

SANDIA REPORT

SAND91-2694 • UC-212
Unlimited Release
Printed December 1991



SAND91-2694
0002
UNCLASSIFIED

12/91
124P STAC

REFERENCE COPY

C.2

Utility Battery Exploratory Technology Development Program Report for FY91

Nicholas J. Magnani, Paul C. Butler, Abbas A. Akhil,
Jeffrey W. Braithwaite, Nancy H. Clark, James M. Freese

Prepared by
Sandia National Laboratories
Albuquerque, New Mexico 87185 and Livermore, California 94550
for the United States Department of Energy
under Contract DE-AC04-76DP00789

Issued by Sandia National Laboratories, operated for the United States Department of Energy by Sandia Corporation.

NOTICE: This report was prepared as an account of work sponsored by an agency of the United States Government. Neither the United States Government nor any agency thereof, nor any of their employees, nor any of their contractors, subcontractors, or their employees, makes any warranty, express or implied, or assumes any legal liability or responsibility for the accuracy, completeness, or usefulness of any information, apparatus, product, or process disclosed, or represents that its use would not infringe privately owned rights. Reference herein to any specific commercial product, process, or service by trade name, trademark, manufacturer, or otherwise, does not necessarily constitute or imply its endorsement, recommendation, or favoring by the United States Government, any agency thereof or any of their contractors or subcontractors. The views and opinions expressed herein do not necessarily state or reflect those of the United States Government, any agency thereof or any of their contractors.

Printed in the United States of America. This report has been reproduced directly from the best available copy.

Available to DOE and DOE contractors from
Office of Scientific and Technical Information
PO Box 62
Oak Ridge, TN 37831

Prices available from (615) 576-8401, FTS 626-8401

Available to the public from
National Technical Information Service
US Department of Commerce
5285 Port Royal Rd
Springfield, VA 22161

NTIS price codes
Printed copy: A04
Microfiche copy: A01

SAND91-2694
Unlimited Release
Printed December 1991

Distribution
Category UC-212

Utility Battery Exploratory Technology Development Program Report for FY91

Nicholas J. Magnani,
Power Sources Department
Paul C. Butler, Abbas A. Akhil,
Jeffrey W. Braithwaite, Nancy H. Clark,
and James M. Freese,
Storage Batteries Division

Sandia National Laboratories
Albuquerque, New Mexico 87185

Abstract

Sandia National Laboratories, Albuquerque, manages the Utility Battery Exploratory Technology Development Program, which is sponsored by the U.S. Department of Energy's Office of Energy Management. In this capacity, Sandia is responsible for the engineering analyses and development of rechargeable batteries for utility-energy-storage applications. This report details the technical achievements realized during fiscal year 1991.

Contents

| | |
|---|------------|
| Acronyms and Abbreviations | vii |
| 1. Executive Summary | 1-1 |
| Introduction | 1-1 |
| Sodium/Sulfur Project | 1-2 |
| Technology Development | 1-2 |
| Technology Evaluation | 1-2 |
| Zinc/Bromine Technology | 1-3 |
| Technology Development | 1-3 |
| Technology Evaluation | 1-3 |
| Applied Research | 1-3 |
| Systems Studies and Advanced Lead-Acid Technology | 1-4 |
| Utility-Specific Systems Studies | 1-4 |
| Advanced Battery Development | 1-4 |
| AC Battery Development | 1-4 |
| Supplemental Evaluations and Field Tests | 1-5 |
| Nickel/Hydrogen Evaluation | 1-5 |
| Aluminum/Air Evaluation | 1-5 |
| 2. Sodium/Sulfur Project | 2-1 |
| Core Technology Development - CSPL | 2-1 |
| Background | 2-1 |
| Results | 2-1 |
| Utility Battery Technology Development - BPI | 2-2 |
| Task 1 - UES Applications Assessment | 2-3 |
| Task 2.1 - Cell Component Development | 2-3 |
| Task 2.2 - Cell Development and Qualification | 2-4 |
| Task 2.3 - Battery Component Development | 2-4 |
| Task 3.0 - Design and Fabrication of UES Module | 2-5 |
| Task 4.0 - Full-Scale Battery Plant Design | 2-5 |
| Technology Evaluation - SNL | 2-5 |
| Technology Evaluation - ANL | 2-9 |
| 3. Zinc/Bromine Project | 3-1 |
| Technology Development - JCBGI | 3-1 |
| Laboratory Battery Testing | 3-1 |
| Other Laboratory Testing | 3-15 |
| Core Technology Advances | 3-27 |

| | |
|---|------------|
| Battery/Station Design | 3-59 |
| Summary and Conclusions | 3-60 |
| Technology Evaluation - SNL | 3-61 |
| Applied Research - SNL | 3-64 |
| Durability Studies | 3-64 |
| Improved Membranes | 3-67 |
| 4. Systems Studies and Advanced Lead-Acid Technology | 4-1 |
| Utility-Specific Systems Studies | 4-1 |
| Bonneville Power Administration | 4-1 |
| San Diego Gas & Electric | 4-2 |
| Oglethorpe Electric Power Corporation | 4-2 |
| Chugach Electric Association | 4-2 |
| Battery System Development - GNB | 4-3 |
| AC Battery Development | 4-4 |
| 5. Supplemental Evaluations and Field Tests | 5-1 |
| Nickel/Hydrogen Evaluation | 5-1 |
| Program Background | 5-1 |
| Battery Design | 5-1 |
| Florida Solar Energy Center Tests | 5-1 |
| Southwest Technology Development Institute Tests | 5-3 |
| 7-kWh Battery (JCBGI) | 5-8 |
| SNL Evaluation | 5-10 |
| Aluminum/Air Evaluation | 5-12 |
| Appendix: Presentations and Publications | A-1 |
| Presentations | A-1 |
| Publications | A-1 |

Figures

| | | |
|-----|--|------|
| 1-1 | SNL Utility Battery Exploratory Technology Development Program | 1-2 |
| 2-1 | Baseline Life-Cycle Test, CSPL Cell #508, Capacity and Resistance | 2-7 |
| 2-2 | Peukert Plot for Sodium/Sulfur Cells 515, 516, and 517 | 2-7 |
| 2-3 | Ragone Plot for CSPL Sodium/Sulfur Cells 515, 516, and 517 | 2-8 |
| 2-4 | Peak Power, CSPL Cell #515 | 2-8 |
| 2-5 | Average Capacity and End-of-Discharge Resistance at Different Temperatures, CSPL Cell #506 | 2-10 |

| | | |
|------|--|------|
| 2-6 | Rc/Rd at Different Temperatures, CSPL Cell #506 | 2-10 |
| 3-1 | Zinc/Bromine Contract - Phase 1 | 3-2 |
| 3-2 | Baseline Cycles, V1-53 | 3-5 |
| 3-3 | Baseline Cycles, V1-55 | 3-5 |
| 3-4 | Baseline Cycles, V1-54 | 3-6 |
| 3-5 | No-Strip Cycle Sets (Average Coulometric Efficiency for Each Set) | 3-7 |
| 3-6 | No-Strip Cycle Sets (Residual Ah on Last Cycle of Set) | 3-9 |
| 3-7 | V1-44: Standloss at Full Charge (Wh Loss Compared to Baseline Cycles) | 3-11 |
| 3-8 | Standloss at Full Charge (Ah Loss Compared to Baseline Cycles) | 3-11 |
| 3-9 | Zinc Loading Study, V1-54 | 3-12 |
| 3-10 | Efficiency vs Operating Temperature, V1-50 | 3-12 |
| 3-11 | Effect of Charge Current Density on Efficiencies, Mini-Cell #2 | 3-15 |
| 3-12 | Baseline Cycle Efficiencies, Mini-Cell #2 | 3-16 |
| 3-13 | Effect of Zinc Loading on Dendrite Height Unsupported Load-Leveling Electrolyte | 3-17 |
| 3-14 | Effect of Current Density on Dendrite Height | 3-18 |
| 3-15 | Effect of Flow Rate on Dendrite Height | 3-19 |
| 3-16 | Effect of Flow Rate on Zinc Thickness | 3-19 |
| 3-17 | Spray-Coat PV2 vs CP4 Carbon Paper Electrodes | 3-22 |
| 3-18 | ESCA-Monitored Changes in PV2 Carbon | 3-23 |
| 3-19 | ESCA-Monitored Changes in CP4 Paper Carbon | 3-23 |
| 3-20 | ESCA-Monitored Changes in PV2 Carbon | 3-24 |
| 3-21 | ESCA-Monitored Changes in CP4 Carbon | 3-24 |
| 3-22 | Polarization Data - Effect of Graphitic and Oxygen Content | 3-25 |
| 3-23 | Resistivity vs Concentration | 3-26 |
| 3-24 | Electrolyte Comparison, V1-59 | 3-26 |
| 3-25 | Interaction Effects of Pressure with Bead Width on Weld Strength, Experiment #1 | 3-29 |
| 3-26 | Interaction Effects of Melt Index with Weld Depth on Weld Strength, Experiment #1 | 3-29 |
| 3-27 | Interaction Effects of Glass Content with Weld Depth on Weld Strength, Experiment #1 | 3-30 |
| 3-28 | Main Effects on Weld Strength (with 95% Confidence Intervals), Experiment #2 | 3-30 |
| 3-29 | Weld Strength (psi) vs Melt Index and Glass Content at Pressure = 140 psi, Bead Height = 0.025", Amplitude = 0.052", Experiment #2 | 3-31 |
| 3-30 | Weld Strength (psi) vs Pressure and Amplitude at Melt Index = 30, Glass Content = 11%, Weld Bead Height = 0.020", Experiment #2 | 3-31 |
| 3-31 | Weld Strength per Linear Inch vs Bead Width (17 Melt Index, 30% Glass Content, various welder parameters), Experiment #3 | 3-32 |
| 3-32 | Weld Strength (psi) vs Weld Bead Size (Weld Pressure = 400 psi, Amplitude = 0.046", Depth = 70%), Experiment #3 | 3-33 |
| 3-33 | Contourplot of Weld Strength vs Welder Parameters (30 Melt Index, 11% Glass; 0.120" Wide, 0.020" High Bead), Experiment #4 | 3-34 |
| 3-34 | 3D Plot of Strength vs Welder Parameters, Experiment #4 | 3-34 |

| | | |
|------|--|------|
| 3-35 | Expansion of Ketjenblack Composites in Bromine Vapor (no glass fiber) | 3-37 |
| 3-36 | Properties of Ketjen Composites (0.3 MI HDPE + 16 wt% glass fiber) | 3-38 |
| 3-37 | Properties of XC-72 Composites (MDI 3/91) (0.3 MI HDPE + 16 wt% glass fiber) | 3-39 |
| 3-38 | Expansion of Ketjenblack/Glass Fiber Composites in Bromine Vapor | 3-39 |
| 3-39 | Expansion of XC-72 Black/16% Glass Fiber Composites in Bromine Vapor | 3-40 |
| 3-40 | Zinc/Bromine Mass and Energy Balance | 3-44 |
| 3-41 | Model Predicted Voltage Profile (15 ohm-cm electrodes) | 3-45 |
| 3-42 | Effect of Electrode and Separator Thicknesses on Energy Efficiency | 3-46 |
| 3-43 | Effect of Electrode Resistivity on Energy Efficiency | 3-46 |
| 3-44 | Effect of Separator Resistivity on Energy Efficiency | 3-47 |
| 3-45 | Effect of Bromine Transport on Energy Efficiency | 3-47 |
| 3-46 | Model Predicted Voltage Profile (2 ohm-cm electrodes) | 3-48 |
| 3-47 | Effect of Bromine Transport on Coulombic Efficiency | 3-49 |
| 3-48 | Effect of Bromine Transport and Separator Resistivity on Energy Efficiency (4-hr discharge rate) | 3-49 |
| 3-49 | Effect of Bromine Transport and Separator Resistivity on Energy Efficiency (10-hr discharge rate) | 3-50 |
| 3-50 | Effect of Discharge Time on Efficiencies (8-cell stack, no pumping losses) | 3-50 |
| 3-51 | Effect of Discharge Time on Efficiencies (8-cell stack, including pumping losses) | 3-51 |
| 3-52 | Effect of Charge Time on Efficiencies (8-cell battery stack; constant zinc loading of 90 mA/cm ²) | 3-51 |
| 3-53 | Effect of Discharge Time on Efficiencies (8-cell stack) | 3-52 |
| 3-54 | Effect of Charge and Discharge Times on Efficiencies (80-cell including pumps) | 3-52 |
| 3-55 | Stand Time Study on V1-44 Compared to Model Predictions | 3-53 |
| 3-56 | Vapor Pressure Over MEPBr Complex | 3-55 |
| 3-57 | Zinc/Bromine Battery Electrolyte Recycling Process | 3-56 |
| 3-58 | Adhesive Bonding Strength | 3-59 |
| 3-59 | Zinc Loading Study at Constant Charge of 20 mA/cm ² and 24°C, Efficiencies | 3-62 |
| 3-60 | Zinc Loading Study at Constant Charge of 20 mA/cm ² and 24°C, Residual and Transport Losses | 3-62 |
| 3-61 | SNL Data (Battery #514), 50-Cell Zinc/Bromine | 3-63 |
| 3-62 | JCBGI and SNL Data (Battery #518), 8-Cell Zinc/Bromine | 3-64 |
| 3-63 | Shear Modulus vs Temperature of HDPE-1 | 3-66 |
| 3-64 | Shear Modulus vs Temperature of HDPE-2 | 3-67 |
| 3-65 | Bromine Permeation (a) and Area Resistivity (b) of Untreated Daramic [®] and Nafion-Treated Daramic [®] as a Function of Aging Time in the Battery Electrolyte | 3-69 |
| 3-66 | Chemical Structure of Eastman Kodak's Sulfonated Polyester: Eastman AQ 55D | 3-70 |
| 3-67 | Normalized Resistance and Permeation of JCBGI's Developmental Separator vs Impregnation Dilution with Eastman AQ 55D | 3-71 |
| 3-68 | Experimental Procedure for Preparing Radiation-Grafted Membranes | 3-71 |
| 3-69 | Effect of Grafting Methacrylic Acid and Divinylbenzene into the Pores of JCBGI's Developmental Separator | 3-72 |
| 5-1 | 10-Cell Battery Stack | 5-2 |

| | | |
|-----|---|-----|
| 5-2 | 2-kWh Batteries in Filament-Wound Vessels | 5-2 |
| 5-3 | Representative Daily Data from Lighting Profile | 5-4 |
| 5-4 | Representative Daily Data from Vaccine Refrigeration Profile | 5-6 |
| 5-5 | Representative Daily Data from Telecommunications Profile | 5-7 |
| 5-6 | Typical Daily Operation of Batteries #P004 and #P005 on the Vaccine Refrigeration Profile | 5-9 |
| 5-7 | 7-kWh Boilerplate CPV Nickel/Hydrogen Battery | 5-9 |

Tables

| | | |
|------|--|------|
| 2-1 | CSPL Cell Test Summary at SNL | 2-6 |
| 3-1 | Modifications to V-Design Stacks | 3-4 |
| 3-2 | Results of No-Strip Cycles | 3-8 |
| 3-3 | Standloss Results | 3-10 |
| 3-4 | Strip Times | 3-13 |
| 3-5 | V1-51 Performance - Energy Losses | 3-14 |
| 3-6 | Separator Comparison from Mini-Cell Testing | 3-16 |
| 3-7 | Plastic Composition | 3-28 |
| 3-8 | Weld Bead Height | 3-28 |
| 3-9 | Burst Tests Results | 3-36 |
| 3-10 | Results of 8/91 MDI Compounding Trials | 3-36 |
| 3-11 | Resistivities of HDPE/Graphite/Carbonblack Composites | 3-37 |
| 3-12 | Properties of Compounded Compression-Molded Separator Materials | 3-41 |
| 3-13 | Predictions from Revised Computer Model | 3-45 |
| 3-14 | Flow Cell Optimization | 3-54 |
| 3-15 | Analysis Types | 3-57 |
| 3-16 | Adhesive Bonding Tests on Polyethylene (11% Glass - 30 Melt Index) | 3-58 |
| 3-17 | Aging Matrix | 3-65 |
| 3-18 | Melting and Heat of Fusion Data on Aged and Unaged Electrodes (1 Mo Data) | 3-66 |
| 3-19 | Sorption Data for HDPE-1 and HDPE-2 | 3-67 |
| 4-1 | Utility-Specific Systems Studies: FY91 | 4-2 |
| 5-1 | Lighting Profile Performance Summary | 5-5 |
| 5-2 | Refrigeration Profile Performance Summary | 5-5 |
| 5-3 | Characterization Cycles of Batteries P004 and P005 | 5-8 |
| 5-4 | Parametric Testing of Series-Configured 10-Cell Modules #1 and #3 from 7-kWh Battery | 5-10 |
| 5-5 | Parametric Testing of Series-Configured 10-Cell Modules #2 and #4 from 7-kWh Battery | 5-11 |
| 5-6 | Configuration and Test Conditions | 5-12 |
| 5-7 | Summary of Test Results (as of 6/30/91) | 5-12 |
| 5-8 | Aluminum/Air Cell SFUDS Discharge Results | 5-13 |

Acronyms and Abbreviations

| | |
|-------|--|
| ABB | Asea Brown Boveri |
| ANL | Argonne National Laboratory |
| ASV | anodic stripping voltammetry |
| BEST | Battery Energy Storage Test Facility |
| BPA | Bonneville Power Administration |
| BPI | Beta Power, Inc. |
| CA | coupling agent |
| CAEDS | computer-aided engineering design system |
| CE | coulombic efficiency |
| CEA | Chugach Electric Association |
| CPV | common pressure vessel |
| CSPL | Chloride Silent Power, Ltd. |
| CV | cyclic voltammogram |
| DOD | depth-of-discharge |
| DOE | Department of Energy |
| DVB | divinylbenzene |
| EDX | energy dispersive X-ray |
| EE | energy efficiency |
| EHP | DOE/Electric and Hybrid Propulsion |
| EOC | end of charge |
| EOD | end of discharge |
| EPRI | Electric Power Research Institute |
| ERC | Energy Research Corporation |
| ESCA | electron spectroscopy for chemical analysis |
| ETD | Utility Battery Exploratory Technology Development |
| EV | electric vehicle |
| FEA | finite element analysis |
| FSEC | Florida Solar Energy Center |
| FTIR | Fourier transform infrared |
| GNB | GNB Industrial Battery |
| GRI | Gorman-Rupp Industries |
| HDPE | high density polyethylene |
| IC | ion chromatography |
| ICE | ion capillary electrophoresis |
| ICP | inductively coupled plasma |

| | |
|--------|--|
| INEL | Idaho National Engineering Laboratory |
| IPV | individual pressure vessel |
| ISOA | improved state-of-the-art |
| JCBGI | Johnson Controls Battery Group, Inc. |
| LBL | Lawrence Berkeley Laboratory |
| LCC | life-cycle cost |
| LCLo | Lethal Concentration Low |
| LLDPE | linear low density polyethylene |
| M | molar |
| MAA | methacrylic acid |
| MDI | Modern Dispersions, Inc. |
| MEM | methyl morpholinium |
| MEP | methyl pyrrolidinium |
| MI | melt index |
| OCV | open-circuit voltage |
| OEM | DOE/Office of Energy Management |
| OPC | Oglethorpe Power Corporation |
| OPS | DOE/Office of Propulsion Systems |
| PGE | Pacific Gas & Electric |
| PP | polypropylene |
| PREPA | Puerto Rico Electric Power Authority |
| PV | photovoltaic |
| SCE | saturated calomel electrode |
| SCP | shunt current protection |
| SDGE | San Diego Gas & Electric |
| SFUDES | Simplified Federal Urban Driving Schedule |
| SNL | Sandia National Laboratories |
| SOA | state-of-the-art |
| SOC | state-of-charge |
| SPS | sulfonated polysulfone |
| T&D | transmission and distribution |
| TDI | Southwest Technology Development Institute |
| TGA | thermal gravimetric analysis |
| UES | utility energy storage |
| UHMWPE | ultra high molecular weight polyethylene |
| UMR | University of Missouri-Rolla |
| VE | voltaic efficiency |
| VRLA | valve-regulated lead-acid |
| XRF | X-ray fluorescence |

1. Executive Summary

Introduction

This report documents the fiscal year 1991 activities of the Utility Battery Exploratory Technology Development Program (ETD), managed by Sandia National Laboratories (SNL) and supported by the U.S. Department of Energy, Office of Energy Management (OEM). (See SAND91-0672, *Exploratory Battery Technology Development and Testing Report for 1990*, for a description of the previous year's activities.) ETD is responsible for the engineering development of battery systems whose basic feasibility has been demonstrated. These systems are being designed for use in utility energy storage and other stationary applications. Battery development is accomplished through cost-shared contracts with industrial partners. SNL's responsibilities include program management and technical direction of the contracts. Additionally, SNL conducts analysis of the benefits of battery storage in utility systems and performs appropriate applied research activities. The performance of batteries or components produced by development contractors is characterized either at SNL or at Argonne National Laboratory (ANL).

Paul C. Butler is the person responsible for activities at SNL. Mr. Butler supervises the Storage Batteries Division under Nicholas J. Magnani, Manager of the Power Sources Department (see Figure 1-1).

ETD was organized into five projects:

- Utility-Systems Analysis
- Sodium/Sulfur Development
- Zinc/Bromine Development
- Advanced Lead-Acid Development
- Supplemental Evaluations and Field Tests.

The results of the utility-systems analyses will be used to motivate and define needed field evaluations of battery systems, inform utilities of the value of batteries, and specify engineering requirements for more widespread application of batteries to utility systems.

Battery technology development utilizes a phased approach from fundamental electrochemical R&D, to component development, and through several steps of battery engineering (conceptual, prototype, and

product). A battery technology suitable for commercial marketing is the desired final product. At SNL, program management involves placing industrial development contracts, monitoring and guiding progress, solving programmatic issues, and coordinating reporting. Under technology evaluation, contract deliverables are tested primarily at SNL to determine performance, lifetime, and failure mechanisms. These data are reported to the developers for use in optimizing designs and resolving problems. Applied research is performed in certain projects where SNL has specific technical expertise to address critical issues facing a technology. This applied work is closely integrated with the prime development contractor.

A separate activity is devoted to miscellaneous testing and evaluation activities. Included are field testing of nickel/hydrogen batteries and laboratory testing of aluminum/air, two technologies no longer being developed by SNL. Also this project enhances and maintains the SNL battery evaluation facilities. Specialized hardware and software are developed to provide unique test capabilities.

For continuity, this report is organized by technology, with one chapter devoted to each technology that was under development and evaluation during FY91, plus a chapter for those testing activities not associated with present technology development. Because the utility-systems studies are currently utilizing the lead-acid technology, progress on this topic is reported in Chapter 4. Specific topics covered in Chapters 2 through 5 include:

2. Sodium/Sulfur Technology
 - Core Technology Development by Chloride Silent Power, Ltd. (CSPL)
 - Utility-Energy-Storage (UES) Battery Engineering by Beta Power, Inc. (BPI)
 - Evaluations at SNL and ANL
3. Zinc/Bromine Technology
 - Development by Johnson Controls Battery Group, Inc. (JCBGI)
 - Evaluations at SNL
 - Applied Research at SNL

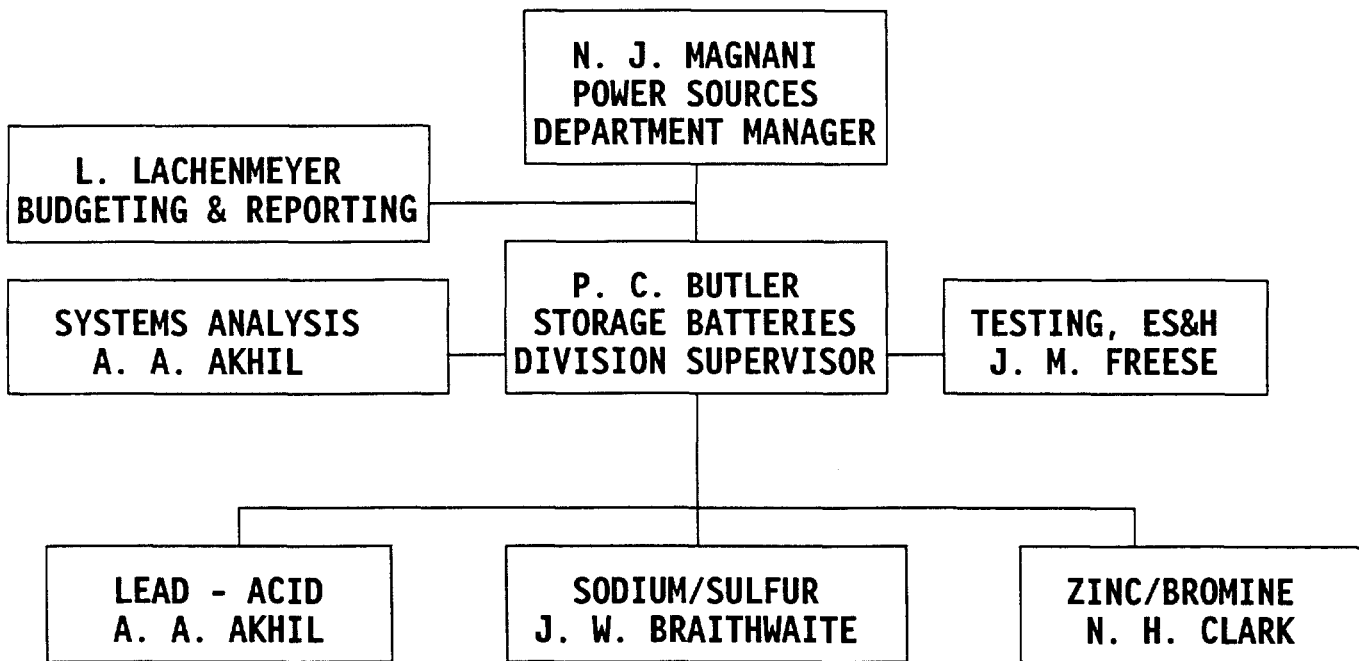


Figure 1-1. SNL Utility Battery Exploratory Technology Development Program

4. Systems Studies and Advanced Lead-Acid Technology

- Utility-Specific Systems Studies
- Battery System Development by GNB Industrial Battery Co. (GNB)
- Technology Evaluation
- AC Battery Development

5. Supplemental Evaluations and Field Tests

- Nickel/Hydrogen Evaluation
- Aluminum/Air Evaluation

A summary of the FY91 highlights follows.

Sodium/Sulfur Project

Technology Development

The 5-yr contract with Chloride Silent Power Limited was successfully concluded in December 1990. The objectives of the CSPL program were to advance the sodium/sulfur technology with respect to compo-

nents, cells, and small batteries for both stationary and mobile applications and to complete initial conceptual studies of sodium/sulfur batteries for large-scale UES.

A new contract was placed with Beta Power, Inc. for the first phase of sodium/sulfur utility-battery engineering. This 2.5-yr contract is being cost-shared at the 24% level. Approximately half of the activity will be performed at CSPL, BPI's inter-divisional partner. The four functional tasks to be completed in this program are structured to address and solve many generic utility-battery issues related to the sodium/sulfur technology. These tasks will define the market opportunities for sodium/sulfur utility batteries; advance the development stage for a number of cell and battery-level components; design, fabricate, and test an advanced small-scale utility module; and finally design and analyze the performance and cost for a full-scale utility battery. As formulated, this program represents a logical initial phase of a larger development effort to commercialize the technology by the turn of the century.

Technology Evaluation

During this fiscal year, SNL evaluated 10 individual PB cells and one 2-cell series string from CSPL. These cells, which were the last ones from the Core Technol-

ogy contract with CSPL, were specifically designed for electric vehicle applications. The DOE/Office of Propulsion Systems (OPS) funded the evaluation.

The cells were subjected to parametric testing to determine the effects of different cycling regimes on service life. One group of cells completed over 700 continuous constant-current cycles. Another group of cells was evaluated using a modified driving schedule and has completed over 200 cycles. The cell capacities remain above their rated capacity of 10 Ah; however, most cell resistances have increased 6 to 7 mohms.

The maximum specific peak power was measured to be ~135 W/kg. Range in the IDSEP vehicle is predicted to be 160 miles.

At ANL, life-testing of a 120-cell (PB) sodium/sulfur module from CSPL continued with SFUDS discharges to 100% DOD. The module has completed 696 cycles and retains ~85% of its initial 292-Ah, 3-hr rate capacity. The specific energy obtained with SFUDS discharges continues to hold at ~80% of its initial 71.5 Wh/kg.

Zinc/Bromine Technology

Technology Development

Zinc/bromine battery technological advances have been realized in several areas in the first year of a 39-month cost-shared contract with JCBGI. At the onset of this contract, criteria were established addressing most of the concerns that were observed in the previous development efforts. These criteria have been met and in some cases exceeded with 1-kWh battery stacks. Prior to the start of Phase 2, these criteria need to be demonstrated on 50-cell battery stacks.

Some of the most significant developments have been in the ability to vibration-weld a battery stack that remains leak free. The task of sealing the battery stack was by no means trivial. However, through several design iterations, a solid base for larger battery stack designs has been established. Internal stack stresses can now be modeled in addition to fluid velocity and fluid pressure distribution through the use of the CAEDS/finite element analysis (FEA) software programs. Additionally, JCBGI's proprietary FORTRAN model has been improved significantly enabling accurate performance predictions. This modeling has been instrumental in improving the integrity and performance of the battery stacks, and should be instrumental in reducing the turnaround time from concept to assembly.

The development highlights of the efforts for the past year are listed below:

- 4 1-kWh battery stacks over 100 cycles
- Less than 10% degradation in performance in these 4 battery stacks
- 1 battery stack over 200 cycles
- 1 battery stack over 300 cycles
- Zinc loading investigation exhibits virtually no loss in performance for loadings up to 125 mAh/cm²
- Charge current densities of 50 mA/cm² have been achieved in minicells
- 14 consecutive no-strip cycles have been successfully conducted on the stack with 300+ cycles
- Safety and environmental studies have been initiated by conducting spill simulations
- Materials research is continuing to provide improvements in the electrode, activation layer, and separator.

Technology Evaluation

During FY91, SNL evaluated two zinc/bromine batteries from JCBGI: one stack consisted of 8 cells while the other had 50 cells. Identical sets of parametric tests, at two different battery temperatures (24°C and 28°C), were conducted on the 50-cell battery along with numerous baseline capacity tests. Results of these tests indicated that, within experimental error, temperature had little or no effect and that a loss in coulombic and energy efficiency of ~10% was measured when the zinc loading was varied threefold. A total of 77 charge/discharge cycles were placed on this battery (20 cycles at JCBGI and 57 cycles at SNL) before it was removed from test due to internal stack leaks and external catholyte tank leaks.

The 8-cell battery has completed a total of 160 charge/discharge cycles (26 cycles at JCBGI and 134 cycles at SNL) and the coulombic and energy efficiencies have decreased less than 3%. The battery will continue to be cycled in an attempt to establish life-cycle capability.

Applied Research

Applied research is being done in the areas of developing advanced membranes and in studying the

durability of electrode materials. Durability studies, which have been 50% completed this year, have shown that High Density Polyethylene (HDPE) with glass content of ~30 is more stable in electrolyte than lower glass content materials and significantly more stable than polypropylene. Advanced membrane work has looked at improving separator performance by impregnation of membranes with ionic polymers including polysulfones, Eastman AQ 55D (sulfonated polyester) and Nafion. Also, radiation grafting, plasma, and sol-gel processes were tried. Currently Nafion shows the most promise in laboratory experiments and will be evaluated by JCBGI in minicells next year. Work will also be continued in the plasma and sol-gel processes since initial studies showed these processes also had promise.

Systems Studies and Advanced Lead-Acid Technology

Utility-Specific Systems Studies

Four utility-specific systems studies were initiated during FY91 with:

- Bonneville Power Administration (BPA)
- San Diego Gas & Electric (SDGE)
- Oglethorpe Power Corporation (OPC)
- Chugach Electric Association (CEA)

The aim of these studies is to identify possible applications of battery energy storage in each utility's network and quantify the benefits that these applications offer. These are screening level studies driven by the needs of each utility's specific operating and generation resource requirements. As such, each study has a relatively short duration of 3-4 mo, during which the operation and planning staff of each utility provides information that forms the basis of the SNL evaluation.

All except the BPA study were started relatively late during this fiscal year, and there are no significant study findings that can be reported at this time. The BPA study started in February, but its original completion was postponed due to revision of the basic planning assumptions by BPA in mid-June. The revised assumptions made a significant impact on their system study. It is expected that the SNL study will now be completed in late 1991.

Advanced Battery Development

The Advanced Lead-Acid battery development cost-shared contract was placed with GNB on May 1, 1991. The 3-yr development effort will focus on the improvement of Valve Regulated Lead-Acid (VRLA) battery designs to meet utility application requirements in the mid-to-late 1990s. The statement-of-work and the make-up of the project team for this contract were specially defined to ensure that GNB obtains first-hand input from utilities about battery storage requirements in their network. This was accomplished by incorporating a "host utility" function that required GNB to form a relationship with one or more electric utilities to support specific tasks.

The GNB effort will study the specific requirements for two utility applications and develop an advanced VRLA battery to meet those requirements. Two host utilities, Pacific Gas & Electric (PGE) and Puerto Rico Electric Power Authority (PREPA), are participating on the GNB project team. Both utilities will identify site-specific battery storage applications in their network and define the requirements that will guide the GNB battery design effort. The utilities will also perform economic analysis of their selected applications to identify the economic feasibility of battery applications using current technology costs as well as the cost for the advanced VRLA design.

Recognizing the near-term market potential, GNB offered 46% cost-sharing, and both host utilities are also cost-sharing their participation as sub-contractors to GNB, PREPA at 100% and PGE at 50%.

The GNB effort is comprised of three tasks. Task 1 is a two-phase activity that seeks performance improvements through changes in battery design. Tasks 2 and 3 involve requirements definition and economic evaluations that require extensive host utility participation.

Progress was made in several subtasks in Task 1, Phases I and II. However, due to the late start-up of the contract and staffing difficulties at GNB, activity on Task 3 was behind schedule.

AC Battery Development

In early FY92, a 15-mo contract will be placed with Omnion Power Engineering Corp., who has patented the AC Battery concept. This contract will implement an engineering development program to build and test the first prototype unit at a utility site in the PGE service area.

Supplemental Evaluations and Field Tests

Nickel/Hydrogen Evaluation

During FY91, SNL contracted JCBGI to provide technical support for four 2-kWh Common Pressure Vessel (CPV) nickel/hydrogen batteries on test at the Florida Solar Energy Center (FSEC) and the Southwest Technology Development Institute (TDI). In addition, JCBGI conducted a series of parametric tests on the 7-kWh module (consisting of four batteries), which was previously on test at SNL. All of these batteries were produced by SNL development contracts in prior years.

The testing of three load profiles at FSEC demonstrated the excellent performance and flexibility of the CPV nickel/hydrogen battery. Simple battery control schemes based on charge pressure and discharge voltage proved adequate. In addition, the ability of the battery to withstand catastrophic system failures and total discharge proved to be a valuable asset. A similar test strategy was developed at the TDI; however, due to an apparent leak in one of the modules, this test plan was not completed.

In preparation for the renewed testing of the 7-kWh module at JCBGI, a brief series of cycles was run, establishing that the batteries were still in excellent condition. The four batteries were then split into two separate sets of series-connected stacks for the parametric tests. To date, a set of C/5 discharge baseline cycles and C/10 rate discharge cycles have been completed. The batteries have been delivering over 190 Ah and 9.5 kWh in total, well over the 7.85 kWh achieved in initial testing.

At SNL, three nickel/hydrogen cells were on test during FY91, each representing a different stage of

development. The capacity of Cell #144 continued to diminish and subjecting it to an activation cycle did not correct the problem. When the capacity declined below 80% of the nominal capacity value, the cell was returned to JCBGI for evaluation.

Due to a tendency to reach the high-temperature limit on discharge, Cell #185 has been running on a test plan that maintained a steady 98% coulombic efficiency without causing as great a temperature rise. Recent fluctuation of the capacity has dropped the efficiency to 96%.

Cell #P003 has a cooling jacket installed on the pressure vessel. Controlling the temperature has resulted in a 6-Ah increase in capacity over that obtained without cooling.

All three of these cells have displayed the phenomena of gradually increasing pressures during charge until a high-pressure alarm at 330 psig necessitates reducing the end-of-discharge (EOD) pressure to 50 psig before resuming testing.

Testing of all cells was suspended on June 30, 1991, until completion of remodeling of the laboratory.

Aluminum/Air Evaluation

Evaluation of the Eltech Research Corp. aluminum/air cell concluded during this reporting period. This cell was produced during a development contract in FY90. Tests were run with pure aluminum anodes and with an advanced aluminum alloy under SFUDS discharge conditions. Under SFUDS, the corrosion rate of the advanced alloy averaged 22.9 mA/cm²; this compares favorably with the programmatic goal of 30 mA/cm². Due to the uncertainty in the scaled weight of the cell, a vehicle range was not predicted.

2. Sodium/Sulfur Project

The sodium/sulfur technology is one of the leading candidates for large-scale mobile and utility-energy-storage applications because of its potential for low-cost, long-life, reliable operation, and excellent performance (e.g., energy and power density, electrical efficiency). During FY91, advancement of this technology continued under ETD support. A major, 5-yr development effort was successfully concluded near the first of the fiscal year under a contract with Chloride Silent Power Limited, Runcorn, England. With the positive results of the CSPL contract providing the basis, a new contract was placed in the third quarter with Beta Power, Inc., Salt Lake City, Utah. (BPI is a wholly owned subsidiary of CSPL.) The objective of this new activity is to complete the first dedicated phase of development specifically addressing UES applications. Additionally, the performance of the CSPL technology was evaluated at SNL and ANL. Accomplishments during FY91 in each of these areas are reported separately in the following four sections.

Core Technology Development - CSPL

The 5-yr SNL contract (#48-8837) with CSPL concluded in December 1990. The objective of the CSPL program was to advance the development state of the sodium/sulfur technology with respect to components, cells, and small batteries for both stationary and mobile applications. Overall, CSPL cost-shared 35% of this \$11.0M effort. The final deliverables from the program included qualified cells suitable for use in both mobile and stationary applications and a subscale battery module (200 cells) that is still being evaluated in a UES mode. As described in detail in the *Exploratory Battery Technology Development Report for FY90*, the objectives for this effort were satisfied.

The activity at CSPL was divided into the following two tasks:

Task 1 - Core Technology Research and Development

Task 2 - Battery Engineering and Testing

Task 1 was devoted to research and development in the areas that are generic to both stationary and electric

vehicle (EV) applications. Major emphases of this task were to improve cell performance, reliability, safety, and cost. The Task 2 effort was directed toward the design and fabrication of batteries for UES applications.

Background

The CSPL sodium/sulfur cell design strategy is based on a family of cells designated the "PB" cells. Two specific sizes were developed with support from this program: a 45-mm-diameter by 45-mm-high cell called the "PB" cell and a 45-mm-diameter by 110-mm-high cell, called the "extended PB or XPB" cell. The cells both utilize a central-sodium configuration and are based on identical components as far as possible, particularly in the seals. The XPB has been proposed for utility applications and the PB for electric vehicle applications.

A notable milestone for CSPL was reached in 1988 when approval was given for the construction of an automated, 5000 cell/week pilot production plant. The output will be used in the construction of batteries for extensive field trials. In March of 1990, a German electric utility, RWE, signed an agreement with Chloride Group, CSPL's holding company. A new joint venture company, C-RWE was established and purchased the Clifton Sodium/Sulfur Production Plant and the associated Electrolyte Plant at Runcorn. This facility was commissioned in late FY91.

A significant effort to transfer the CSPL technology to the U.S. commenced during 1989. This is being accomplished by means of a phased schedule in which parts of the manufacturing processes are introduced to the BPI facility at Salt Lake City, Utah. BPI now has the capability to manufacture cells using the CSPL technology.

Results

During FY91, CSPL prepared a draft of a comprehensive final report that is now in the review process. In addition, CSPL continued testing cells and modules and completed a short study to identify issues related to optimum cell size and configuration for UES applications.

Cell and Module Evaluation

As mentioned above, during FY91, CSPL commissioned their new sodium/sulfur battery pilot production plant. The first unit operation to become fully functional was the electrolyte facility. This highly automated process is capable of manufacturing 5000 usable shapes per week. Two important advances have already been achieved: 1) new processing conditions have resulted in an ~10% increase in electrolyte conductivity, and 2) because of the use of automated handling, thin-walled electrophoretic-deposited tubes have been successfully made for the first time in relatively large quantities.

These advances are significant because cells can now be produced with lower resistance (and thus higher power). Typical 1990 PB cell resistance (e.g., those in the ETX-II battery) is 30-32 mohms. This value drops to the high twenties using the new electrolyte production procedure. Finally, cells made with the new thin-walled material show resistance values approaching 20 mohms. Because power is the primary design criterion in mobile applications (and even possibly in UES), fewer cells will be needed in each battery. These improvements will allow the CSPL cell technology to at least match the power density and continue to exceed the energy density observed in the competing Asea Brown Boveri (ABB) systems. The unanswered question is the effect of the thinner electrolyte on cell durability.

A problem that has existed for an extended period in a current version of the PB cells has been empirically solved. This problem was characterized by a rising resistance followed by a stable, elevated resistance plateau. Subtle contaminant reactions are believed to be the cause. As mentioned, electrolyte from the new pilot production plant has a higher conductivity than observed before. This improvement is probably due to better powder mixing and less contamination during processing. A second positive result is that cell resistance now slightly decreases during the break-in cycles instead of increasing.

Testing continued with a 120-cell module being used to determine if a new glass seal material is superior to their old material. This module contains 15, 4-cell strings of cells made with each material. The test procedure consists of performing 80 baseline electrical cycles and then one freeze/thaw cycle (with a 24-hr hold at ambient). At the 720 cycle point, 8 freeze/thaw cycles had been logged. All 15 control strings failed, compared with only one cell in 60 with the improved seal material. These results indicate that a dramatic improvement has been attained.

The most significant single deliverable from this contract was the 200-XPB-cell UES module described

in detail in the *Exploratory Battery Technology Development Report for FY90*. This module was tested at temperature for over a year. The durability of the cells was much lower than expected based on the excellent results obtained from qualification tests that used single cells and a 40-cell module. The cause of this reduced service life is believed to be very poor thermal uniformity and especially the existence of "cold-spots." Heat was lost in many directions due to the large busbars and the complicated thermal management system. A full description will be included in the final report.

UES Cell Size Study

A preliminary analysis was undertaken to investigate the effects of cell size and configuration on UES plant investment cost, operating cost, and safety. Safety was emphasized because the information from the core development part of this contract indicated that factors associated with increased size can dramatically and adversely impact operational safety.

A prerequisite cell design study had to be completed to ensure that practical configurations were considered in this system-level study. The cell design was driven by performance capability, gravimetric energy density, manufacturing yields, and safety. Although volumetric energy and power density are probably most important for UES applications, gravimetric energy density and manufacturing yield were considered because they were assumed to be proportional to selling cost. Other important factors include current collection techniques, cell orientation, discharge time, and specifics of how sodium flow is effectively regulated. Because of the sensitivity to confidential information, a description of the results will be deferred to the upcoming final report.

Utility Battery Technology Development - BPI

The goal of the ETD Sodium/Sulfur Project is to advance the development state of the sodium/sulfur battery technology specifically for UES applications. In pursuit of this goal, a new 2.5-yr, \$3.1M contract was placed with BPI in July 1991. Approximately half of the activity will be performed interdivisionally at CSPL. The general objective of this 24% cost-shared contract is to resolve a number of issues related to the feasibility of utilizing the sodium/sulfur technology in these relatively large-scale utility-based applications. Successful completion of this program will result in the identification of quantitative long-term development and demonstration objectives. As such, this "core utility battery technology" activity represents the first phase of

an integrated, long-term DOE/industry effort to produce a viable commercial battery system. Because of the status and needs of the technology, the current lack of identified near-term markets, and the synergism with complementary EV battery developments, commercialization is targeted for the 2000 - 2002 timeframe.

A very important aspect of this new program is battery requirements. Current DOE/Electric Power Research Institute (EPRI) goals for installed sodium/sulfur utility batteries include a 20- to 30-yr service life, 80% ac-to-ac energy efficiency, and an installed cost of under \$100/kWh. Power and energy specifications remain undefined because many diverse candidate applications exist (e.g., load leveling, area regulation, frequency control, spinning reserve). However, it appears from the characterization and analyses that have been done that these electrical requirements can be satisfactorily met with an optimization of the current tubular cell designs. If the development effort is successful, not only would lead-acid options be replaced, but other market opportunities could be opened and/or further expanded.

The tasks that are being performed under the BPI contract include the following:

1. Assessment of UES Applications
 - 1.1 – Utility-application identification
 - 1.2 – Utility-application evaluation and selection
 - 1.3 – Detailed battery specification preparation
2. UES Cell and Battery Component Development
 - 2.1 – Cell component development
 - 2.2 – Cell development and qualification
 - 2.3 – Battery component development
3. Preliminary Engineering of UES Modules
 - 3.1 – Module design
 - 3.2 – Module fabrication
 - 3.3 – Module evaluation
 - 3.4 – Commissioning support
4. Full-Scale Battery Plant Design
 - 4.1 – Utility battery design
 - 4.2 – Performance and cost analysis

The remainder of this section contains a description of the results obtained during the first active quarter for this contract (fourth quarter of FY91):

Task 1 - UES Applications Assessment

Discussions with A. Akhil at SNL have helped identify specific utilities with ongoing UES battery programs that may be receptive to advanced battery discussions. In addition, the pertinent reports from EPRI on strategic and dynamic benefits of UES have

been reviewed, along with progress reports on the battery-energy-storage projects at Puerto Rico Electric Power Authority (PREPA) and the San Diego Trolley. The latter two projects have been targeted to serve as a preliminary design basis for demonstrating the benefits of sodium/sulfur advanced batteries. Battery designs are being formulated in preparation for discussions with the operations personnel of selected utilities. To aid in these discussions, a brochure is also being drafted that identifies the benefits of sodium/sulfur batteries in various UES applications. Utility visits will be made during the coming quarter to enable the development of a representative load profile model and a subsequent design study of the applications. The selection of relevant UES applications is scheduled for January 1992.

The subject of using advanced batteries with the AC Battery concept being developed at Omnion was discussed with H. Meyer. A preliminary design of a 1 MWe (1 MWh) transportable AC Battery unit was generated. The building block of this battery is a self-contained module, two to three times the size of an electric-van battery and weighing nearly 4000 lb (forklift handling capability). Eight such modules would be utilized in bipolar pairs to provide 1 MWh of installed capacity. The benefit offered by the use of sodium/sulfur batteries is that twice the capacity can be delivered to a site in a single haul, at 25% of the volume (lower footprint). Although these benefits offer a cost savings, the overall battery plant installed cost will be the most significant challenge to bolster a battery UES market.

Task 2.1 - Cell Component Development

To design a cell and battery properly for UES applications, the criteria must be considered from two opposing perspectives: 1) the overall battery requirements down to the cell level, and 2) from the cell level back to the battery plant. That is, because safety, cost, and reliability are the key design criteria for UES applications, it is important to develop the design from the top down as well as from the bottom up.

The emphasis for UES cell design is directed initially to considering a central/sulfur configuration. This conclusion was reached as a way to extend life by reducing the potential for corrosion-related effects. In this regard, a prototype cell design and performance study was completed to serve as a baseline for UES applications. The design is based on the use of CSPL XPB electrolyte. Although this decision has an expeditious, practical aspect, it is also appropriate based on safety and reliability results obtained in the UES cell size study

noted in the previous CSPL section. The CSPL "TD" cell design also served as a design reference. The latter cell is also a central-sulfur configuration and utilizes electrolyte of equivalent size to XPB. This cell has the longest cycling performance (in excess of 8000 cycles) in the history of the sodium/sulfur technology, and for this reason, it offers an excellent basis for a UES cell design.

The proposed prototype cell has a usable energy of 49 Wh and has the capability for steady-state discharge at rates up to C/2 without loss of capacity. The cell can be discharged at a 2C rate loss of capacity with some limited loss of capacity. The total cell equivalent resistance is expected to average 11.7 mohms. The performance densities are expected to be 155 Wh/kg and 296 Wh/l at the cell level, and approximately 87 Wh/kg and 139 Wh/l at the integrated module level. It must be emphasized that cell weight, unlike EV applications, is not a major issue for UES battery designs. On the contrary, motivation in UES applications may be to provide sufficient thermal mass in the design to preclude the need for an active cooling system.

Task 2.2 - Cell Development and Qualification

Component drawings have been completed, but are awaiting vendor feedback and final internal review before the package is considered ready for quotation. A cell design review is scheduled for January 1992 to coincide with the selection of the UES application. By that time, it is expected that sufficient assembly experience will have occurred to permit the first build group to be assembled and placed on test.

The cell testing/qualification subtask is divided into design build groups. Initially, BPI will characterize performance (capacity and resistance) with 10-cell populations to verify component designs. Freeze/thaw durability could be the single largest issue regarding the acceptability of the central-sulfur cell design. As such, the cells that remain after performance testing, will be subjected to freeze/thaw testing to explore the conditions that may permit the design to withstand freeze/thaw events. Such testing is scheduled to begin during April 1992 and continue for the duration of the program. Starting in December 1992, the cell test population will increase to permit a statistical cell reliability database to be established.

Safety trials will be performed to establish a statistical basis for safety performance. In particular, cells intended for safety testing will be subjected to a suffi-

ciently high overvoltage to fail the electrolyte catastrophically. The highest temperature, subsequent to the event, will be recorded as a basis for establishing probability of exceeding a specific temperature.

Task 2.3 - Battery Component Development

Battery components being considered for development include the thermal management system, the interconnection and busplate/busbar, and a viable failure device. While the main thrust in cell design is to control temperature rise with "meaningful" thermal mass, it is necessary to include design and development activities associated with a compact cooling scheme that can be integrated into the modular design. Such a component may be necessary based on the power requirements of the application. To this end, BPI is performing specific experiments to identify appropriate heat transfer schemes and define limits of operation and preferred control approaches.

The design for interconnection of cells will be verified via weld trials and mounting experiments to insure minimal stress on the sulfur seal. Due to the larger capacities of UES cells, the cell tab must be thicker to handle higher current levels. A stiffer interconnection is produced yielding the potential for imposing higher stresses on the seal.

The cell mounting scheme is dependent on the specification of the string building block. In the previous UES battery designs, an open-circuit failure device was assumed to exist in series with each cell, permitting self-supporting parallel arrays, or trays, of cells. In this latest modular concept, the design is recognizing the reality that no such reliable, low-cost failure device exists. Instead multi-cell series strings will be the building block for the module, and it will be imperative to design a cell that achieves high Weibull characteristic life and shape factor. The mounting scheme (busplate/busbar design) and interconnect scheme will be important aspects of a successful module design. For this reason, BPI will be attempting to verify the design in specific experiments.

Although a difficult task, the development of a viable failure device to enhance battery overall reliability will also be continued. Ideas that were advanced in the proposal, as well as new concepts that develop over the course of the program, will be prioritized and explored to the extent that prototypes will be fabricated and tested.

Task 3.0 - Design and Fabrication of UES Module

The design and fabrication of a representative UES module is scheduled to begin during the fourth quarter of 1992. This module will utilize XPB cells, 1/3 of which will be assembled by BPI and the remainder supplied by CSPL. Two modules are scheduled for assembly by BPI: one a deliverable to SNL; the other to be tested at BPI.

Task 4.0 - Full-Scale Battery Plant Design

The battery approach that is currently being pursued is based on a modular, self-contained battery that is manufactured and shipped to the site as a stand-alone unit, requiring minimal field work. Inherent in the modular concept is the maintenance strategy that simply dictates replacement of modules using a forklift at ambient-temperature conditions. A 15-MWh plant size, for example, would have to contend with replacement of only 120 such modules over its lifetime. This situation contrasts with a more typical custom battery design in which overhead crane access and costly field labor must be provided. In this way, the design effort is being directed toward one which, in principle, should offer low life-cycle cost (LCC). The diversification offered by the PREPA and San Diego Trolley projects is expected to provide an early assessment of the benefits of an advanced sodium/sulfur battery design for UES applications.

Following selection in Task 1 of an actual UES application, the design of the full-scale battery plant will be initiated. This design will be completed in sufficient detail to allow the development of detailed plant costs. A subcontract to an A&E firm will be pursued to support the balance of plant costing. This task is not scheduled to begin until October 1992.

Technology Evaluation - SNL

One of the last deliverables from the core technology contract with CSPL was received by SNL and placed on test in FY91. This deliverable consisted of 12 PB cells specifically designed for electric vehicle applications. The DOE/OPS funded the evaluation. All of these 10-Ah cells have the MkIII seal design/safety features and are similar to those contained in the ETX-II battery now being tested at Idaho National Engineering Laboratory (INEL).

The 12 cells were divided into groups of three cells each and a different test plan was conducted on each group. The intent of this series of tests was to determine the effects of different cycling regimes on service life. The first group of cells was continuously life-cycled using baseline constant current parameters while the second group of cells was evaluated using a modified driving schedule. The third group of cells was evaluated using a proposed DOE/Electric and Hybrid Propulsion (EHP) general test plan. Two of the remaining untested cells were connected in series and placed on a SFUDS life-cycle test regime. Table 2-1 is a summary of the tests conducted on the 12 cells. The results indicate that the present capacity, for all the cells, exceeds their rated capacity value of 10 Ah.

Figure 2-1 is a plot of cell resistance and capacity vs cycle life for cell #508 and is typical for the rest of the cell population on baseline cycling. Approximately 50 cycles were placed on the cell before the cell resistance reached a minimum value. This decrease was attributed to wetting of the electrolyte. Over the next 450 cycles, the cell resistance increased 5 mohms or ~ 0.011 mohm/cycle. This was consistent with results observed by CSPL and ANL. The increase in cell resistance was attributed to the corrosion of the surface of the container and redistribution of corrosion products. Following cycle 499, a power outage occurred, and all cells experienced a freeze/thaw cycle. Prior to the power outage, all cells were fully charged. When the cells were reheated and placed on test, a sharp increase of from 1-3 mohms in cell resistance was observed. Again, this was probably due to poor wetting of the electrolyte. Since the freeze/thaw, a slight decrease in cell resistance has been measured on all the cells as cycling continued.

The second group of cells (SNL# 509, 510, and 511) was evaluated using a modified driving schedule. This test plan consists of a continuous alternate frequency cycle representing 5-day use of the vehicle followed by a 2-day rest period. A 1-day simulated cycle is represented by a 3-hr rate discharge to 1.9 V followed by a 6-hr rest period. The cells are then charged at the 5-hr rate to 2.4 V followed by a 10-hr rest period. This cycle is repeated 5 times representing the 5 days of usage followed by the 48-hr rest period representing the weekend. These cells have completed a total of 206 commuter cycles. As shown in Table 2-1, the capacity for two of these cells also declined slightly from the value that was initially measured. The end-of-discharge cell resistance for these three cells has increased ~ 6 mohms.

The third group of cells (SNL# 515, 516, and 517) was evaluated using the proposed EHP Testing Task Force test plan. Characterization tests consisting of

Table 2-1. CSPL Cell Test Summary at SNL

| SNL Number | Capacity (Ah) | | Total Number Cycles | No. Cycles 4 th Qtr. | Test Regimes | Cell Resistance (mohms) | |
|---------------|---------------|---------|---------------------------|---------------------------------------|-----------------|----------------------------|---------|
| | Initial | Present | | | | Minimum | Present |
| 506 (PB) | 10.8 | 10.3 | 140 | 140 | 1,5 | 34 | 32 |
| 507 (PB) | 10.4 | 10.2 | 710 | 182 | 1 | 29 | 36 |
| 508 (PB) | 10.6 | 10.4 | 742 | 227 | 1 | 27 | 34 |
| 512 (PB) | 10.5 | 10.5 | 710 | 212 | 1 | 31 | 35 |
| 509 (PB) | 10.6 | 10.2 | 206 | 53 | 2 | 29 | 35 |
| 510 (PB) | 10.6 | 10.6 | 206 | 53 | 2 | 31 | 37 |
| 511 (PB) | 10.5 | 10.3 | 206 | 53 | 2 | 28 | 35 |
| 515 (PB) | 10.5 | 10.4 | 243 | 158 | 3,5 | 30 | 32 |
| 516 (PB) | 10.5 | 10.1 | 289 | 171 | 3,6 | 29 | 34 |
| 517 (PB) | 10.5 | 10.4 | 308 | 232 | 3,6 | 27 | 30 |
| 519 (PB) | 10.6 | 10.6 | 44 | 44 | 4 | 62 | 62 |

Notes:

Cell Initial Capacity: Discharge @ C/3 to 1.9 VOC and Charge @ 2.0 A to 2.4 V
519 = Two-Cell String

Test Regimes

1. Baseline Life Cycles (discharged at 3.3 A to 1.9 V o/c; charged at 2 A to 2.4 V)
2. Modified Driving Schedule
3. EHP Task Force Test Plan
4. Life Cycle SFUDS
5. Parametric Test Matrix
6. Limited DOD (2 hr)

three different discharge rates (C/3, C/2, and C/1) were run on the three cells. Figure 2-2 is a Peukert plot showing the results of these tests. Next, constant power tests were run on the three cells using an encumbered weight of 0.207 kg/cell. This encumbered cell weight was based on the projected 600 kg weight of the ETX-II battery. A Ragone plot of the resultant data is shown in Figure 2-3. The specific energy behavior of the three cells at specific power levels of 25, 40, and 55 W/kg was similar. At the end of this parametric testing, SFUDS cycling was performed.

The range of these cells in average equivalent miles was 160. These results were slightly higher than the 148-mile range ANL reported for the 120-cell CSPL sodium/sulfur module. The difference can be explained by the fact that SNL based the burden weight of a single cell on the projected weight of the advanced ETX-II battery (600 kg) while the burden of the 120-cell module

was based on an existing CSPL battery, the 700-kg Griffon battery being tested at Electrotek Concepts.

Figure 2-4 is a plot of specific peak power vs depth-of-discharge for cell #515. These results were similar to the results obtained on two other cells. Again, an encumbered weight of 0.207 kg was used and the tests were performed at five different depth-of-discharge values (0%, 5%, 20%, 50%, and 80%). At full state-of-charge, the cell resistance was high, and thus the specific peak power was only around 73 W/kg. The maximum specific peak power achieved on this cell was approximately 137 W/kg with the cell being discharged to 2/3 of the open-circuit voltage.

Another cell (SNL #506) exhibited a high resistance problem during its break-in cycles. Continued cycling brought the cell resistance down to a near-normal value of 34 mohms. The cell was then subjected to baseline cycling at four different temperatures to determine the effect of temperature on electrical performance. Initial-

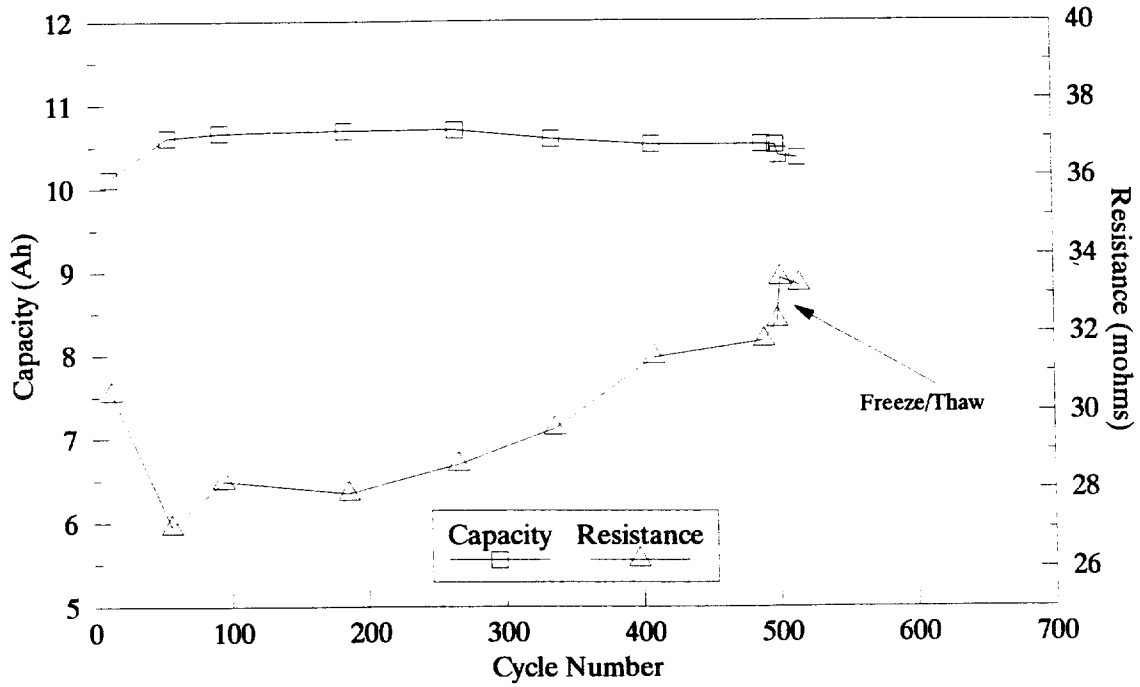


Figure 2-1. Baseline Life-Cycle Test, CSPL Cell #508, Capacity and Resistance

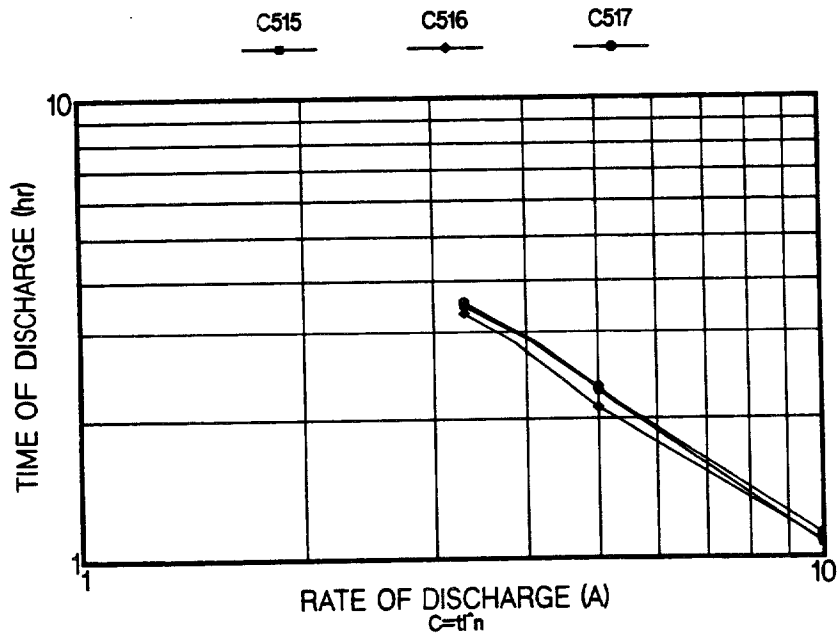


Figure 2-2. Peukert Plot for Sodium/Sulfur Cells 515, 516, and 517

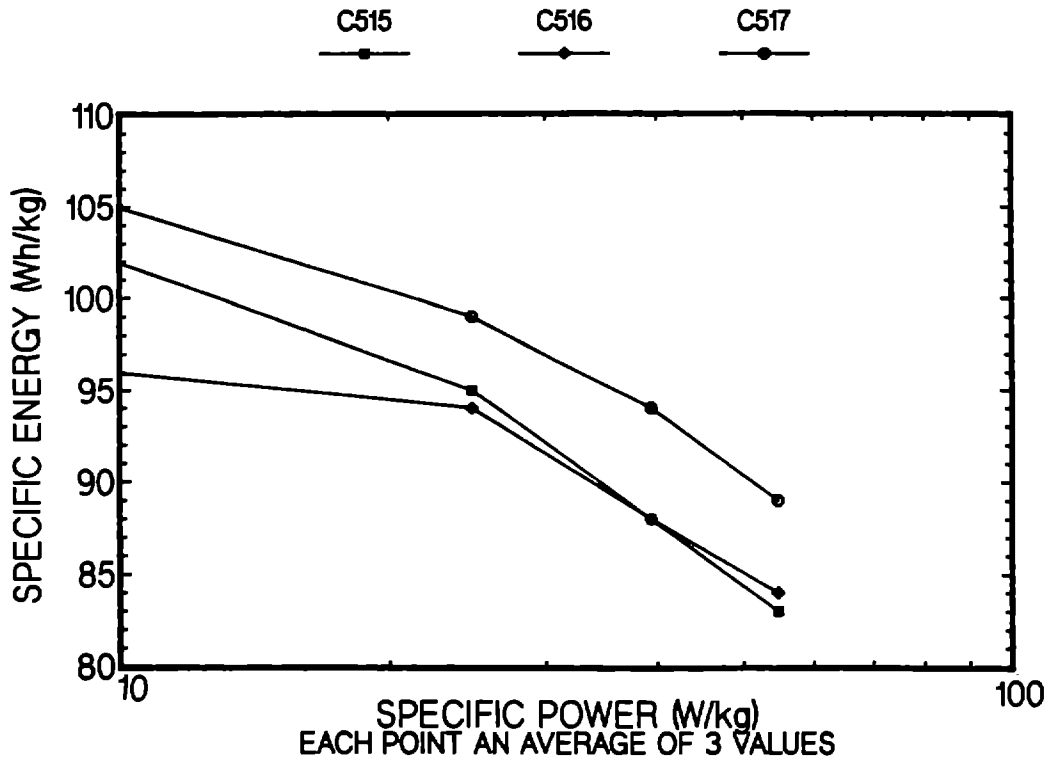


Figure 2-3. Ragone Plot for CSPL Sodium/Sulfur Cells 515, 516, and 517 (results based on an encumbered cell weight of 0.207 kg)

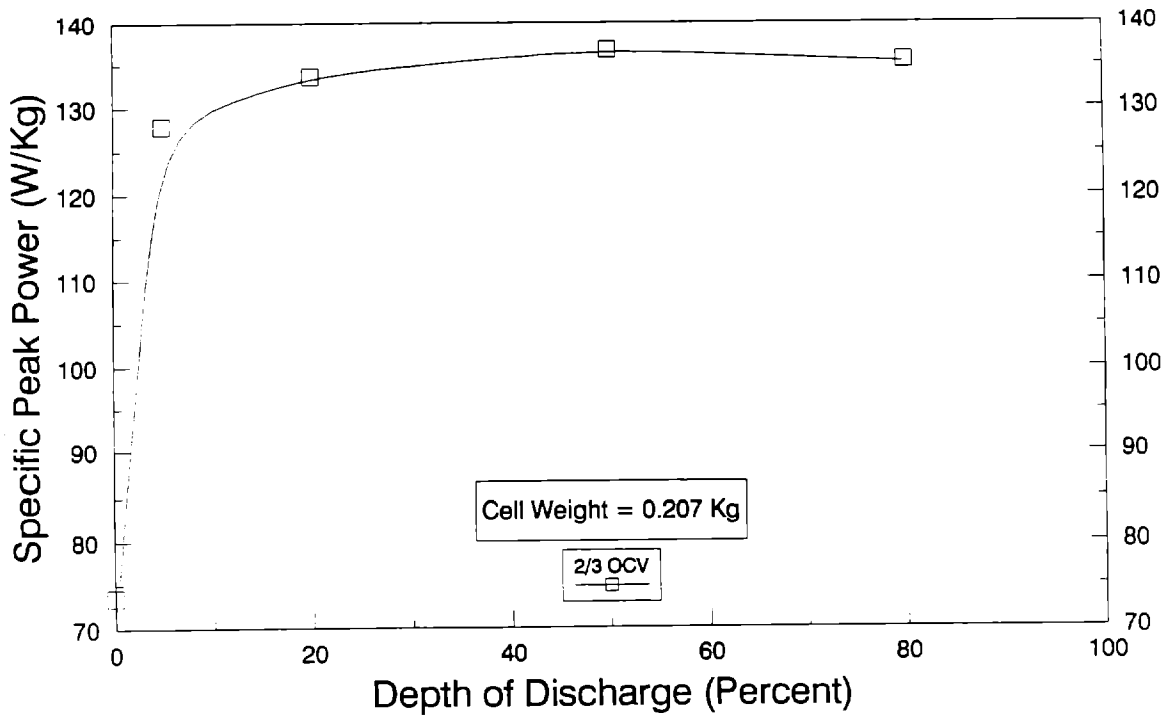


Figure 2-4. Peak Power, CSPL Cell #515

ly, changes in capacity, cell resistance, and cell polarization were measured. CSPL previously found that the ratio of cell resistance during charge to discharge at ~20% depth-of-discharge is a good indicator of cell polarization. For a properly functioning cell, CSPL found empirically that this quotient should be lower than 1.2. Results are shown in Figures 2-5 and 2-6. These results demonstrated that the end-of-discharge resistance and polarization measure have little effect on capacity using the baseline C/3 discharge and C/5 charge rates. Although increased polarization is occurring during charging at 310°C (Figure 2-6), the effect on capacity is minimal, probably because mass transport rates are not significantly affected. The expectation is then that a higher charge rate than was used in this study would negatively impact capacity. This has potential implications on low-temperature regenerative braking and/or charging.

In July 1991, a life-cycle SFUDS test regime was initiated on a 2-cell string (SNL #519). A total of 12 SFUDS tests has been completed. A burdened weight of 0.414 kg was used again, based on the projected 600 kg weight of the ETX-II's battery. The range of these cells in average equivalent miles varied between 141 and 163.

These power profile test results apply to UES applications. Certain utility applications (such as frequency regulations and system stability) require pulsed power discharges similar to those of EV batteries.

Technology Evaluation - ANL

Life-testing of the 120-cell (PB) sodium/sulfur module from CSPL continued at ANL with SFUDS discharges to 100% DOD. As noted previously, battery burden was based on the 28-module CSPL Griffon battery that weighs 700 kg. The module has completed 696 cycles and retains ~85% of its initial 292-Ah, 3-hr rate capacity. The specific energy obtained with SFUDS discharges continues to hold at ~80% of its initial 71.5 Wh/kg. Hence, the module has been operating at a performance level near the end-of-life level. Module resistance vs life data show that the end-of-discharge resistance has increased from 5.4 mohms on cycle 31 to about 6.9 mohms on cycle 605. The total Ah capacity loss with life indicates that four 4-cell strings are no longer operational (40-Ah loss).

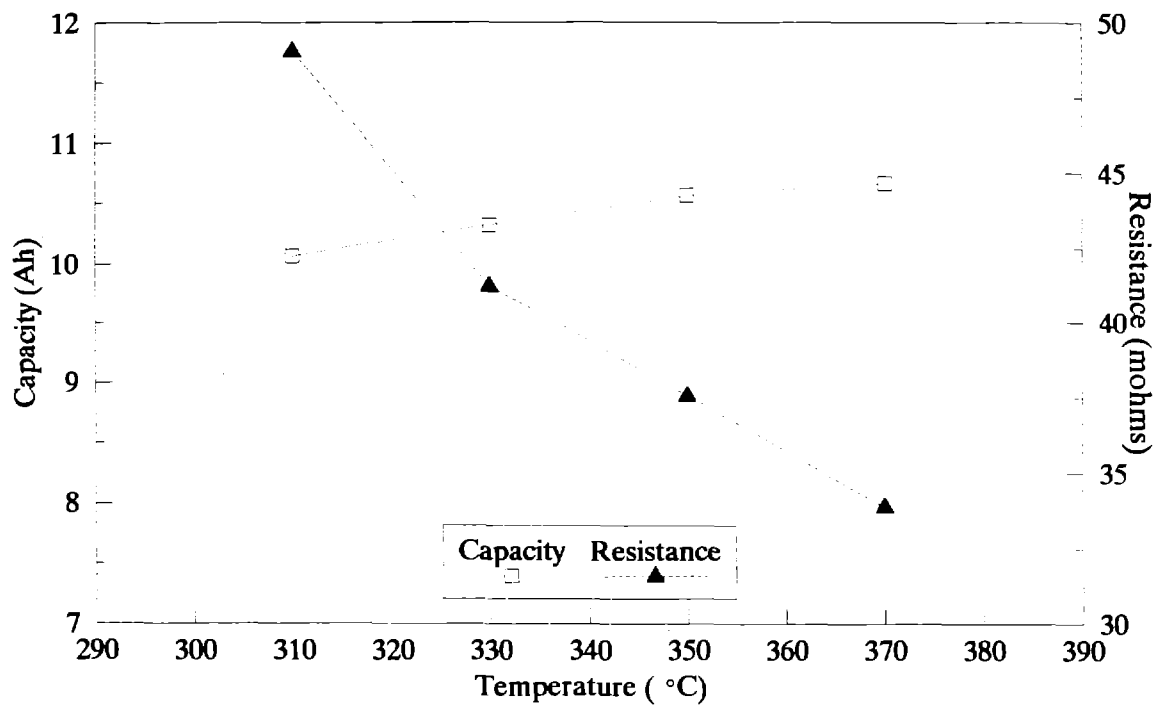


Figure 2-5. Average Capacity and End-of-Discharge Resistance at Different Temperatures, CSPL Cell #506

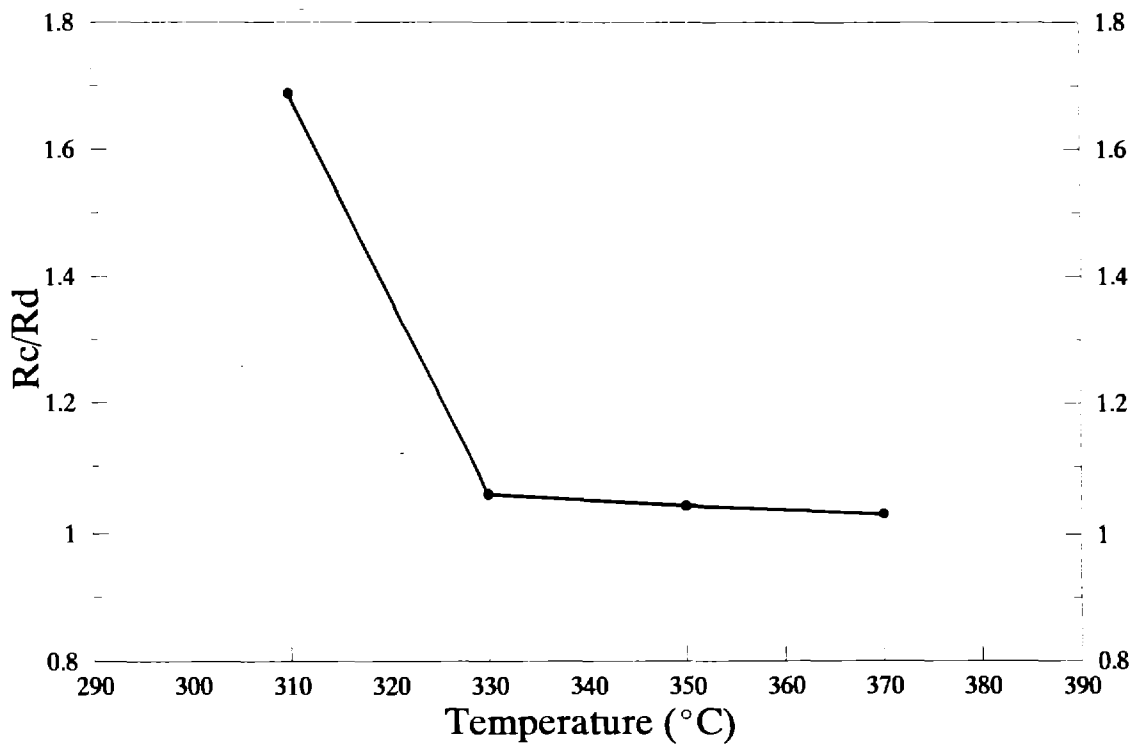


Figure 2-6. Rc/Rd at Different Temperatures, CSPL Cell #506

3. Zinc/Bromine Project

Zinc/bromine batteries are attractive candidates for utility applications because they offer 2-3 times the specific energy of lead-acid batteries, have sufficient power, operate near room temperature, are capable of being recycled, can be built at low cost, and have potentially long lifetimes. A 39-mo cost-shared contract with Johnson Controls Battery Group, Inc., was initiated in August 1990 with the objective of extending the JCBGI technology from an electric vehicle design to utility applications. This effort is organized into two 18-mo technical phases followed by a 3-mo reporting period. Satisfactory technical progress is required during Phase 1 prior to initiating Phase 2. The objectives of this program are to design, fabricate, evaluate, and optimize a zinc/bromine battery system suitable for utility applications. As well as technical direction of the contract, SNL conducts technology evaluation of contract deliverables and applied research. Accomplishments in FY91 in each of these areas are reported separately in the following sections.

Technology Development - JCBGI

JCBGI is currently working on Phase 1 of the technical effort. The major activities of Phase 1 center on developing a full-size prototype cell with an area of 1170 cm². Larger areas may be needed to optimize performance in these utility applications, but they will not be built until Phase 2.

Validation tests of both 8- and 50-cell configurations are currently under way. In addition, design activities have begun to scale up these cells to an optimized size.

Phase 1 of the program has met several criteria proposed by SNL to demonstrate the soundness of the technology. These criteria are:

1. Demonstrate leak-free battery stacks.
2. Demonstrate steady long-term operation by achieving over 100 cycles with <10% drop in energy efficiency.
3. Achieve energy efficiencies of ~75%.
4. Demonstrate adequate performance with six consecutive, no-strip cycles.

5. Verify battery cost of \$150/kWh or less.
6. Address safety issues associated with the battery.

Details will follow on how most of these criteria have been met, as well as on further work which has been done on improving the battery materials, the assembly processes, and the ability to recycle the batteries.

The goal of Phase 1 of the contract is to develop zinc/bromine battery technology to the point that significant progress has been made to show it is suitable for utility applications. This goal can be broken down into several separate tasks as shown in Figure 3-1, the project schedule.

The core research program is on schedule. The modeling and spreadsheet work is essentially done and can be used to size battery parts and predict performance. Work on electrodes, separators, and bromine electrode activation layers is ongoing. Success in these programs will mean improved battery performance or lower cost. Laboratory battery testing is confirming the advantages of recent changes to the welding process, and new information is being collected on cycle life, stand loss, no-strip cycles, temperature effects, zinc loading, etc. Miniature cells have been developed to facilitate investigations into zinc plating, flow rates, etc. New flow frame models are being written. A transparent flow-test fixture has been used to video-tape single-phase and two-phase electrolyte movement, to verify the improved electrolyte flow uniformity resulting from a redesigned flow frame.

An 8-cell state-of-the-art (SOA) battery station was delivered to SNL at the beginning of the project. Work is now under way on a twin 50-cell stack improved state of the art (ISOA) station to be delivered by the end of December 1991. This new battery will include most of the technology improvements made so far, and will demonstrate the capabilities of zinc/bromine batteries for utility operation.

Laboratory Battery Testing

Battery Stack Integrity

Of the battery stacks built early in the program, from the beginning of the program in August of 1990

through February of 1991, several failed when electrolyte began to leak from the stacks. One developed dendrites, and another was assembled with experimental electrode material that had unwanted porosity. To increase the reliability of the battery stack welding process, it was first necessary to identify all possible causes of battery stack failure. Based on previous experience with zinc/bromine technology, the failures of the battery stacks built during this period could be attributed to the following causes:

1. **Faulty Builds**—Problems traceable to less than optimum assembly, such as insufficient welds, parts not in full contact, and foreign objects or oil in the weld area. The problem was often detected before or during the initial pressure and flow checks. These problems tended to be one-of-a-kind because immediate corrective action usually was effective.
2. **Stack Leaks**—After a number of otherwise normal cycles, the stack would split open at a weld and leak electrolyte. Most of these weld failures were design related, the result of insufficient weld surface or improper positioning. Some of the leaks were also the result of an imperfect vibration-welding process or slightly defective parts.
3. **Electrolyte Crossflow**—The battery efficiency suffers if the rate of electrolyte crossflow across the separators increases. Normally, a small amount of electrolyte will transfer due to pressure-gradient-driven diffusion. Abnormally high crossflow usually indicates a separator-to-frame weld failure, but could also result from dendrite penetration or long-term degradation of the separator.
4. **Rapid Performance Decline**—This usually has taken place after a number of cycles at normal energy efficiency. The causes can include dendrites, dendrite holes, cell reversal, poor electrolyte flow within a cell, or poor electrolyte distribution between cells. The predominant underlying cause is likely to be electrode warpage.

After the first few months of the program, it became clear that nearly all of the stack failures to that time could be traced to an initial failure of a specific weld in the stack. Steps were taken to increase the strength of this weld, including doubling the effective weld bead in areas subject to high stress and modifying the welding tooling to ensure complete weld uniformity.

Two assembly techniques were developed to guard against the formation of zinc dendrites at the edges of electrodes. Dendrites may result if the active bromine electrode area on one side of a bipolar electrode is larger than the active zinc electrode area on the other side of

the same electrode. Both new assembly techniques ensure that the active cathode area is slightly smaller than the active anode area in order to prevent current density from concentrating at the edges of the zinc anodes. The first technique removed a small zone of the activation layer around the edges of the cathode. The second method involved reversing the direction that the electrode insert was welded into the frame so that the electrode-to-frame weld automatically covered part of the edge of the cathode activation layer. Later, after several stacks were built, electrode-to-frame welds proved to be weak unless the cathode activation layer was removed in the weld area.

As of this writing, eleven 8-cell stacks have been made with the latest vibration-welding process. A summary of the changes made to the parts throughout the first part of the contract is shown in Table 3-1. None of the stacks with the recent weld-improvement modifications has failed due to electrolyte leaking from the stack. Two or possibly three have failed due to the loss of an internal electrode-to-frame weld. One other stack has operated poorly because the experimental separator used allowed high bromine transport.

Cycle Life and Performance

Laboratory batteries are not immediately used for life-cycle testing. Rather, they are typically used in various tests and exposed to operating conditions which, along with a high number of cycles, have induced cell stack failure in the past. After a battery has achieved between 100 and 200 cycles, it is tested primarily for cycle life.

Currently, four 8-cell batteries have exceeded 100 cycles. Their voltaic and consequently energy efficiencies exhibit some decline, but not more than 6%. The coulombic efficiencies of these batteries have shown virtually no decline thus far. Peak energy performance has been in the range of 75% efficiency. These battery stacks were manufactured using the improved techniques that have corrected the problems of internal and external leakage, dendrite shorting along the edges of the electrode, and blocked flow channels.

The cycle-life results are given in terms of three efficiencies: coulombic (CE), voltaic (VE), and energy (EE). The CE is the ratio of amp-hr discharged to the amp-hr charged. The EE is the ratio of watt-hr discharge to the watt-hr charged. The VE is found by dividing the EE by the CE. It is average discharge voltage divided by average charge voltage.

Battery V1-53 was placed on test March 25, 1991. Initial testing started at baseline and then proceeded to a no-strip cycle study. Baseline testing has been resumed.

Table 3-1. Modifications to V-Design Stacks

| Stack | Start Test Date | Double Weld Beads: | | | Filled EB** | Improved | Edge Treatment | |
|--|-----------------|--------------------|---------|---------|-------------|-------------------|----------------|----------|
| | | Anode Te* | Bipolar | Cath Te | | Surface Treatment | Edged | Reversed |
| V1-38 | 8/7/90 | ✓ | | | | | | |
| V1-39 | 9/6/90 | ✓ | | | | | | |
| V1-40 | 9/17/90 | ✓ | | | | | | |
| V1-41 | 10/5/90 | ✓ | | | | | | |
| V1-42 | 12/14/90 | ✓ | | | | | | |
| V1-43 | 12/20/90 | ✓ | | | | | | |
| V1-44 | 1/4/91 | ✓ | | | | | ✓ | |
| V1-45 | 1/14/91 | ✓ | | | | | ✓ | |
| Upper Tooling on Vibration Welder Modified | | | | | | | | |
| V1-46 | 2/5/91 | ✓ | | | | | ✓ | |
| V1-47 | 2/13/91 | ✓ | ✓ | ✓ | | | ✓ | |
| V1-48 | 3/1/91 | ✓ | ✓ | | | | | ✓ |
| V1-49 | 3/4/91 | ✓ | ✓ | ✓ | ✓ | | ✓ | |
| V1-50 | 3/7/91 | ✓ | | | ✓ | | ✓ | |
| V1-51 | 3/18/91 | ✓ | ✓ | ✓ | ✓ | | | ✓ |
| V1-52 | 3/20/91 | ✓ | ✓ | ✓ | ✓ | | | ✓ |
| V1-53 | 3/21/91 | ✓ | ✓ | ✓ | ✓ | | | ✓ |
| V1-54 | 4/2/91 | ✓ | ✓ | ✓ | ✓ | | | ✓ |
| V1-55 | 4/2/91 | ✓ | ✓ | ✓ | ✓ | | | ✓ |
| V1-56 | 4/4/91 | ✓ | ✓ | ✓ | ✓ | | | ✓ |
| V1-57 | 4/22/91 | ✓ | ✓ | ✓ | ✓ | | | ✓ |
| V1-58 | 6/4/91 | ✓ | ✓ | ✓ | ✓ | | | ✓ |
| V1-59 | 8/16/91 | ✓ | ✓ | ✓ | ✓ | ✓ | | ✓ |
| V1-60 | 8/16/91 | ✓ | ✓ | ✓ | ✓ | ✓ | | ✓ |

* Terminal Electrode

** End Block

At 289 cycles, V1-53 performs at 96% of its peak energy efficiency as shown in Figure 3-2.

Stack V1-55 has cycled continuously at baseline for 4 mo. At 192 cycles, it is operating at energy efficiencies only 2-3% below its peak performance. The efficiencies vs cycle number are shown in Figure 3-3.

At 118 cycles, V1-54 has exhibited only a minimal decline in efficiency as shown in Figure 3-4, the base-

line efficiency measurements through the current cycle. A zinc loading study on this battery is in progress.

The SNL deliverable battery V1-57(SNL #518) has completed 152 cycles. It is also leak-free with less than 10% degradation in the energy efficiency.

No-Strip Cycling

Typically, laboratory batteries are stripped at the end of a discharge by shorting for an extended period.

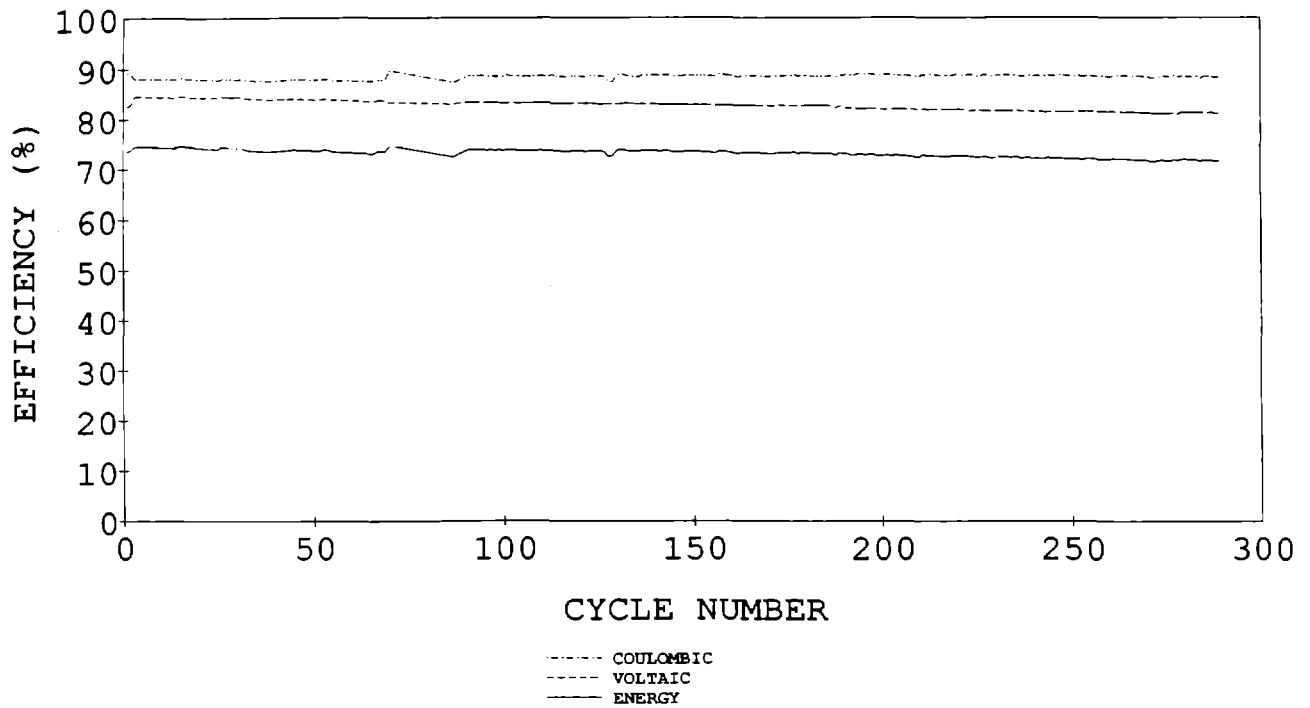


Figure 3-2. Baseline Cycles, V1-53

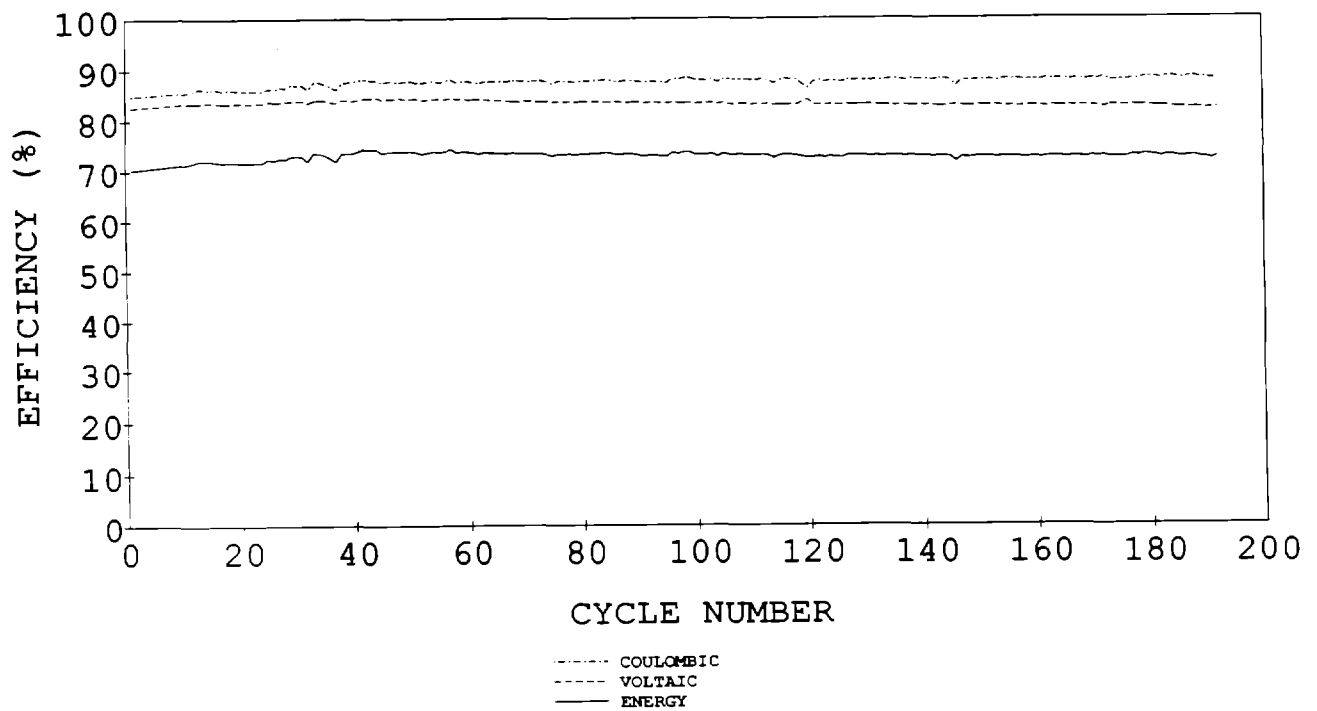


Figure 3-3. Baseline Cycles, V1-55

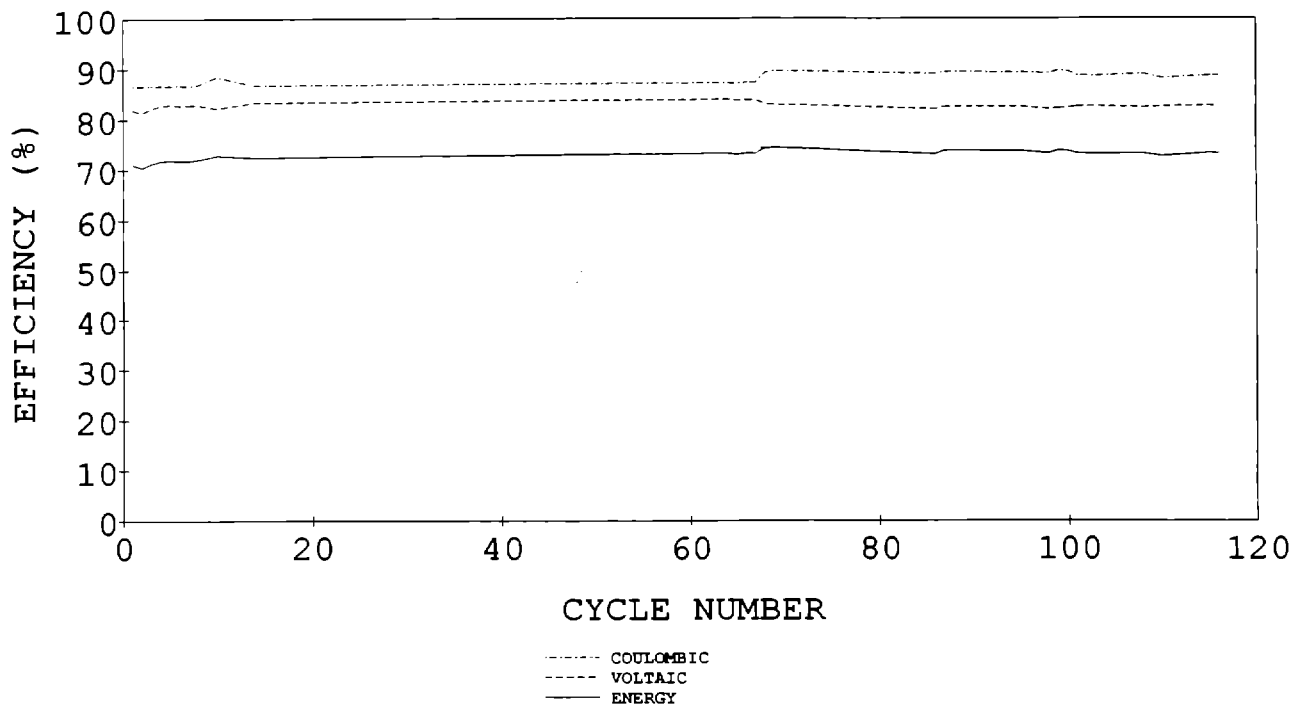


Figure 3-4. Baseline Cycles, V1-54

Stripping insures that zinc is deposited on a fresh surface, rather than on top of what could possibly be uneven zinc deposits remaining from previous cycles. It also simplifies the accounting procedure involved in monitoring a zinc/bromine battery's true state-of-charge. Although it is a simple and convenient procedure for laboratory batteries in commercial applications, stripping will not necessarily be done on every cycle. For example, a utility battery may be required to operate for at least six cycles without stripping because an electric utility would be able to fully strip the batteries only during a weekend. These considerations have prompted investigations of multiple charge/discharge cycling without stripping.

Efficiency actually increases when a zinc/bromine battery is operated without stripping the last remaining zinc from the electrode after the battery has discharged. The average CE of no-strip cycles is initially higher because a portion of the amp-hr normally lost to stripping is retained in the battery. After a number of cycles, however, the CE may decline to less than that of the baseline cycles as shown in Figure 3-5. For batteries built prior to V1-59, this decline occurs after three or four no-strip cycles. Battery V1-59 and later batteries were built with improved electrolyte flow diverters, and

the CE decline is less and occurs after more cycles. Within a set of no-strip cycles, this efficiency loss takes the appearance of decreasing capacity. Each cycle discharges fewer watt-hr than the previous cycle. A summary of the efficiency values for all of the no-strip tests is given in Table 3-2.

In Table 3-2, the three efficiencies are calculated as before, except they are an average taken over the whole set of cycles. The transport inefficiency is the percent of the total amp-hr charge that is lost to bromine transport. The residual inefficiency is the percent of the amp-hr charged that remain in the battery after the discharge is terminated at the cut-off voltage, which is 1 V/cell. The values of the CE, and the two inefficiencies sum to 100%.

The progressive decrease in efficiency results from an accumulation of zinc on the anodes. This is clearly apparent from the amp-hr value of the final strip cycle immediately following each set of no-strip cycles. All the zinc that accumulated during the no-strip cycles is removed during this cycle. As the number of no-strip cycles in a set increases, there is a progressive rise in residual amp-hr for the final cycle that does include full strip, as shown in Figure 3-6.

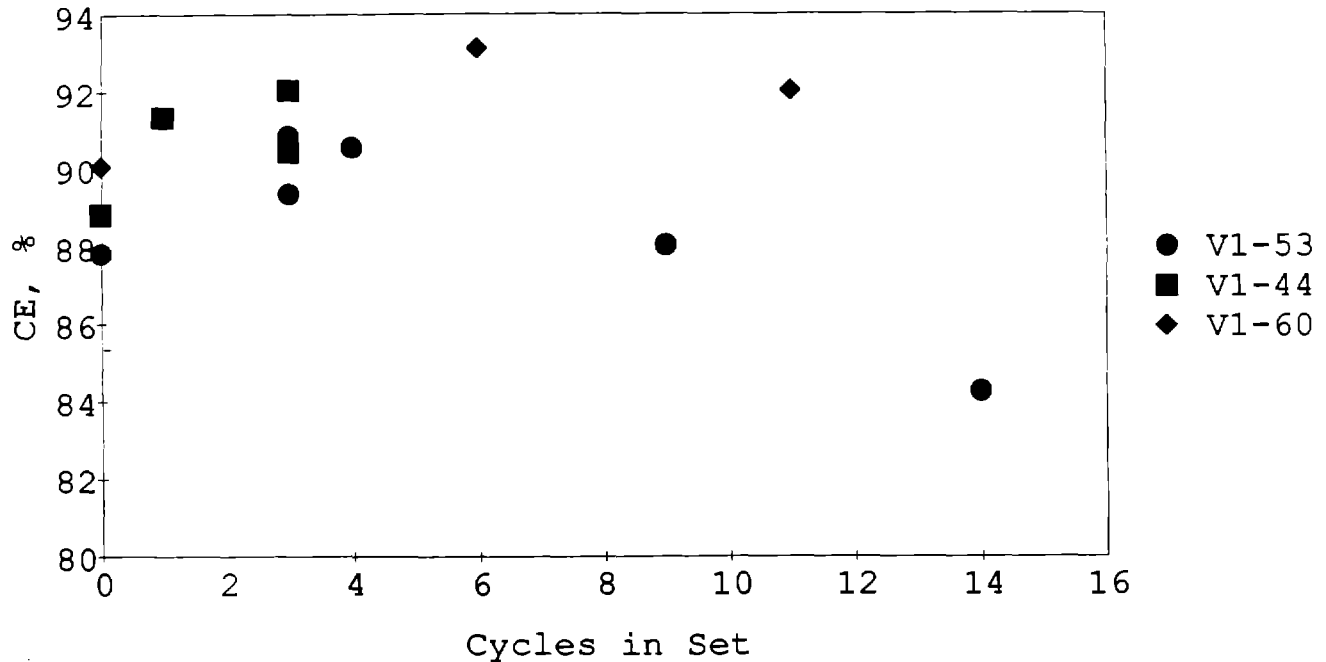


Figure 3-5. No-Strip Cycle Sets (Average Coulometric Efficiency for Each Set)

The zinc accumulation is most likely occurring in zones of lower activity on the anodes. From observations made in teardowns, these zones are located in the corners away from the flow entry points and along the center rib. The improved performance of V1-60 is undoubtedly the result of more uniform electrolyte flow distribution. Warps in the electrode material can also create low activity zones where the electrolyte gap is very thin, so improvements in electrode materials will also lead to improved no-strip performance.

Stand Tests

In utility service, there is a period of time in the duty cycle during which the battery must stand fully charged, waiting to be discharged. There will be some energy loss during this time due to self-discharge. As of now, there is no standard utility duty cycle to use for testing. It is very likely that the utility battery will experience a stand period lasting for 2-4 hr after the charge period.

A study of energy lost during stand was done in two parts. In the first part of the study, tests for the optimum standing conditions were performed. Battery V1-44 was tested by adding stand periods of various durations directly after the end of charge. In some cases, the second phase valve was open, and other times it was closed; also, the electrolyte was sometimes continu-

ously pumped, and other times it was pumped only periodically. Some pumping is needed to remove self-discharge heat from the stack. In the second part of the study, the tests were continued to higher number of cycles to determine if there was a limiting energy loss.

As shown in Table 3-3, the energy efficiency drop was hardly noticeable in first half hour of stand. By the second hour of stand, the EE drop is 0.8%. The minimum loss occurred when the second phase valve was closed, and the electrolyte circulated only periodically as was done in cycles 45 and 46. In later tests, this became the standard procedure. At cycle 90, the baseline cycle was repeated with little change from the cycle 36 baseline.

The coulombic efficiency decreased slightly during both the 1-hr and 2-hr stands as expected. However, during the 1-hr stand test, residual inefficiency, not transport inefficiency, increased. This may be attributed to an unevenness in the plating that developed during the stand due to preferential bromine attack at the bottom of the zinc electrode. During the 2-hr stand tests, the transport was slightly higher as well.

The most significant evaluation of the stand loss of a battery system is determining the amount of energy lost and the rate at which it is lost. The results from the tests of battery V1-44 have been evaluated in terms of

**Table 3-2. Results of No-Strip Cycles
Averages for Sets of Cycles**

| | CE (%) | VE (%) | EE (%) | T (%) | R (%) |
|--------------------------|-----------|-----------|-----------|----------|----------|
| V1-44 | | | | | |
| Baseline (#2,5,10) | 88.9 | 82.9 | 73.7 | 6.1 | 5.0 |
| One cycle (#3) | 91.4 | 83.0 | 75.9 | 5.9 | 2.7 |
| Three cycles (#6-8) | 90.5 | 82.8 | 74.9 | 6.6 | 1.9 |
| Three cycles (#12-14) | 92.1 | 82.7 | 76.2 | 5.4 | 2.4 |
| V1-53 | | | | | |
| Baseline (#28-31) | 87.9 | 84.4 | 74.2 | 7.6 | 4.4 |
| Baseline (#51-55) | 87.8 | 83.9 | 73.7 | 7.5 | 4.7 |
| Three cycles (#21-24) | 90.6 | 84.6 | 76.7 | 7.1 | 2.4 |
| Three cycles (#47-50) | 90.9 | 84.0 | 76.4 | 5.8 | 3.3 |
| Four cycles (#15-19) | 90.6 | 84.6 | 76.7 | 7.1 | 2.4 |
| Nine cycles (#56-65) | 88.1 | 85.2 | 75.0 | 8.9 | 3.0 |
| Fourteen cycles (#72-86) | 84.3 | 83.0 | 69.9 | 12.5 | 3.1 |
| V1-60 | | | | | |
| Baseline (#11-14) | 90.1 | 85.9 | 77.4 | 5.9 | 4.0 |
| Six cycles (#15-21) | 93.2 | 85.6 | 79.8 | 5.1 | 1.7 |
| Eleven cycles (#43-54) | 92.1 | 85.5 | 78.7 | 5.8 | 2.2 |

CE = Coulombic Efficiency
VE = Voltaic Efficiency
EE = Energy Efficiency
T = Transport Inefficiency
R = Residual Inefficiency

the watt-hr capacity lost as compared to a baseline discharge. In this test, the battery is held for a predetermined time at full charge. The second phase valve is closed, and the electrolyte is circulated periodically. The results indicate a roughly linear 1%/hr loss in capacity as shown in Figure 3-7. At some point, the capacity loss must level out to a constant value, since most of the bromine in the stack will have been exhausted. This test series will be continued to find when the capacity loss decreases, and at what total loss that occurs.

Two special tests were performed to see if the energy lost on stand could be limited. If the stand period was followed by a discharge, the amount of bromine in the stack would be taken to nearly zero and the following diffusion loss would also be lower. Two special tests were done to check this concept. In the first

test, the battery was discharged at decreasing current so that almost all of the second phase in the stack was consumed. The battery then stood for 15.5 hr before it was discharged. As can be seen in Figure 3-8, the amp-hr loss was only about 1% above that of a baseline discharge. However, the energy in the first discharge period was removed at a low voltage (average = 3.7 V) so that few watt-hr were recovered. That is why the energy loss shown in Figure 3-7 appears high.

In the second special test, the battery was discharged at the full C/3 rate until the voltage fell to the normal cut-off value (average = 12.8 V). However, so few amp-hr were taken out that the amp-hr lost to diffusion during the shutdown remained high, as seen in Figure 3-1 at 20 hr of stand. The energy lost shown in Figure 3-8 was close to what would be predicted from an

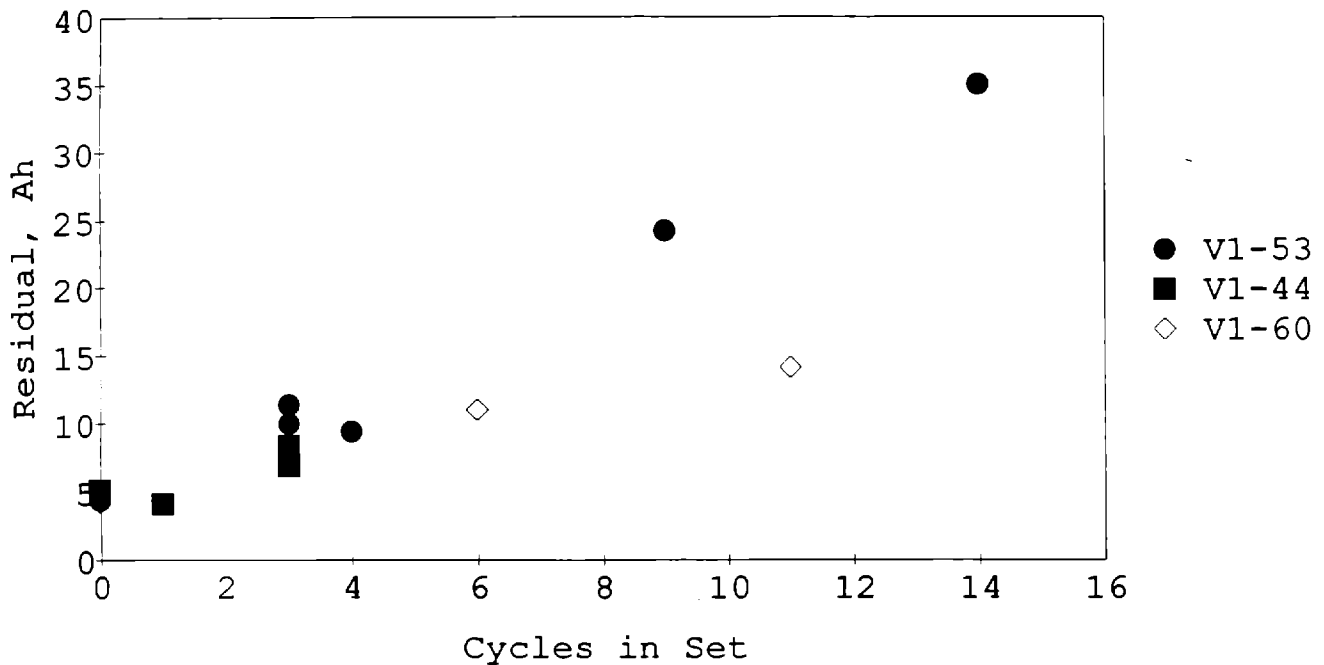


Figure 3-6. No-Strip Cycles Sets (Residual Ah on Last Cycle of Set)

extrapolation of the results of the standard shutdown tests.

There should be a natural limit to the amount of standloss that can be expected because once the bromine in the stack has been consumed, all reactions stop. Testing will be continued to find this level of standloss.

Self-Discharge Current Equivalent to Bromine Transport

One of the questions that came up at the August 1991 quarterly review was, "What is the relationship of the bromine transport measurement for separators to the observed rate of self-discharge in batteries?" The answer is straightforward to calculate, as follows:

3.4×10^{-9} mol Br₂/cm²-sec, measured for SF-600 in LL electrolyte

$\times (1175 \text{ cm}^2)(3600 \text{ sec/hr})(2 \text{ equiv./mol Br}_2)(26.8 \text{ Ah/equiv.}) = 0.77 \text{ A.}$

Thus, 0.77 amp is the equivalent self-discharge current resulting from bromine diffusion across the separator. This measurement can be viewed as a somewhat high estimate of self-discharge, since it uses a bromine concentration gradient corresponding to the worst-case

battery condition (100% state-of-charge). Also note that the bromine flux value of 3.4×10^{-9} mol/cm²-sec for Asahi varies somewhat, and has at other times been as high as about 4.0 under these conditions.

Agreement with JCBGI's spreadsheet calculation, derived from "transport losses" calculated from lab battery tests, is fairly good. This number is 0.883 A.

Zinc Loading

A study is now in progress to establish the zinc loading limitations and to evaluate the effect of zinc loading on the performance of the zinc/bromine battery using standard load-leveling electrolyte (2.25 M ZnBr₂, 0.5 M ZnCl₂, 0.8 M MEPBr). All the trials are constant-current cycles run at baseline current density, zinc bromide utilization (80%), and temperature (30°C).

The zinc loading study began at 45 mAh/cm² and has progressed in increments of 5 mAh/cm² to a loading of 125 mAh/cm² (the standard loading in a baseline cycle is 90 mAh/cm²). The results have indicated that there is virtually no change in the coulombic, voltaic, and energy efficiencies up to a loading of 115 mAh/cm². The results achieved to date with battery V1-54 are shown in Figure 3-9. Since the cycle life of V1-54 is

**Table 3-3. Standloss Results
V1-44 - 100% SOC (Per = Periodic)**

| | Pumps/2 nd Phase | CE (%) | VE (%) | EE (%) | T (%) | R (%) |
|-------------------------|-----------------------------|--------|--------|--------|-------|-------|
| Baseline | | | | | | |
| Cycle 36 | No Stand | 87.4 | 82.3 | 71.9 | 8.6 | 4.1 |
| Half-Hour Stand | | | | | | |
| Cycle 61 | On/Open | 87.2 | 82.4 | 71.8 | 8.4 | 4.5 |
| Cycle 62 | Off/Closed | 87.2 | 82.3 | 71.7 | 8.5 | 4.3 |
| One-Hour Stand | | | | | | |
| Cycle 37 | Per/Closed | 86.3 | 82.4 | 71.1 | 8.7 | 5.1 |
| Cycle 38 | Off/Closed | 85.3 | 82.0 | 69.9 | 8.1 | 6.6 |
| Cycle 39 | On/Open | 86.3 | 82.6 | 71.3 | 8.6 | 5.2 |
| Two-Hour Stand | | | | | | |
| Cycle 44 | On/Closed | 84.9 | 82.7 | 70.3 | 10.0 | 5.1 |
| Cycle 45 | Per/Closed | 86.5 | 82.2 | 71.1 | 9.3 | 4.1 |
| Cycle 46 | Per/Closed | 86.2 | 82.4 | 71.0 | 8.7 | 5.2 |
| Four-Hour Stand | | | | | | |
| Cycle 50 | Per/Closed | 85.4 | 82.2 | 70.2 | 10.1 | 4.5 |
| Cycle 51 | On/Closed | 82.5 | 82.1 | 67.8 | 12.0 | 5.6 |
| Six-Hour Stand | | | | | | |
| Cycle 53 | Per/Closed | 83.1 | 82.1 | 68.2 | 11.3 | 5.6 |
| Cycle 54 | On/Open | 79.9 | 81.9 | 65.4 | 13.0 | 7.2 |
| Cycle 58 | On/Closed | 80.5 | 81.8 | 65.9 | 13.2 | 6.3 |
| Baseline | | | | | | |
| Cycle 90 | No Stand | 87.7 | 81.4 | 71.4 | 6.2 | 6.1 |
| Six-Hour Stand | | | | | | |
| Cycle 93 | Per/Closed | 85.0 | 81.1 | 68.9 | 9.7 | 5.3 |
| Eight-Hour Stand | | | | | | |
| Cycle 95 | Per/Closed | 83.2 | 80.8 | 67.3 | 10.9 | 5.9 |
| Cycle 97 | Per/Closed | 84.2 | 80.7 | 68.0 | 9.9 | 5.9 |

now 118, the performance has declined slightly; the baseline performance is at 98.4% of the peak energy efficiency. This experiment will continue until some significant deterioration in performance is seen.

Temperature Effect

Battery operation has been studied in the range of 21°C to 45°C in order to establish the temperature range

in which performance is optimized with load-leveling electrolyte. The test was conducted at constant temperature to within 1°C.

Results, shown in Figure 3-10, indicate that the energy efficiency is greatest at 30°C and decreases by 3% at 45°C. The temperature effect operates through two factors: electrolyte resistance and bromine diffusion rate. Elevating the operating temperature lowers

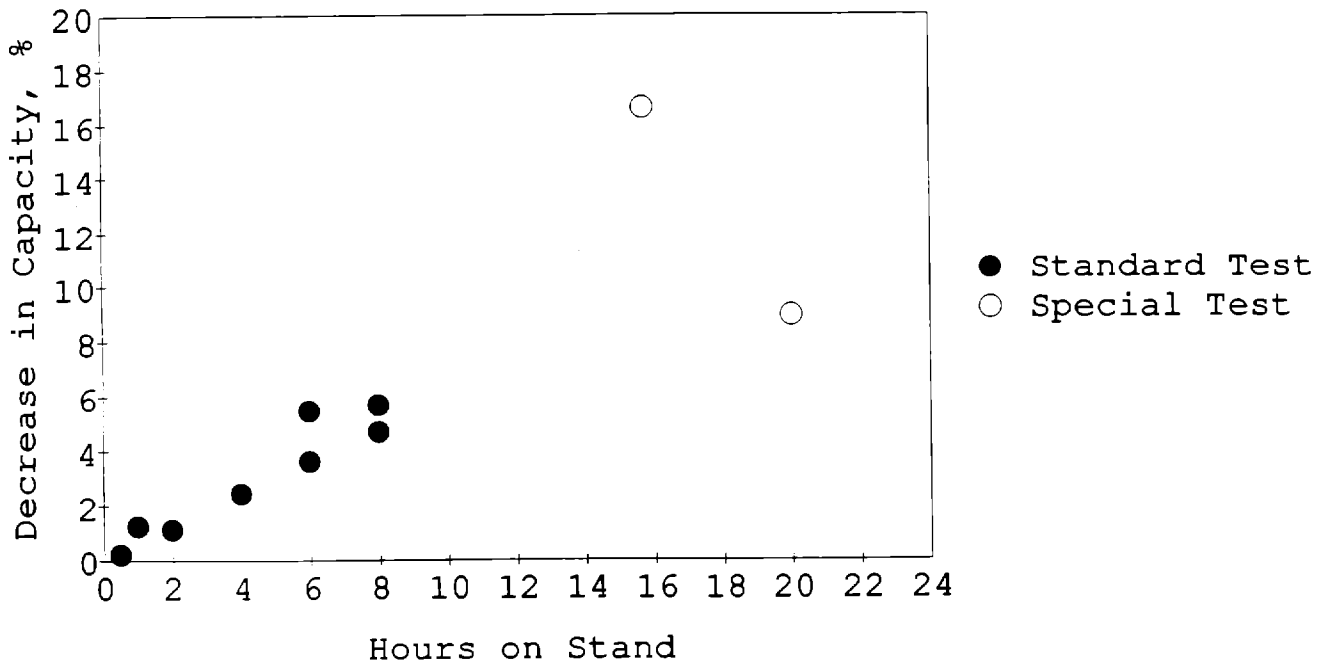


Figure 3-7. V1-44: Standloss at Full Charge (Wh Loss Compared to Baseline Cycles)

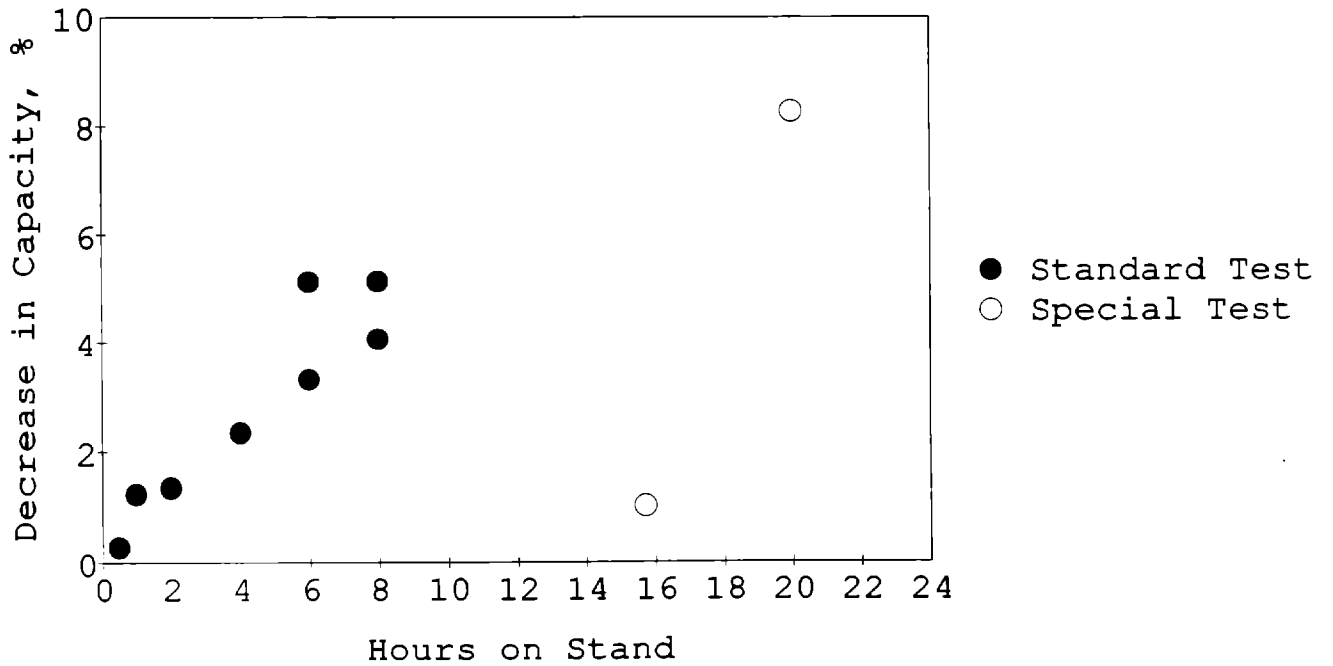


Figure 3-8. Standloss at Full Charge (Ah Loss Compared to Baseline Cycles)

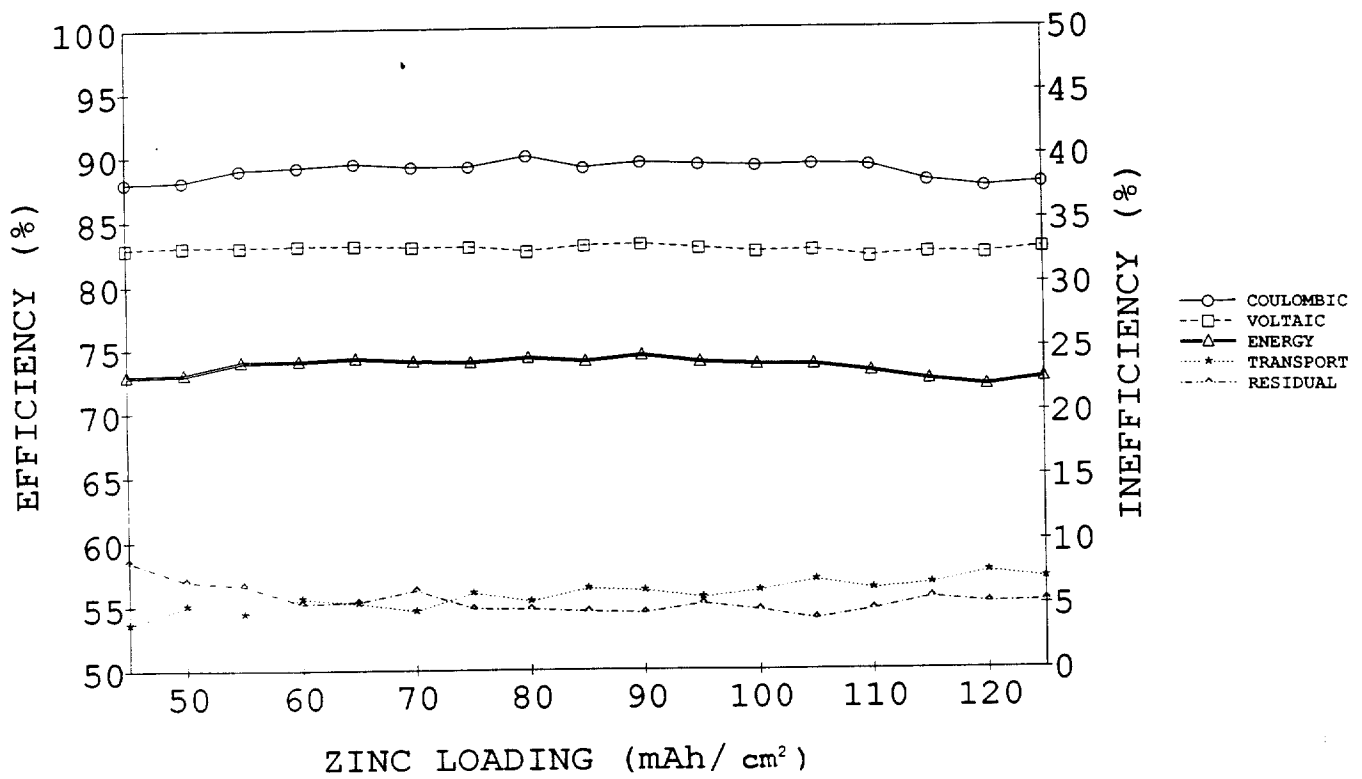


Figure 3-9. Zinc Loading Study, V1-54

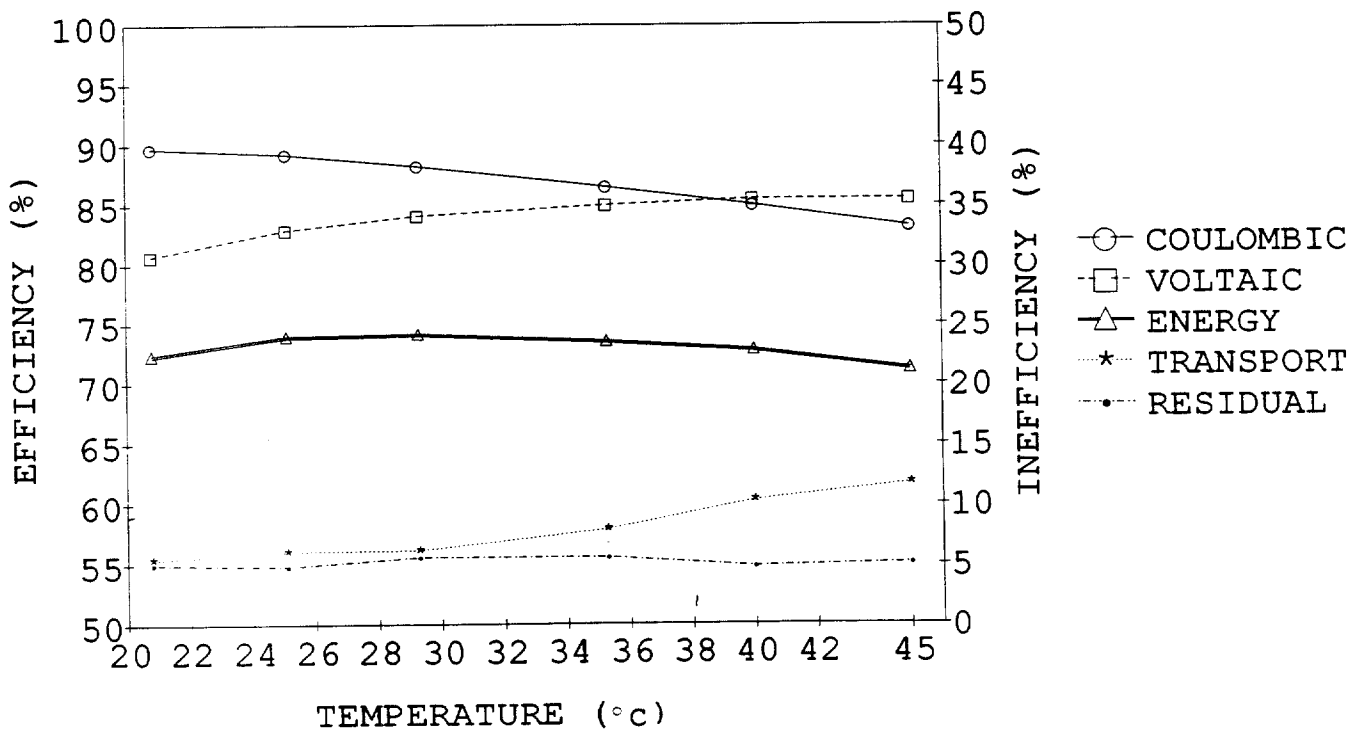


Figure 3-10. Efficiency vs Operating Temperature, V1-50

the electrolyte resistivity, and this improves the voltaic efficiency. From 21°C to 45°C, the transport inefficiency increases, which decreases the coulombic efficiency. Maximum coulombic efficiency in the test was achieved at 21°C, the lowest temperature. Between 21° and 45°C, the coulombic performance decreased by 6.5%.

Fast-Strip Cycling

In many zinc/bromine battery applications, there may be only limited opportunities for stripping the remaining zinc from the negative electrode. Therefore, the battery needs to be stripped as quickly as possible. One way to do this is to mix the two electrolytes when the stripping process begins so that the remaining bromine can react directly with the plated zinc.

Two batteries were fast-stripped by switching the electrolytes at the beginning of the strip period. The strip times listed in Table 3-4 show that in each case, the fast-strip method was more effective than the conventional method.

Two methods were used to measure the strip time. In the first, the time until the total amp-hr no longer changed (0.1 Ah increments) was used; in the second, the time until the voltage fell below 0.01 V/cell was recorded. In general, the strip times determined by voltage reading were shorter, but all except for the V1-53 voltage times were rather scattered. The exact decrease in strip time would be difficult to determine. The test does demonstrate that the strip period can be limited to

1.5-2.0 hr by admitting bromine-containing electrolyte to the zinc electrodes.

Experimental Separator Battery Test

After peaking at 72.6% energy efficiency during the first week of operation, battery V1-51 (Experimental separator) returned increasingly lower efficiencies. By cycle 40, the energy efficiency fell to 66.3%. A calculation using the mass and energy spreadsheet indicated that the losses are occurring in bromine transport and residual capacity. The calculated values are shown in Table 3-5.

The energy lost to bromine diffusion showed the largest increase. This may indicate some partial dendrite penetration or other deterioration of the separator. Surprisingly, the energy lost to resistance decreased slightly, even though the voltaic efficiency also decreased. The VE drop might occur if the average voltage on discharge decreased but was not due to a change in resistance. A decrease in the discharge voltage would also explain the increase in residual loss.

Shunt Current Protection

In the present V-design, Shunt Current Protection (SCP) is provided by a set of electrodes and tunnels through the stack. The current in the tunnels sets up a potential field that matches the potential expected from the shunt current in the electrolyte channels and thus removes the driving force for shunt currents in the channel.

Table 3-4. Strip Times

| Battery/Cycle | To $\Delta Ah = 0$ (min) | To $V < 0.01$ (min) |
|---------------|-----------------------------|------------------------|
| V150/23 | 386 | 190 |
| V150/24 | 346 | 282 |
| V150/25* | 95 | 85 |
| V150/26 | 160 | 125 |
| V153/29 | 206 | 135 |
| V153/30 | 176 | 136 |
| V153/31 | 569 | 136 |
| V153/32* | 131 | 96 |
| V153/33 | 333 | 136 |

* Fast-Strip Test

Table 3-5. V1-51 Performance - Energy Losses

| | Cycle 4 | Cycle 41 |
|-------------------|---------|----------|
| Efficiency | | |
| CE | 84.6% | 79.4% |
| VE | 85.5% | 83.5% |
| EE | 72.4% | 66.3% |
| Categories | | |
| Resistance, Wh | 225 | 218 |
| Overvoltage, Wh | 34 | 33 |
| Shunt Current, Wh | <1 | <1 |
| Diffusion, Wh | 152 | 199 |
| Residual, Wh | 81 | 114 |

The protection currents measured at the SCP electrodes of V1-39 were typically 400 mA, but when the opposing electrode was disconnected, the current dropped by about 110 mA. Assuming that this change in the current was the true tunnel current, the remaining current must be diverting to the main electrodes. There are two tunnels connected to each SCP electrode, so assuming an equal split of the tunnel current, each tunnel had about 55 mA. This is a good match to the 48 mA tunnel current calculated in the manner described in the following paragraph.

The tunnel current required to stop shunt currents was calculated by putting the P. Grimes equation in a spreadsheet format. The minimum tunnel current needed is much smaller than the current actually seen at the SCP electrodes. The tunnel current is set by a combination of the stack voltage, the size of the resistors that connect the SCP electrodes, the resistance of the electrolyte, and the diameter of the tunnels. Since the diameter of the electrodes is relatively large in the present 8-cell stacks, the tunnel current is expected to be larger than the minimum required to block the shunt current.

SCP Calculations

From the spreadsheet used to calculate the tunnel current, the currents are:

| | |
|--------------------------|-------|
| Minimum tunnel current | 2 mA |
| Expected tunnel current* | 48 mA |

* Using 5/64" (0.2 cm) diameter tunnels. Predicted diameter is 0.04 cm for minimum current

The results indicate:

1. The tunnel holes should theoretically be much smaller to approach the minimum tunnel current. This could be a problem, since small holes are likely to plug easily with either carbon particles or second phase particles.
2. The individual SCP electrode currents were larger than expected, and must have been composed of more than just tunnel currents.

Other Laboratory Testing

Miniature Cell Testing

Miniature cells with half the active electrode area of a standard V-battery have been developed to investigate operating conditions, i.e., charge current density, zinc loading, electrolyte compositions (i.e., plating additives), and battery material. The initial work has been to establish baseline performance levels for the cells, to investigate the effects of plating current density on zinc dendrite formation, and to test samples of chemically treated separator.

Current Density Studies

Baseline cycles use a charge current density of 20 mA/cm² with the total zinc loading set at 90 mAh/cm². To test the effect of current density on zinc plating, cycles were run at charge current densities ranging from 20 mA/cm² to 50 mA/cm², with the zinc loading held at 90 mAh/cm². A minimum of three complete charge/discharge cycles was run, after which the cell was opened and inspected at 100% SOC to observe the zinc plating. Before each set of cycles, a baseline cycle was used to compare battery performance with previous baseline cycles.

Figure 3-11 shows the effect of charge current density on efficiencies for mini-cell #2. The main effect is a decrease in voltaic efficiency due to ohmic losses associated with the increased current density. The coulombic efficiency appears to increase slightly as current density is raised. This is presumed to be due to the reduced time available for bromine transport at higher current densities.

The decrease in performance is exaggerated somewhat in Figure 3-11 because of an overall reduction in performance of the battery during baseline cycles (see Figure 3-12). The general downward trend in voltaic efficiency as the number of cycles increases is most likely due to corrosion of the copper screen in the terminal electrodes. The mini-cell electrodes were prepared with only one layer of carbon plastic on the active side of the electrode, instead of three as in standard terminal electrodes. This was done to improve voltaic efficiency at the expense of long life. In earlier mini-cells made with the standard terminal electrode construction, the voltaic efficiency was poor because the carbon plastic available at the time was too resistive. The next set of electrodes will use two layers of carbon plastic. The newer carbon plastic is less resistive, so two layers are expected to give adequate voltaic performance.

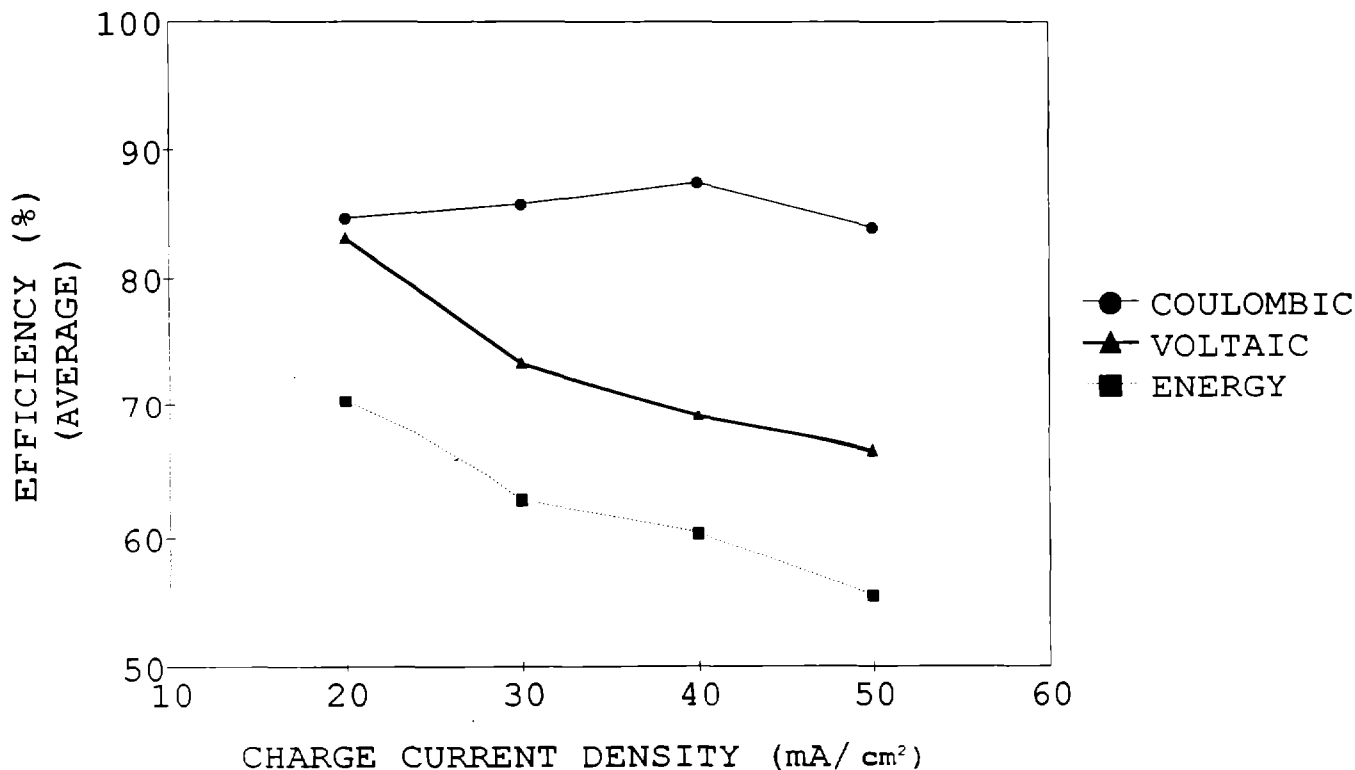


Figure 3-11. Effect of Charge Current Density on Efficiencies, Mini-Cell #2

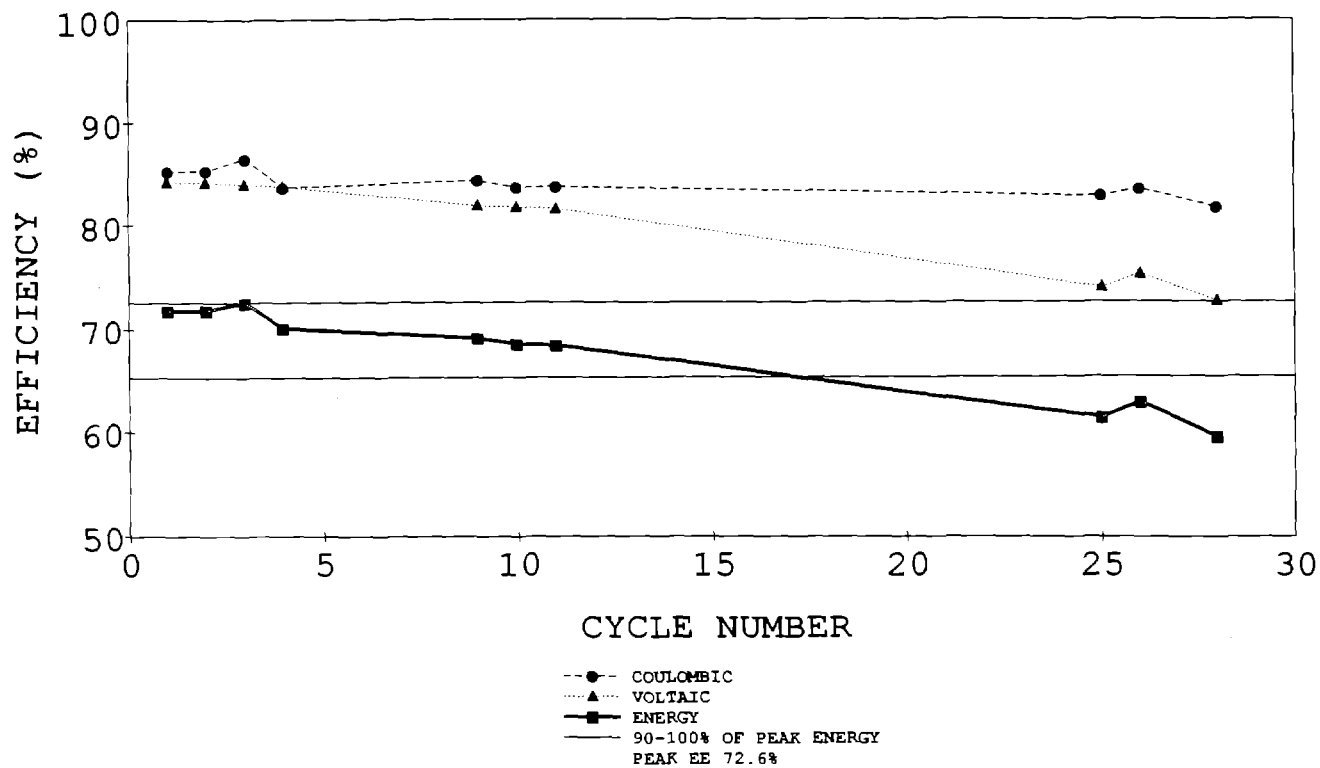


Figure 3-12. Baseline Cycle Efficiencies, Mini-Cell #2

Tear-downs of the cell at 100% SOC did not show any significant differences between cycles run at different charge current densities. The plated zinc at 40 mA/cm² looked essentially the same as the zinc plated at 20 mA/cm². Slightly dendritic zinc was seen near the outside edges of the electrode when the cell was inspected at 100% SOC after a 50 mA/cm² (1.8-hr) charge. Charge current densities will be increased until very poor zinc plating is observed. At this point, plating additives will be introduced to the system to determine concentrations needed to obtain smooth zinc plating.

Separator Testing

Mini-cells are also being used to test various separators. Samples of Asahi separator were coated with a sulfonated polyester resin at SNL. The coated material was compared to uncoated Asahi separator by cycling at standard conditions. Results are shown in Table 3-6.

The coated separator gave a coulombic efficiency increase of 2%, by decreasing the bromine transport. The voltaic efficiency decreased by about 1%, due to the slightly higher resistivity of the coated separator. The net increase in energy efficiency was about 1%.

Table 3-6. Separator Comparison from Mini-Cell Testing

| Separator Type | Standard | Chemically Coated |
|----------------|----------|-------------------|
| Coulombic % | 86.4 | 88.4 |
| Voltaic % | 80.2 | 79.3 |
| Energy % | 69.3 | 70.1 |
| Transport % | 11.4 | 8.9 |
| Residual % | 2.2 | 2.4 |

Zinc Plating

Testing Methods

A variety of tests have been performed using 6-cm² flow-by test cells to better understand factors that affect zinc plating morphology. Screening studies were performed to determine how such factors as charge current density, zinc loading, electrolyte flow rates, and plating additives affect zinc plating in unsupported, 0% SOC load-leveling electrolyte. Results were consistent with previous studies using electric vehicle battery electrolyte (containing KCl to increase the conductivity). The zinc plating became rougher with increasing charge current density and zinc loading. Electron spectroscopy chemical analysis (ESCA) studies have also been used to help identify the causes of rougher zinc plating normally observed in the presence of KCl-supported electrolytes. These studies indicated that a greater propensity towards zinc oxide surface growths could be causing the rougher plating in KCl-supported electrolytes.

Zinc plating morphology was examined both qualitatively and quantitatively. Photographs of zinc plating samples were taken for visual comparisons under the various testing conditions. Dendrite heights

were measured from the tip of the dendrite to the base of the zinc plate using the Neophot incident light microscope. Five dendrites of about average height (eliminating very large and small dendrites and edge effects) were measured to obtain an average dendrite height. Another measurement taken was the thickness, using a calipers, from the backside of the plate to the tip of the largest peak.

Zinc Loading and Current Density

Dendrite heights were plotted vs zinc loading at a constant current density of 18 mA/cm² and vs current density at a constant zinc loading of 90 mAh/cm² in Figures 3-13 and 3-14, respectively. From Figure 3-13, it can be seen that dendrite height increases with zinc loading, which could be expected. It also shows that plating additives can be effective in reducing dendrite formation, even at very high zinc loadings of 180 mAh/cm². Figure 3-14 illustrates that dendrite height increases with increasing current density and that 3 M KCl-supported electrolyte gives rougher plating than unsupported electrolyte at a given current density.

Some reports in the scientific literature have indicated that zinc plating morphology in acid media may become smoother if plating current densities are in-

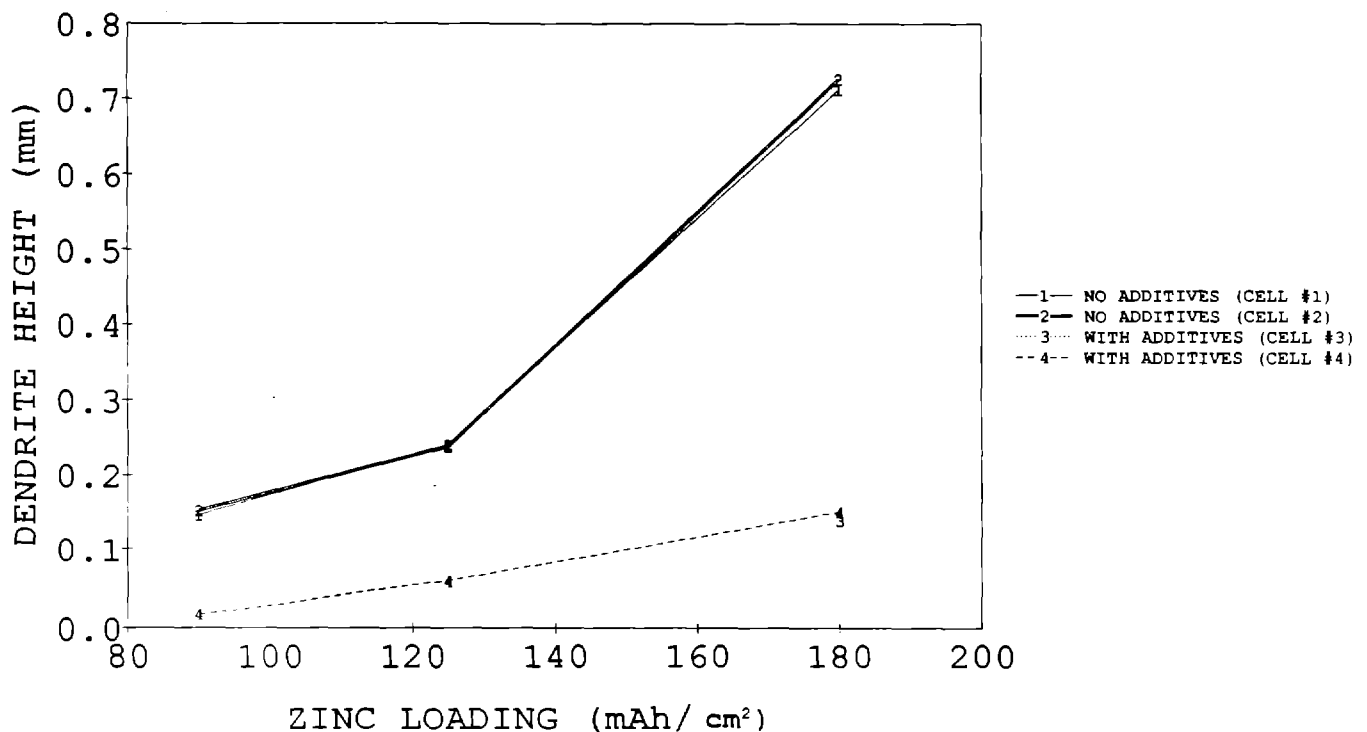


Figure 3-13. Effect of Zinc Loading on Dendrite Height Unsupported Load-Leveling Electrolyte (constant current density of 18 mA/cm²)

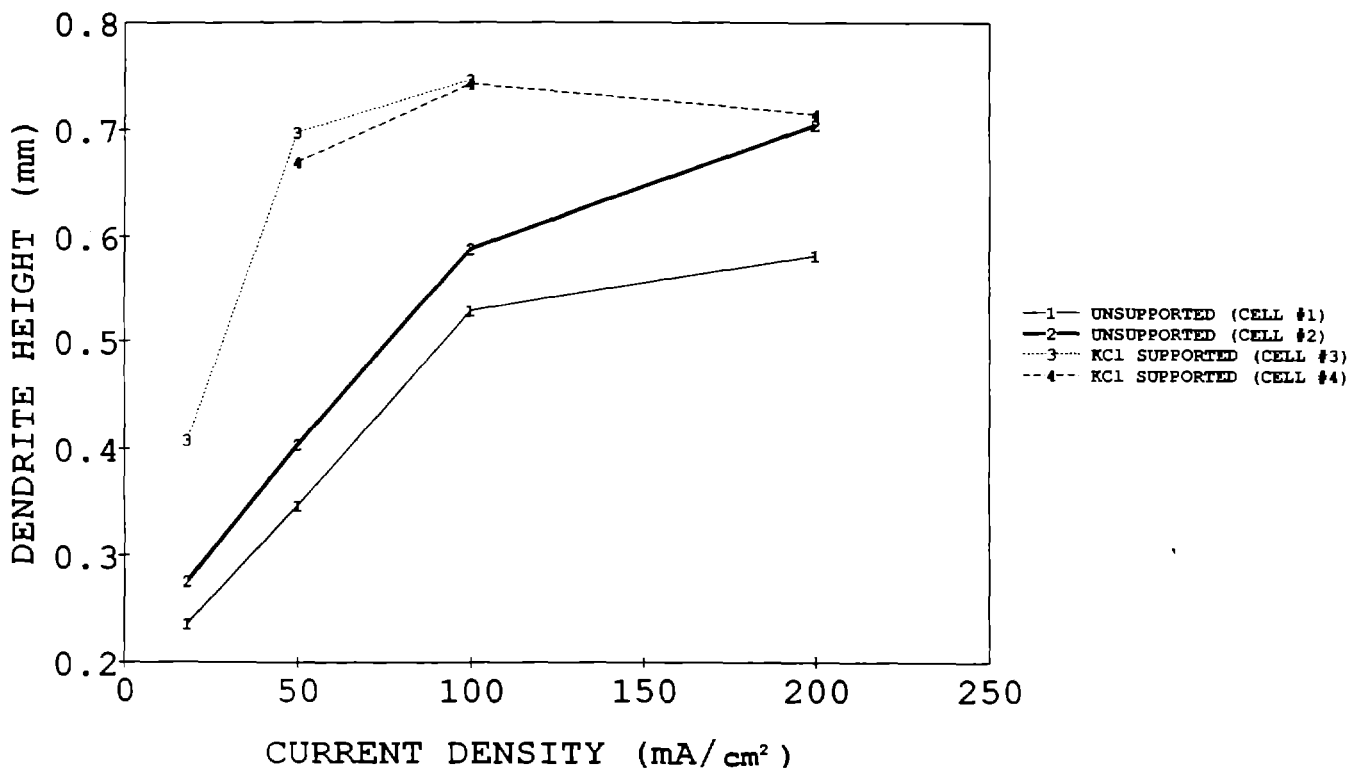


Figure 3-14. Effect of Current Density on Dendrite Height (constant zinc loading of 90 mAh/cm²)

creased to 100 mA/cm² or greater. Some of these studies were conducted at very high flow rates compared to the standard laminar flow conditions in JCBGI's plating studies. Experiments with up to 65 times the standard flow rate and up to 200 mA/cm² were completed to examine these factors. In every case, zinc plating appeared rougher at higher current densities for both unsupported and KCl-supported electrolytes. Figure 3-15 shows that measured dendrite height does decrease as flow rate becomes very large. Also, at each flow rate, the lower current density gives a smoother surface for both unsupported and supported electrolytes, with supported being rougher than unsupported in each case. It has been concluded that high charge-current densities should be avoided to minimize dendritic growth at both high and low flow rates.

The dendrites appear to be smaller at higher flow rates (Figure 3-15). However, Figure 3-16 shows that overall plating thickness is independent of flow rate.

ESCA Surface Studies

In other experiments, ESCA surface spectroscopy studies of zinc plating samples have been used to deter-

mine if zinc oxide growth on the electrodes was influencing zinc plating morphology. The zinc that had been plated from KCl-supported electrolytes had zinc oxide surface layers that were consistently about two times thicker than in unsupported electrolytes. There were no observed differences in trace adsorbed impurities on the surfaces of these two types of zinc plating samples. Argon gas purging of the zinc plating cell both prior to and during zinc plating did not reduce the thickness of the zinc oxide surface layers. This indicates that the oxide is not forming due to dissolved oxygen in the electrolyte. Instead, the zinc oxide layer was likely forming when zinc metal reacted with water to form hydrogen gas. This reaction was fairly rapid and self-limiting, since the oxide layer thicknesses were essentially the same for samples exposed to electrolyte for 30 or 240 min at open circuit following plating.

Argon ion sputtering inside the ESCA instrument was used to determine the approximate oxide layer

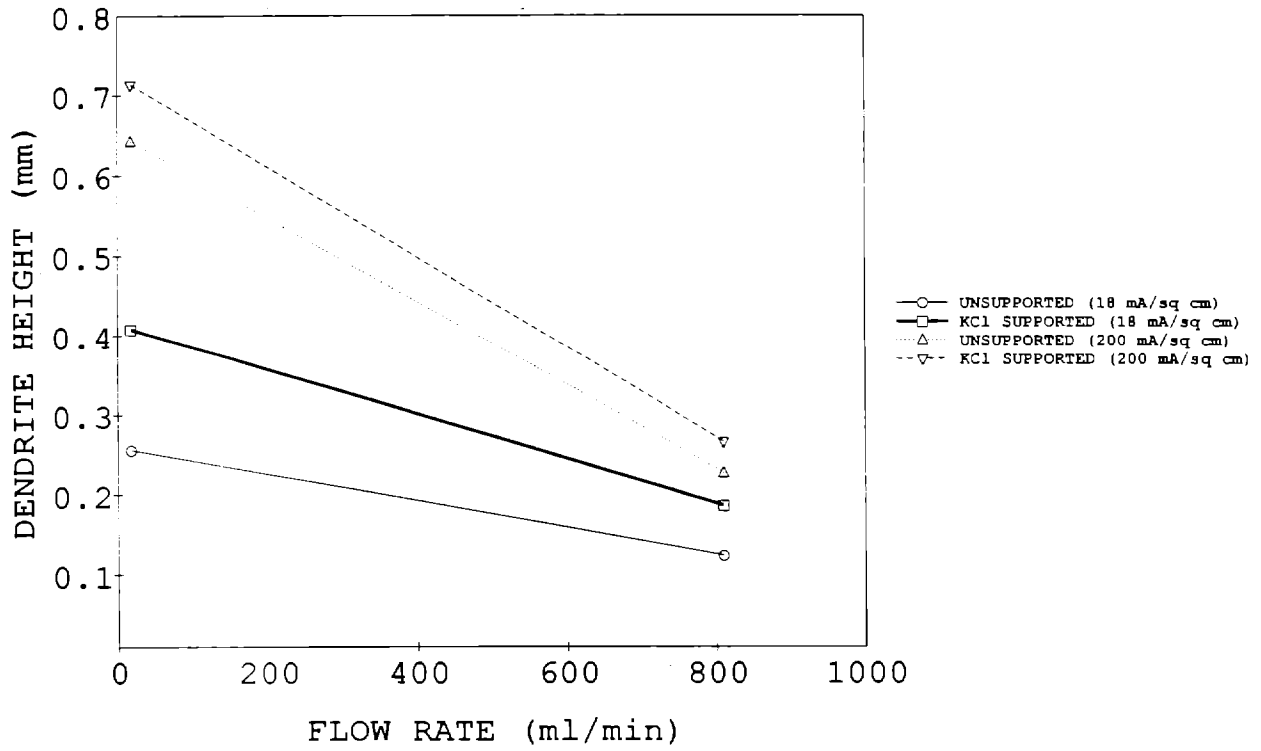


Figure 3-15. Effect of Flow Rate on Dendrite Height

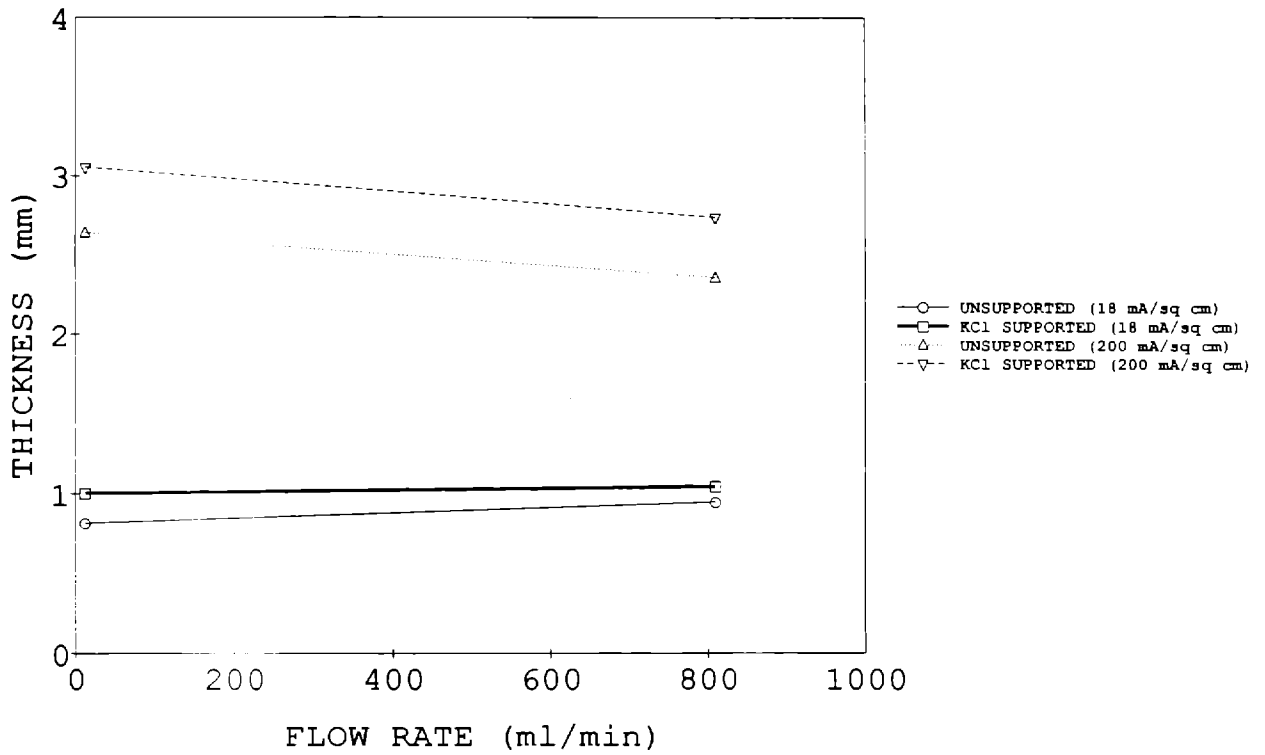


Figure 3-16. Effect of Flow Rate on Zinc Thickness

thicknesses. Therefore, it was possible that differences in surface roughnesses between the two types of plating samples, supported vs unsupported electrolytes, could have artificially influenced their relative oxide layer thickness determinations. Consequently, follow-up experiments were conducted to measure zinc oxide layer thicknesses on the smooth back faces of the zinc plating samples that had been peeled away from the carbon-plastic electrode backbones. The electrodes were then immersed at open circuit in the different electrolytes for 30 min. As before, the samples were then transferred to the ESCA instrument under an argon atmosphere. The smooth back faces of these electrodes had oxide surface layers that were three to ten times thinner than that of the front electrode surfaces that were exposed to electrolyte throughout plating. However, just as before, the electrodes exposed to KCl-supported electrolytes exhibited oxide surface layers approximately two times thicker than those of electrodes plated in unsupported electrolytes.

The ESCA experiments indicated that a greater propensity for zinc oxide growth could be the cause for the rougher zinc plating observed in KCl-supported electrolytes. The zinc plating additive package could improve zinc plating by reducing zinc oxide surface layer thicknesses by at least 20%. Zinc oxide growths could cause rougher zinc plating by creating surface inhomogeneities that act as dendrite precursor sites. Experiments will be performed in unsupported load-leveling electrolytes to determine if zinc oxide growths cause rougher zinc plating onto unstripped, partially discharged zinc layers.

In summary, it has been shown that KCl-supported electrolyte consistently gives rougher plating than unsupported electrolyte, and that an increased tendency towards zinc oxide growth is a possible cause for this increased roughness. JCBGI's proprietary zinc plating additive package functions just as well in load-leveling electrolyte as previously confirmed in EV electrolyte. Incorporation of the plating additives has yielded very smooth plating at loading levels as high as 180 mAh/cm².

Bromine Electrode

Background/Introduction

To date, most of JCBGI's full-size test batteries have been constructed using bromine electrodes that contain conventional PV-2 type cathode activation layers. These electrodes have generally shown good performance, at least up to the presently achieved 300 charge/discharge cycles. However, a variety of beaker-scale experiments have been done to further assure the

optimal fabrication, performance, and long-term cycle life of bromine electrode cathode activation layers.

A newly developed electrochemical surface area measurement technique, coupled with ESCA carbon surface spectroscopy analyses, has indicated that declines in bromine electrode performance with increasing accelerated cycle life are often attributable to changes in carbon surface chemistry, as opposed to physical losses of electrode surface areas. ESCA surface spectroscopy studies of various types of cathode layer carbons have identified how carbon surface chemistries can be optimized to improve the long term cycle life performance of bromine electrodes.

Experiments have also been done to evaluate the use of noncarbonaceous cathode layer materials such as ruthenium dioxide (RuO₂), titanium oxide (TiO_x, also known as Ebonex), and a JCBGI proprietary mixed metal oxide, M₁M₂O_x. Based on these studies, carbon is still the cathode layer material of choice. The poor performance of the aforementioned noncarbonaceous cathode layer materials was attributed to their very low surface areas. Ruthenium dioxide had previously been used in bromine electrodes developed by Energy Research Corp. (ERC), but they supported this material on high surface area carbon to increase the electroactive area. JCBGI prefers to avoid such fabrication complications by instead identifying and using a carbon with very good performance as the sole cathode layer material.

Electrochemical Surface Area Determinations

During accelerated cycle-life testing, the electrochemical performance of bromine test electrodes declines with increasing cycle life. A surface area measurement technique was required to determine if this declining electrode performance was due to a simple physical loss of electrode surface area, e.g., spalling off of surface carbon. BET surface area measurements have not proven sensitive or reproducible enough to measure the bromine electrode surface areas, especially if the areas are less than about 1000 cm² actual area per cm² geometric area.

A cyclic voltammetric technique was developed to more accurately determine the electroactive surface areas of bromine test electrodes. The technique measures double-layer capacitance, which is directly proportional to the electroactive surface area of the electrodes. Using this technique, it was determined that neither PV-2 nor CP-4 carbon paper type cathode layers lose electroactive surface area during accelerated cycle-life tests. Therefore, the declines in electrode performance were attributable to something other than physical losses in electrode surface areas. As described

later, ESCA studies indicated that changes in carbon surface chemistry were the likely cause of declines in electrode performances during accelerated cycle-life testing.

The details of the electrochemical surface area test are as follows. Cyclic voltammograms (CVs) are run on 4-cm² bromine test electrodes in 0.1 M KCl electrolytes in a nonfaradaic potential region of 0.6 - 0.1 V vs saturated calomel electrode (SCE) reference electrode. A voltage scan rate of about 0.5 mV/sec gives the best results. Test electrodes that have received exposure to bromine must first be electrochemically stripped of the adsorbed bromine prior to the CV tests. The capacitance of the electrodes, C, is calculated from the double-layer charging current of its cyclic voltammogram using Equation 1:

$$C \text{ (Farads)} = I \text{ (charging current in amps)} / \text{scan rate (V/sec)} \quad (1)$$

The electroactive surface area of the electrode is then calculated using Equation 2:

$$\text{Area (cm}^2\text{)} = C \text{ (Farads)} / C_{dl} \text{ (Farads/cm}^2\text{)} \quad (2)$$

The proportionality constant, C_{dl} , in Equation 2 is a factor that depends on the composition and concentration of the electrolyte. Typically, C_{dl} has a value of about 20×10^{-6} Farads/cm². However, it is possible that this value could change for different types of carbons. Therefore, this surface area test is most accurate for comparing changes in surface area for a given carbon type. Under these conditions, the relative accuracy of the test is better than 20%. Comparisons of surface areas for different carbon types must be made with a little more caution unless an accurate value of C_{dl} can be calculated using accurate BET data.

Optimization of Carbon Surface Chemistry for Long Cycle Life

ESCA surface spectroscopy has been used to monitor the changes in carbon surface chemistry during the cycle life testing of various types of cathode layer carbons. In essentially all cases, the carbons lose graphitic character and gain in surface oxygen content during accelerated charge/discharge cycling. Based on these findings, it is proposed that the best long-life bromine electrode carbons should have an optimum combination of high graphite content, low oxygen content, and high surface area. Pure graphite powder did not perform well in a cathode layer owing to the naturally low surface area of very highly graphitic carbon. Thus, there are some restrictions as to just how highly graphitic the carbons can be. However, partial graphitization and removal of surface oxygen from a

poor cycle-life carbon converted it into one of the best cycle-life carbon cathode layers.

Bromine electrodes containing spray-coated PV-2 or heat-pressed CP-4 carbon paper cathode layers were analyzed by ESCA surface spectroscopy as a function of cycle number during accelerated cycle-life testing. The ESCA analyses were performed on a V.G. Scientific Model VG ESCALAB instrument located at the University of Wisconsin, Milwaukee. The ESCA oxygen peak at 531 eV was used to measure changes in surface oxygen contents of the carbons, while the carbon energy loss region of 305 - 315 eV was used to monitor changes in the graphitic character of the carbons. The peak intensity at 314 eV is a measure of the amount of delocalized electron character, i.e., graphitic content of the carbons, while the peak intensity at 305 eV is a measure of the amorphous content of the carbons. The ratio of these peak intensities was taken to be a semi-quantitative measure of the ratio of graphitic to amorphous content of the various cathode layer carbons.

The bromine peak at 70 eV was also monitored to measure changes in the amount of strongly bound bromine. The bromine content of all electrodes remained at about 2 atom % independent of cycle life number. This bromine was undoubtedly chemically bound to the carbons. Weakly adsorbed bromine would have been removed during the successive aqueous and acetone rinses of the electrodes, which were followed by > 24-hr vacuum treatments prior to their introduction into the ESCA instrument. The bromine content of the carbons did not correlate with their cycle life performance. However, as described below, an increasing oxygen content and decreasing graphitic character of the carbons appeared to correlate with the increasing polarization of the cycling electrodes.

The 4 cm² bromine test electrodes were subjected to accelerated cycle life testing, which consisted of a total of 7000 10-min charge/10 min discharges at a current density of 100 mA/cm². The tests were conducted over a 3-mo period at room temperature in a simulated constant composition 35% SOC catholyte electrolyte. The relatively high current density used in this cycling has been shown to accelerate the degradation of the cathode activation layers.

The correlation between battery cycle life and these accelerated cycles is such that the 7000 accelerated cycles are believed to approximately correspond to about 2000 battery cycles. However, this correlation is quite tenuous, since it is primarily based on the testing of a limited number of battery electrodes that had less than 200 cycles. Thus, the accelerated cycle-life testing is used mainly as a comparative screening tool for various types of cathode activation layers. IR-free

polarization curves were taken every 1000 to 2000 cycles to periodically monitor electrode performance as a function of cycle life. Following the polarization tests, washed bromine electrode samples were submitted for ESCA analyses.

Figure 3-17 shows polarization vs accelerated cycle-life data for both the spray-coated PV-2 and CP-4 carbon paper cathode layers. As described in the previous section, the observed increases in electrode polarization with increasing cycle-life were not due to physical losses in electrode surface areas. Figures 3-18, 3-19, 3-20, and 3-21 show plots of amorphous/graphitic carbon ratios and surface oxygen contents versus electrode polarizations for PV-2 and CP-4 carbon layers. There is some scatter in the data, but increasing oxygen content and increasing amorphous/graphitic carbon ratios appeared to correlate with increasing electrode polarization that was observed with increasing cycle numbers.

With the exception of the PV-2 surface oxygen data, multiple regression statistical analyses showed that the aforementioned correlations were statistically significant with greater than 90% confidence. The correlation between PV-2 oxygen and polarization was significant at only a 76% confidence level. Still, analyses of other

cathode layer carbon types other than CP-4 and PV-2 have always revealed an increase in oxygen content and a decreasing graphite content after 7000 cycles. Therefore, JCBGI is fairly confident in making the statement that increasing oxygen content and decreasing graphite content of cathode layer carbons plays a role in the increase in electrode polarization during increasing cycle numbers.

The correlation between carbon surface chemistry and cycle life has been confirmed by treating a carbon to increase its graphite content and decreasing its oxygen content to improve the carbon's cycle life performance. A high surface area wood-based carbon was found to give good initial polarization performance, but this polarization increased to unfavorably high levels after only 1000 accelerated cycles. The carbon supplier was asked to treat this given batch of carbon to increase its graphitic content and lower its oxygen content. This treatment increased the ratio of graphitic/amorphous carbon from 1.22 to 1.58, while decreasing the surface oxygen content from 8 to 4 atom %. As seen in the polarization plots of Figure 3-22, the high graphite content, low oxygen content carbon showed improved cycle life performance compared to the original carbon which had low graphite and high oxygen content. Also note that this improved wood-based carbon was performing

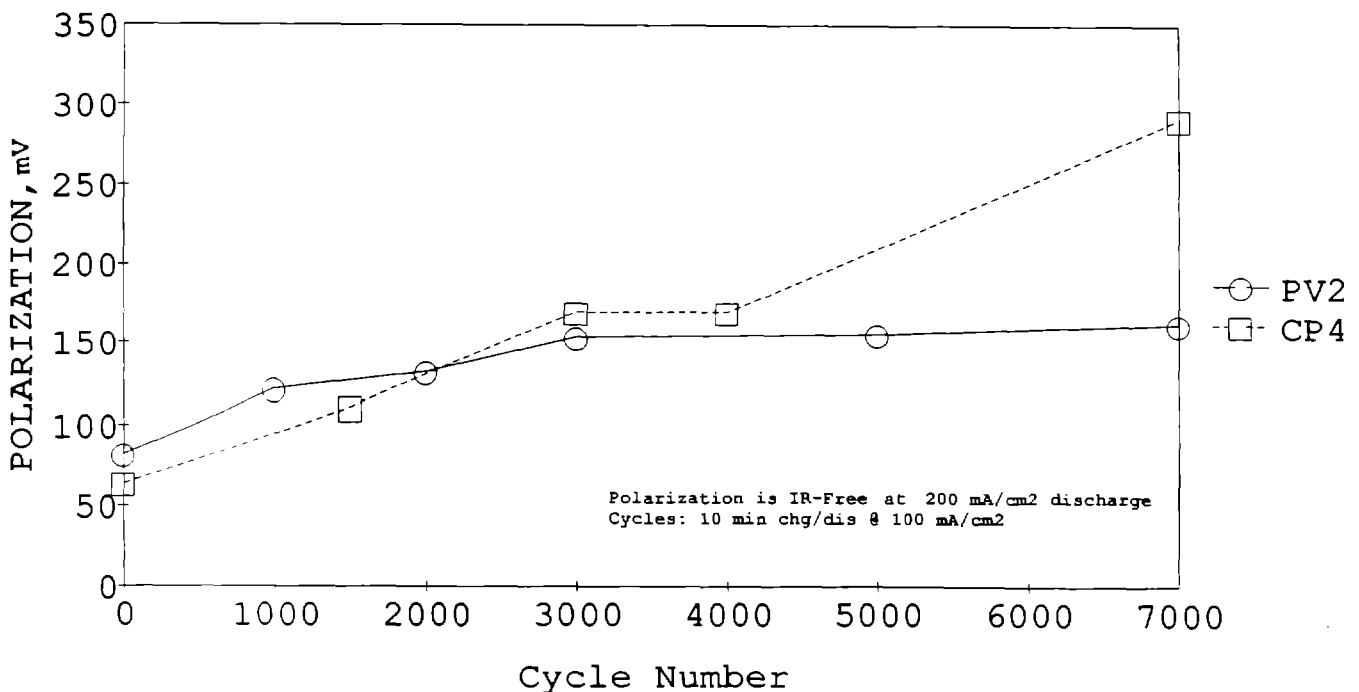


Figure 3-17. Spray-Coat PV2 vs CP4 Carbon Paper Electrodes (data are average of > 2 electrodes per run)

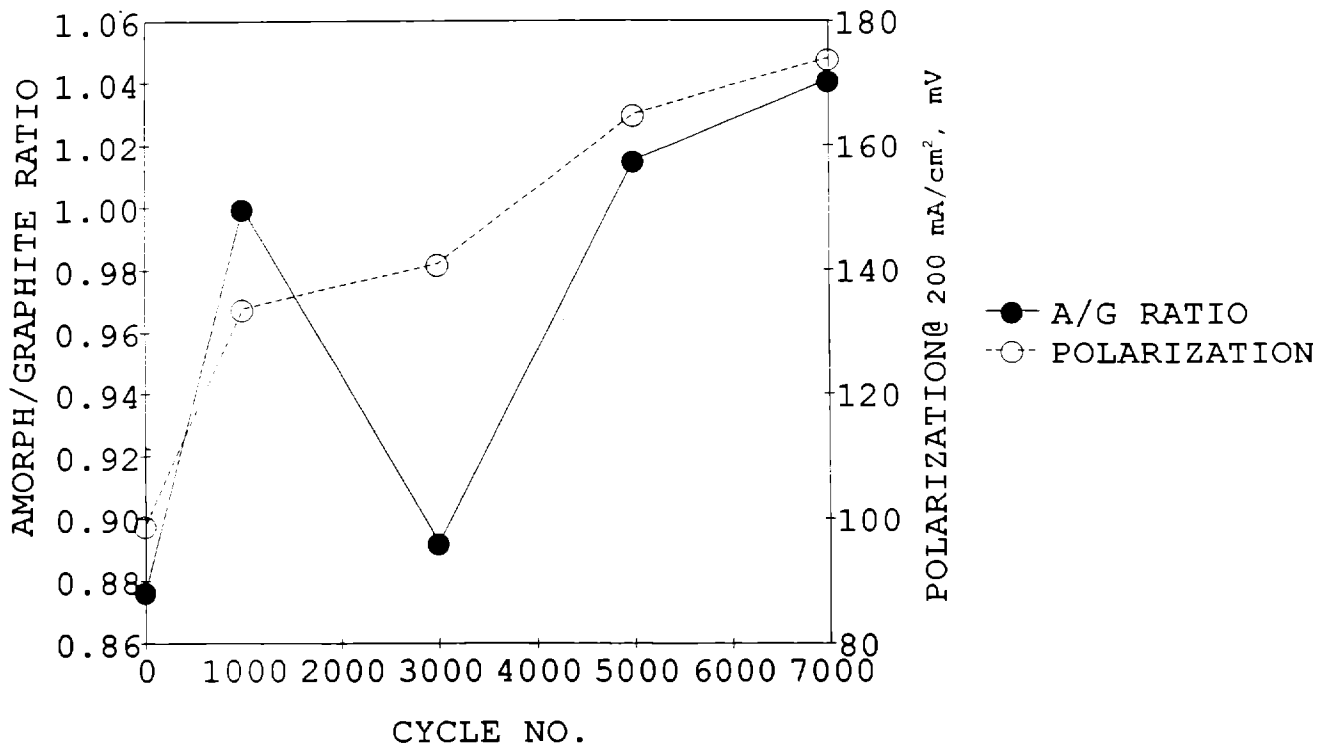


Figure 3-18. ESCA-Monitored Changes in PV2 Carbon

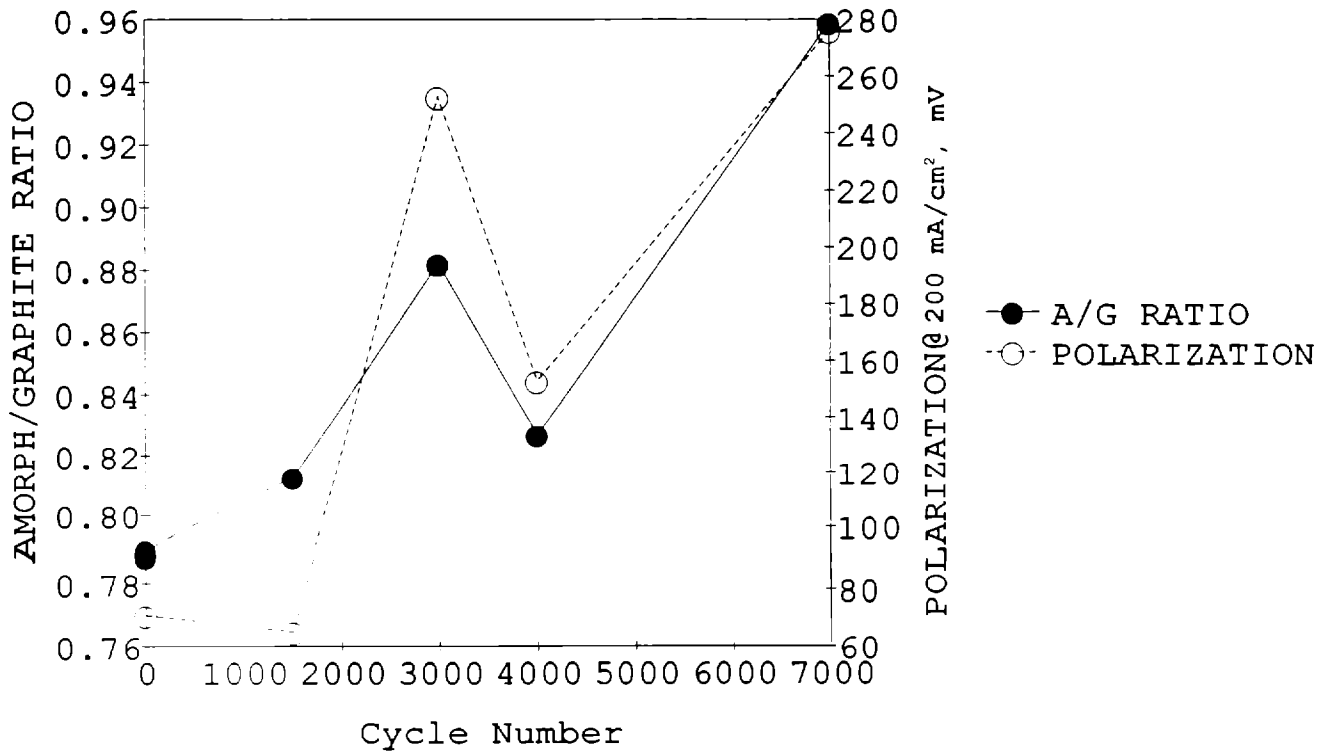


Figure 3-19. ESCA-Monitored Changes in CP4 Paper Carbon

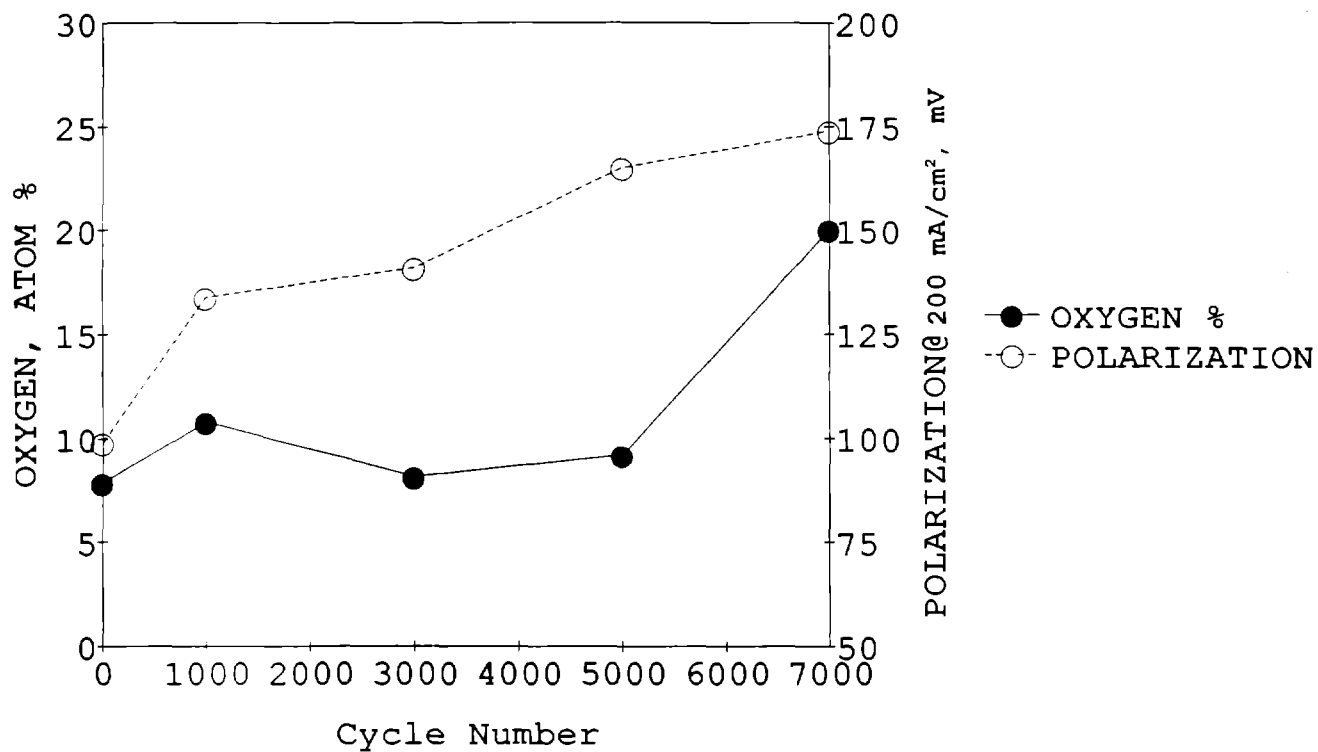


Figure 3-20. ESCA-Monitored Changes in PV2 Carbon

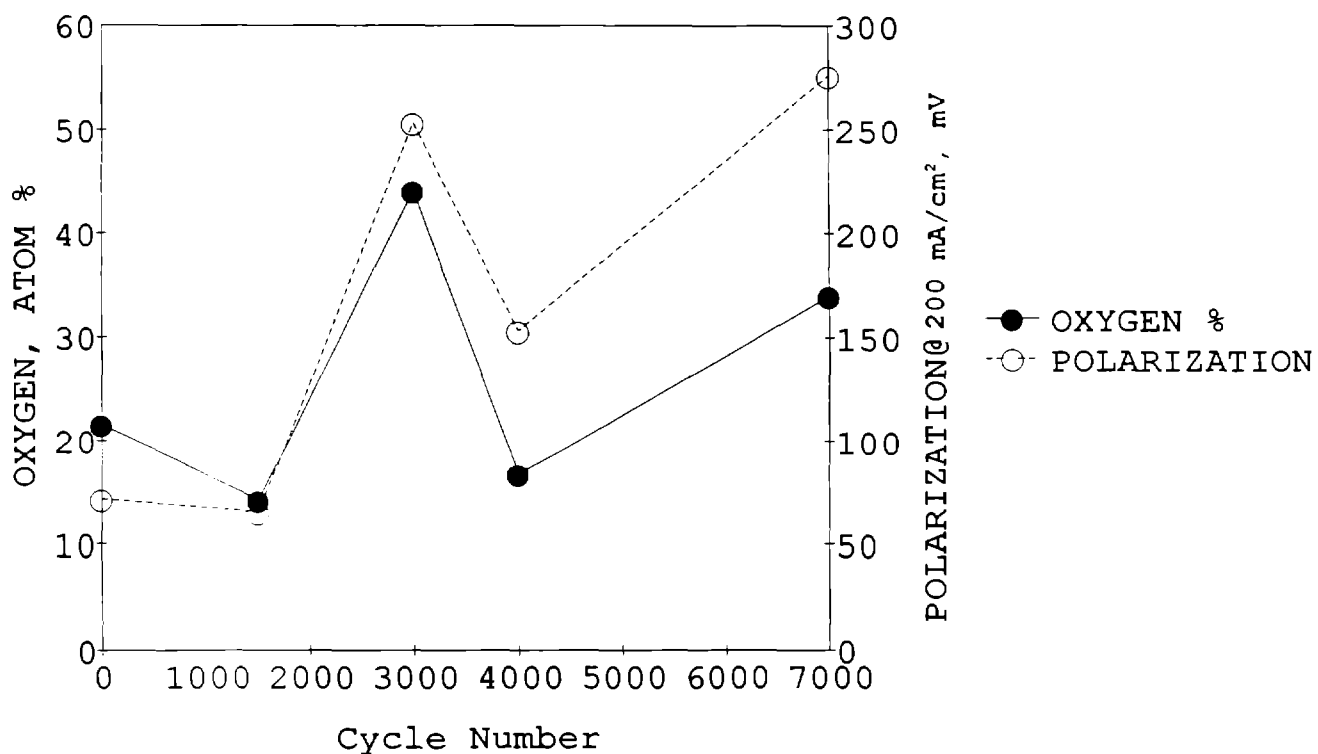


Figure 3-21. ESCA-Monitored Changes in CP4 Carbon

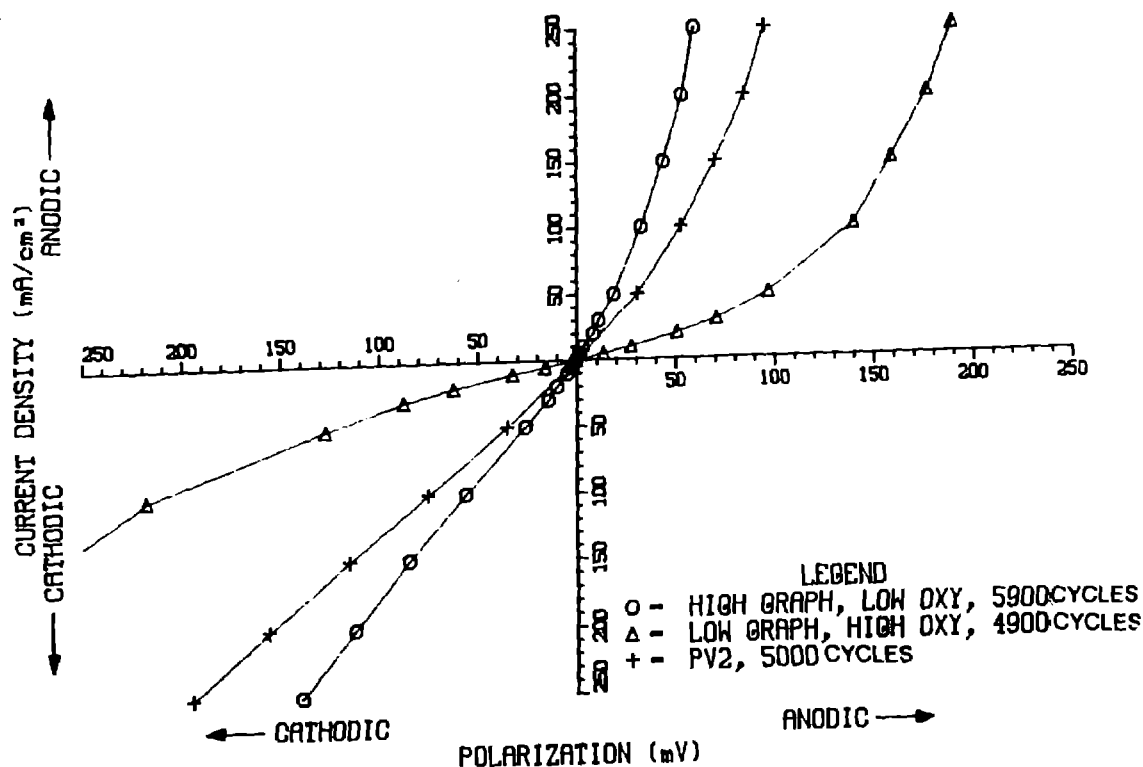


Figure 3-22. Polarization Data - Effect of Graphitic and Oxygen Content

significantly better after 5900 cycles than PV-2 after 5000 cycles.

Electrolyte Composition

Consideration of some of the basic properties of electrolyte leads to the conclusion that higher energy efficiencies may be attainable by using a more dilute electrolyte composition. Naturally, this entails some sacrifice in energy density, but this may be warranted for load-leveling batteries, where energy density is not a primary consideration.

Previous zinc plating studies have shown that unsupported electrolyte tends to produce better zinc plating, with higher coulombic efficiencies, than supported electrolyte. Also, as a rule, lower concentrations of zinc bromide tend to give better zinc plating. These observations may be at least partially explained by the fact that less complexation occurs in electrolyte with lower concentrations of halide ion (either Br⁻ or Cl⁻). Complexation can make zinc ion in solution less available for the zinc ion reduction reaction ($Zn^{++} + 2e^{-} \rightarrow Zn^0$).

In addition to improved coulombic efficiency, the use of more dilute electrolyte would, under certain conditions, be expected to produce improved voltaic

performance. Figure 3-23 shows the resistivity of zinc bromide solutions, methyl pyrrolidinium (MEP) Br solutions, and mixed ZnBr₂/MEP Br solutions as a function of concentration. Note that for the mixed solutions, the resistivity decreases as the ZnBr₂ concentration is decreased, until it reaches a minimum at about 1 M. These data suggest that the voltaic efficiency of present batteries may improve slightly by substituting the present concentration of 2.25 M ZnBr₂ with a more dilute composition (e.g., 1.8 M). It must be pointed out that a sufficient volume of electrolyte must be available so that at the end of charge the zinc bromide concentration does not become significantly lower than the concentration at which the resistivity is lowest (1 M in this case). If the concentration becomes too dilute, the resistivity will increase.

Studies with more dilute electrolyte are under way on battery V1-59. At cycle 17, the standard load-leveling electrolyte composition of 2.25 M ZnBr₂, 0.55 M ZnCl₂, 0.8 M MEP Br was replaced by a similar composition electrolyte with 1.83 M ZnBr₂. Figure 3-24 shows the improvement obtained using the more dilute electrolyte. Contrary to expectations, most of the improvement was in coulombic efficiency, with a slight decrease in voltaic efficiency. The energy efficiency

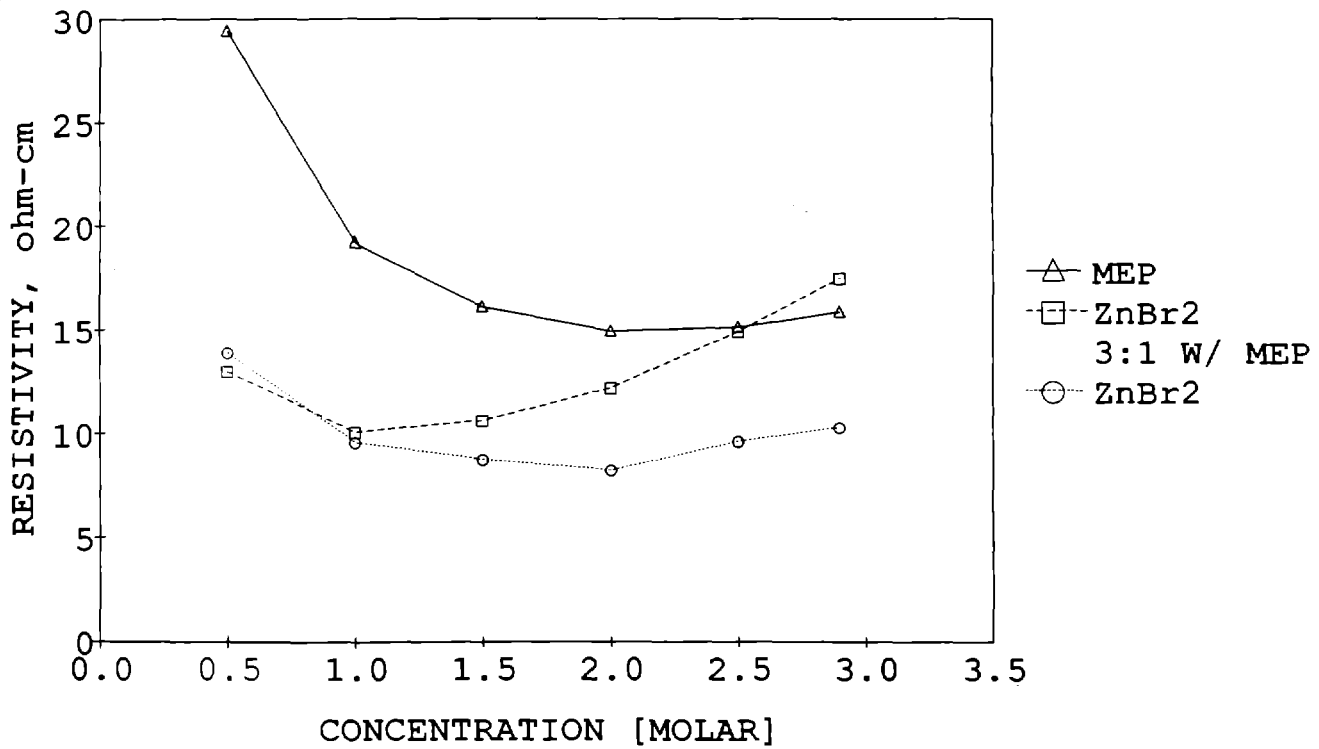


Figure 3-23. Resistivity vs Concentration

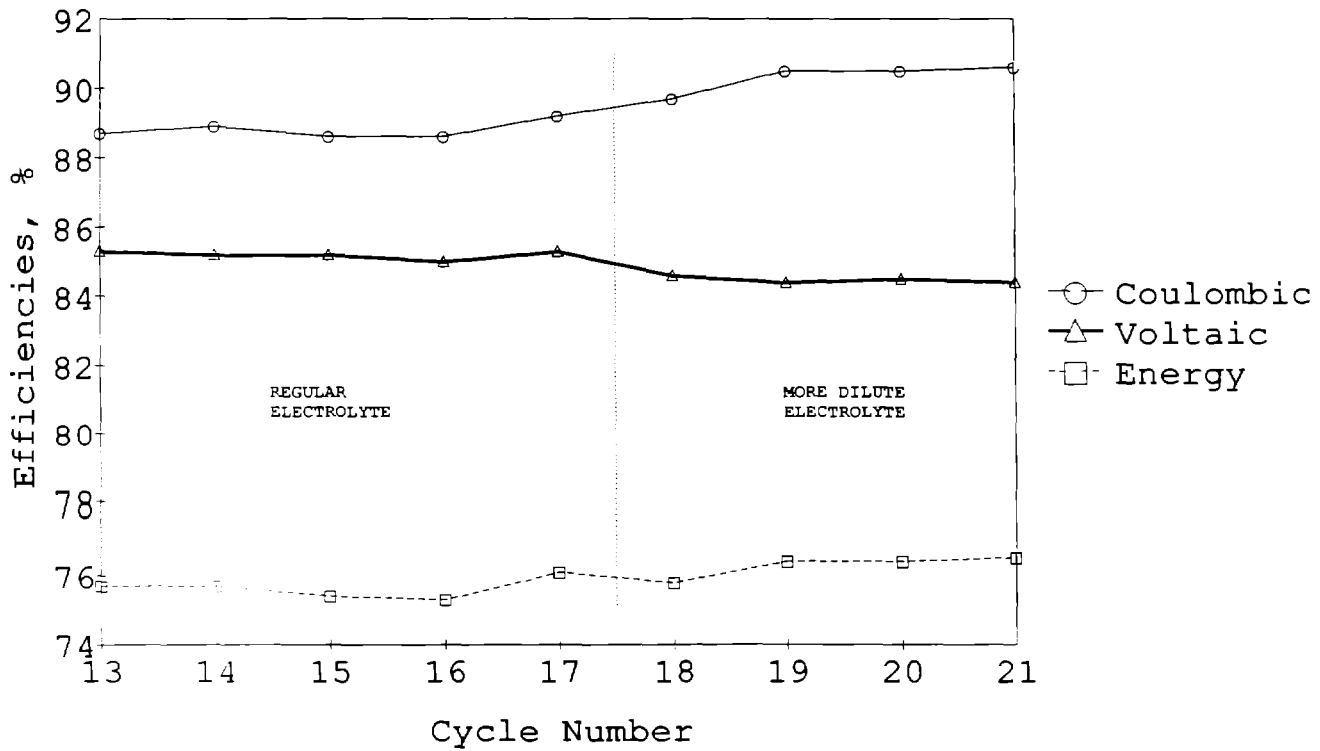


Figure 3-24. Electrolyte Comparison, V1-59

underwent a slight, but statistically significant improvement of 0.7%.

These studies will continue at lower zinc loadings. The lower loadings will result in a smaller zinc/bromine concentration change throughout the cycle.

Core Technology Advances

Welding Study

Literature Search

A literature search for information on vibration welding of thermoplastic materials was done in preparation for the experimental design study, and results are summarized as follows:

- **The vibration welding process goes through four phases:**
 1. Solid friction, heat generated but no welding occurs.
 2. First melt, friction increases, some melt extrudes but not steadily.
 3. Steady-state melt, melting rate = extrusion rate.
 4. Vibration stops, penetration slows then stops, solidification occurs.

Surprisingly, the friction is reported in one source to be higher after the plastic melts. This is because the friction force derives from viscosity and shear. While the viscosity goes down on melting, the shear goes up even more. It is generally recommended that the operating parameters be studied to learn the "window of operation" for each particular material and weld shape. The most important parameters are weld time, amplitude, and pressure. An experimental design using RS/1TM software found that amplitude and pressure interacted, so they should not be studied independently.

- **Some of the published general observations are listed below:**
 1. Poor welds can result when insufficient energy has been directed into the weld, making a cold-weld; or when too much energy has been absorbed, resulting in orientation of the polymer chains.
 2. Reinforced plastics can experience welding problems when the fiber filler is above 40% by volume. One way around the problem is to form the weld bead out of virgin resin.

3. Tests of the weld strength have been done by uniaxial tensile testing with a peel rate of 25-100 mm/min.
4. It is generally beneficial to use as high an amplitude as possible without causing damage to the parts.
5. Amplitude has a greater effect than welding pressure. There are time limits at high amplitudes. If these limits are exceeded, the welds will be damaged.
6. Welds requiring short times at high pressure are good, but at long times the high pressure makes for poor welds. There is too much expulsion of the melt, the heat zone becomes too large, and the weld cools too slowly.

Weld Strength Test

The weld strength test was conducted to eliminate poor weld quality as a cause of battery stack leaks. The objective was to acquire a base of information that will be used to maximize the weld strength, given the constraints encountered in building battery stacks, such as vibration welder limitations, injection mold filling problems, and excessive flash production.

The approach taken was to test the three following general areas of flow frame design and welding processes: 1) Materials, 2) Weld Bead Geometry, 3) Vibration Welder Parameters.

To test the battery stack frame materials used in vibration welding, 16 different combinations of the polyethylene melt index and fiberglass content were tested as shown in Table 3-7.

The weld bead geometry was tested by cutting the mold for 12 different weld bead sizes, all combinations of four heights and three widths. Test frames were manufactured from all materials in each of the 12 weld bead sizes as shown in Table 3-8.

The vibration welder operation has three variables: two that can be altered to maximize strength, i.e., amplitude and clamp pressure, and one that can be designed into the flow frame, i.e., depth of weld.

The depth of weld is expressed as a percentage of bead height, and indicates at what point the vibration stops while the pressure continues. This parameter cannot be varied for a given frame, since the ending weld depth is important in the final electrode spacing gap. The amplitudes used in the test were 0.058", 0.052", and 0.046". The pressures chosen to test were 140 psi, 270 psi, and 400 psi. The original vibration welder did not have enough power to weld at more than about

Table 3-7. Plastic Composition

| | 17 melt HDPE | 30 melt HDPE | 40 melt LLDPE | 52 melt HDPE |
|------------------|--------------|--------------|---------------|--------------|
| 5% glass-filled | ✓ | ✓ | ✓ | ✓ |
| 11% glass-filled | ✓ | ✓ | ✓ | ✓ |
| 20% glass-filled | ✓ | ✓ | ✓ | ✓ |
| 30% glass-filled | ✓ | ✓ | ✓ | ✓ |

Table 3-8. Weld Bead Height

| | 0.020" | 0.025" | 0.030" | 0.034" |
|-------------|--------|--------|--------|--------|
| 0.080" wide | ✓ | ✓ | ✓ | ✓ |
| 0.120" wide | ✓ | ✓ | ✓ | ✓ |
| 0.160" wide | ✓ | ✓ | ✓ | ✓ |

140 psi on the bipolar flow frame. Therefore, this was chosen as a low starting point, since excess flash (excessive molten plastic extruding from the weld area) was already a problem at this setting.

Samples for testing were prepared by welding an initial test frame to a square block of polyethylene for fixturing convenience. Two more test frames were then welded one by one to the initial frame with pull tabs extending in opposite directions. Since each welded frame set was square in shape, it had four potential coupons. Two were cut and tested; two were saved for retest if needed.

The two coupons from each run were sent to the Analytical Services Division of JCBGI where they were tensile-tested at 5 mm/min (the weld itself was in shear), and the results analyzed by the RS/Discover computer program. A total of four design experiments were run, each one concentrating on different factors based on the previous experiments, or on the availability of test frames at that time.

Experiment #1: Screening for Two-Factor Interactions

Of the 21 possible two-factor combinations, three show interactions. A pressure with bead width interaction is shown in Figure 3-25. As pressure is decreased, strength increased for the narrower (0.080") weld bead, but did not change for the wider bead. The effect was more pronounced at low weld pressures than at high

ones. However, this strength was given per square inch of weld bead area, and the wider bead was actually stronger per linear inch of weld.

The data in Figure 3-26 indicated that the melt index and the weld depth interacted. Increasing melt index decreased strength, while decreasing weld depth decreased strength. In both cases, the strength was affected to a different extent, depending on what level the other factor was set at, which implied interaction.

The third interaction is given in Figure 3-27: glass content and weld depth. Increasing glass content increased strength, but not as much for 50% depth of weld as for 70%. Again, decreasing weld depth decreased strength, but the levels of glass content make a difference in how much.

Experiment #2: Response Surfaces

In Figure 3-28, the main effects are shown in the order of magnitude: melt index, glass content, pressure, weld bead height, and amplitude. The materials clearly had the greatest effect on weld strength. The variation of strength with material is shown in Figure 3-29, a response surface contourplot of strength vs material.

The 3D plot of strength vs welder parameters shown in Figure 3-30 indicates that at low pressures, strength increased with increasing amplitude, and at high pressures, it increased with decreasing amplitude. This saddle was more pronounced in experiment #4.

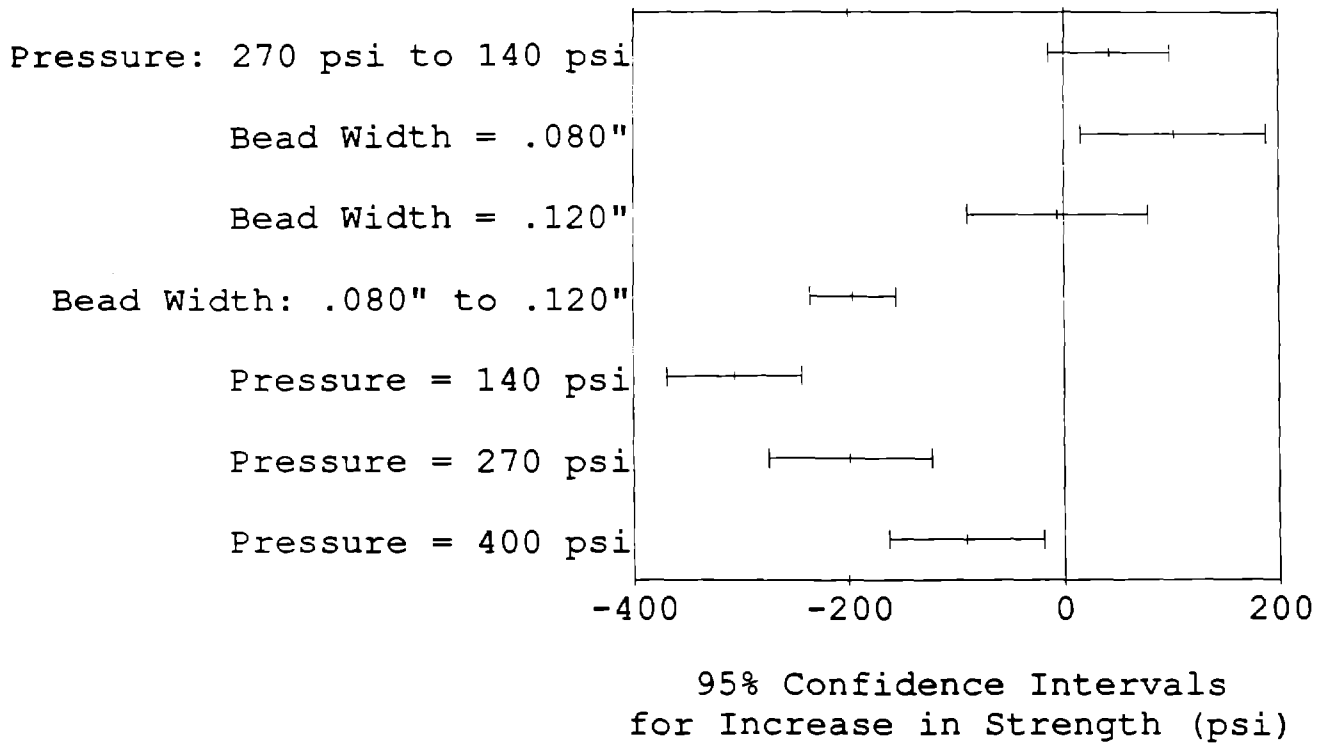


Figure 3-25. Interaction Effects of Pressure with Bead Width on Weld Strength, Experiment #1

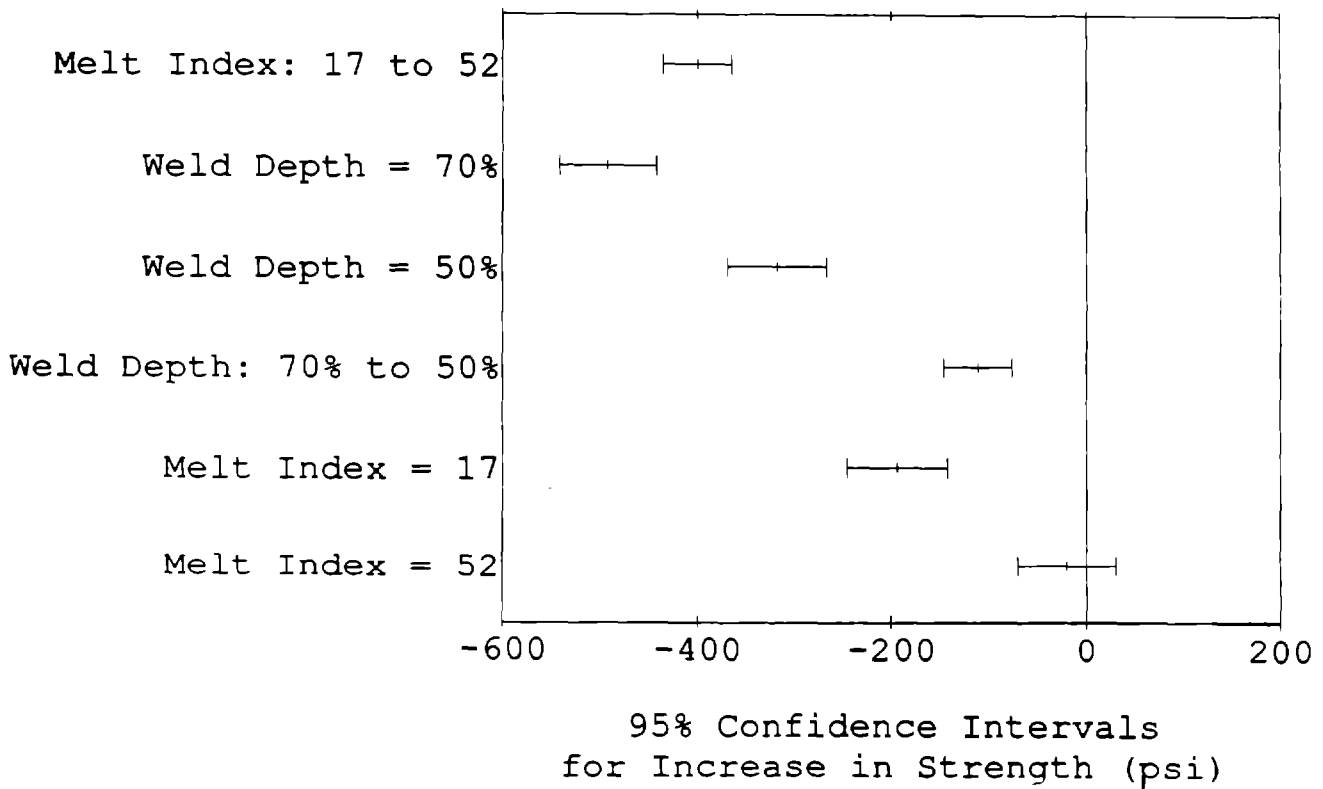


Figure 3-26. Interaction Effects of Melt Index with Weld Depth on Weld Strength, Experiment #1

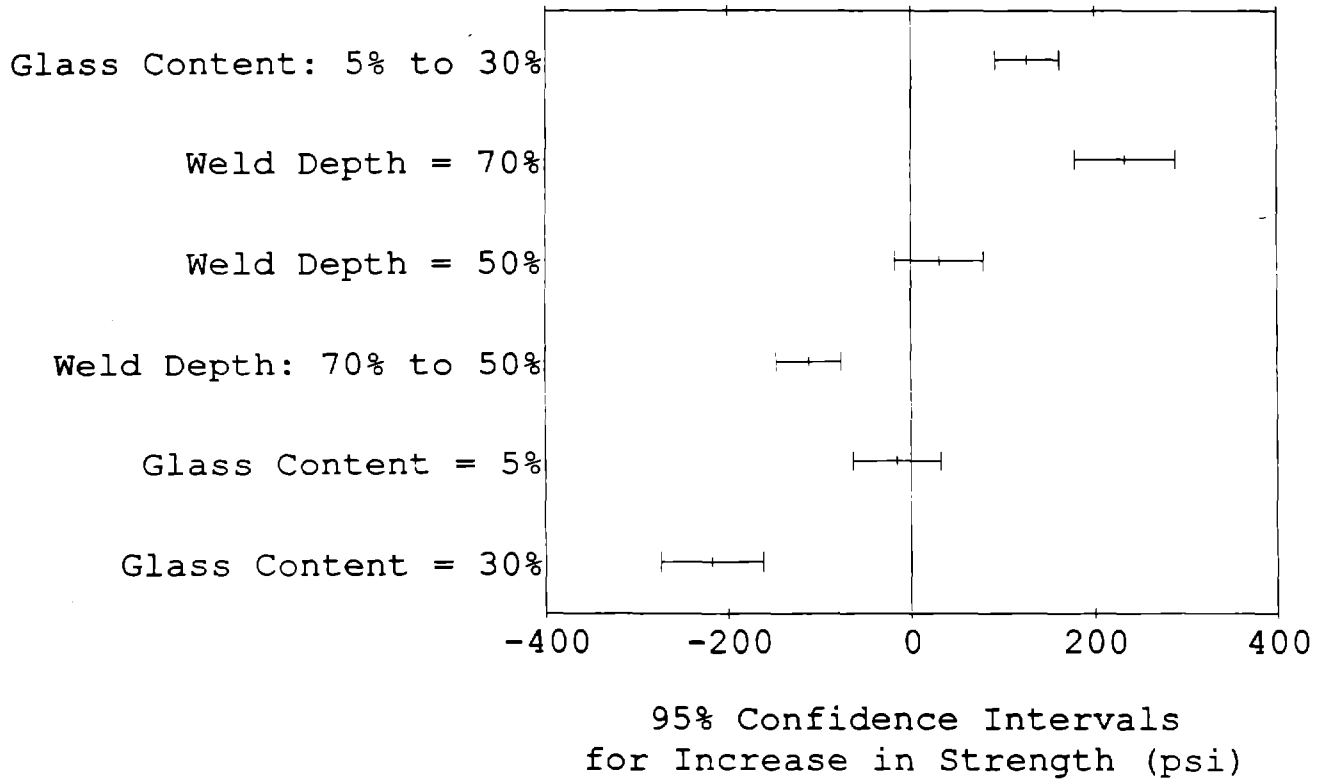


Figure 3-27. Interaction Effects of Glass Content with Weld Depth on Weld Strength, Experiment #1

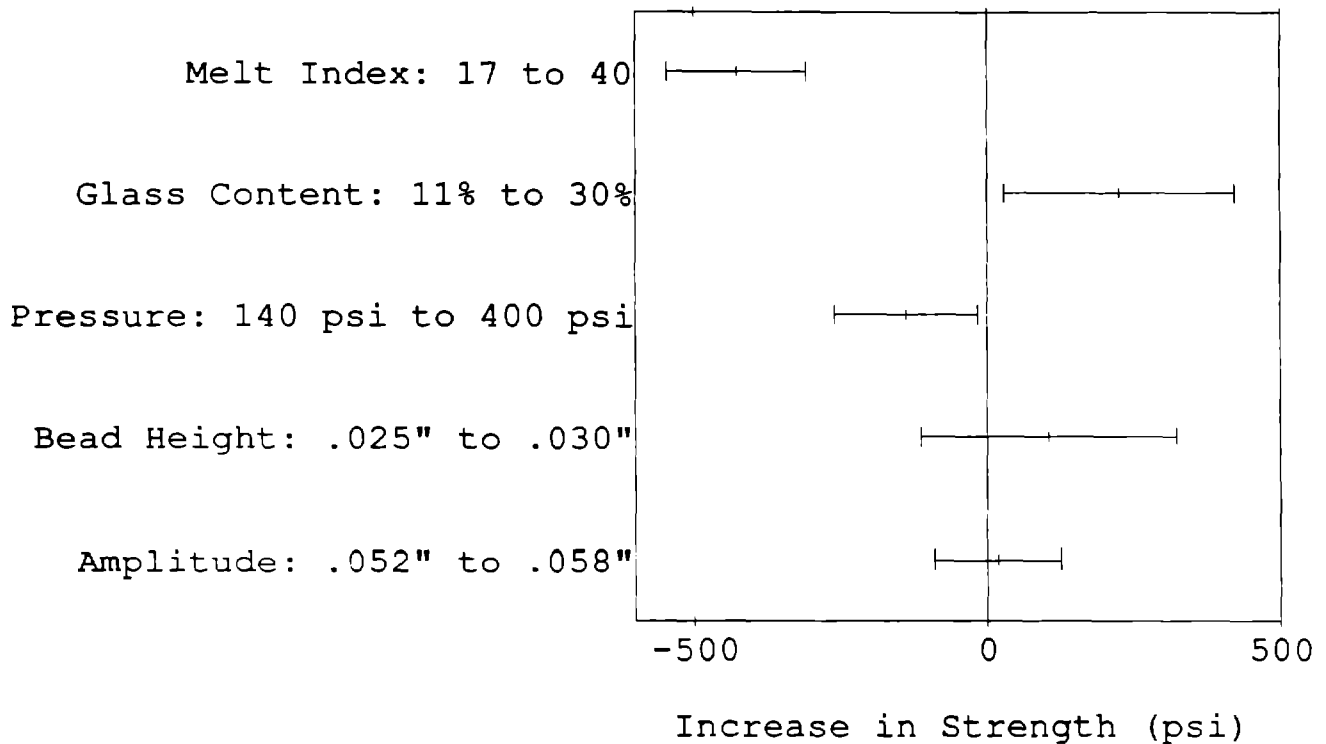


Figure 3-28. Main Effects on Weld Strength (with 95% Confidence Intervals), Experiment #2

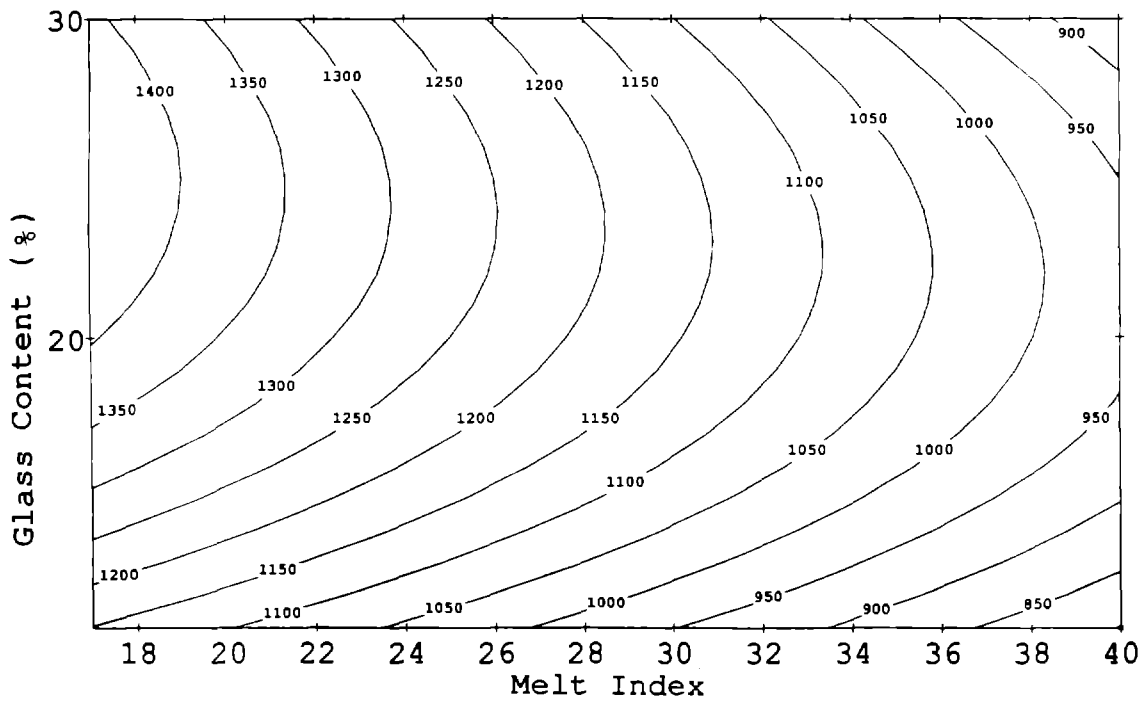


Figure 3-29. Weld Strength (psi) vs Melt Index and Glass Content at Pressure = 140 psi, Bead Height = 0.025", Amplitude = 0.052", Experiment #2

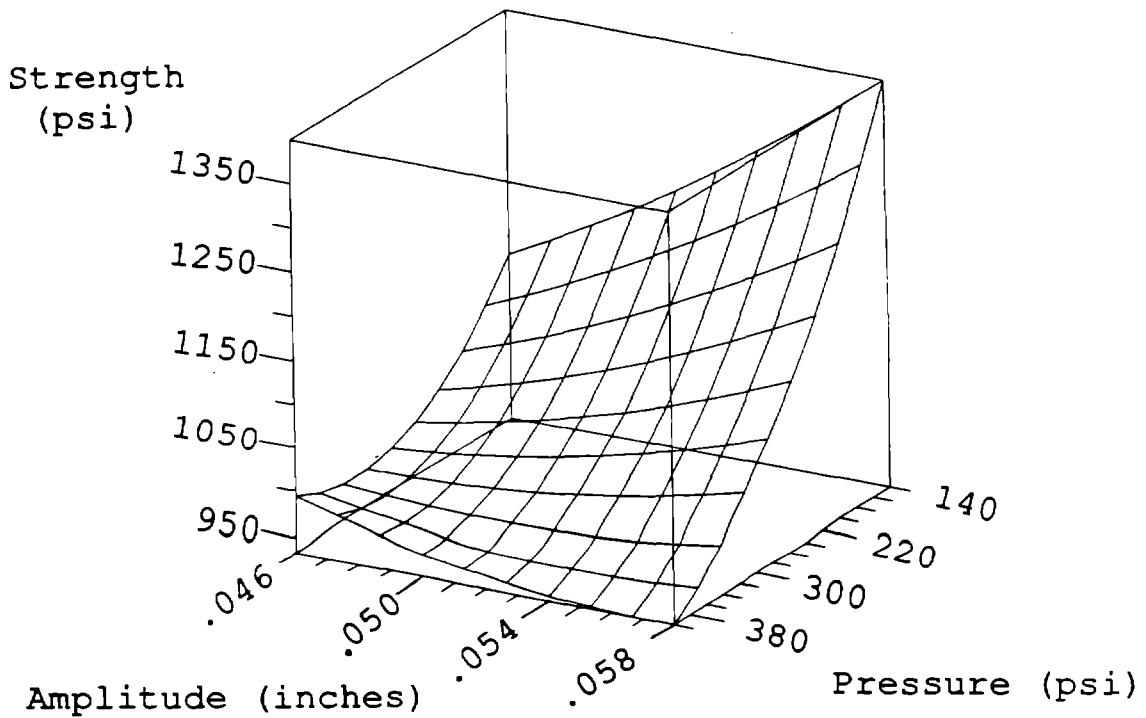


Figure 3-30. Weld Strength (psi) vs Pressure and Amplitude at Melt Index = 30, Glass Content = 11%, Weld Bead Height = 0.020", Experiment #2

In experiment #2, the strength variation with respect to direction of vibration, i.e., vibration along the length of the weld bead as opposed to across the bead, was found to be negligible.

Experiment #3: Emphasis on Weld Bead Size

Three weld bead widths and heights were compared. The strength in pounds per linear inch of weld bead vs weld bead width are given as raw data in Figure 3-31. The 0.160"-wide beads showed unexpectedly high strength, but it was due at least in part to the curvature of the cross section of the weld bead frames. These 0.160" frames were made thicker to hold up to the expected higher force required to shear the welds, and as a result, more distortion occurred in the injection molding. This resulted in the edges of the frame being welded in addition to the weld bead itself and skewed the data. An attempt is being made to retest some of these samples to confirm the wide bead results.

For the widest beads, strength increased with decreasing bead height, but the opposite was true for the narrowest beads. Figures 3-32a and 3-32b are response surfaces of strength vs weld bead height and bead width showing these effects. The "edge-welding" effect may have occurred here, also.

Experiment #4: Emphasis on Welder Parameters

The effect of welder pressure and amplitude on strength described in Experiment #2 is more apparent here. The strength is quantified in Figure 3-33, while a more intuitive view of what happens is shown in Figure 3-34, a 3D plot of the same parameters.

In summary, the type material used in the battery flow frame currently is 30 melt index, 11% glass content. The strongest welded material was 17 melt index, 30% glass content. Therefore, the glass content should be increased to perhaps 20% or even higher along with a corresponding increase in melt index to compensate for the anticipated difficulty in successfully producing injection molded parts. These parameters will have to be changed cautiously, to ensure that the mold filling will not be a problem.

The study to find the height for the strongest weld bead was inconclusive. However, 0.020" seems to be as strong or stronger at wide bead widths, and should be more conducive to successful mold filling. The wider beads are stronger, and should be used with space constraints in mind. The analysis done in Computer-Aided Engineering Design System (CAEDS) in conjunction with this study indicates that a double 0.120"-wide bead should be used for the center bead on the new frame.

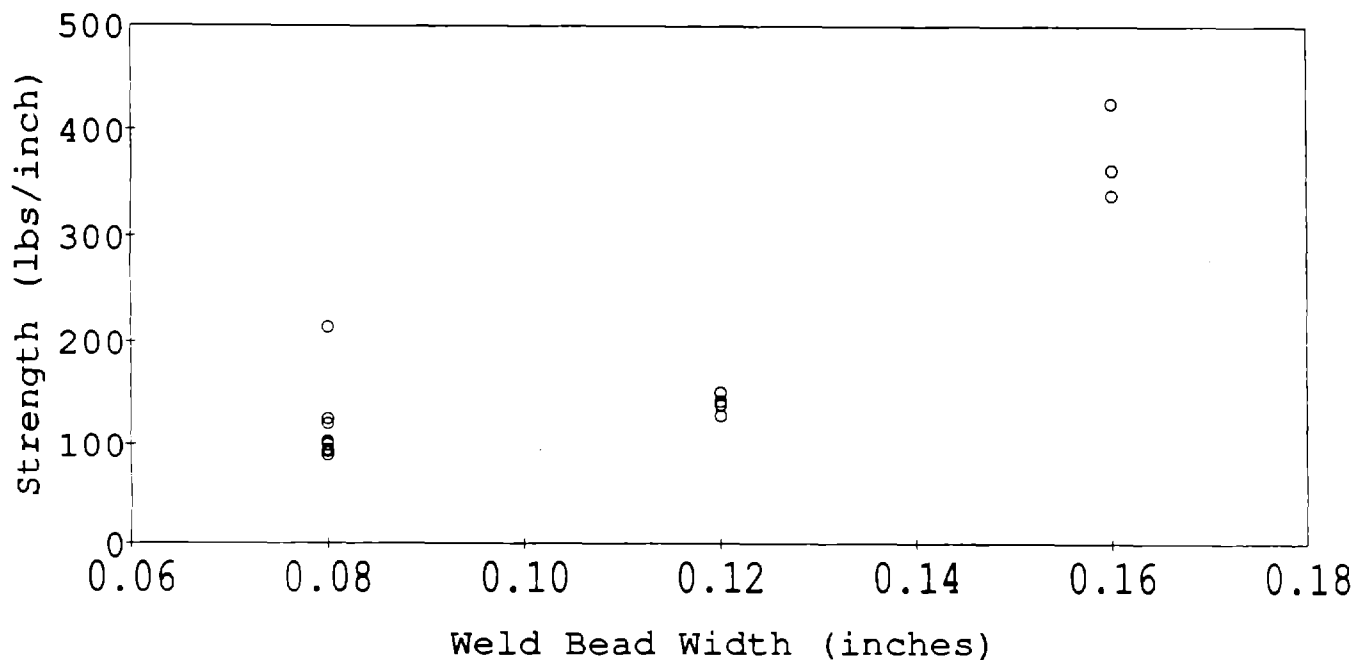
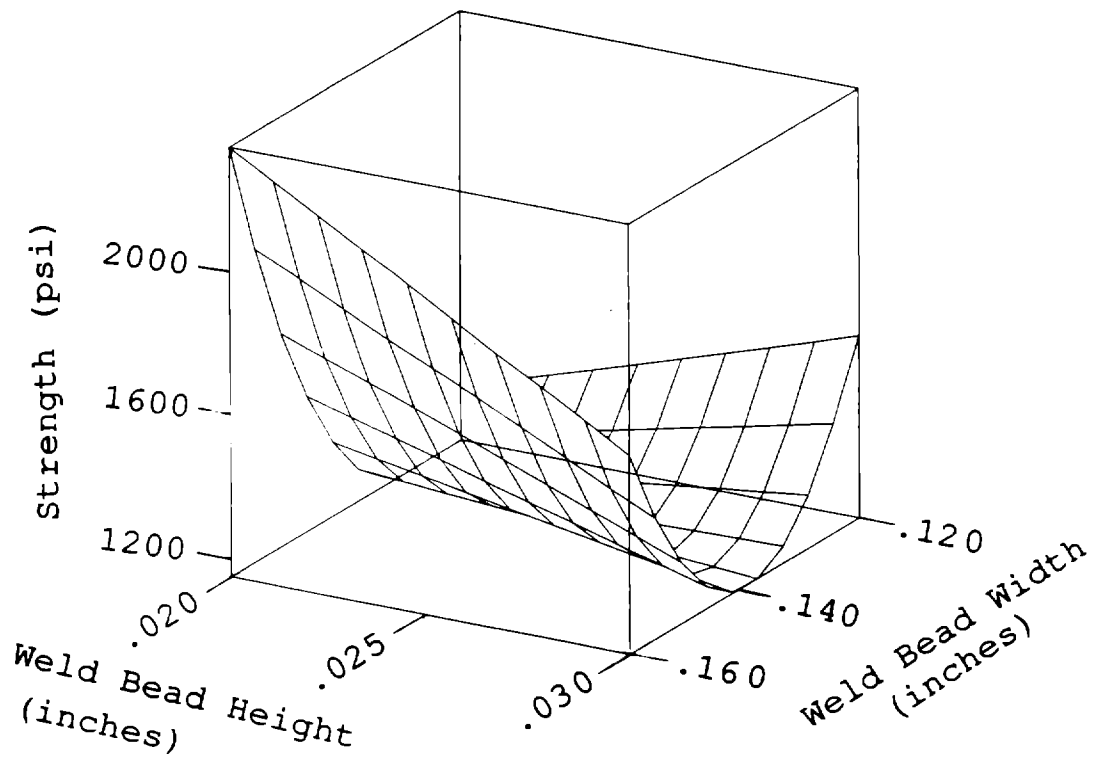
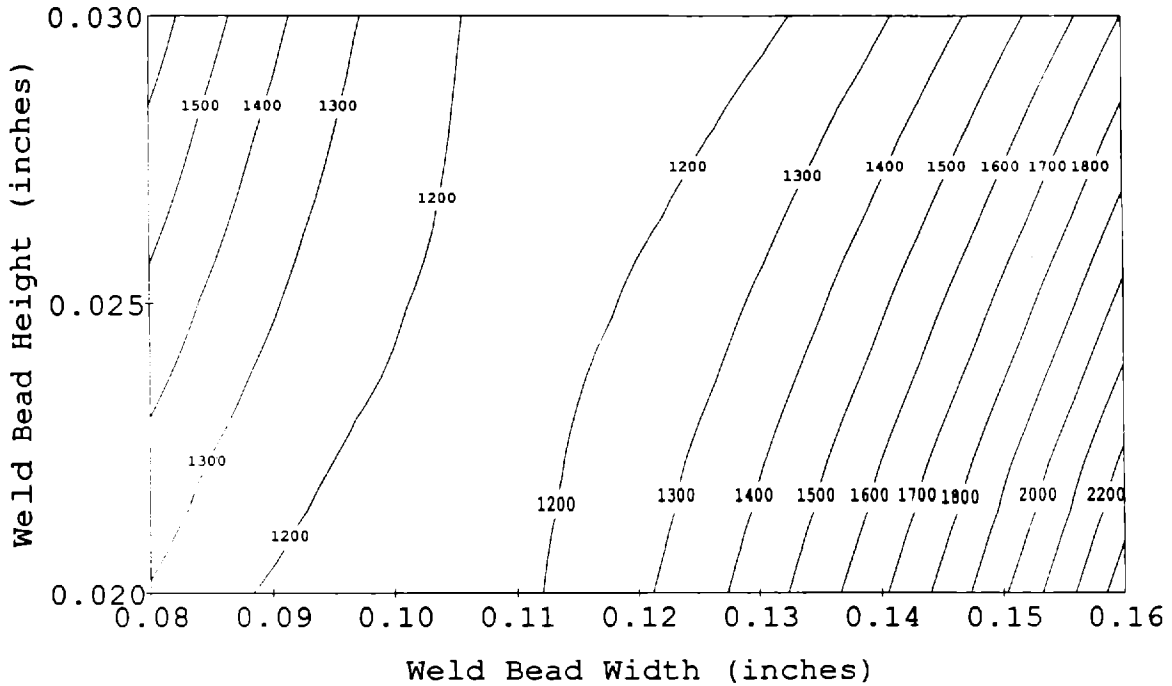


Figure 3-31. Weld Strength per Linear Inch vs Bead Width (17 Melt Index, 30% Glass Content, various welder parameters), Experiment #3



(a)



(b)

Figure 3-32. Weld Strength (psi) vs Weld Bead Size (Weld Pressure = 400 psi, Amplitude = 0.046", Depth = 70%), Experiment #3

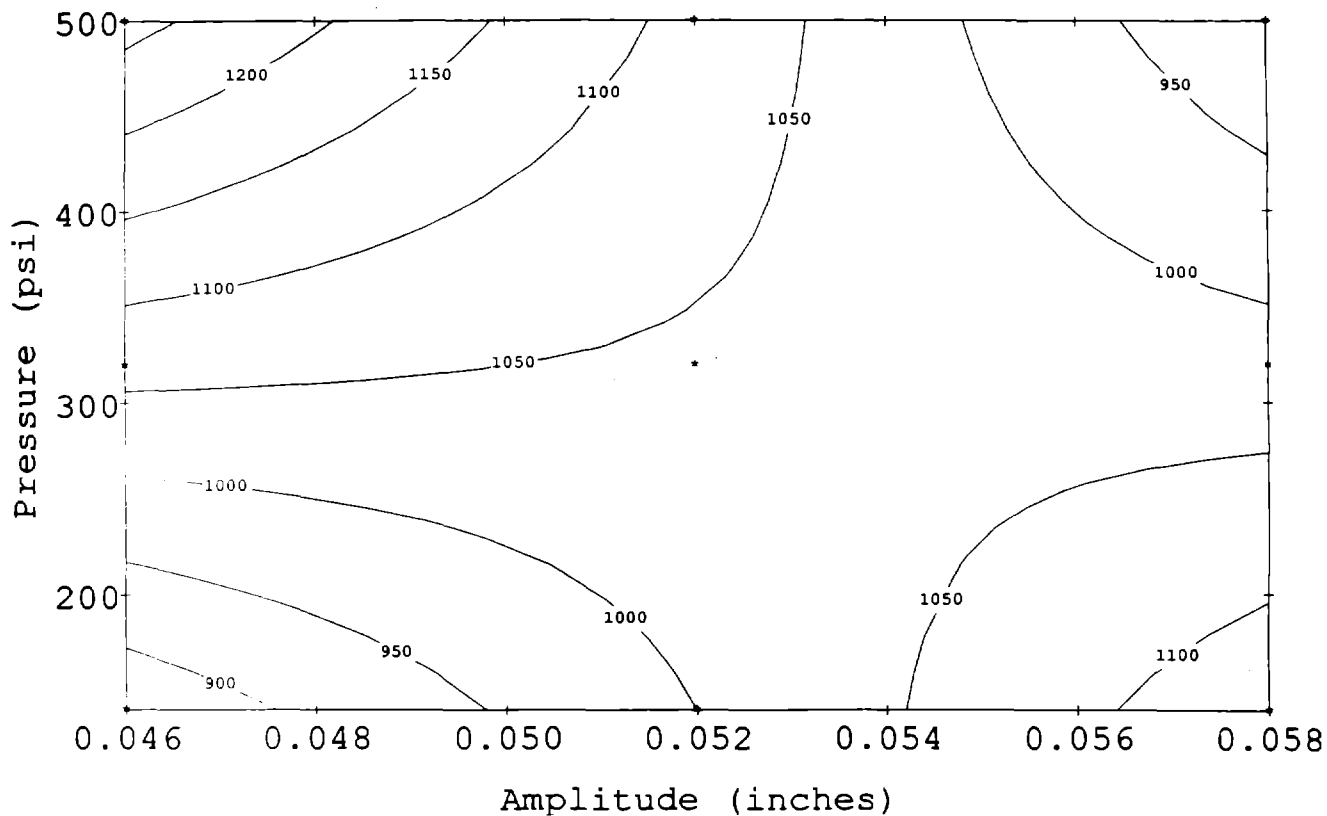


Figure 3-33. Contourplot of Weld Strength vs Welder Parameters (30 Melt Index, 11% Glass; 0.120" Wide, 0.020" High Bead), Experiment #4

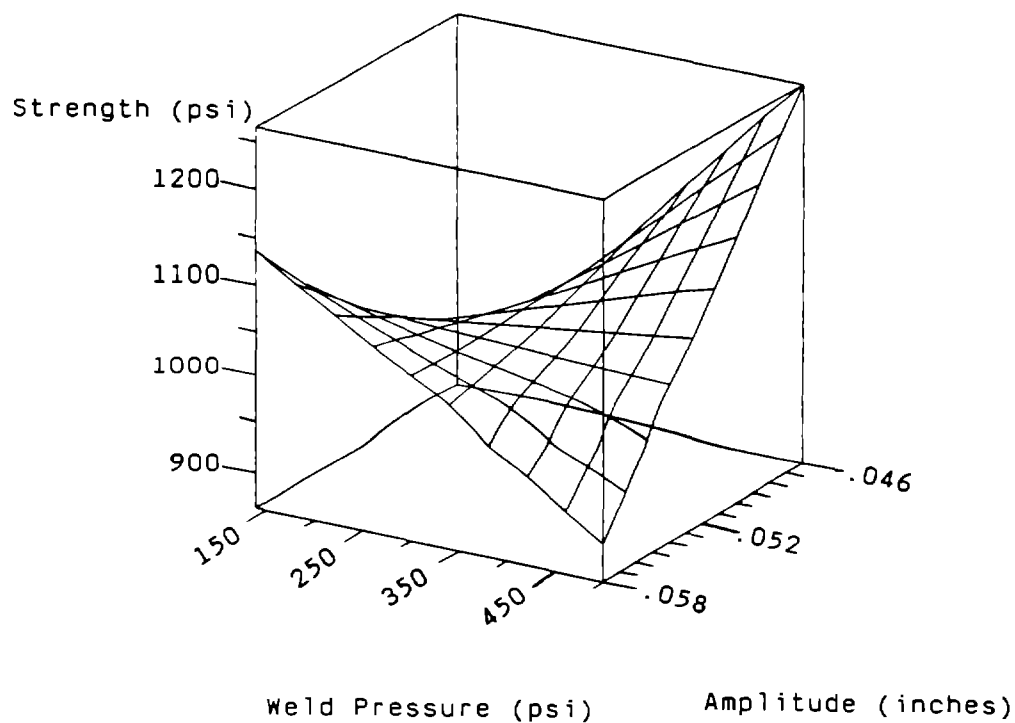


Figure 3-34. 3D Plot of Strength vs Welder Parameters, Experiment #4

The optimal vibration welder parameters for strong welds are: at high pressure, use low amplitude; and at low pressure, use high amplitude. Since previous experience has shown that plastic flash is more of a problem at low pressures, the parameters should be set for high-pressure operation. Alternatively, low pressure with a corresponding increase in amplitude could be used if tooling slippage were encountered.

Finite Element Analysis Modeling

The finite element analysis package used for frame design modeling is CAEDS. The weld beads were analyzed for stresses to find out where the highest stresses occur, and what the magnitudes of the stresses are at that location. The flow distribution over the frame was also analyzed to make the flow more uniform.

Only one quarter of a flow frame is modeled. Symmetry is used to reduce the size of the model, and still get accurate results. For modeling weld bead stresses in normal operation, a 10 psi electrolyte pressure was applied. At this pressure, the highest stress is 395 psi and is located at the center weld bead. In actual battery stack burst tests, the stacks failed at 26 psi. The equivalent weld bead stress at this pressure is 1028 psi. The welded coupon strength of this material is 985 psi, which is in agreement to within about 4%.

On a 2330 cm² electrode, a double 0.120"-wide center weld bead on the frame will see a stress of 992 psi at 26 psi electrolyte pressure, which gives a similar factor of safety.

When analyzing the flow distribution over the current frame, the model predicted a flow very similar to what was seen in the videotaped flow tests. The diverter pattern was changed for improved flow, and that new pattern is being modeled to determine if it can be further improved.

In the new flow frame design, CAEDS will reduce the design time by balancing the flow before cutting the mold, as well as assure a properly sized weld to avoid leaks.

Burst Tests

Several stacks were pressurized with air to determine the failure pressure and mechanism. The stacks were built by vibration welding four flow frames between standard endblocks. All of the parts had two weld beads in the center. Table 3-9 summarizes the tests, failure points, and failure pressures. The unfilled and filled centers refer to the open groove in the terminal plate. In some cases, the welds failed; in other cases, the stack material broke.

The test results indicate that the stacks can withstand a pressure of 26 psi before failure. Since the batteries are operated at design pressure of 10 psi, this gives a safety factor of 2.5.

Materials

Electrodes

Extruded Materials

A series of carbon plastics was compounded by Modern Dispersions in August 1990. Table 3-10 lists the compositions, with their measured resistivities and expansion in bromine vapor.

These compositions used no glass fiber. The first six materials were prepared according to a preplanned experimental design, whose purpose was to explore effects of composition, amount of shear, and presence or absence of coupling agent. The results from the first series were used to determine the direction of the second series. In the second series, high density polyethylene (HDPE, melt index of 20) was used, with a higher loading of Ketjenblack EC300J (20 wt%, materials 7A and 7B). Material 11 was made at an earlier time, but was included in this table as another data point. It used 23.5% Ketjenblack and the same HDPE.

The other materials in the second series used linear low density polyethylene (LLDPE) with Cabot XC-72 carbonblack. LLDPE is almost as stable to bromine as HDPE, but it is more flexible. XC-72 is a lower-surface-area, less-expensive carbonblack than Ketjenblack. Modern Dispersions, Inc. (MDI) recommended XC-72 because they have more experience with it.

The effect of Ketjenblack loading on expansion in bromine vapor is shown in Figure 3-35. The expansion increases with loading, to a high of about 2.5%. The XC-72/LLDPE materials expanded about the same amount as the Ketjenblack/HDPE compositions.

Controlling the shear rate via the RPMs of the compounding machine did not appear to have a clear effect on the resistivity, nor was it practical. According to MDI personnel, the shear experienced by the compound was a function not only of the machine speed but also the viscosity of the compound (which changed with composition).

Somewhat later in the year, a second set of electrode composition experiments was done. The purpose was to investigate ways to maximize the conductivity. As before, these compositions did not use any glass fiber. Combinations of graphite and Cabot XC-72 black were used to impart conductivity. Graphite particles are

Table 3-9. Burst Tests Results

| Test | Failure Point | Pressure (psi) |
|---------------------------|--------------------------|----------------|
| 1. Unfilled center | Interior frame | 17 |
| 2. Filled center - w/Like | Endblock cover weld | 21 |
| 3. Filled center - w/HDPE | Endblock cover weld | 26 |
| 4. Standard build | Endblock material | 26 |
| 5. Standard build | Frame material and welds | 26 |

Table 3-10. Results of 8/91 MDI Compounding Trials

| Material | Composition | Resistivity (Ω -cm) | Expansion* (%) |
|----------|-----------------------------------|-----------------------------|----------------|
| 1 | HDPE, 16% K**, lo shear, no CA# | 22.1 | 1.94 |
| 2 | HDPE, 16% K, med shear, CA | 10.2 | 2.10 |
| 3 | HDPE, 16% K, hi shear, no CA | 12.3 | 1.80 |
| 4 | HDPE, 18% K, lo shear, CA | 6.4 | 2.00 |
| 5 | HDPE, 18% K, med shear, no CA | 6.5 | 2.06 |
| 6 | HDPE, 18% K, hi shear, CA | 4.5 | 2.27 |
| ----- | | | |
| 7A | HDPE, 20% K, lo shear, CA | 4.6 | 2.70 |
| 7B | HDPE, 20% K, hi shear, CA | 5.7 | 2.47 |
| 8 | LLDPE, 36% XC-72, lo shear, CA | 2.2 | 2.73 |
| 9 | LLDPE, 36% XC-72, lo shear, no CA | 2.2 | 2.90 |
| 10A | LLDPE, 32% XC-72, lo shear, CA | 3.0 | 1.94 |
| 10B | LLDPE, 32% XC-72, hi shear, CA | 2.5 | 3.61 |
| 11 | HDPE, 23% K, no CA | 13.0 | 2.59 |

* After 24 hr in bromine vapor

** K = Ketjenblack

Organotitanate coupling agent, 0.5 wt%.

CA - coupling agent

plate-shaped so they have a higher aspect ratio than amorphous carbon; this means for a given volume percent loading, graphite is expected to impart better conductivity than spherically or irregularly shaped carbon particles (assuming equal bulk conductivities for the two fillers). Unlike Ketjenblack, graphite was found to be capable of being incorporated in very high loadings

(40% or higher). The compounding was done simply by mixing the materials as powders, then compression molding. The resistivities of these formulations are given in Table 3-11.

Note that these measurements were for 0.100"-thickness sheets. For thinner sheets, resistivity was

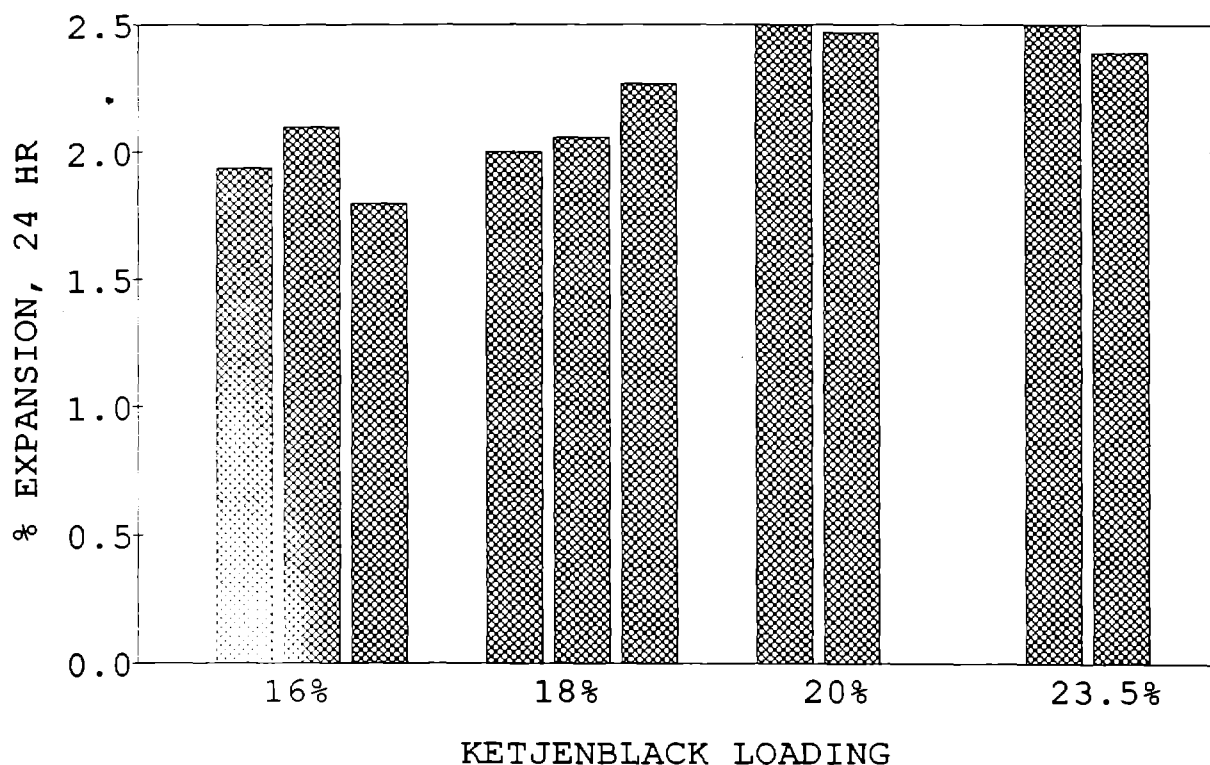


Figure 3-35. Expansion of Ketjenblack Composites in Bromine Vapor (no glass fiber)

Table 3-11. Resistivities of HDPE/Graphite/Carbonblack Composites

| Wt% LDPE (4.5 MI) | Wt% Graphite | Wt% XC-72 | Resistivity (Ω -cm) |
|-------------------|--------------|-----------|-----------------------------|
| 80 | 20 | 0 | 402 |
| 80 | 10 | 10 | 336 |
| 80 | 0 | 20 | 44 |
| 60 | 40 | 0 | 338 |
| 60 | 20 | 20 | 3.1 |
| 60 | 0 | 40 | 0.39 |
| 40 | 60 | 0 | 13.5 |
| 40 | 30 | 30 | 0.19 |
| 40 | 0 | 60 | (brittle) |

higher. As an example, a 0.025"-thick sheet of the 40/30/30 material had a resistivity of 1.10 Ω -cm.

The results of this study showed that formulations could be made with substantially lower resistivities than that of typical extruded glass-fiber filled conductive plastics. However, the usefulness of these formulations

is limited because the present state-of-the-art extruded materials require glass fiber to resist bromine-induced expansion.

In March 1991, MDI compounded another set of carbon plastic compositions, this time with glass fiber. Two series of compositions were made. Both series

used 16 wt% glass fiber. One series used Ketjenblack; the other used Cabot XC-72. Again, XC-72 was used because MDI's equipment was reportedly more suited to it.

The Ketjenblack compositions ranged from 13% to 20.5% Ketjenblack, in increments of 1.5%. Higher loadings were planned, but were not feasible to run on MDI's equipment. Similarly, Cabot XC-72 compositions ranged from 25% to 28%, in increments of 1.5%.

Resistivity and tensile strength results are shown in Figures 3-36 and 3-37. Note that while it is possible to achieve somewhat lower resistivity with Ketjenblack compositions, this is done at the expense of the tensile strength. In addition, the properties of the Ketjenblack compositions are very sensitive to the loading, compared to the Cabot XC-72 compositions that do not vary nearly so much with loading. Again, these results may only hold for the type of equipment used for the compounding.

Bromine expansion test results are shown in Figures 3-38 and 3-39. Figure 3-38 shows the results for the Ketjenblack compositions. The expansion results are for 24 hr and did not increase substantially after several more days. They are all in the range of 1.0 to 1.5%, and

do not increase with increased loadings of Ketjenblack. In this respect, the results are different than for composites of Ketjenblack and HDPE (without glass fiber) shown in Figure 3-35. Note also that the addition of glass fiber greatly reduces the total amount of expansion.

Figure 3-39 shows expansion of XC-72 (+ glass fiber) composites. The expansion of these composites is slightly less (at an equivalent resistivity) compared to that of the Ketjen composites. This may be due to the slightly lower plastic content of the XC-72 composites.

Approximately 1000 lb. of 0.025" nominal thickness electrodes were extruded by Penn Fibres on 5-17-91. The composition was 26.5% Cabot XC-72 black, 16% glass fiber, and 57.5% HDPE [0.29 melt index (MI)]. MDI compounded the mixture. A resistivity of 9.1 Ω -cm was measured for the 0.025" extruded sheet. The previous batch of extruded electrode sheet from Penda measured 27.1 Ω -cm using the same method. The conductivity improvement in the May 1991 electrodes was attributed to MDI's better capability for compounding formulations with Cabot XC-72 carbon black.

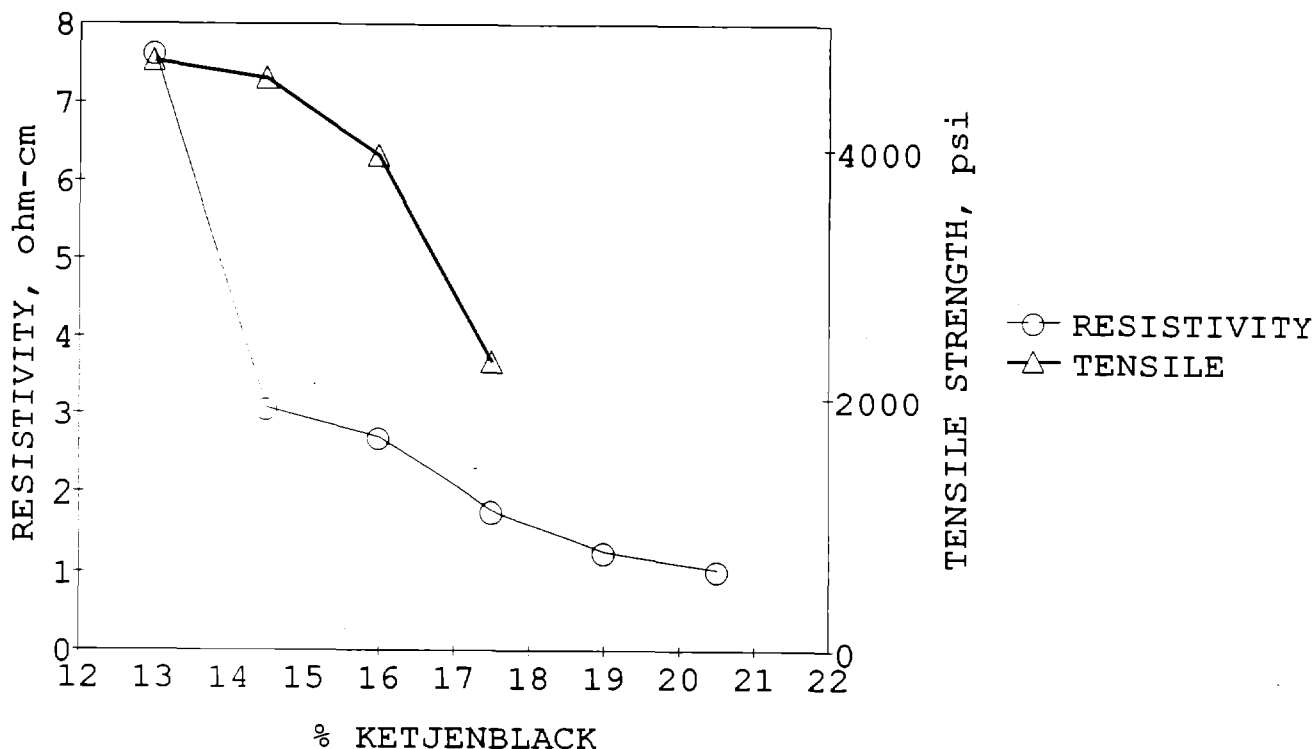


Figure 3-36. Properties of Ketjen Composites (0.3 MI HDPE + 16 wt% glass fiber)

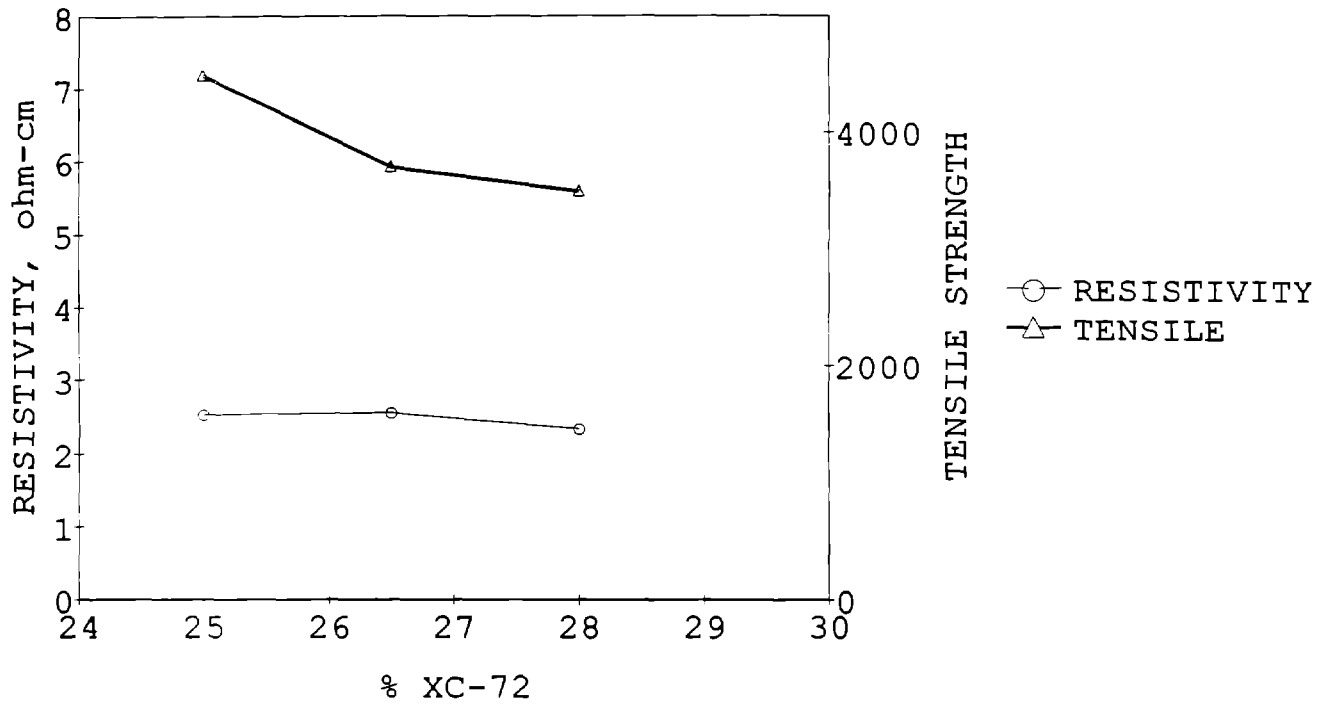


Figure 3-37. Properties of XC-72 Composites (MDI 3/91) (0.3 MI HDPE + 16 wt% glass fiber)

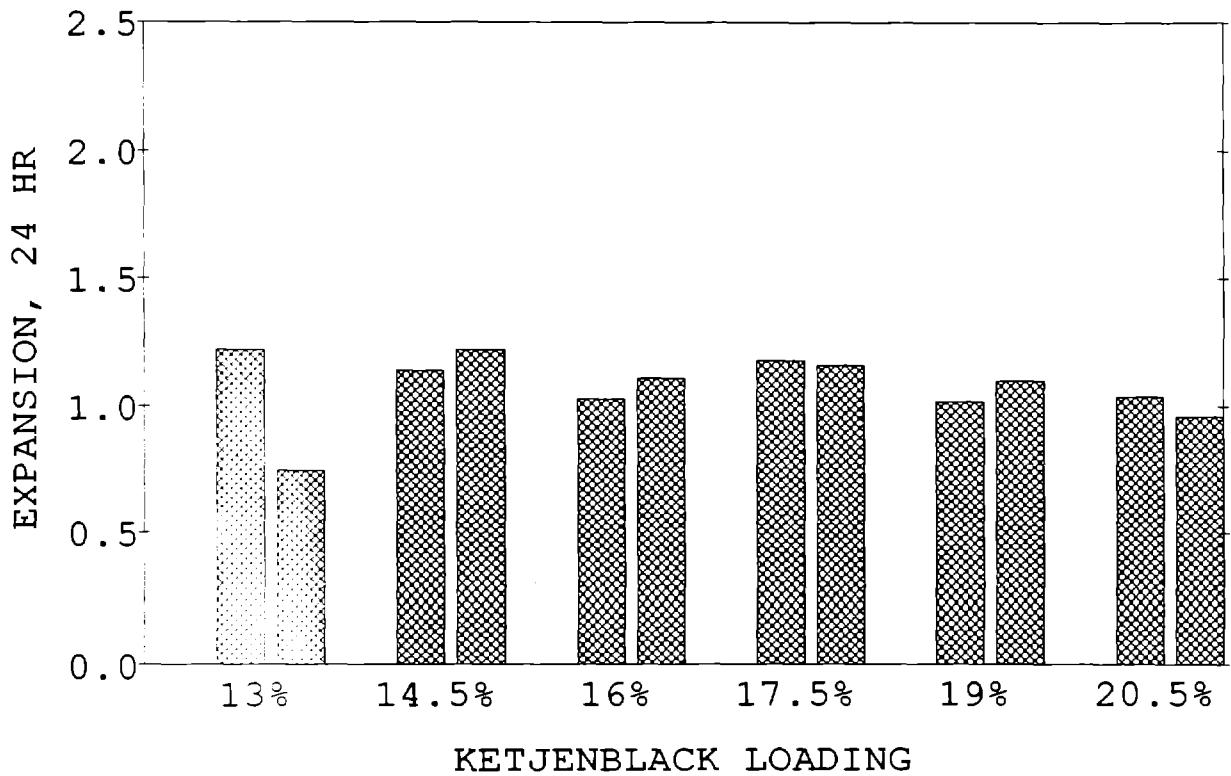


Figure 3-38. Expansion of Ketjenblack/Glass Fiber Composites in Bromine Vapor

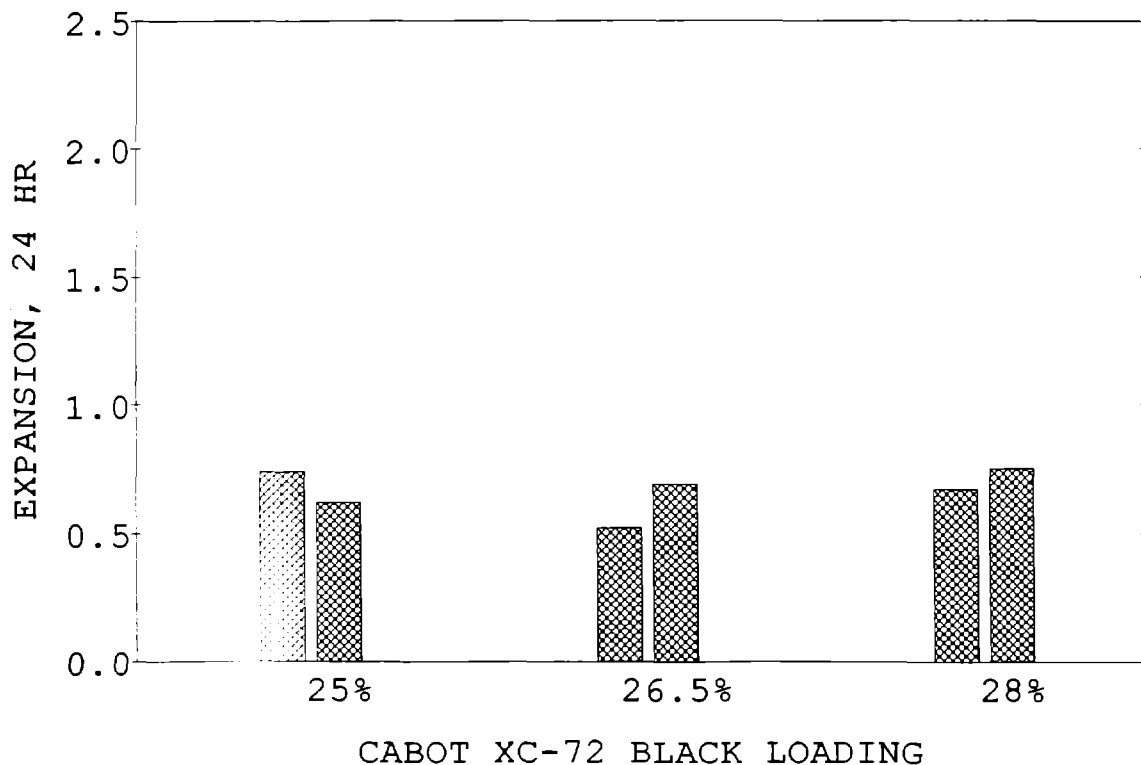


Figure 3-39. Expansion of XC-72 Black/16% Glass Fiber Composites in Bromine Vapor

Expansion of the May 1991 material after 48 hr in bromine vapor was 0.38% in the machine direction, 1.64% in the cross-machine direction, and 2.13% in thickness.

Water Slurry Process Electrodes

The first large run of the Radlite electrode material took place at Azdel, Inc., on September 13, 1991, and produced about 900 lb. of 52" x 12" sheet. Radlite is the trade name for Azdel's water slurry process for making polyolefin sheet with high loadings of very long glass fibers. The composition was specified to be 35-40 wt% glass fiber, 14 wt% Ketjenblack, and the remainder, 20 melt index polyethylene.

Reportedly, there were no major problems with the run; thicknesses of the semi-consolidated sheet were approximately 0.050" to 0.060". Small pieces of this material were able to be consolidated (densified by hot-pressing) down to 0.025" to 0.030". The resistivity is in the range of 5 Ω -cm after consolidation. Pieces of this material large enough for batteries were extremely difficult to consolidate due to the high pressures required.

Battery V1-42 was made with Radlite electrodes. It was torn down at 47 cycles because it leaked from the anode studs. The Radlite electrodes (surprisingly) did show some warpage. The warpage did not appear quite

as extensive as with extruded electrodes, but was greater than expected from accelerated tests of Radlite in bromine vapor. Additionally, zinc plating was spotty in places, suggesting porosity or disruption of plating by large concentrations of glass fiber just under the surface.

A general problem with Radlite (as well as with Taffent, its counterpart material made by Exxon) is that the consolidation process they use only applies very light pressure (around 30 psi). Azdel supplied their material to JCBGI in "semi-consolidated" form, so it required further pressing. Unless the plastic has a very low viscosity, the final consolidated product tends to be porous. The direction of future effort will have to be to make carbon plastic with as low a viscosity as possible, to maximize the wet-out of the glass fibers, and probably to use a glass fiber content considerably lower than the present 40 wt%. Even with these modifications, it is almost certain that Azdel will only be able to semi-consolidate the sheet. Full densification will have to be accomplished through a secondary batch process that consists of hot pressing in a very large hydraulic press, which will add considerably to the cost.

Exxon prepared a similar material for JCBGI, from a formulation of 36% Cabot XC-72 black in 20 MI linear low density polyethylene. About thirty 11"x16" pieces of the product were received. The specification called

for 35-40% glass fiber loading. Thermal gravimetric analysis (TGA) indicated a glass fiber loading of 29.4 wt% in the product. As received, the thickness of these electrodes was 0.025" and the resistivity was excessively high, in the 50 to 200 Ω -cm range. When the electrodes were held in front of a light, some pinholes were visible.

These electrodes were fairly easily hot-pressed (two electrodes pressed to 0.025" thickness) and the pinholes were eliminated. The resistivity also decreased to 16 Ω -cm. Obviously, the Taffent electrodes as supplied were incompletely consolidated, resulting in voids and less-than-optimum particle-to-particle contact. When asked about this, Exxon replied that they could try to laminate thin pieces of carbon plastic on either side of the porous material. However, this is not really a viable approach, since very thin carbon plastic is not readily available.

Presently, extrusion appears to be the only viable process for economically producing electrodes.

Experimental Separator

Experimental Separator Materials

Along with extruding, small batches of separator base materials were compounded and compression molded to produce 0.025" sheets that could then be tested using standard methods. Little or no difference in properties could be determined between extruded and compression molded sheets having the same composition. An advantage of this approach is that it costs less per sample than extrusion.

Several small (50-70 g) batches of polyethylene- and kynar-based separator compositions were produced this way. Table 3-12 shows the test results of these samples. These were the first results using the load-leveling electrolyte formulated for this program. With this electrolyte, bromine transport measurements tend to be lower and resistivity measurements tend to be higher than with EV electrolyte. Asahi SF-600 and "standard" extruded zinc/bromine separator properties are compared against those of samples made with different silica-to-plastic ratios and with kynar instead of polyethylene.

The most important finding from this testing was that the bromine transport, for the most recently produced experimental material, was much higher than expected. At first it was not clear whether this increase

Table 3-12. Properties of Compounded Compression-Molded Separator Materials

| Separator Material | Thickness (mm) | Resistance (Ω -cm ²) | Br ₂ Flux* (10 ⁻⁹ mole/sec-cm ²) |
|---|----------------|--|---|
| Asahi SF-600 | 0.60 | 1.28 | 3.3 |
| Advanced Zn/Br EV* (extruded) | 0.61 | 0.75 | 6.0 |
| EV, comp. molded (180°C) | 0.40 | 0.67 | 6.4 |
| EV, comp. molded (190°C) | 0.40 | 0.68 | 7.1 |
| EV, comp. molded (200°C) | 0.46 | 0.66 | 6.8 |
| 55% SiO ₂ /45% UHMWPE** | 0.53 | 1.59 | 10.7 12.6 |
| 55% SiO ₂ /22.5% UHMWPE/22.5% HDPE | 0.51 | 1.79 | 11.7 8.6 |
| 60/40 Kynar/SiO ₂ (DBP plasticized) | 0.60 | 1.76 | 7.6 |

* proprietary material

** ultra high molecular weight polyethylene

was caused in part by the different electrolyte used for the test, since earlier runs of extruded separator had properties closer to that of the Asahi material. Later investigations found that the type of silica was different from previous extrusion runs. The separator manufacturer claimed that the two types of silica were equivalent and had been used somewhat interchangeably in their commercial product. They report that there were few detectable differences in the properties of the two silicas. So while this may be a factor, it is probably not the entire cause of the problem. Another possible factor was that the silica loading may have been too low. Ash tests of the experimental separator showed slightly less silica than the specification.

Future work will explore the use of other types of silica, and will investigate polymers other than polyethylene.

Ion-Exchange Coatings for Separators

Several pieces of 10.5" x 12" experimental separator and Asahi SF-600 were sent to C. Arnold of SNL for coating with Nafion and other ion-exchange resins. Nafion is a fluorocarbon polymer with sulfonic acid groups. The separator sheets sent to SNL were of a size large enough for testing in JCBGI's miniature cells.

The coated SF-600 samples received from SNL were tested for bromine transport. The results were 1.26 and 1.29×10^{-9} mol/cm²-sec. For untreated SF-600, the measurement was 3.37. However, the increase in resistivity as measured by JCBGI was of the same magnitude. An additional problem was that the coated separators could no longer be welded into polyethylene frames. A method was worked out to allow the coated separators to be tested in cells without having to weld them.

Asahi separator treated with a similar type ion-exchange resin from Eastman fared somewhat better. The treatment increased the resistivity by only 17%, while it decreased the bromine transport by 43%. When this material was tested in a miniature cell, it gave an improvement in coulombic efficiency of about 2% and a slight decline in voltaic efficiency. The net result was an energy efficiency improvement of about 1%. This is a small but significant improvement. It may prove to be more significant under different cycle conditions, e.g., slower charge/discharge rates and/or long stand times.

Glass Fiber-Filled Polyethylene for Frames

Owens-Corning 415-CA chopped glass fibers used in the preparation of extruded electrodes and injection-molded frames show a surface effect when exposed to standard load-leveling electrolyte and two phase

catholyte solution. To test the fibers, they were initially dried for 2 hr at 250°F, weighed to three decimal places, and immersed in the two solutions for one week at room temperature. Then the fibers were filtered and rinsed thoroughly with distilled water. Finally the fibers were dried at 250°F and weighed after 2 hr, and again after 4 hr of drying.

The weight of the fibers in each case was essentially the same after 4 hr as it was after 2 hr, indicating that the fibers were thoroughly dried after 4 hr. In the case of standard load-leveling electrolyte, the weight increased 2.4% after immersion for 1 week. These fibers were also noticeably a darker yellow color than the original fibers. The weight of the fibers immersed in the two-phase catholyte solution increased 1.9% after 1 week and the color changed from a light yellow to a grey-brown color.

The glass fibers were analyzed by Energy Dispersive X-Ray (EDX) to determine the elemental make-up of the surface. No zinc or bromine was found on the surface of the untreated fibers, but both were found to be on the surface of the treated fibers. The fibers immersed in load-leveling electrolyte contained 0.81 atom% zinc and 1.47 atom% bromine, while the fibers treated with two phase catholyte had 0.61 atom% zinc and 1.75 atom% bromine. These results indicate that zinc bromide electrolyte alters the surface of the glass fibers, but the effect this has on actual battery component properties is not known at this time.

Several pieces of frame material used in weld study testing (11% glass, 30 MI) were exposed to two-phase catholyte and pure polybromide complex phase for one week and compared to the virgin material using ESCA. Surface studies indicate significant decreases in the silicon and oxygen contents at the surface, which suggests degradation of the silane coupling agent used in processing the fibers. Also the bromine appears to have reacted with some of the carbon atoms at the interface. The carbon could be from the HDPE, the silane coupling agent or an organic binder used on the glass fibers. Similar results were confirmed using FTIR and TGA to examine the bulk material. Bromine reacting with silanes and binders at the glass/HDPE interface may weaken the bulk frame material.

Spreadsheet Mass and Energy Balance

A Lotus-compatible spreadsheet was written that describes some of the mass balance and energy losses of test batteries. The spreadsheet does not predict energy losses, but shows which factors account for the measured loss. The value of the spreadsheet is that it can calculate how much of the electrolyte is being utilized

(important information when chloride salts are substituted for bromide), and the various trade-offs between diffusion losses and resistance losses can be clearly shown.

A copy of the spreadsheet written for the SNL #514 battery is given in Figure 3-40. The data entered consist of the volume and concentration of electrolyte, the amp-hr and watt-hr readings from a typical cycle, an estimate of the overvoltage at the zinc and bromine electrodes, and an estimate of the per cell resistance. From these numbers, the utilization of the zinc, bromide, etc., is calculated, and the ratio of bromine to complexing agent is determined. The overall efficiencies are calculated and can be compared to the results of the cycle from which the data were taken. The average voltage on charge and discharge are calculated.

The losses due to shunt currents are found through a multi-step process. First, the electrode and electrolyte gaps and resistivities are used to calculate resistances in the channels and manifolds. A calculation of the expected cell resistance is also made from component resistivities and dimensions. The calculated value is relatively close to the observed value. In the attached spreadsheet of battery SNL#514, the cell resistance is entered as 5.5 mohms, is calculated from the resistivities as 5.1 mohms, and is verified from the results as 6.0 mohms. A Basic language program supplied by S. Lott (SNL), based on work by Kaminski and Savinell, calculates the shunt currents in the channels and manifolds depending on the conditions. The program is run three times, one each for the different voltages on charge, open circuit, and discharge. The total current in the manifold is found by adding the current at each cell, and then the equivalent amps/cell are found by dividing by the number of cells. Since there are four manifolds, this value is multiplied by four. This represents the current that bypasses the cells in the battery and is entered into the spreadsheet.

The energy losses are calculated individually and the sum is compared to the actual measured loss. A difference of less than 10% is considered good. The energy losses are restated in terms of percent of the total. A slope of the overvoltage-free volts/amps taken from the currents and average voltages is calculated, as a check on the entered ohmic resistance. These numbers should also be in agreement.

The weakness of the spreadsheet is that it is a summary of the whole cycle. The resistance, concentration, diffusion rates, etc., change during the cycle. The spreadsheet calculations are based on the total performance during a cycle. As such, it is at best a semi-average.

The energy lost to bromine diffusion now closely matches that predicted by the FORTRAN Zinc/Bromine Model. However, the energy lost to shunt currents is still only half that predicted by the model.

Modeling

Battery Test Simulation

Many improvements and changes have been incorporated into JCBGI's Fortran zinc/bromine computer model to better calculate voltage profiles similar to those of an actual battery. This in turn means that efficiencies and discharge energy predictions have become more accurate. The battery voltage profile (V1-53, cycle #3) is compared to the original and improved models in Table 3-13 and Figure 3-41. Output from the model compares to an actual battery cycle as in Table 3-13.

Effect of Material Properties

Computer modeling has been used to examine the effects of material properties on zinc/bromine battery performance. Iterations over a range of material (electrode and separator) properties were run on the model and are plotted in Figures 3-42 to 3-45. Figure 3-42 shows the variation in energy efficiency with changes in electrode and separator thicknesses. Figure 3-43 demonstrates the effect of electrode resistivity on energy efficiency, while Figures 3-44 and 3-45 show the relationship of energy efficiency with separator resistivity and bromine transport respectively. These four plots indicate that improvements in resistivities and bromine transport could significantly improve battery performance.

Figure 3-42 indicates that decreasing electrode thickness could show a 0.5% increase in energy efficiency. The lower limit on electrode thickness would be determined by material property and warpage considerations. The separator thickness shows a peak in efficiency at 0.025" due to a trade-off between resistivity and bromine transport. The increase shown at very small separator thicknesses is due to an assumption in the model that bromine diffusion is governed by the smaller of the separator and bulk diffusion terms, but again lower limits would be dependent on the physical properties of the separator.

Figure 3-43 shows that improvements of 2% in energy efficiency could be obtained by using lower resistivity electrodes. Actual improvements of 1-2% (from 74-75% to 76-77%) in energy efficiency were observed when lower resistivity electrodes were used in V1-59 and V1-60. The model predicted voltage profile for a battery with low resistivity electrodes is compared

Inputs:

Electrolyte:

| | | | |
|-------------------|-------------|---------------------|----------------------|
| Volume | 54.57 liter | Number of Cells | 50 |
| ZnBr ₂ | 2.25 M | Area per cell | 1170 cm ² |
| ZnCl ₂ | 0.5 M | Anode Overvoltage | 0.011 V |
| Quat | 0.8 M | Cathode Overvoltage | 0.011 V |

| | | | |
|-------------------------------|-----------|--------------------|-----------------------|
| Resistivity | 14 Ohmcm | Meas. Resis. /cell | 5.5 mohm |
| Electrode C-Plastic Separator | 5.5 Ohmcm | Manifold Len./cell | 0.301 cm |
| Separator | 40 Ohmcm | Manifold Diameter | 1.5 cm |
| Electrode Thickness | 30 mil | Channel Length | 45.7 cm |
| Electrolyte Gaps | 65 mil | Channel Area | 0.051 cm ² |
| Separator Thickness | 23.5 mil | Resistance (calc) | 5.1 mohm |
| Electrode Thickness | 0.076 cm | R channel | 12545 Ohm |
| Electrolyte Gaps | 0.165 cm | R manifold/cell | 2.39 Ohm |
| Separator Thickness | 0.060 cm | | |

| | | | |
|----------------|----------|-------------------|-----------|
| Charge Current | 23.5 Amp | Discharge Current | 24.2 Amp |
| Charge Time | 4.7 hour | Discharge Time | 3.9 hour |
| Amp Hours in | 110.6 | Amp Hours out | 94.7 |
| Watt Hours in | 10529.0 | Watt hours out | 7456.0 |
| Stand time | 0.0 hour | Strip | 7.3 AmpHr |

| | | | |
|------------------|-----------|---------------------|-----------|
| Equiv. SC Charge | 0.131 Amp | Equiv. SC Discharge | 0.096 Amp |
| | | Equivalent SC Stand | 0.117 Amp |

Results:

| | | | |
|-------------------------------|---------------------------|---------------------------|-------------------------------|
| Total Zinc | 150.07 Moles | Stack Efficiencies: | |
| Zinc Plated | 103.17 Moles | Coulombic | 85.62 % |
| Zinc Plated | 94.53 mAh/cm ² | Voltaic | 82.70 % |
| Zinc remaining | 46.90 Moles | Energy | 70.81 % |
| Zinc Utilization | 68.75 % | Trans | 7.78 % |
| ZnBr ₂ Utilization | 84.03 % | Resid | 6.60 % |
| Total Bromide | 289.22 Moles | Charge Voltage | 1.9 V |
| Bromide Available | 245.57 Moles | Discharge Voltage | 1.6 V |
| Bromide remaining | 39.22 Moles | Shunt Current | 0.99 Ah |
| Bromide Utilization | 84.03 % | Br ₂ Diffusion | 3.9e-09 mol/cm ² s |
| Total Bromine | 103.17 Moles | equil. current | 0.754 mA/cm ² |
| Bromine/Quat | 2.36 | Stack current | 0.883 A |

| | | | |
|--------------------|-------------|--------------------|---------|
| Resistance Losses | 1344.98 Whr | Resistance Losses | 44.6 % |
| Overvoltage Losses | 225.83 Whr | Overvoltage Losses | 7.5 % |
| Shunt Curr Losses | 88.33 Whr | Shunt Curr Losses | 2.9 % |
| Diffusion Losses | 661.57 Whr | Diffusion Losses | 21.9 % |
| Residual Losses | 694.95 Whr | Residual Losses | 23.0 % |
| Total | 3015.66 Whr | Total | 100.0 % |
| Actual | 3073.00 Whr | | |
| Deviation | 1.87 % | | |

Check Value:
(Average volt/curr 6.0 mohm)

Figure 3-40. Zinc/Bromine Mass and Energy Balance (first order calculation of energy loss; based on SNL #514/27, no SCP in operation)

Table 3-13. Predictions from Revised Computer Model

| | V1-53 (cycle #3) | Original Model | Improved Model |
|-------------|------------------|----------------|----------------|
| Amp-hr in | 105.6 | 123.2 | 105.2 |
| Watt-hr in | 1604.3 | 1890.5 | 1608.2 |
| Disch. Time | 228.7 | 178.6 | 232.3 |
| Amp-hr out | 93.0 | 72.9 | 93.5 |
| Watt-hr out | 1195.7 | 877.7 | 1192.7 |
| Coulombic % | 88.1 | 68.2 | 88.9 |
| Voltaic % | 84.6 | 75.0 | 83.4 |
| Energy % | 74.5 | 51.2 | 74.2 |

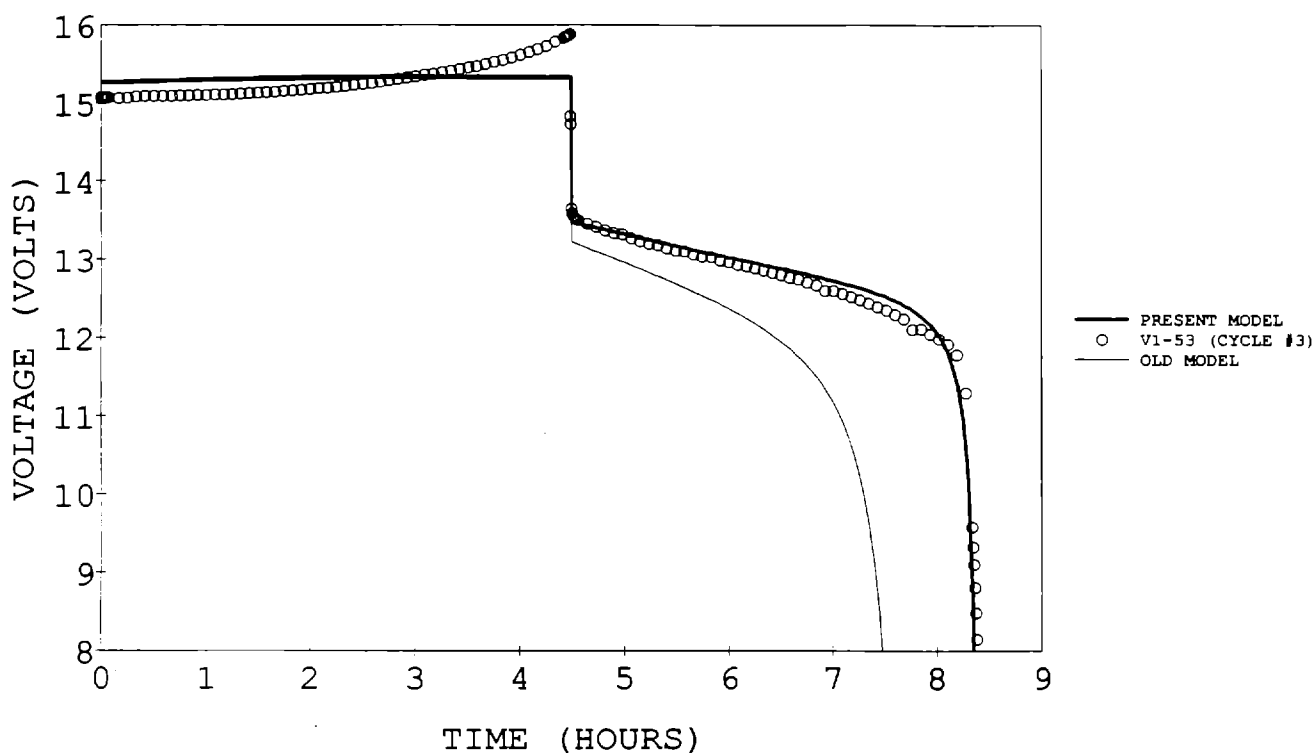


Figure 3-41. Model Predicted Voltage Profile (15 ohm-cm electrodes)

to an actual battery cycle in Figure 3-46. This again shows a very good correlation between the model and actual results.

Similarly, an increase of 1% could be observed by decreasing the separator resistivity as seen in Figure 3-44. A very critical property appears to be separator bromine transport (See Figure 3-45).

Significant improvements in energy efficiency could be observed by decreasing the bromine transport property, but this is not a simple property to improve. Also there appears to be a physical trade-off between bromine transport and separator resistivity, which may need to be optimized for the best battery performance.

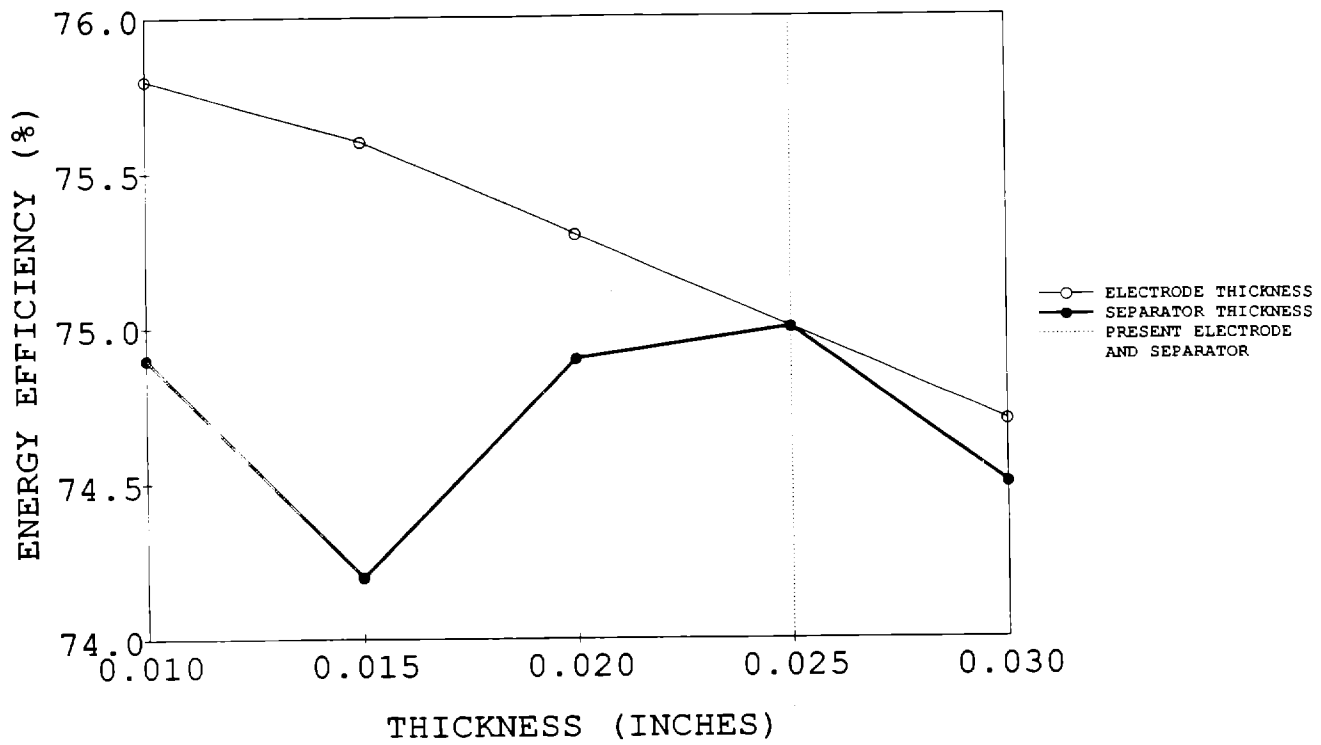


Figure 3-42. Effect of Electrode and Separator Thicknesses on Energy Efficiency

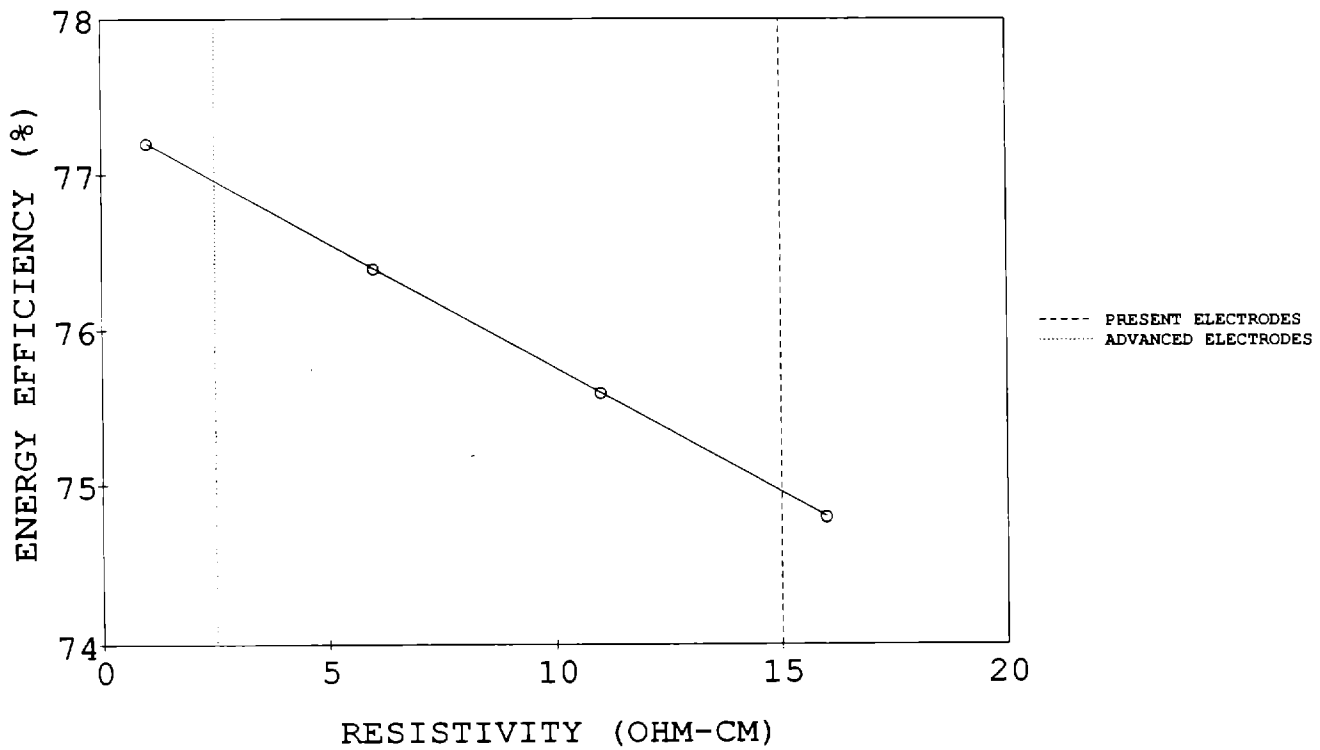


Figure 3-43. Effect of Electrode Resistivity on Energy Efficiency

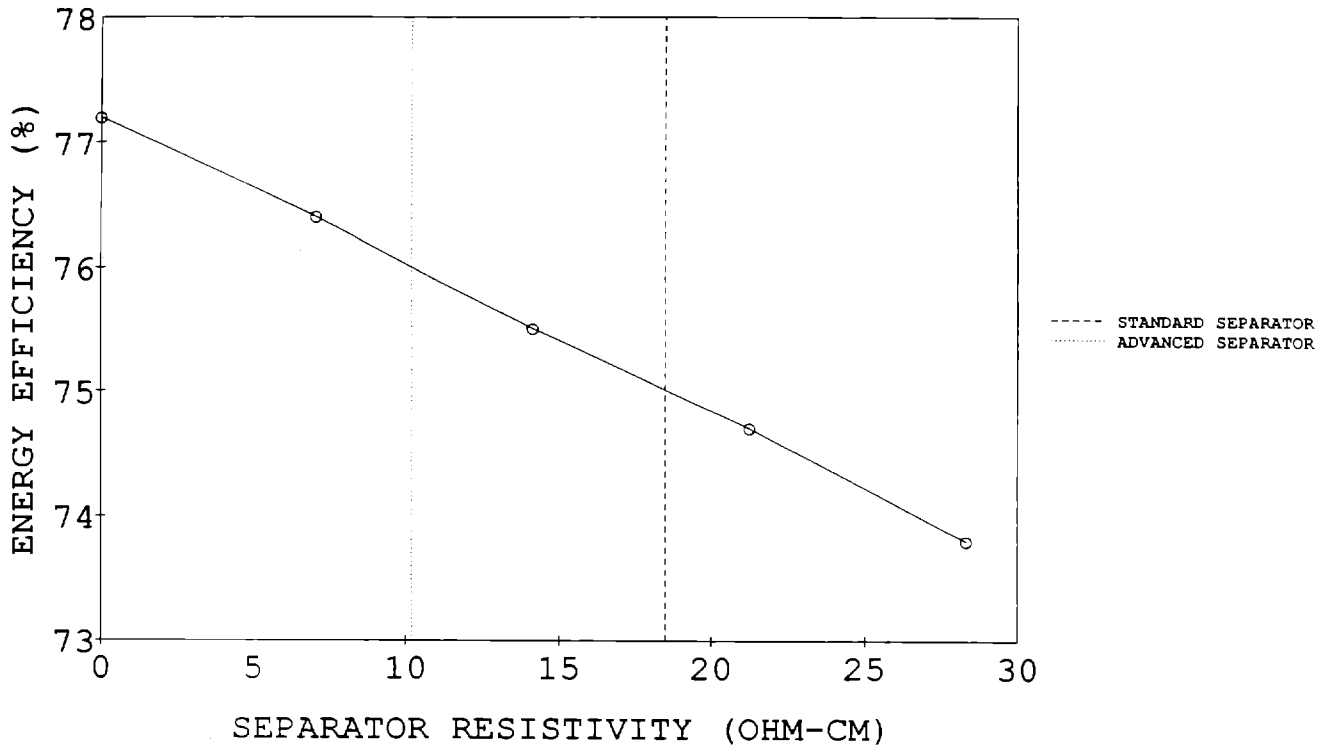


Figure 3-44. Effect of Separator Resistivity on Energy Efficiency

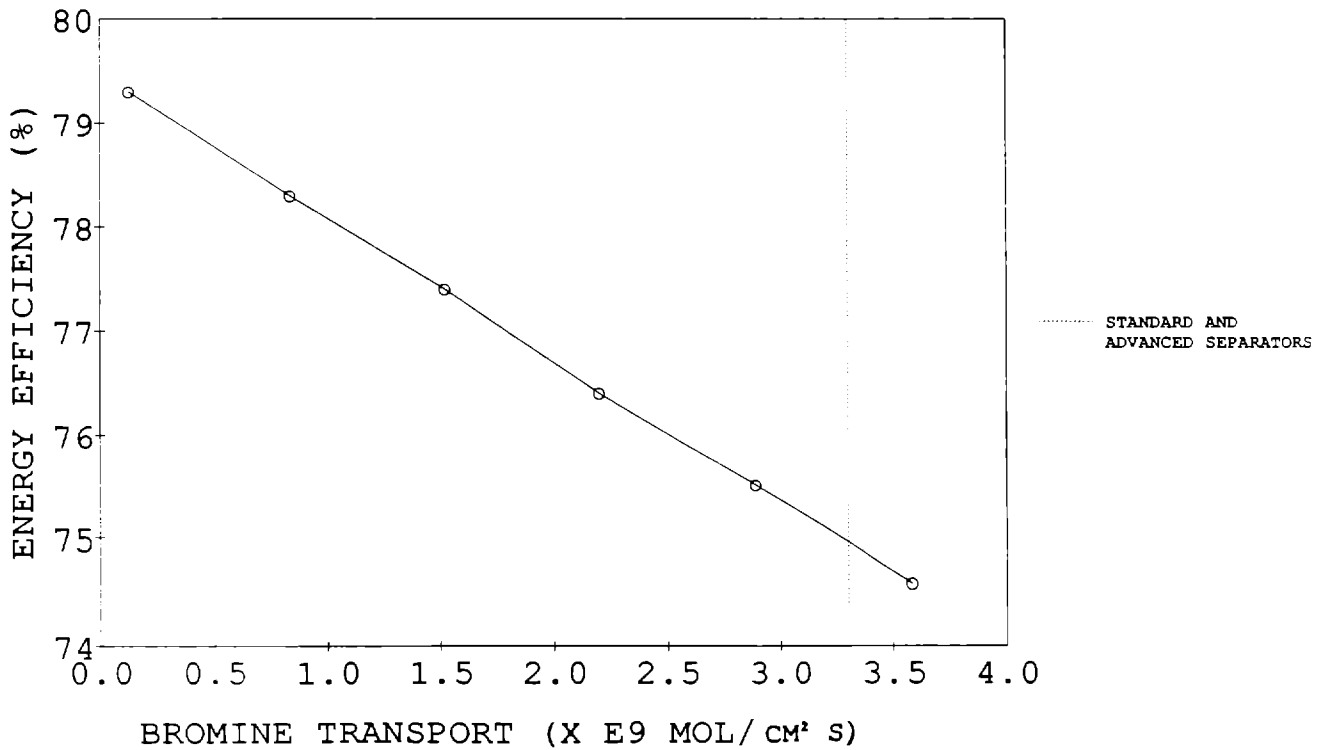


Figure 3-45. Effect of Bromine Transport on Energy Efficiency

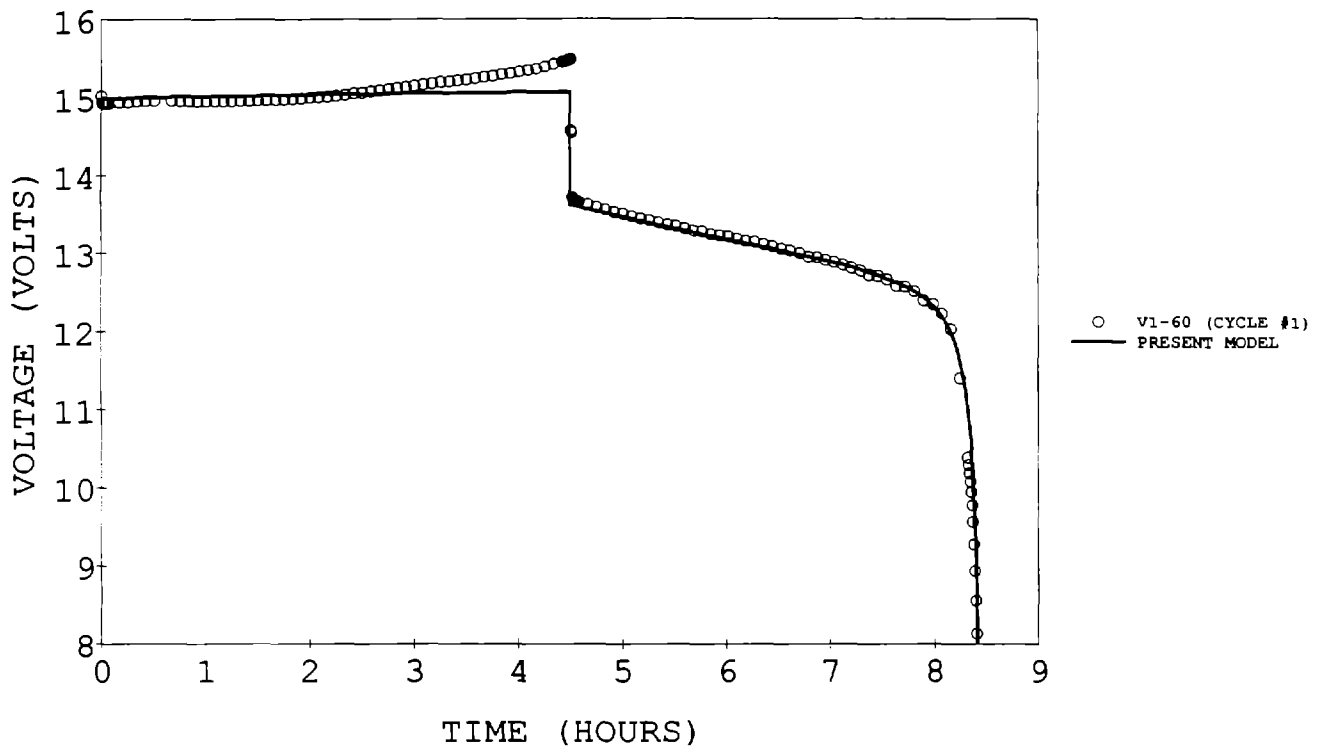


Figure 3-46. Model Predicted Voltage Profile (2 ohm-cm electrodes)

Effect of Discharge Rates

The computer model was used to examine the effects of bromine diffusion and separator resistivity on efficiencies for 4-hr and 10-hr discharge rates. Figure 3-47 shows how coulombic efficiency is affected by bromine diffusion for both discharge rates. It can be seen that coulombic efficiency is more sensitive to bromine diffusion for the 10-hr discharge than for the 4-hr discharge, which would be expected due to the extended time available for bromine diffusion.

Figures 3-48 and 3-49 show the trade-off between bromine diffusion and separator resistivity on energy efficiency for 4-hr and 10-hr discharge rates, respectively. These plots indicate that by lowering the bromine transport, a higher resistivity separator could be used to obtain the same energy efficiency. This trade-off appears to be more important at the 10-hr discharge rate than for the 4-hr rate.

The effect of discharge time on battery stack performance can be seen in Figure 3-50 for a standard 8-cell battery. The stack energy efficiency reaches a maximum at about a 7-hr discharge, while present batteries are run with a 4-hr discharge. It appears that a slight increase in stack energy efficiency could be obtained by going to a 6-8 hr discharge. When examining the entire

system (including pumping losses), a shorter discharge time would be more favorable as seen in Figure 3-51. The optimum energy efficiency would be obtained with approximately a 4-hr discharge rate.

A similar analysis was performed considering the charge cycle for an 8-cell zinc/bromine battery. The effect of charge time (keeping the total zinc loading constant at 90 mAh/cm^2) is seen in Figure 3-52 for an 8-cell battery with and without pumping losses. This indicates that the energy efficiency would peak at about a 7- to 8-hr charge rate when pumping losses are not included, while the peak shifts to a shorter charge time of 6 hr when including pumping losses.

During actual battery testing using V1-52, it was observed that residual losses are affected by discharge current density. An empirical relationship between residual losses and discharge current density was added to the computer model to adjust for this fact. This allows a very good correlation between the model and actual results as seen in Figure 3-53.

Similar analyses were performed for the final 80-cell (2300-cm^2 electrode) deliverable battery system. The effects of discharge and charge times can be seen in Figure 3-54 for an 80-cell battery system including pumping losses. Results appear to be similar to the

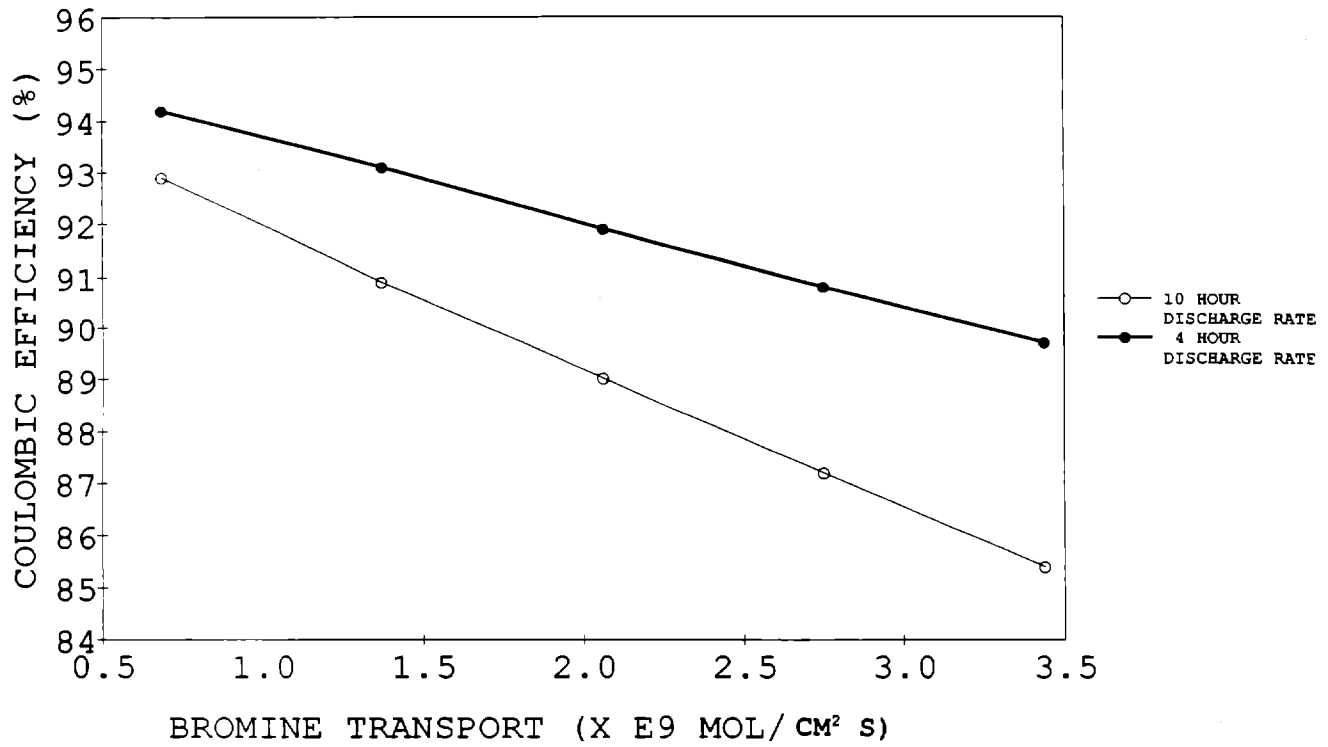


Figure 3-47. Effect of Bromine Transport on Coulombic Efficiency

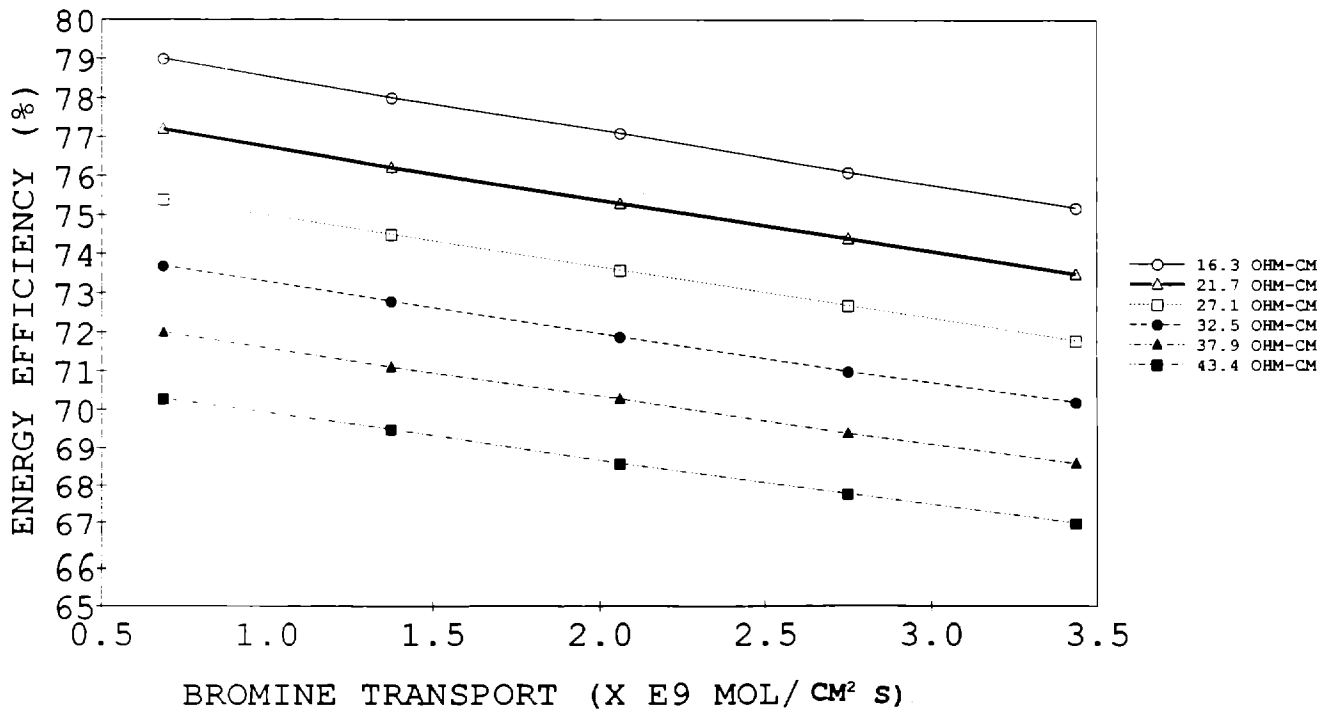


Figure 3-48. Effect of Bromine Transport and Separator Resistivity on Energy Efficiency (4-hr discharge rate)

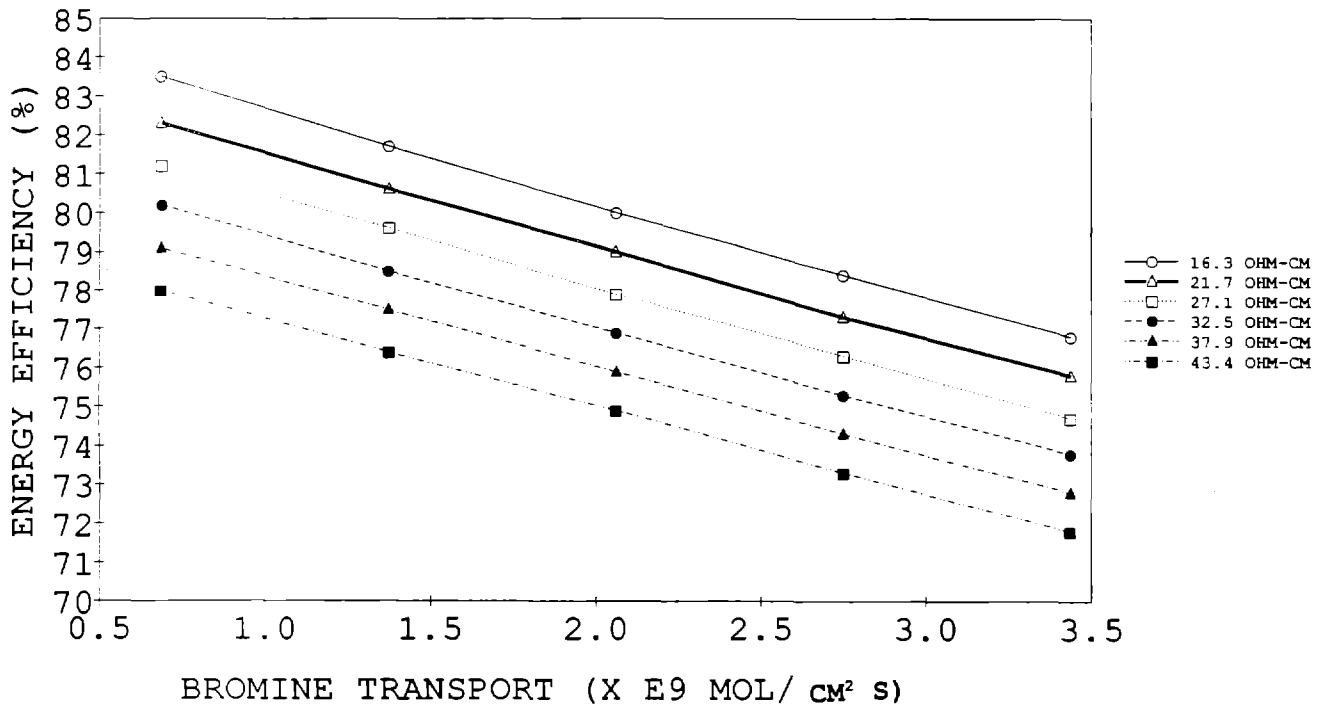


Figure 3-49. Effect of Bromine Transport and Separator Resistivity on Energy Efficiency (10-hr discharge rate)

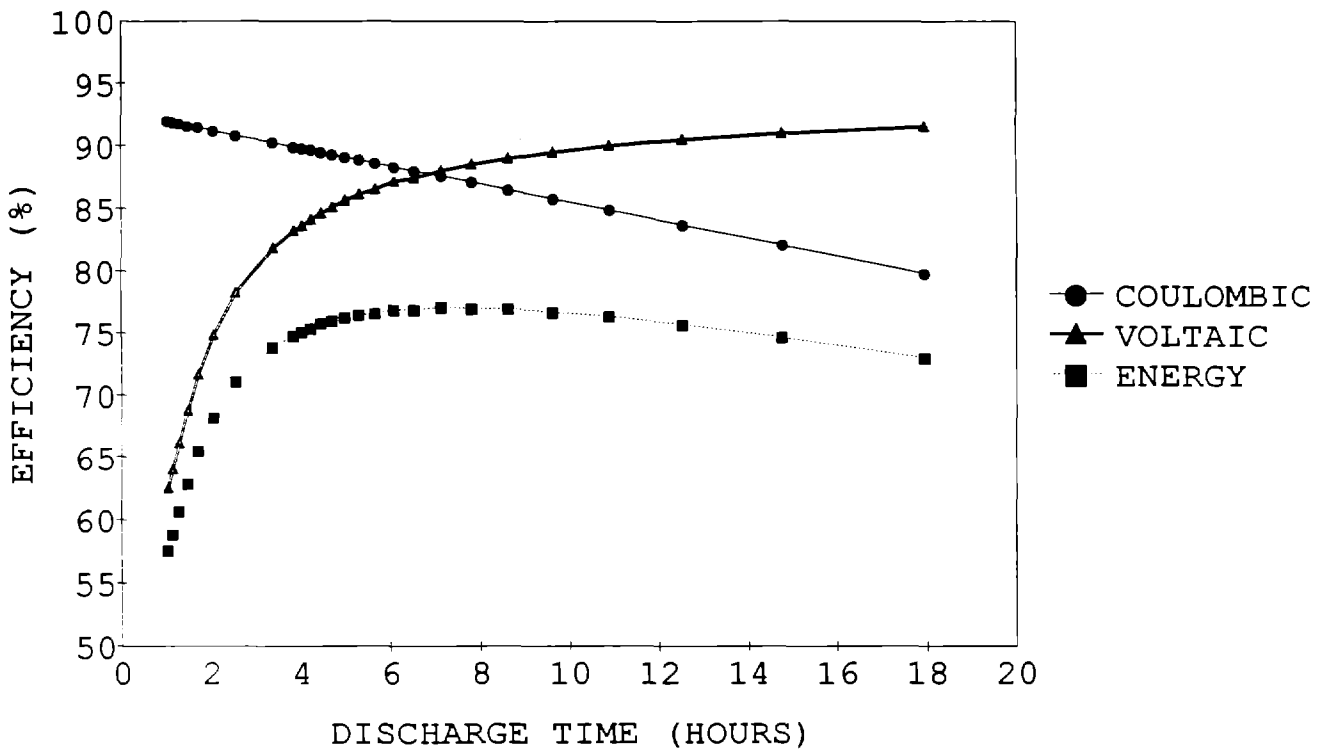


Figure 3-50. Effect of Discharge Time on Efficiencies (8-cell stack, no pumping losses)

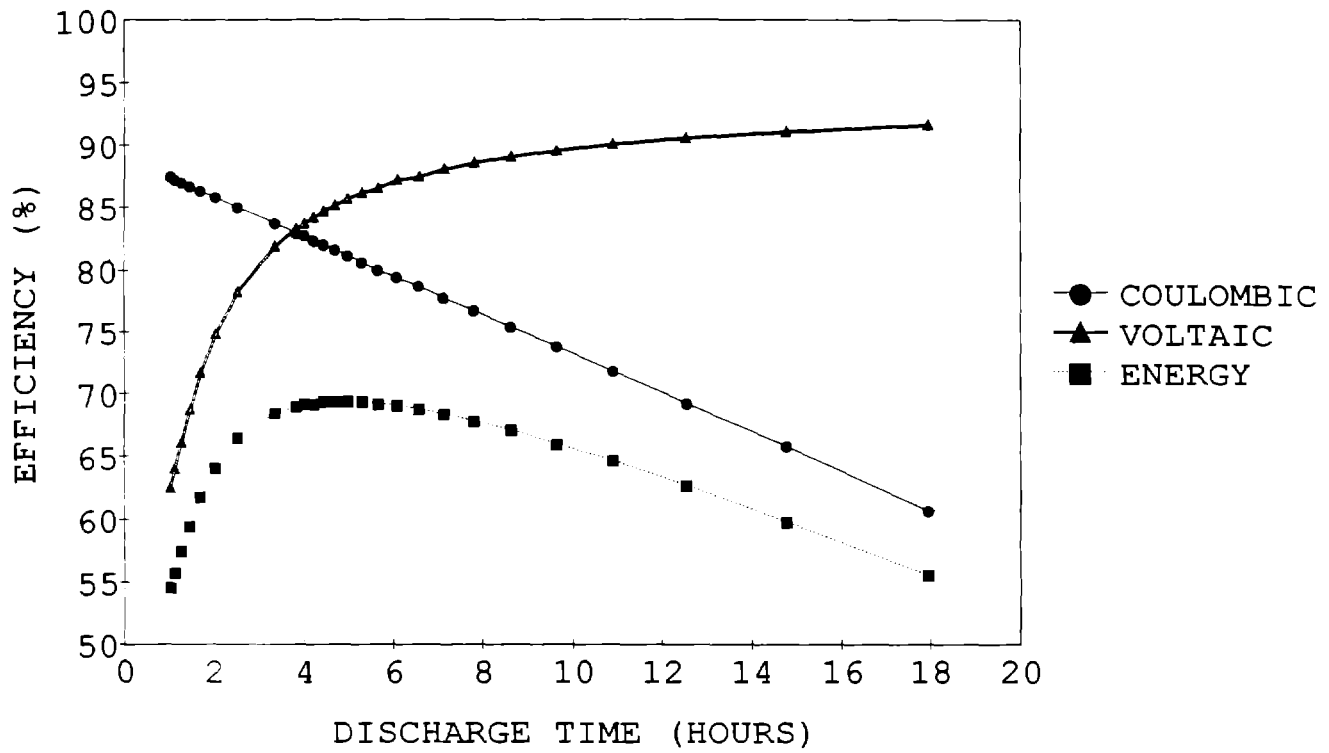


Figure 3-51. Effect of Discharge Time on Efficiencies (8-cell stack, including pumping losses)

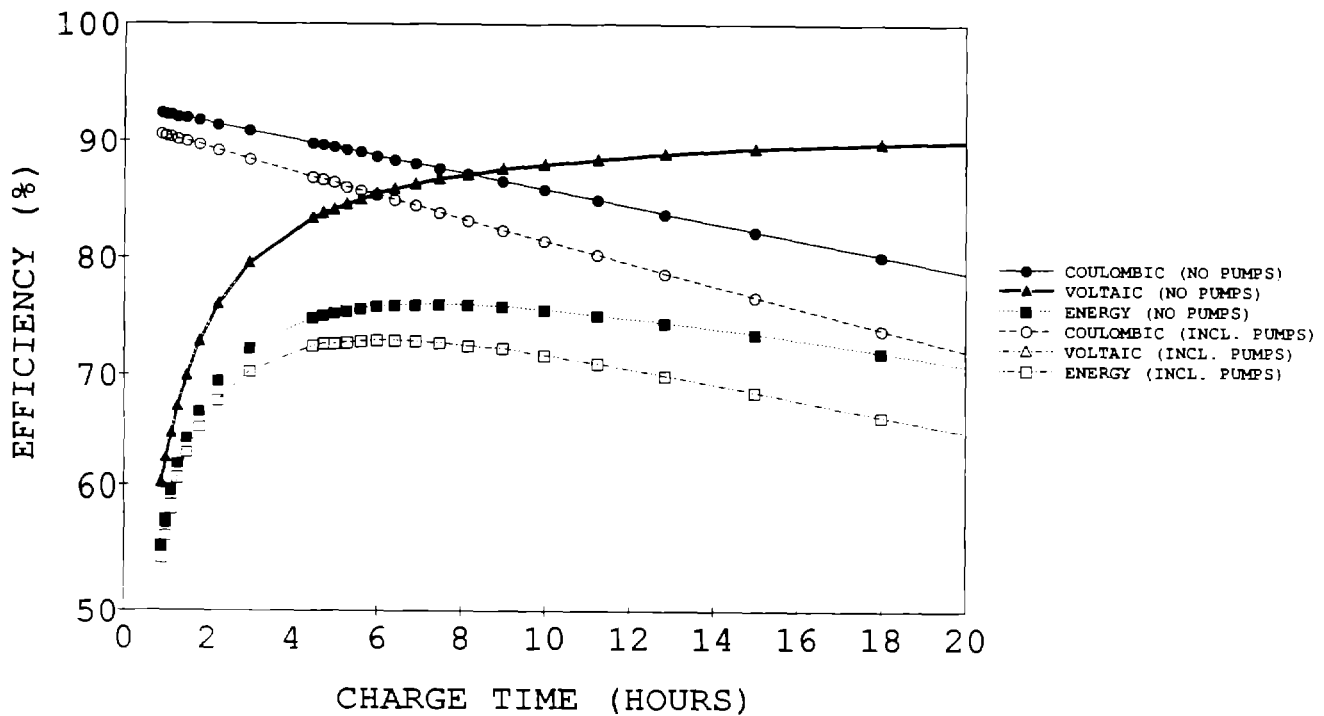


Figure 3-52. Effect of Charge Time on Efficiencies (8-cell battery stack; constant zinc loading of 90 mAh/cm^2)

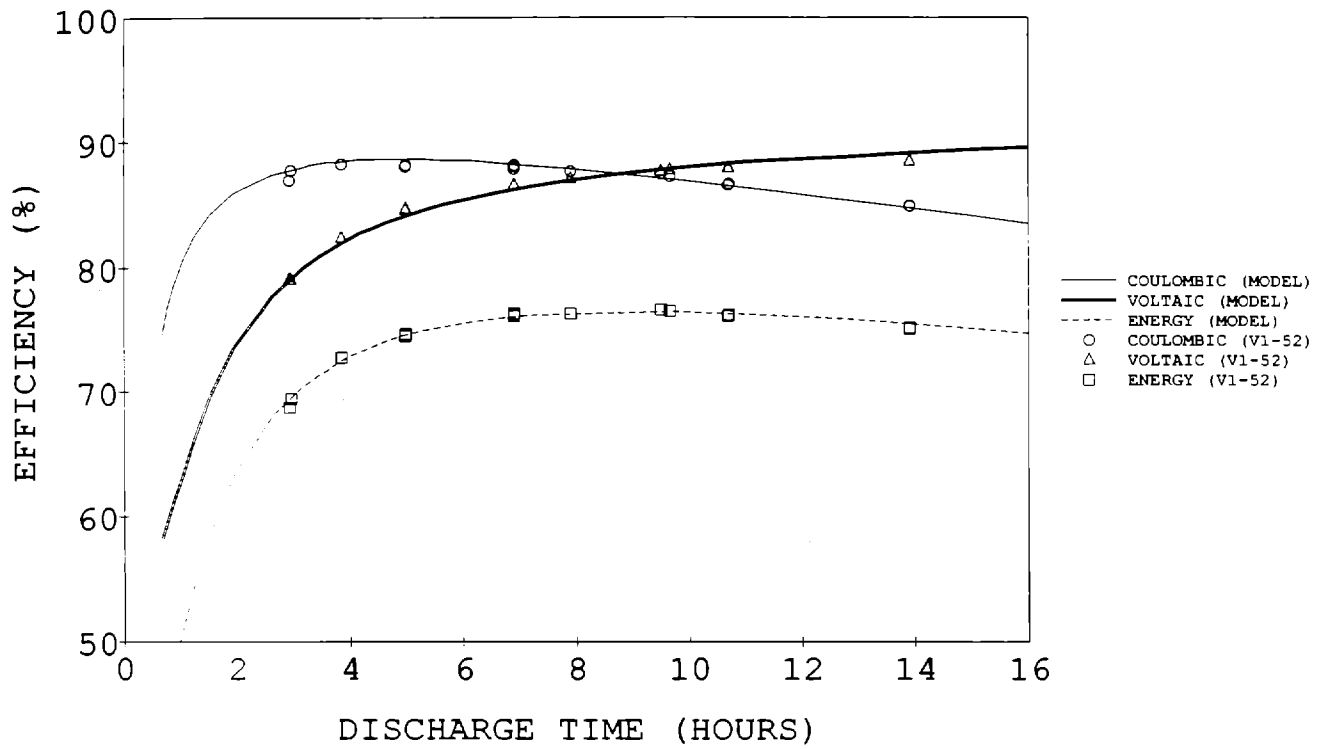


Figure 3-53. Effect of Discharge Time on Efficiencies (8-cell stack)

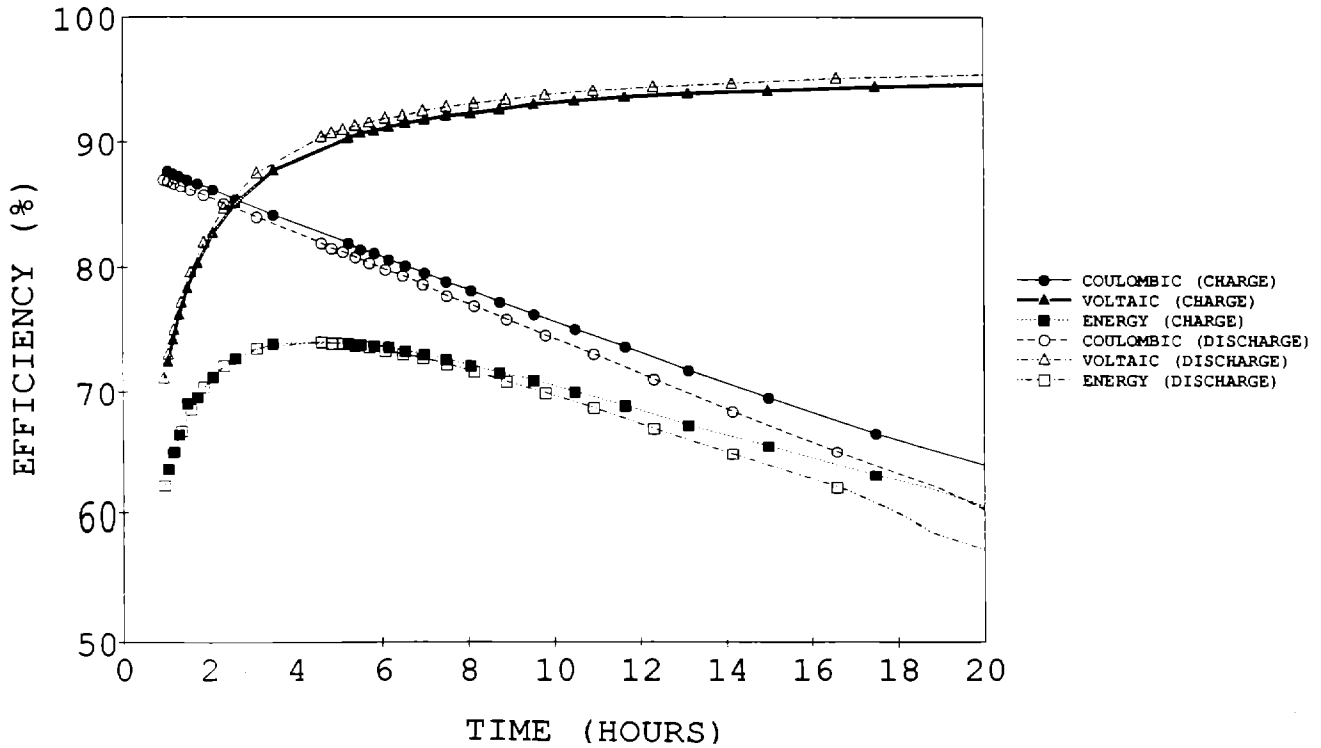


Figure 3-54. Effect of Charge and Discharge Times on Efficiencies (80-cell including pumps)

results observed for an 8-cell battery system. The best energy efficiencies could be obtained with about a 5-hr charge and a 5-hr discharge. By increasing or decreasing these times, the performance will decline due to either coulombic or voltaic effects.

Stand Testing

A new attribute of the computer model is the capability to calculate efficiencies when stand times (open circuit) are added to the charge/discharge cycles. This enables the model to simulate utility duty cycles. The computer program estimates losses due to bromine transport and shunt currents during open circuits of a given length of time. Results of stand times from 0-6 hr are compared to V1-44 stand test results in Figure 3-55. The model gives slightly higher efficiencies than the battery, but V1-44 was not running at peak performance at the time of the tests. Even though the model results do not exactly match the battery results, the general downward trend in energy and coulombic efficiencies are similar.

Battery Design Optimization

Optimization studies were run for the final 80-cell deliverable battery system with and without shunt current losses. Iterations over the channel dimensions,

manifold diameter, and anolyte and catholyte gaps were run to determine the dimensions that would provide the optimum battery performance. Initial estimates for the cell parameters came from doubling the sizes used in the present battery design. Results of the optimization can be seen in Table 3-14 for cases with and without shunt current losses.

The results in Table 3-14 indicate that optimum energy efficiencies could be obtained with anolyte and catholyte gaps of 0.015". These results are based only on pumping, shunt current, and resistivity trade-offs. Other considerations could include air bubble formation and uneven zinc plating (due to poor flow) at higher loadings if the anolyte gaps are too small. The best configuration due to these possible problems may be a 0.015" catholyte gap with a 0.020" anolyte gap.

One design consideration for the 80-cell battery is whether to have the electrolyte feeds in the center or the ends of the stack. A center feed would give 1/2 the channel lengths needed for an end feed. It is interesting to note that if shunt currents could be eliminated, a center feed configuration would give the best performance, while end feeds would give the optimum performance when shunt current losses are included.

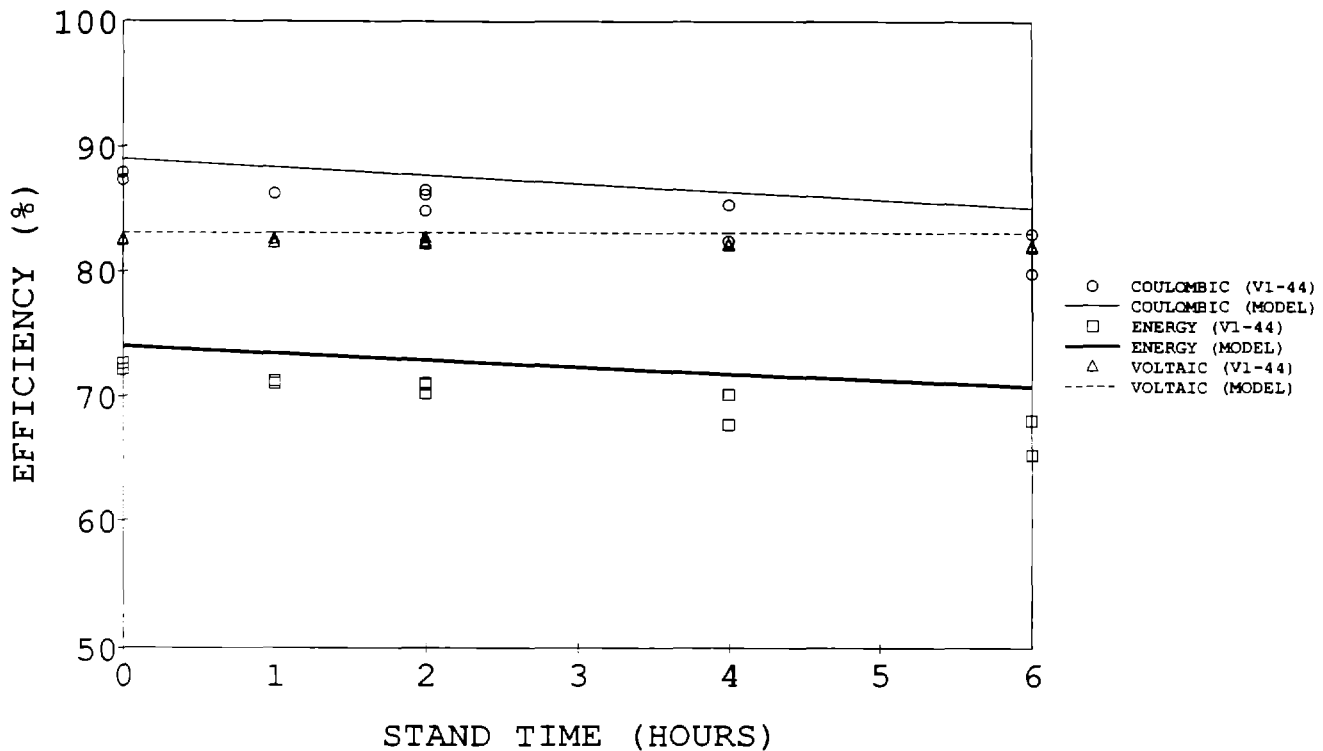


Figure 3-55. Stand Time Study on V1-44 Compared to Model Predictions

Table 3-14. Flow Cell Optimization

| | Including Shunt Current Losses | | No Shunt Current Losses | |
|-------------------|--------------------------------|-----------|-------------------------|-----------|
| | Original | Optimized | Original | Optimized |
| Manifold Diameter | 0.625" | 1.0" | 0.625" | 1.0" |
| Channel Length | 25.0" | 25.0" | 25.0" | 12.0" |
| Channel Width | 0.24" | 0.50" | 0.24" | 0.40" |
| Anolyte Gap | 0.032" | 0.015" | 0.032" | 0.015" |
| Catholyte Gap | 0.032" | 0.015" | 0.032" | 0.015" |
| Coulombic % | 81.1 | 82.2 | 83.0 | 86.7 |
| Voltaic % | 87.4 | 90.1 | 87.3 | 90.0 |
| Energy % | 70.9 | 74.1 | 72.5 | 78.1 |

Safety Study

An investigation into the various safety factors of the zinc/bromine battery has been initiated. A possible roadblock to the acceptance of zinc/bromine batteries is the perception of danger due to bromine. In fact, exposure to bromine is the only serious hazard of the battery other than electrical shock, a hazard shared by all technologies. The battery electrolyte is relatively nontoxic and not very harmful to contact except for the eyes.

The bromine hazard is actually rather small. There is little or no pure bromine in the battery. The bromine that is present is tied up as either Br₃-ion in the aqueous portion of the electrolyte, or as quaternary complexes in the "red oily phase" of the electrolyte. Both forms of bromine have greatly reduced activity and volatility compared to elemental bromine. Testing has focused on the quaternary complex because the second phase contains nearly all of the bromine that might escape from the battery.

To properly understand the bromine hazard in a utility facility, it is necessary to make reasonable estimations of the following:

1. The concentration at which bromine becomes dangerous.
2. The rate of evaporation expected from an electrolyte spill.
3. The degree of dispersal and dilution of the bromine vapors.

The lowest concentration at which an animal or human has been known to die is called the Lethal Concentration Low (LCLo). For bromine, it is 180 ppm, the concentration that was lethal to rabbits after seven hours exposure. However, bromine gas becomes distressing when inhaled at concentrations between 1 and 5 ppm, which means the gas will not be inhaled at injurious levels without the exposed person being aware of it.

The bromine evaporation rate can be approximated if the vapor pressure and temperature of the sample are known. The measurements of the total pressure over the polybromide complex in 100% state-of-charge load-leveling electrolyte (Figure 3-56) show how the pressure increases with temperature. The values are slightly higher than those reported for MEM Br complex in the final report for EPRI Project RP1198-4 (*Comparative Hazard Investigation for a Zinc/Bromine Load-Leveling Battery*). However, when the composition of the vapor was tested by titration, it was found to be only about 50% bromine. The remainder was probably mostly water of hydration in the complex.

The safety enhancement of bromine complex formation is apparent from Figure 3-56. The pressure of bromine (uncomplexed) is so high that it boils; i.e., the vapor pressure equals atmospheric pressure, at about 60°C. But when complexed, the bromine pressure is only 10% of atmospheric at 60°C.

The evaporation rate was simulated by CAMEO II (*The Computer-Aided Management of Emergency Operations* Department of Commerce report) for a spill in an enclosed area. For a room of 300 m³ area with

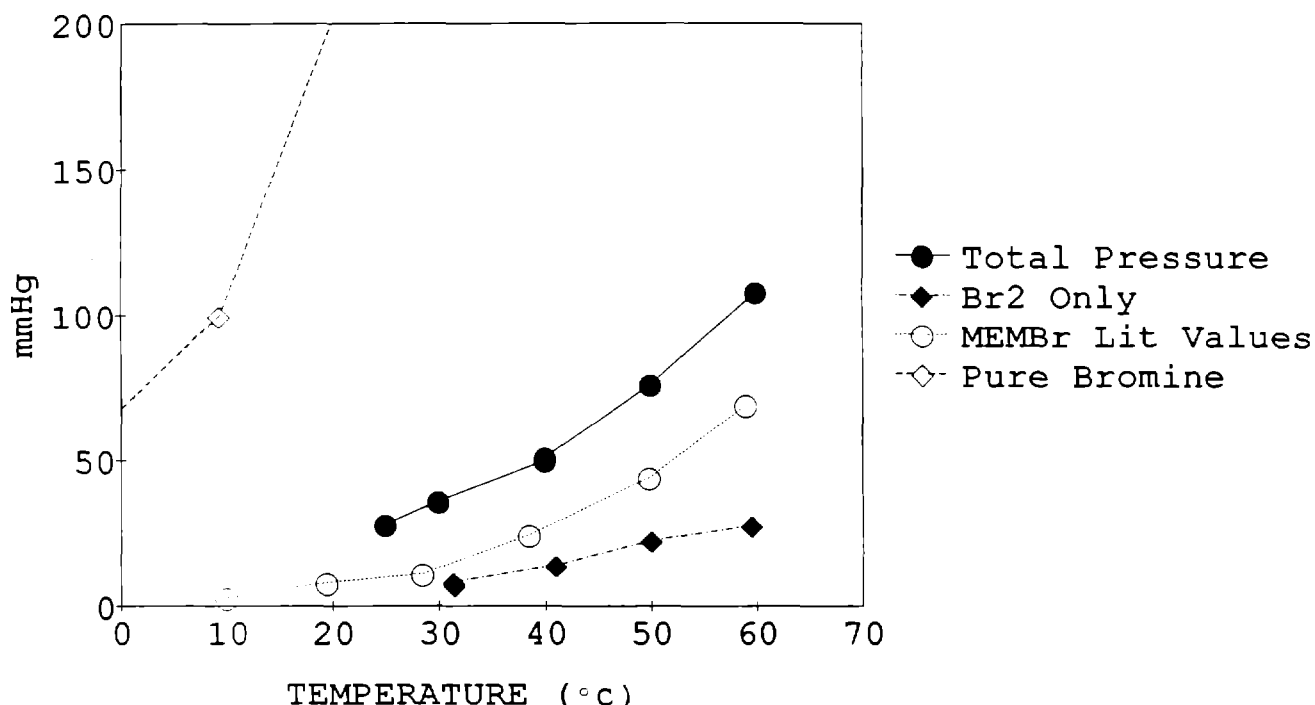


Figure 3-56. Vapor Pressure Over MEPBr Complex

well-mixed air, the evaporation rate was calculated to be 0.015 g/min, which would bring the area to the LCLo in 73 min. This would be plenty of time to evacuate or to initiate cleanup efforts that would prevent further evaporation of bromine.

Electrolyte Recycle Program

The electrolyte in the zinc/bromine battery shows no evidence of deterioration over time. Only contamination of the used electrolyte would prevent immediate electrolyte reuse. Some possible sources of contamination might be internal corrosion from the stack or station, and sloppy handling and storage in "dirty" containers. In earlier studies on the electric vehicle program, some impurities, especially transition metals, were found to be readily removable.

A preliminary plan will be proposed for the handling of recycled electrolytes. A schematic flow sheet is shown in Figure 3-57. The major steps are analysis for purity and composition, treatment to reduce transition metals, and filtration. If the recycling process can be carefully controlled so that electrolyte is removed from old batteries without introducing new contaminants, it should be possible to return it to service easily with only a cursory check of the purity and composition. The

more electrolyte that can be recycled without having to repurify it, the less expensive the process will be.

Undoubtedly, some material will be nonrecycleable for various reasons. There are two possible ways to recover valuable electrolyte materials from this waste. First, zinc could be separated by electrodeposition and then reacted with the bromine that would evolve at the counter electrode to reconstitute pure zinc/bromine. Second, the zinc could be precipitated by adjusting the pH to alkaline. The remaining NaBr solution would be purified of metals by ion-exchange. The NaBr could be converted to HBr and NaOH by a "water splitting membrane" process, and the HBr reacted with the ZnO to regain the zinc/bromine. A good way to purify the quaternary ammonium salts has not yet been found. Possibly, separation could be effected from a contaminated aqueous solution by use of bromine to form a second phase.

The two main analytical tools needed for electrolyte recovery will be an inductively coupled plasma (ICP) analyzer for determining ppm levels of metals, and an ion chromatograph for doing composition/concentration analysis of the electrolyte. An X-ray fluorescence (XRF) machine might be substituted for the ICP. At the present time, ICP Emission Spectroscopy is used to analyze metal impurities. However, the ICP is a large,

- Used Electrolyte
 - Source
 - Known
 - Segregate
 - Electric Vehicle
 - Load Leveling
 - Neutralize bromine
 - Analyze Purity, Evaluate, and Mix
 - Pure
 - Impure/metals
 - Zinc Treat
 - Carbon Filter
 - Impure/solids
 - Particle Filter
 - Analyze Concentration
 - OK
 - Concentrated
 - Dilute with water
 - Dilute
 - Make up with concentrate
 - Return to service
 - Not recyclable
- Neutralize Bromine
 - Unknown
 - Analyze Components
 - Assign type
 - Analyze Purity, Evaluate, and Mix
 - Pure
 - Impure/metals
 - Zinc Treat
 - Carbon Filter
 - Impure/solids
 - Particle Filter
 - Analyze Concentration
 - OK
 - Concentrated
 - Dilute with water
 - Dilute
 - Make up with concentrate
 - Return to service
 - Not recyclable

Figure 3-57. Zinc/Bromine Battery Electrolyte Recycling Process

expensive piece of equipment, and a worker is needed full-time to keep it operational. At present, only a few analyses are done per week. In a recycling facility, the number might go up to several dozen per day. This means the analytical procedures will need to be automated and have a low cost per sample. Vendors who supply Ion Chromatography (IC) and Ion Capillary Electrophoresis (ICE) equipment have been contacted. Both methods should be able to provide accurate analyses of the composition rapidly, on equipment that is relatively low on the scale of advanced technology.

ICE equipment is capable of resolving ppm concentrations of most ions. If this is true, it might be preferred over the ICP. Also, recent advances in the electrochemical technique, Anodic Stripping Voltammetry (ASV) allow it to resolve ppm levels of transition metals (basically anything that can be plated out of aqueous solution). The major difficulty of this particular application is the high background of zinc/bromine. The real test will be if different procedures are capable of analyzing actual electrolyte. Future plans are to send samples of clean and dirty electrolyte to each of the equipment suppliers.

Table 3-15 is a short summary of the methods of analysis and applications.

Adhesive Bonding

It is possible that the battery assembly process could be accelerated if the stacks were put together using adhesive bonding instead of thermal welding. There has been much recent progress in new structural adhesives that can bond to polyethylene and are chemically inert. The three adhesives selected for testing were Dexter/Hysol EA-9430 and EA-9460, and Conap FR-1210 adhesives.

Samples of the 30 melt index and 11% glass fiber frame plastic were cut to 2" size and glued with wide beads (using the whole frame width, about 0.5") and narrow adhesive beads (the size of the weld bead, 0.08"). Some samples were exposed to bromine vapor for five days; others were exposed to sulfuric acid for five days. They were then tensile-tested to failure.

A list of the samples and test results is shown in Table 3-16. The surface preparation was critically important to the adherence of the joint as can be seen in the results of the tensile tests. All samples were cleaned with acetone, but the plastic was still too slippery unless it was specially prepared. Samples that were treated with chromic acid and physically roughened with sandpaper were noticeably stronger.

The EA-9430 adhesive did not appear to be as strong as the EA-9460, and the EA-9430 overheated when it was mixed so that much of the adhesive in the mixing pot was lost. Since it was more difficult to work with and showed no advantage over the other Dexter/Hysol adhesive, it was not used in the chemical exposure tests.

Samples of Dexter/Hysol EA-9460 and Conap FR-1210 adhesives were tested for adhesion and resistance to two chemicals: bromine vapor and sulfuric acid. Tests results listed in Table 3-16 are given in pounds/inch of glue bead and so are readily comparable to weld bead data. Both adhesives had softened after five days in bromine vapor, but the EA-9460 was still holding tightly, while the FR-1210 adhesive had nearly fallen off. In five days of exposure to sulfuric acid, the EA-9460 was almost unaffected, while the FR-1210 showed some surface crazing.

The results are shown in Figure 3-58. The narrow glue bead was not as strong as a vibration weld bead of

Table 3-15. Analysis Types

| | <u>Impurity</u> | <u>Composition</u> |
|-------------------------------|-----------------|--------------------|
| ICP | √√ | |
| Anodic Stripping Voltammetry | √ | |
| Ion Chromatography | √ | √√ |
| Ion Capillary Electrophoresis | √ | √√ |

√ = might give satisfactory results.
 √√ = likely or known to give satisfactory results.

**Table 3-16. Adhesive Bonding Tests on Polyethylene
(11% Glass - 30 Melt Index)**

| Sample | Bead | Adhesive Type | Failure Load Pounds/inch | Chemical Exposure | Surface Preparation |
|--------|--------|---------------|--------------------------|--------------------------------|-------------------------|
| 3A | Narrow | EA-9460 | 28.4 | | |
| 4A | Narrow | EA-9460 | 28.2 | | |
| 1A | Wide | EA-9460 | -- | | Failed in Handling |
| 2A | Wide | EA-9460 | 32.0 | | Not Prepared |
| 9A | Narrow | EA-9460 | 75.2 | | Chromic Acid |
| 10A | Narrow | EA-9460 | 55.6 | | Chromic Acid |
| 11A | Wide | EA-9460 | 142.5 | | Chromic Acid, Roughened |
| 12A | Wide | EA-9460 | 124.8 | | Chromic Acid, Roughened |
| 5A | Narrow | EA-9430 | 20.9 | | |
| 6A | Narrow | EA-9430 | 25.2 | | |
| 7A | Wide | EA-9430 | 50.9 | | Roughened |
| 8A | Wide | EA-9430 | 60.1 | | Roughened |
| 13A | Narrow | EA-9460 | 56.3 | H ₂ SO ₄ | Chromic Acid |
| 14A | Narrow | EA-9460 | 52.1 | H ₂ SO ₄ | Chromic Acid |
| 15A | Narrow | EA-9460 | 56.1 | Bromine | Chromic Acid |
| 16A | Narrow | EA-9460 | 12.2 | Bromine | Chromic Acid |
| 20A | Narrow | FR-1210 | 72.3 | | Chromic Acid |
| 19A | Narrow | FR-1210 | 36.0 | Bromine | Chromic Acid |
| 17A | Wide | FR-1210 | Tab | | Chromic Acid, Roughened |
| 18A | Wide | FR-1210 | Tab | H ₂ SO ₄ | Chromic Acid, Roughened |

EA-9460 was produced by Dexter/Hysol, Inc.
FR-1210 was produced by Conap, Inc.

All narrow adhesive beads were milled, but not further roughened.

Tab means the base material failed before the bond.

the same size. However, a wide glue bead was quite strong. In fact, two of the samples broke before the glue to plastic bond did. The narrow bead glued samples showed the effect of exposure to bromine. Visually, the weld bead softened in the bromine, then became brittle when the bromine evaporated. The sulfuric acid had little or no apparent effect on the EA-9460 samples, but did attack the FR-1210 samples. Wide glue bead

samples did not seem to be attacked, but in time, they probably would be.

In summary, one adhesive (EA-9460) has been identified that could be used to bond plastic parts in sulfuric acid service, and possibly zinc/bromine electrolyte as well. Another adhesive (FR-1210) provided a strong bond, but should not be used where it would be exposed to battery electrolytes. Despite the lower

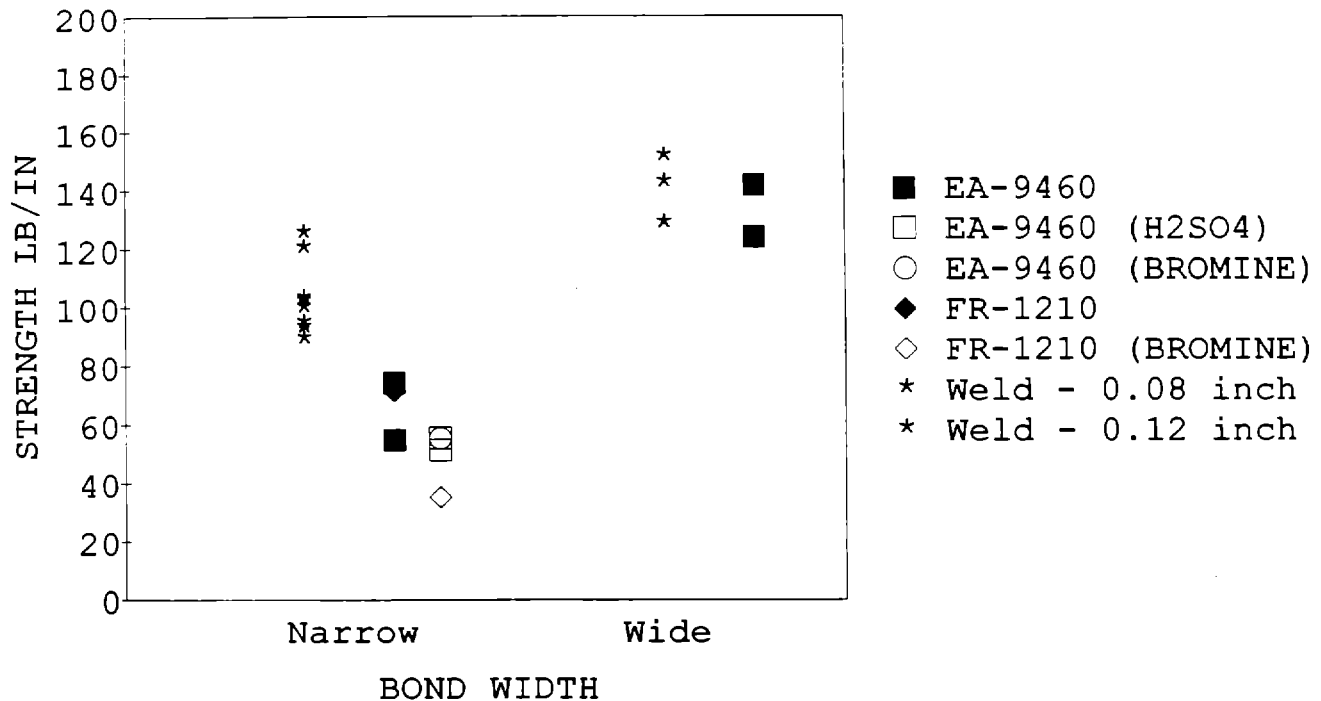


Figure 3-58. Adhesive Bonding Strength

chemical resistance, the FR-1210 adhesive wetted the plastic surfaces very well and gave excellent adhesion values. In fact, the tabs on the wide bead samples failed before bonds. If used for stack assembly, both adhesives should be applied in a wider bead than the vibration weld bead. If that is done, the bond can be as strong as a vibration weld, and certainly would be suitable for service in non-chemical exposure applications.

Battery/Station Design

Cooling

The heat that is generated by a battery can be estimated from the efficiency of operation. Every kilowatt-hour not utilized in discharge is converted to heat. Recently tested batteries have shown typical energy efficiencies of 70-75%. For every kWh of energy delivered, 1.43 to 1.33 kWh must be charged, and 0.43 to 0.33 kWh of heat will be generated. Therefore, the starting point for determination of battery cooling requirements is to use a design value of about 40% of the battery rated capacity.

JCBGI 8-cell battery stations typically use 36" of 1/4"-O.D. titanium tubing for the heat exchanger. Cooling water flows through the tubing, and warm electrolyte is on the outside. The tubing is placed where it will contact returning anolyte. The cooling water is supplied from the tap, at a temperature of about 13°C. Since titanium tubing is costly, other materials should be considered for better cost effectiveness. Plastic tubing has been used in a larger size station.

Data from battery VL-14 have been used as a starting point for designing the cooling system for the dual-stack 50-cell battery deliverable. VL-14 is a 50-cell (single-stack) battery which has been satisfactorily kept at an operating temperature of 30°C by using 19 feet of 1/4"-O.D. teflon tubing. The water inlet and outlet temperatures are typically 14°C and 17°C, respectively; the flow rate is about 3/4 gallon/min, and the water line pressure about 40 psi.

VL-14 has an energy capacity of about 6.25 kWh. The dual-stack deliverable battery will have a capacity of about 12.5 kWh. Therefore the cooling capacity of the next deliverable station should be twice that of VL-14. Two heat exchanger configurations are being considered.

Electrolyte Level Control

The operation of the zinc/bromine battery depends on facile transport of ions through the separator to carry the electrical current and to maintain charge neutrality. Since the ions have differing numbers of water molecules in their hydration spheres, there may be a water imbalance between the two electrolytes. In previous JCBGI station designs, this imbalance could be counteracted by setting the pump pressures so that a slight amount of electrolyte was transported by the pressure difference across the separator. In that way, there would be no net gain of one electrolyte over the other. Unfortunately, adjusting the pumps was a trial-and-error process that could be difficult and tedious. For example, a balance might be achieved after several valve adjustments, but the overall pressure might then be too low. The valves would have to be opened up, and the process started over. Until a balance was achieved, a tie-line tube between the two reservoirs would allow excess electrolyte to return to the reservoir with the lower level. But this would result in a lower coulombic efficiency.

The solution to the electrolyte balance problem is to seal the catholyte reservoir so that pressure in the reservoir is held constant. One reservoir needs to remain vented to allow pressure relief in response to volume changes resulting from temperature and concentration fluctuations. Since the anodes have the possibility of venting small amounts of hydrogen, the anolyte reservoir needs to be vented.

The strategy of sealing the catholyte reservoir sets up a water balance at the separator. If an excess amount of water begins to accumulate, it increases the pressure in the reservoir. This forces some of the catholyte back across the separator until the electrolyte levels became stabilized. Sealed catholyte reservoirs have successfully been used on the 8-cell stations for some time. The pump pressures still should be balanced when the battery is initially filled with electrolyte, but after that, the operation is "hands-off." The concept was not extended to large batteries in the past because a pressure-sealed reservoir has heavier walls that decrease the specific energy. Also the reservoirs should be cylindrical for strength, but that is volume-inefficient. For load-leveling applications, some weight and volume advantage can be traded off for gains in reliability and ease of operation.

Pump/Motor Procurement

The centrifugal electrolyte pumps in recent use have been made of Ryton (polyphenylene sulfide) and have proven to be only marginally adequate for this

application. Ryton is quite brittle. Polypropylene pump heads identical to the Ryton pump heads have been used with limited success.

The 14518 model pump manufactured by Gorman-Rupp Industries (GRI) is somewhat oversized for the 8-cell station. When the pump is throttled to restrict its outflow, the forward thrust on the impeller becomes excessive. This forward thrust is designed into the pump to compensate for the rearward thrust seen during normal operation. The front bearing supports of these polypropylene pump heads do not hold up for an acceptable length of time under these conditions.

Two gear pump/dc motor systems have also been purchased. The motor is a 24-V variable speed brushless dc motor with integral electronics, and is coupled with a gear pump made with a glass-filled Ryton body, titanium shafts and magnet cup, Ryton gears and bearings, and Viton O-rings. The performance curves of these match the requirements for 8-cell zinc/bromine battery stations.

The dual 50-cell station due to be delivered in October will use the GRI 14520 centrifugal pumps with polypropylene bodies. They will be powered by either the standard ac motor or the brushless dc motors if the latter system can be proven to be effective and reliable. These motors are manufactured by EG&G Rotron of Woodstock, New York, and are adapted for use with these same model GRI pumps.

Discussions with another major pump manufacturer have been initiated in an attempt to develop polyethylene pumps of a suitable size for the dual-stack 50-cell battery.

Summary and Conclusions

In Phase 1 of the contract, the zinc/bromine battery technology has been significantly improved. The sealed cell stack has been shown to be leak-free when properly designed and manufactured. The stack energy efficiency results are 75% and higher for the most recently built batteries. Several life tests of 8-cell battery stacks have achieved more than 100 cycles with only minor performance degradation. One stack has achieved over 250 cycles. All of the life tests are continuing at this time. Work is under way to identify the causes of the efficiency decline and to improve the retention of high performance.

Supplemental tests of battery performance under no-strip cycling regimes have shown that the battery is capable of performing over a dozen cycles without stripping the zinc. With more uniform electrolyte flow in the

most recently built stacks, the energy efficiency is improved. This is because fewer watt-hr are lost to unreacted zinc and bromine left in the battery at the end of the cycles. Standlosses have been found to be initially about 0.66% of the energy capacity per hr. Although this is a relatively high rate, the loss is limited to the bromine that is in the cell stack. In future tests, the maximum loss will be measured, and work will be done to lower the standloss rate. Although in the present baseline battery cycle the stack is charged to 90 mAh/cm², the loading has been tested to 115 mAh/cm² without any apparent negative effects. The battery was found to operate at peak energy efficiency at 30°C. Higher losses to resistance occurred at lower temperature, and bromine transport increased at higher temperature. The ability to accelerate the stripping process to as short as 1.5 hr was demonstrated.

A welding study and a modeling study of the battery operation were used to prepare for the next stage in the utility battery design. The optimum weld bead size, materials, and welding parameters were developed for the production of a new cell stack. The battery model was improved to the point where it not only can predict trends but now closely matches the observed results of charge/discharge cycles. Initial work on battery recycling and safety suggests that these will be positive factors in the adoption of the zinc/bromine technology.

In this first year of the utility applications contract, the basic design and performance of the zinc/bromine battery has been demonstrated to be appropriate for utility use. A number of the tests to explore the operating parameter envelope of the zinc/bromine battery are still ongoing, as are investigations into improved zinc plating and bromine electrode surfaces. In the next phase of this program, the improved state-of-the-art zinc/bromine technology will be scaled up to a size appropriate for a submodule of a 100-kWh battery suitable for use in a utility facility.

Technology Evaluation - SNL

During FY91, SNL evaluated two state-of-the-art zinc/bromine batteries. These batteries were part of the deliverables under the utility battery development contract with JCBGI. The first was a 50-cell, 6.5-kWh battery (JCBGI #VL-12/SNL #514) with an electrode size of 1,170 cm². The battery was cycled 20 times prior to delivery to SNL using zinc loadings ranging from 10 to 45 mAh/cm². At a zinc loading of 45 mAh/cm², the best efficiencies achieved at JCBGI were the following:

Coulombic efficiency = 88.0%

Energy efficiency = 73.1%

Voltaic efficiency = 83.1%

The battery was then delivered to SNL and placed on test in November 1990. Initial cycles were performed and the results of these tests at 45 mAh/cm² were slightly higher than what JCBGI had achieved; the coulombic efficiency was 91%, the energy efficiency was 75.8% and the voltaic efficiency was 83.3%. These cycles were followed by several cycles at 90 mAh/cm² and were considered as baseline. For this baseline cycle, the battery was charged at a constant current of 23.5 A for 270 min. After a 5-min open-circuit wait, the battery was then discharged at a constant current of 24.2 A until the battery voltage reached 1 V/cell. The battery was then discharged completely (0 V).

During the second quarter of the fiscal year, a parametric test plan was started. In this plan, the zinc loading was varied from 30-90 mAh/cm². This loading was achieved by keeping the charge and discharge currents the same as the baseline values but varying the charge time. The temperature of the battery also remained constant at approximately 24°C. Figure 3-59 is a plot showing how the efficiencies varied with zinc loading. The results of these parametric tests indicated that the voltaic efficiency remained constant. The coulombic and energy efficiencies, however, were affected as the zinc loading changed. Low CE at low loading is caused by the effect of the residual zinc and bromine. The residual inefficiency is part of the coulombic efficiency. When discharged at constant current density, there will always be about the same number of amp-hr of zinc and bromine left over at the end of each cycle. If only a few amp-hr were put in during charge, then the residual amp-hr will be a large proportion of the charge and the CE will be very low. As more amp-hr are put in during charge, the residual inefficiency becomes a progressively smaller portion of the CE. This was illustrated in Figures 3-59 and 3-60. Low CE was seen at low loading, and the amp-hr loss to residual was unchanged over the loading range. The amp-hr loss to transport increased with loading. That was because higher loading was achieved by longer running times and, therefore the bromine had more time to diffuse through the separator. Figure 3-60 is a plot showing the losses that were seen in residual and transport as the zinc loading was varied. It appears that for this battery, a constant residual loss of 6.5 Ah/cm² was seen while the transport loss increased with zinc loading because of the additional time that the bromine had to pass through the separators.

The operating temperature of the battery was increased to 28°C and the parametric tests were repeated.

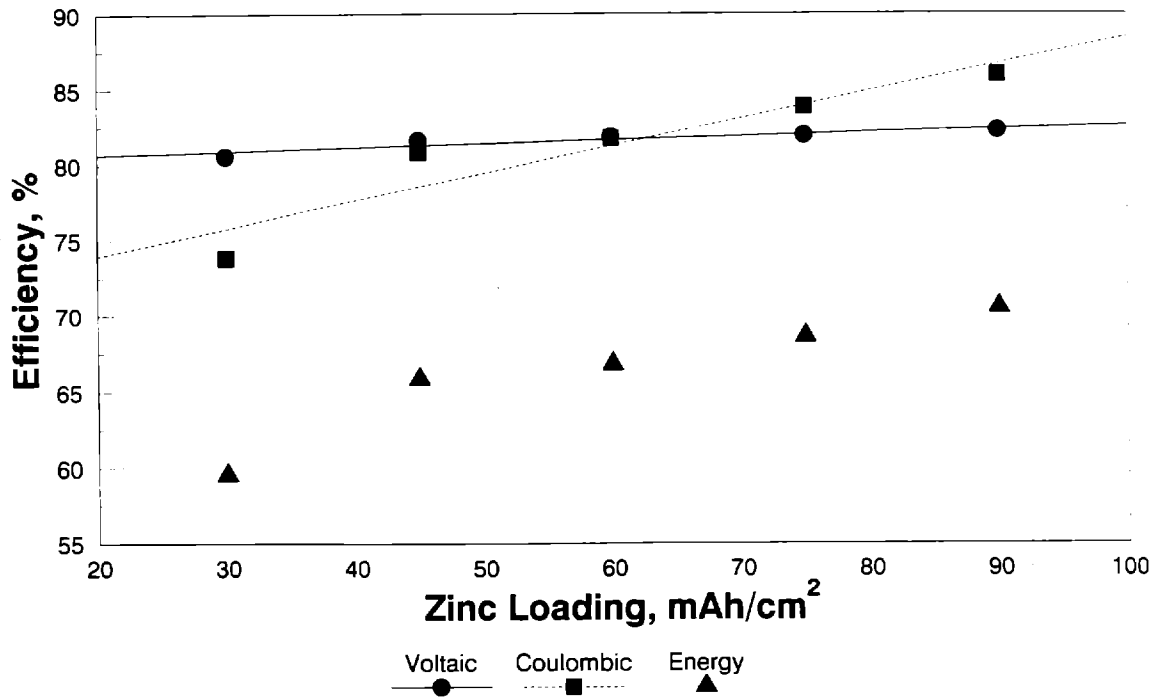


Figure 3-59. Zinc Loading Study at Constant Charge of 20 mA/cm² and 24°C, Efficiencies

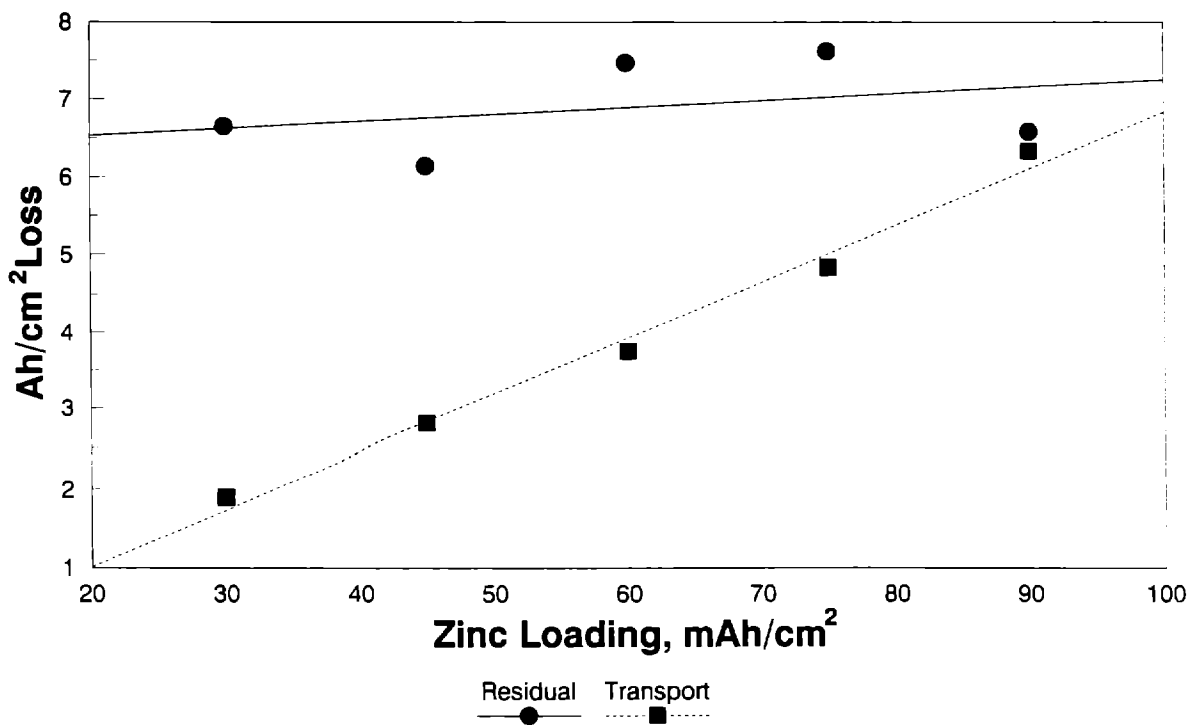


Figure 3-60. Zinc Loading Study at Constant Charge of 20 mA/cm² and 24°C, Residual and Transport Losses

Midway through the tests, testing was suspended when an electrolyte leak was discovered at the cathode terminal electrode. Also, an oil leak in the catholyte pressure gauge was detected, making it difficult to read the pressure accurately. These problems were addressed and testing resumed. Upon completion of the second set of parametric tests, the results were compared with the first set. The conclusion was that, within experimental error, the results were the same and battery temperature, at these two temperature values, had little or no effect.

After completing 57 cycles (Figure 3-61), the battery was removed from test due to continuing problems with leaks both internal to the battery stack and in the catholyte tank. Also during the testing of this battery, leaks were encountered in the catholyte pump. This problem was addressed by JCBGI and was resolved so that it would not be an issue in future deliverables. The battery was disassembled and returned to JCBGI for post-test analysis.

On May 15, 1991, the second battery (JCBGI #VI-57), an 8-cell, 1-kWh unit was delivered to SNL. Due to splitting of an internal weld on the previous deliverable, as well as several other JCBGI laboratory batteries that led to failures, an improved weld was incorporated on this battery. It included a mold modification that changed the weld bead to a double weld in the center of

the flow frame. A total of 26 cycles was run on the battery at JCBGI before it was shipped to SNL. The first cycle was run at a zinc loading of 45 mAh/cm², the next two cycles were run at 75 mAh/cm², and the remainder of the cycles were run at 90 mAh/cm². The coulombic efficiency on cycle 26 was 88.9% while the energy efficiency was 75.1% and the voltaic efficiency was 84.7%.

Upon arrival at SNL, the battery was assembled and designated SNL #518. Tests were then started at 90 mAh/cm². Figure 3-61 is a plot of the battery efficiencies for all the cycles run at JCBGI and SNL. Initial start-up efficiencies at SNL compared well with the results achieved at JCBGI. However, a fairly substantial decline in efficiency was observed during the first 12 cycles at SNL. This decline was caused by an imbalance in the electrolyte tanks when the valve in the 1/4" reservoir tie-line, which is used to balance the tanks, was left partially open. Once the electrolyte tanks were balanced and the tie-line valve was closed, the battery efficiencies returned to values close to the JCBGI results.

This battery station was built such that the levels in the reservoirs could be controlled by sealing the catholyte reservoir tightly after the system had stabilized at start-up. The air head above the electrolyte will

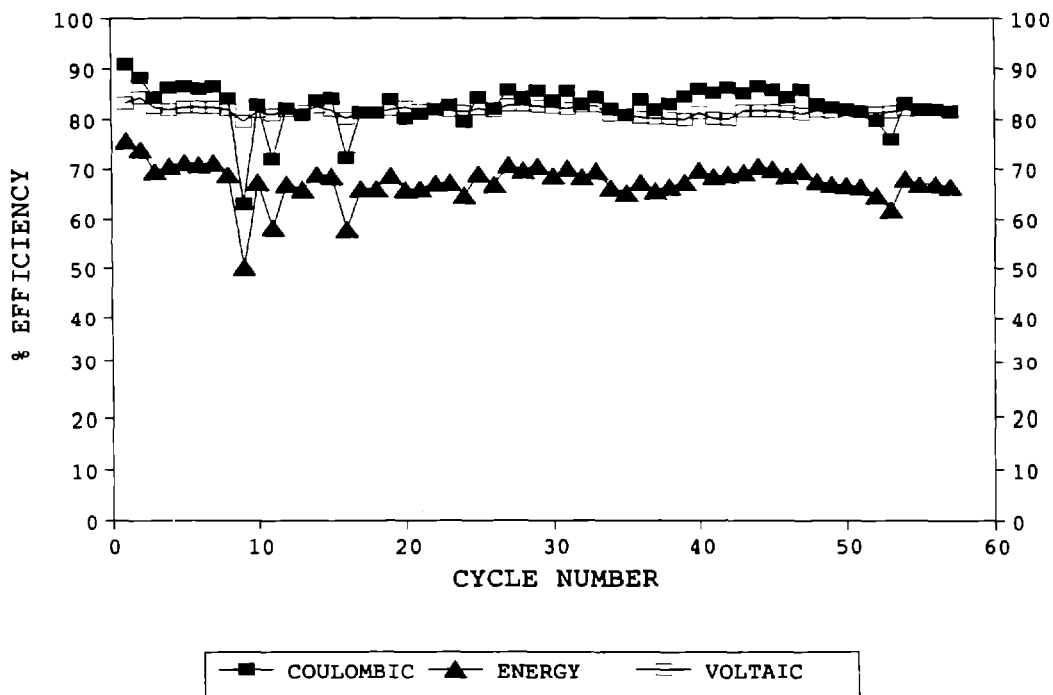


Figure 3-61. SNL Data (Battery #514), 50-Cell Zinc/Bromine

either create a vacuum if the level falls or build pressure if the level rises. By sealing the reservoir, the levels on both sides remain relatively constant. During the first hundred or so cycles, a poor seal in the catholyte tank caused an imbalance to occur that produced a gradual decline in coulombic and energy efficiency. This gradual decline can be seen in Figure 3-62. After several cycles, the tanks were balanced and the efficiencies returned to their initial values. This pattern occurred several times during the life of the battery.

A total of 160 cycles has thus far been placed on this battery. The majority of these cycles are baselines; however, two other types of cycles have also been run. Between cycles 108-117, the discharge current was lowered from 24.2 A to 13.7 A; this produced an increase in both the voltaic and energy efficiencies. The other type of test performed on the battery was a series of no-strip cycles. This occurred between cycles 133 and 137 as shown in Figure 3-62. An increase in coulombic and energy efficiency occurred during the first two or three no-strip cycles but started to decline on subsequent no-strip cycles.

This battery continues to perform well with losses in coulombic and energy efficiency of less than 3% over 160 cycles. There have been no leaks from weld failures or connections and the pumps have performed

without any problems. The battery will continue to be cycled using baseline parameters in an attempt to establish a life-cycle capability.

Applied Research - SNL

Durability Studies

Warping of the first carbon-plastic electrodes that were used in the zinc/bromine batteries during operation resulted in disruption of the electrolyte flow, loss of efficiency, and ultimately was suspected to be the cause of battery failure. In previous work at SNL, it was demonstrated that warpage was caused by both sorption and chemical attack by the electrolyte. The plastic used in these early electrodes was polypropylene (PP). PP contains tertiary hydrogens at every other carbon in the chain; tertiary hydrogens are prone to both oxidation and bromination. Studies showed that both these types of degradation reactions did take place when the electrodes were exposed to the electrolyte used in the zinc/bromine battery. Furthermore, in accelerated aging studies it was shown that the lifetime of these electrodes might be limited to about 96 months. HDPE has physical properties that are similar to that of PP but

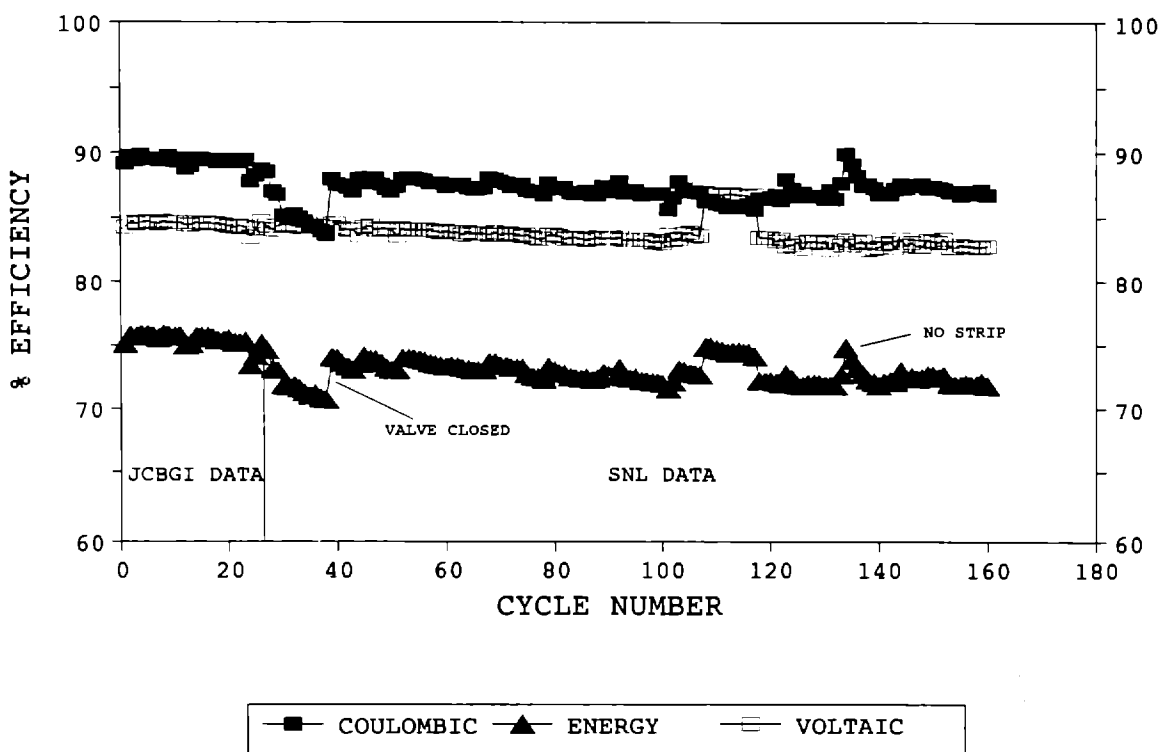


Figure 3-62. JCBGI and SNL Data (Battery #518), 8-Cell Zinc/Bromine

does not contain tertiary hydrogens. Because of the lack of tertiary hydrogens, HDPE should be more stable in bromine-containing electrolytes. On the premise that this was true, JCBGI made two developmental electrodes that used HDPE as the plastic binder. The purpose of this SNL work was to evaluate the stability of these new electrodes toward the electrolyte that is used in the zinc/bromine battery.

The electrodes evaluated in this study were glass-filled formulations that are proprietary to JCBGI. These electrodes are considered to be developmental in nature and were designated as HDPE-1 and HDPE-2. Historically, HDPE-1 was developed at an earlier date than HDPE-2. These electrodes were aged in synthetic electrolyte having the following composition: 1 M ZnBr₂, 3.5 M NH₄Cl; 0.8 M methyl morpholinium (MEM) Br (bromine complexing agent); 0.8 MEP Br (bromine complexing agent); 2 M Br₂. The aging matrix is shown in Table 3-17. Agitation of the electrolyte was provided in the ambient-temperature runs. In these runs, the electrode samples were contained in two Erlenmeyer flasks mounted on a Labline Orbital Shaker to ensure better contact with the bromine complexing agents. Samples in the elevated temperature runs were suspended in the aqueous phase of the electrolyte and there was no agitation.

Electrode properties that can change as a result of chemical attack or sorption include mass, size, modulus, melting behavior, volatiles content, and electrical conductivity. These changes were monitored using the following instrumentation: a five-place Mettler balance (mass); calipers (length, width, and thickness); a Rheometrics Mechanical Spectrometer (shear modulus as a function of temperature); differential scanning calorimetry, DSC (melting temperature and heat of fusion); thermogravimetric analysis, TGA (volatiles and residuals); Signatone four-point probe (conductivity). Changes in chemical structure can be monitored directly by FTIR.

On the basis of 1-mo (mostly complete) and 3-mo (partial) data, HDPE-2 appears to be more resistant to the effects of electrolyte exposure than HDPE-1. HDPE-2 is the newer version of the electrode that has a higher glass content than HDPE-1. This was confirmed by TGA; in this analysis all of the organics and carbon were burned off, leaving only the glass fibers as residue. The glass fiber contents of HDPE-1 and HDPE-2 were found to be 21 and 32%, respectively. There was no evidence within a 1-mo time frame for chemical degradation of either HDPE-1 or HDPE-2 even at 60°C. FTIR spectra for all of the aged samples were essentially identical to the unaged controls. Furthermore, no significant changes in melting point and only relatively small changes in crystallinity (as measured by heats of fusion) were observed by DSC analysis (Table 3-18).

More pronounced differences between HDPE-1 and HDPE-2 were evident, however, in another thermomechanical analysis, namely shear modulus (*G'*) vs temperature. It is possible that shear modulus is more sensitive to sorption effects, which, in general, would be expected to lower the shear modulus. One- and 3-mo data of *G'* vs temperature data for HDPE-1 and HDPE-2, which were aged at 60°C in the electrolyte vs unaged samples, are shown in Figures 3-63 and 3-64.

The shear moduli of both the controls and the aged electrodes decrease with temperature rather gradually up to about 120°C where a very large decrease in modulus occurs. This large decrease in modulus is attributable to the melting transition of polyethylene. Notice that the moduli of HDPE-1 are uniformly lower after 1- and 3-mo aging at 60°C prior to reaching the melting point. This trend, however, was not apparent with HDPE-2. The decrease in modulus as a function of aging time at 60°C was well outside the experimental error, which was determined to be plus or minus 18%. Since there was no evidence of chemical attack by FTIR, the difference in aging between HDPE-1 and HDPE-2 was attributed to physical effects such as electrolyte

Table 3-17. Aging Matrix

| Temperature (°C) | Time (months) | | |
|------------------|---------------|---|---|
| | 1 | 3 | 6 |
| Ambient | X | X | X |
| 40 | X | X | X |
| 50 | X | X | X |
| 60 | X | X | X |

Table 3-18. Melting and Heat of Fusion Data on Aged and Unaged Electrodes (1 Mo Data)

| Electrode | Melting Point (°C) | Heat of Fusion (J/g) |
|------------------|--------------------|----------------------|
| HDPE-1 (Control) | 125 | -91.2 |
| RT | 126 | -88.1 |
| 40°C | 125 | -88.5 |
| 50°C | 124 | -85.4 |
| 60°C | 124 | -86.1 |
| HDPE-2 (Control) | 125 | -64.1 |
| RT | 125 | -70.8 |
| 40°C | 125 | -67.1 |
| 50°C | 124 | -72.8 |
| 60°C | 124 | -68.7 |

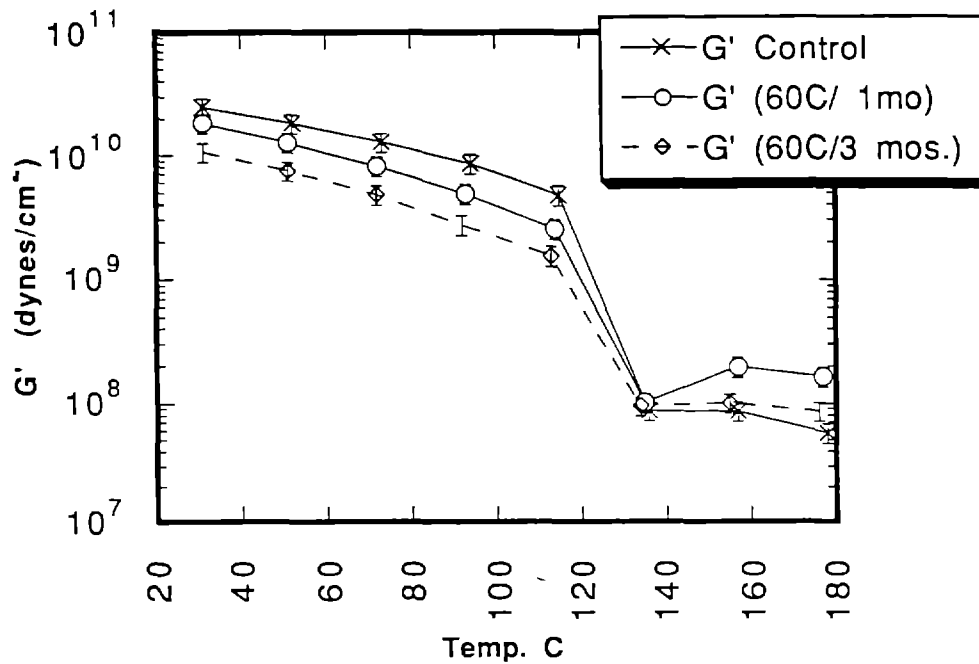


Figure 3-63. Shear Modulus vs Temperature of HDPE-1

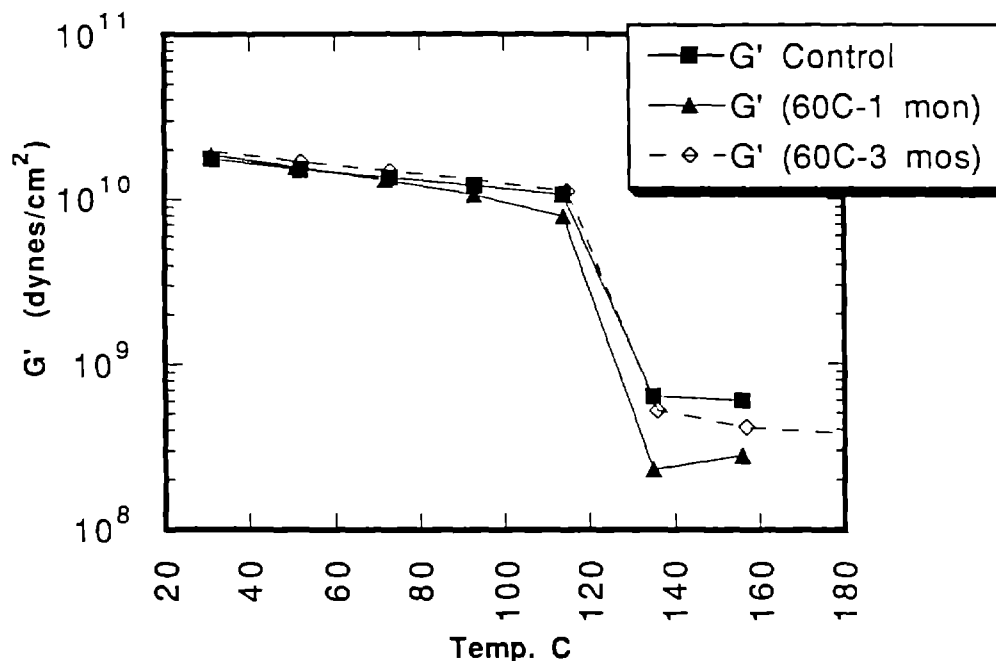


Figure 3-64. Shear Modulus vs Temperature of HDPE-2

sorption. Comparative sorption data for HDPE-1 and HDPE-2 are shown in Table 3-19.

The study will be completed in FY92.

Improved Membranes

The efficiency of zinc/bromine flow batteries is highly dependent on material used to separate electrolyte in the anode compartment from the electrolyte in the cathode compartment. In very early work, the highest efficiencies were reported with ion exchange membranes. These membranes were not considered to

be economically feasible, however, and were replaced by very inexpensive separators such Daramic[®]. Daramic[®] is a silica-filled microporous polyethylene material that is made by extrusion in the presence of a pore-forming oil. The problem with Daramic[®] and other similar separators such as Asahi's SF-600 is that they are nonselective. Because separators are without fixed charges on a molecular level, they do not discriminate or reject either negative or positive ions. They are also highly permeable to neutral species in the electrolyte such as dissolved bromine. The rate of migration of all these species, however, is reduced by separators because of the reduced available volume

Table 3-19. Sorption Data for HDPE-1 and HDPE-2

| Electrode | Temperature (°C) | Time (mo) | % Weight Gain* |
|-----------|------------------|-----------|----------------|
| HDPE-1 | 60 | 1 | 4.6 |
| HDPE-1 | 60 | 3 | 4.4 |
| HDPE-2 | 60 | 1 | 2.0 |
| HDPE-1 | 60 | 3 | 1.7 |

* After water washing off excess electrolyte salts and drying.

compared to the bulk solution and because of the tortuosity of the pores. Permeation of bromine and negatively charged bromine complexes is sufficiently high that the energy efficiency of zinc/ bromine batteries seldom exceeds an average of 65% over numerous charge-discharge cycles. Previous work showed that the rate of bromine permeation could be reduced by as much as an order of magnitude by impregnating the separator with an ionic polymers such as sulfonated polysulfone (SPS) or Nafion. During the past year, methods were investigated to reduce the leaching of SPS that occurred when these SPS-modified membranes were cycled in single-cell batteries; studies were also carried out to assure there were not any age-related problems associated with the Nafion modified membranes. In addition, new approaches to the preparation of membranes were investigated that offer the potential of either improved performance or reduced costs.

Leaching Problem

In early work, it was found that the stability of cast films of SPS appeared to be satisfactory based on exposure tests in which the films were immersed in the two-phase bromine electrolyte at elevated temperatures (50°C) for time periods up to 1 mo. No change in the modulus of the film was observed. Nevertheless, when Daramic[®] was impregnated with SPS and cycled in a single-cell battery, some SPS leached out and caused plugging of the electrolyte plumbing. The discrepancy between SNL aging experiments and battery observations may be due to enhanced contact of the oily phase in the electrolyte with the SPS, which resulted in a deterioration of the adhesive bond of the SPS and the polyethylene substrate. Softening of the SPS by the oily phase of the electrolyte may have also contributed to the loss of SPS from the substrate.

Another possibility is that the SPS simply dissolved in the electrolyte after being attacked by the bromine phase. One possible way of preventing leaching is to crosslink the SPS. This might be accomplished thermally or by exposure to ionizing radiation. Previous work demonstrated that the acid form of SPS can be crosslinked at 250°C. At these temperatures, SPS thermally decomposes and evolves sulfuric acid. This reaction is accompanied by the formation of sulfone crosslinks. This procedure would be impractical for SPS-impregnated Daramic[®] because Daramic[®] melts at about 100°C. To determine if SPS can be crosslinked thermally at lower temperatures, it was heated at 95°C for varying time periods up to two weeks and tested for crosslinking by looking the the formation of sulfone groups by Fourier Transform Infrared Spectroscopy. The solubility of SPS in dimethyl formamide was also

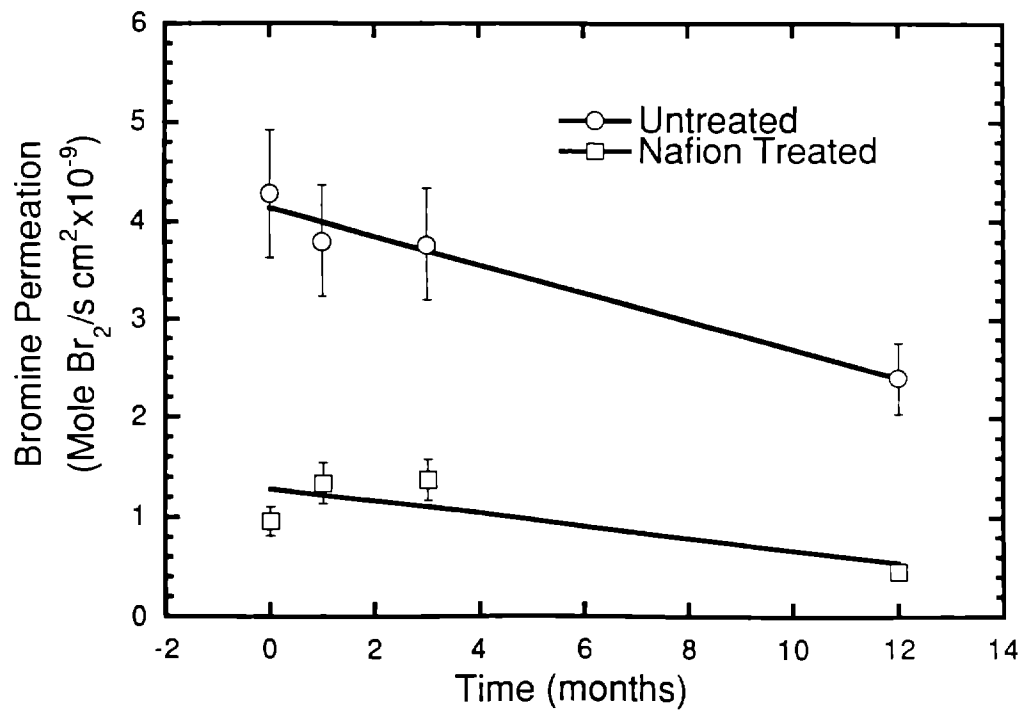
monitored. No crosslinking was observed under these conditions. The effect of exposing SPS to gamma radiation in a cobalt⁶⁰ source did not appear to significantly decrease the solubility of SPS.

Durability of Nafion-Treated Separators

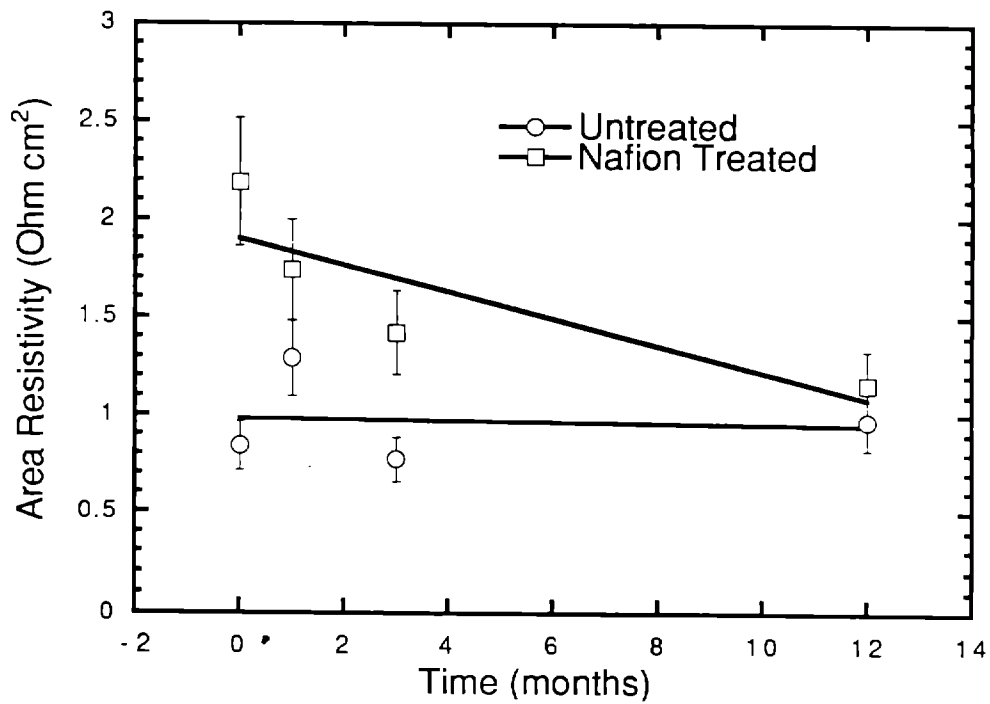
Nafion-treated separators have shown considerable promise in both laboratory screening tests and single-cell cycling experiments. These membranes substantially reduced bromine permeation with a very modest increase in area resistance. Furthermore, Nafion-treated membranes were not stained after exposure to the electrolyte, which suggests that the oily bromine phase of the electrolyte was excluded from the membrane. In this respect, Nafion-treated separators differ from the SPS-treated separators. Durability tests were carried out with the Nafion-treated separators to see if problems similar to those encountered with the SPS membranes exist. In these tests, the membranes were immersed in the two-phase electrolyte and stirred at ambient conditions. The membranes were removed at regular intervals and tested for area resistivity and bromine permeation. The results are shown in Figure 3-65. The permeation of the untreated and Nafion-treated Daramic[®] decreased somewhat during the 12-mo aging process while the area resistivity of the Nafion-treated Daramic[®] decreased by approximately a factor of two. These results suggest that the aging process would improve the performance of the Nafion-treated membrane. Larger sheets of Nafion-treated separators were fabricated and sent to JCBGI for evaluation.

New Membranes

Other microporous substrates and other ionic resins are being investigated. JCBGI has begun a program to develop an improved microporous separator. SNL has evaluated the effect of impregnating this separator with a commercial sulfonated polyester obtained from Eastman Kodak (Eastman AQ 55D). The structure of Eastman AQ 55D is shown in Figure 3-66. The potential advantages of this ionomer is that it is relatively inexpensive and can be chemically crosslinked with either polyvalent metal ions or aminoplast resins, if necessary. It can be obtained in either solid form (pellets) or as a 28% aqueous solution. In initial tests, Eastman AQ 55D appeared to be insoluble in the electrolyte used in the zinc bromine battery. Precipitation occurred when an aqueous solution of the sulfonated polyester was added to the electrolyte. One possible explanation for this is that zinc ions, being polyvalent, caused the resin to crosslink. A series of membranes was prepared by immersion of the separator



(a)



(b)

Figure 3-65. Bromine Permeation (a) and Area Resistivity (b) of Untreated Daramic[®] and Nafion-Treated Daramic[®] as a Function of Aging Time in the Battery Electrolyte

Structure of Eastman AQ-55D

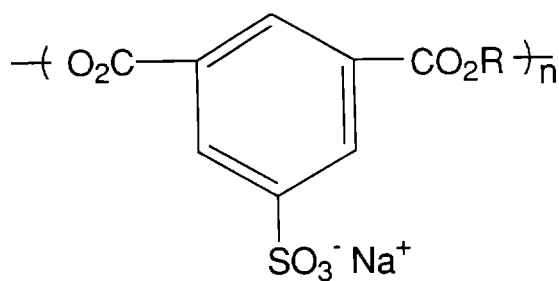


Figure 3-66. Chemical Structure of Eastman Kodak's Sulfonated Polyester: Eastman AQ 55D

in aqueous solutions of Eastman AQ 55D at various dilution levels followed by a drying step. The normalized area resistivity and bromine permeation rates of these membranes as a function of the dilution ratio are shown in Figure 3-67. At the highest concentration of the sulfonated polyester, i.e., 0 dilution, the bromine permeation was reduced by almost two orders of magnitude but the area resistivity increased to a level that is probably not acceptable. Better trade-offs between area resistivity and the bromine permeation rate were achieved at higher dilutions of the polyester ionomer. Experiments are under way to determine if the sulfonated polyester is leached from the separator by the electrolyte over time. JCBGI has evaluated this membrane and found that the resistance increased only 17% while the bromine permeation decreased by 43%. JCBGI uses a catholyte that has a higher bromine content than that used for permeation tests at SNL.

In all of the separator treatments described above, the ion exchange capacity of the impregnating agents was relatively low. It has been established in structure-property relationship studies that increasing the ion exchange capacity results not only in lower area resistivities but also improved selectivity. These effects are attributable to the increased concentrations of both

mobile and *fixed* ions in the membrane. On the basis of these findings, *composite* membranes with relatively high ion exchange capacities were prepared by radiation grafting and plasma deposition techniques.

The radiation grafting experiments were carried out in a cobalt⁶⁰ source, which is available at SNL. In all of these experiments, methacrylic acid (MAA) was grafted into the pore structure of JCBGI's developmental separator. The experimental procedure for the preparation of radiation-grafted membranes is shown in Figure 3-68. To determine the conditions required for effective grafting, a scoping type study was carried out in which the following experimental parameters were evaluated: 1) type of solvent; 2) concentration of MAA; 3) use of cheesecloth as a standoff material (in these experiments the separator was wrapped around a steel bar; to assure adequate contact with the grafting solution, cheesecloth was inserted between the separator and the steel bar); 4) effect of a crosslinker (divinylbenzene, DVB) 5) effect of cuprous chloride (an agent which is alleged to reduce the extent of homopolymerization); 6) total dose; and 7) dose rate. Graft yields were found to be a function of the concentration of monomer and increased markedly when 1-3% of the crosslinker was added. Normalized bromine permeation and area resistivity as

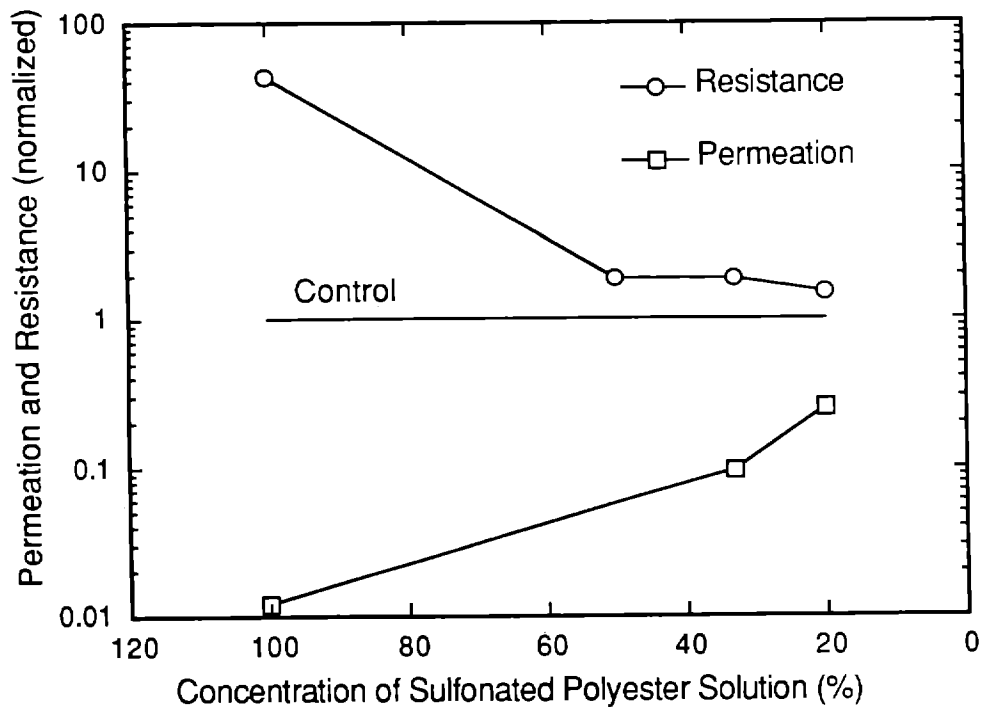


Figure 3-67. Normalized Resistance and Permeation of JCBGI's Developmental Separator vs Impregnation Dilution with Eastman AQ 55D

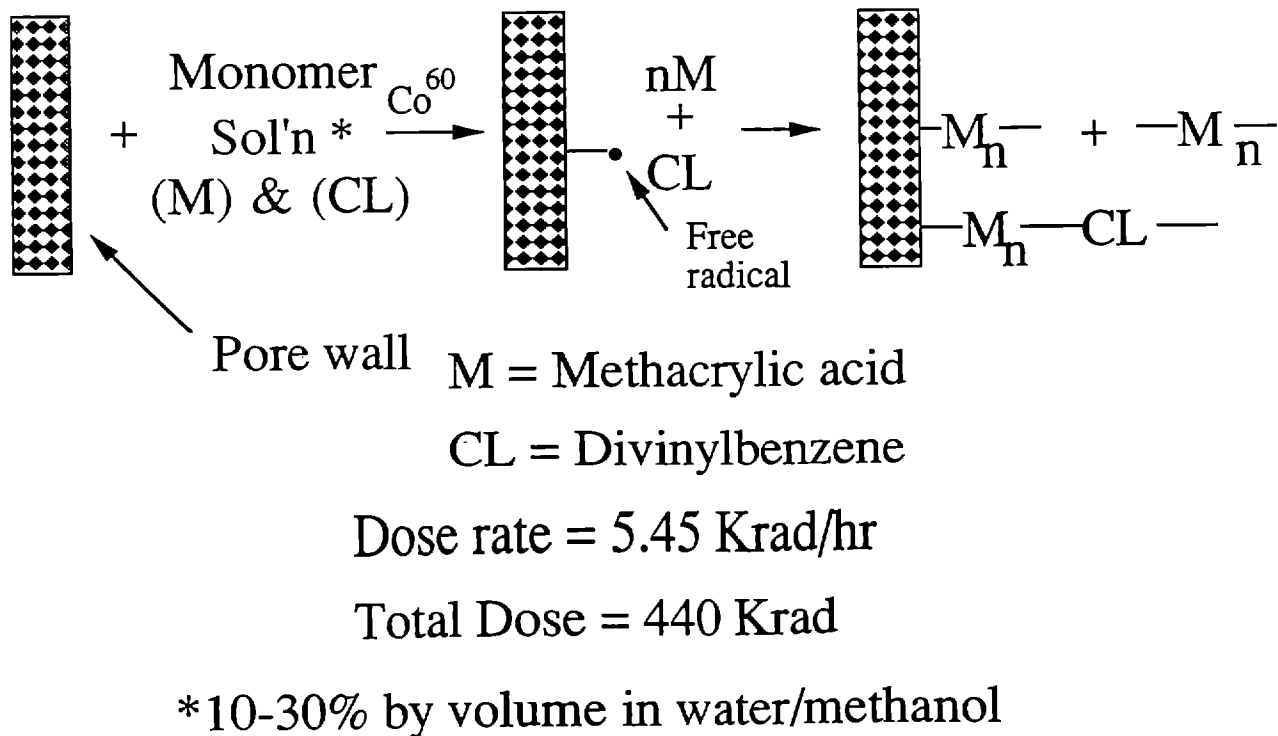


Figure 3-68. Experimental Procedure for Preparing Radiation-Grafted Membranes

a function of graft yield are shown in Figure 3-69. The permeation of bromine was substantially reduced, although the area resistivity of the membrane increased. Samples of this membrane have been sent to JCBGI for evaluation.

The solubility and structure of plasma coatings made from MAA and mixtures of MAA and DVB using a capacitively coupled plasma unit were evaluated. In previous work, we found that the power levels used to create the plasma should be kept as low as possible so as not to destroy the ionic functionality in the deposited film. FTIR analysis of coatings made from pure MAA showed absorption bands for carboxylic acid groups indicating that ionic functionality had *not* been destroyed in the plasma. Unfortunately, these coatings were soluble in both water and acetone and would probably dissolve in the battery electrolyte. Coatings made from mixtures of MAA and DVB were insoluble and should survive dissolution by the electrolyte. FTIR analysis of these coatings was consistent for what one would expect for a crosslinked copolymer of MAA and DVB. Absorption bands for both aromatic and carboxylic acid groups were present in the spectrum of the deposited film. SNL is now in the process of modifying microporous polyethylene substrates with this coating.

The utility of modifying the Daramic[®] membrane with a silica coating prepared by the sol-gel process is

being investigated. Sol-gel technology provides a means to prepare glass-like materials at low temperatures. Ceramists at SNL have developed procedures to tightly control the pore sizes of these materials when used as coatings. The average pore diameter of the untreated Daramic[®] substrate is 360 nm. This is several orders of magnitude larger than the molecular diameters of the electrolyte species. Thus, the Daramic[®] substrate cannot discriminate between electrolyte species on the basis of their size, but can only decrease the volume of electrolyte and provide a tortuous pathway. The pore sizes of the silica coatings, when applied to bulk substrates, can be specified from 0.4-2.0 nm. These diameters are comparable to the diameters of the electrolyte molecules and are therefore expected to discriminate on the basis of size. The silica coating may offer a substantial improvement in performance if the selectivity of the membrane can be increased. The initial sol-gel coating applied to Daramic[®] was prepared using a formulation developed for bulk substrates. The coating decreased bromine permeation by only 20%, while the resistance was not affected significantly. It is believed that the relatively minor improvement indicates that the silica coating may not have completely spanned the pores of the Daramic[®] substrate. Future preparations will be modified accordingly and/or multiple coatings will be applied.

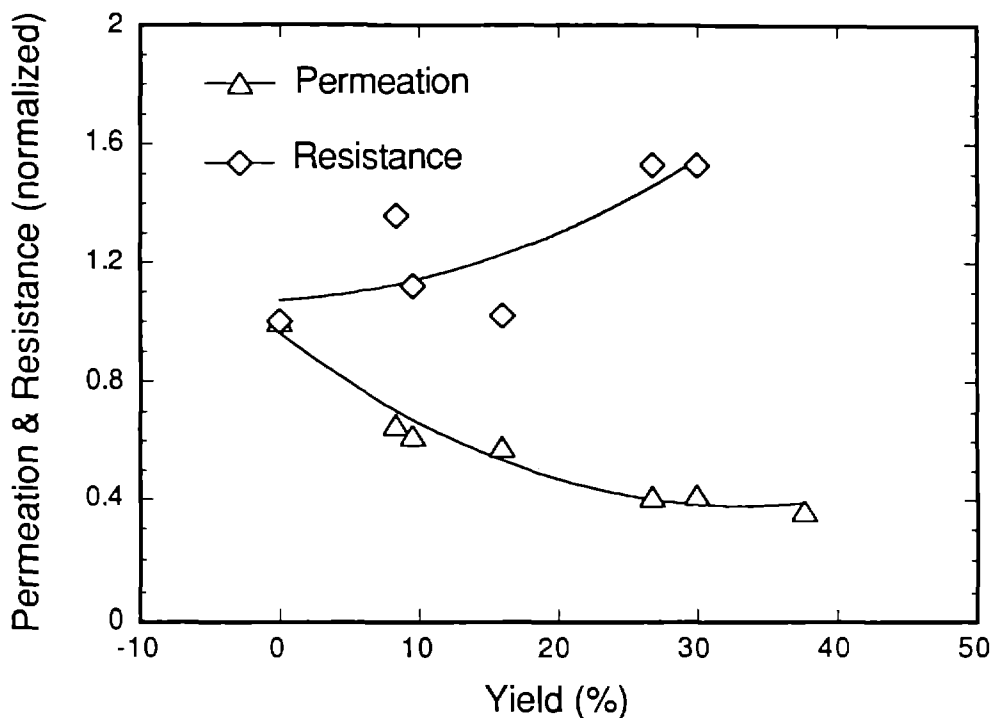


Figure 3-69. Effect of Grafting Methacrylic Acid and Divinylbenzene into the Pores of JCBGI's Developmental Separator

4. Systems Studies and Advanced Lead-Acid Technology

The Systems Studies and Advanced Lead-Acid Technology activities are aimed at near- to mid-term goals of the overall program. The Systems Studies activities seek to quantify the benefits that utilities could obtain if battery energy storage were included in the utility network. Since existing planning tools used by utilities do not have the capability of estimating the benefits of battery energy storage, it is necessary to develop such tools and methodologies to enable utilities to assess the impact of storage in their electric networks.

The Advanced Lead-Acid Technology activities focus on improvements to battery energy storage systems leading to advanced designs that meet utility application requirements. The goal is to have such advanced lead-acid battery designs available for utility applications in the mid- to late-1990s, preceding the commercial introduction of other advanced battery technologies in the year 2000 and beyond. Specific activities include development of advanced VRLA batteries and a modular battery concept called the "AC Battery."

Utility-Specific Systems Studies

The widespread commercialization of battery energy storage technology in utility networks is contingent on the demonstration of quantifiable benefits it can offer to the utility industry. However, current planning tools and methodologies used by utilities are not capable of evaluating the net economic impact of the wide range of benefits that battery energy storage could potentially offer the utility network. Analytical tools that can perform such evaluations have to be developed and accepted by utility planners in order to achieve the commercialization goal for this technology.

A specific task of this program is aimed at developing such analytical tools to assist utility planners in evaluating the potential benefits of battery storage for their systems. Such tools will allow utility planners to quantify the benefits of battery storage that are otherwise overlooked by current techniques. During FY91, four utility-specific systems studies were initiated to determine the economic value of battery storage for utilities with widely differing operating environments.

These studies are aimed at achieving several objectives. First, the experience gained from performing these and related studies would be the basis for developing more generalized, global benefit screening methodologies. Next, the studies involve the participant utilities in actively evaluating battery storage in their system and perhaps implementing a battery storage project if it is deemed economically feasible. Finally, the results of these and other future studies will allow a more accurate assessment of the size of the battery energy storage market in the utility sector. Market size projections that are based on generic, regional assumptions tend to yield inaccurate and inflated estimates that are not indicative of the true market size.

In FY91, studies were initiated with four utilities:

- Bonneville Power Administration (BPA)
- San Diego Gas & Electric (SDGE)
- Oglethorpe Power Corporation (OPC)
- Chugach Electric Association (CEA)

Table 4-1 summarizes the schedule and costs to SNL for each study. All except the Bonneville Power Administration study were started too late for any significant results to be reported at this time. Instead, some of the salient features of each system study are described below.

Bonneville Power Administration

The BPA study initially focused on the potential for solving transmission reliability problems encountered in the Puget Sound area using battery storage to stabilize the system and also defer planned generation capacity additions to meet growing load requirements.

Due to rapid load growth in the Puget Sound area, the existing BPA transmission network across the Cascades that supplies the major portion of the region's power requirements was approaching its stability limits under certain weather conditions. Load management strategies to limit the loading on these transmission lines would offer temporary relief until transmission and distribution (T&D) growth catches up at some future time.

Table 4-1. Utility-Specific Systems Studies: FY91

| Utility | Sandia Contract | Utility Cost Share | Start Date | End Date |
|---------------------------------|-----------------|--------------------|------------|----------|
| Bonneville Power Administration | \$70K | No | 2/91 | 11/91 |
| San Diego Gas and Electric | \$46K | Yes | 8/91 | 12/91 |
| Oglethorpe Power Corp. | \$47K | Yes | 7/91 | 11/91 |
| Chugach Electric (Alaska) | \$43K | Yes | 9/91 | 1/92 |

An initial fact-finding meeting was held with BPA staff in February 1991. At that time, BPA was evaluating nine scenarios that could potentially offer solutions to these regional problems. However, these nine planning scenarios were modified by BPA in June, changing the basic assumptions governing the SNL system study. As a consequence, another meeting was held with BPA in July 1991 to obtain the revised planning scenarios. Under the revised scenarios, BPA was implementing an intertie of two existing transmission lines that would increase the reliability of the transmission system and defer the need for a new transmission line for several years. The new scenarios also assumed that the local Puget Sound utilities would install additional combustion turbines to meet peak loads.

The intertie option substantially impacts the ability for battery storage to compete as a viable option. SNL will continue to evaluate the revised BPA scenarios in early FY92.

San Diego Gas & Electric

The SDGE system study was started in August 1991. Meetings were held with various departments at SDGE to obtain generation and transmission and distribution planning information. The SDGE system has a base load of about 1,200 MW and a peak of about 300 MW that lasts ~3 hr. SDGE is interconnected to other utilities that make up the Western System Coordinating Council, and has access to a large power pool through this council.

The approach in this study will be to examine the benefits of battery storage to offset conventional spinning reserve generation capacity, change the unit commitment schedule, or capture some savings from changing unit ramping rates. In the area of T&D, battery

storage benefits for accommodating load growth at substation sites will be investigated to determine if there are potential benefits to be obtained.

By the end of this reporting period, the SNL study had not progressed to a point where any specific results could be disclosed. However, it is planned that a presentation of the preliminary results will be made to the SDGE staff in late November 1991.

Oglethorpe Electric Power Corporation

The OPC study commenced in July 1991. OPC sells power to 39 electric member coops with a peak load of approximately 3,500 MW. OPC buys the bulk of its power from Georgia Power Company and also owns its own generation plants, including the Rocky Mountain pumped storage facility.

Due to the presence of substantial hydro-pumped storage on the OPC system, it is unlikely that there are any generation-side benefits that battery storage may offer. However, the vast, sparsely populated service area of the OPC system offers a strong opportunity to utilize battery storage in key locations in the transmission network and capture substantial T&D-side benefits. The SNL study is pursuing this approach, and it is expected that results could be reported early in FY92.

Chugach Electric Association

CEA serves the Anchorage and Kenai peninsula area in Alaska. CEA is interconnected with other Alaskan utilities via a single transmission corridor that runs from Juneau through Anchorage to Fairbanks. CEA generation sources include a mix of coal, hydro, and combustion turbines. The SNL system study was

started on September 16, 1991, and it is focusing on both generation and T&D benefits of battery energy systems.

Due to the sharing of a single transmission corridor by several utilities and the geographic location of the generation plants, it appears that CEA might benefit from battery storage to displace substantial amounts of spinning reserve capacity. The SNL study will also examine the potential for battery energy storage to displace planned transmission line additions.

Completion of the CEA study is scheduled for no later than January 1992.

Battery System Development - GNB

A 3-yr, \$2.83M development effort was initiated with GNB Industrial Battery for the improvement of VRLA battery designs to meet utility application requirements in the mid to late 1990s. Current VRLA battery designs are geared to meet the needs of automotive and industrial applications and are not optimized for utility applications that have different operating requirements. The GNB effort will develop an advanced VRLA battery designed to meet utility needs. The statement-of-work and the make-up of the project team for this contract were specially defined to ensure that GNB obtains first-hand input from utilities about battery storage requirements in their network. A host-utility function was incorporated that required GNB to form a relationship with one or more electric utilities to understand the function of battery storage in the utility network and obtain information on battery operational requirements and economics.

The GNB effort will study the specific requirements for two utility applications and develop an advanced VRLA battery to meet those requirements. Two host utilities, Pacific Gas & Electric (PGE) and Puerto Rico Electric Power Authority (PREPA) are participating on the GNB project team. Both utilities will identify site-specific battery storage applications in their network and define the requirements that will guide the GNB battery design effort. The utilities will also perform economic analysis of their selected applications to identify the economic feasibility of battery applications using current technology costs as well as the cost for the advanced VRLA design.

Recognizing the near-term market potential, GNB is cost-sharing the contract at 46%. Both host utilities are also cost-sharing their participation as sub-contractors

to GNB—PREPA at 100% and PGE at 50%—which is indicative of their strong interest in this effort.

The GNB effort is comprised of three tasks. Task 1 is a two-phase activity that seeks performance improvements through changes in battery design. Tasks 2 and 3 are based on requirements definition and economic evaluations that require extensive host utility participation.

Due to the late start-up of the contract and staffing difficulties at GNB activities were not begun until September. Progress has been made in several subtasks in both Phase I and II of Task 1.

Task 1: VRLA Cell Technology Improvement Study

Phase I: Absolute Improvements

Work on some of the activities in this task was initiated, including improvements in thermal management, ground fault elimination, and production process improvements. Test set-ups for conducting this work have been defined and test equipment is being purchased at GNB's cost as proposed. It is expected that the equipment will be operational in late December 1991 or January 1992.

Phase II: VRLA Advancements

Several activities aimed at improving positive active material utilization, inhibiting grid corrosion mechanisms, and improving grid alloys are under way, with the aim of reducing battery cost and increasing battery life.

Task 2: Development of Specifications and Baseline Design

The activity under this task is subcontracted to the University of Missouri-Rolla (UMR), PGE, and PREPA. A delay in negotiating the final contracts with all three entities affected the timely start-up of work in this task.

At the end of FY91, the UMR contract was executed and the PGE and PREPA contracts were in the final negotiation stages.

Task 3: Cost/Benefit Study and Improved Design

This activity follows on to Task 2. It commences after the baseline design specification is completed in that task.

AC Battery Development

Omnion Power Engineering Corp. has patented an AC Battery concept, which is a modular, transportable battery system of 500-kW/500-kWh capacity. The unit contains 36 modules of nominally 14-kW/14-kWh each, that have built-in power conditioning and control electronics. At present, the AC Battery is in the concept stage and needs engineering development to reach an operating system stage. Early in FY92, a 15-mo con-

tract will be placed with Omnion to implement the engineering development program to build and test the first prototype unit at a utility site in the PGE service area. A review team comprised of PGE operations and engineering staff will provide various specifications for the control of and communication with the prototype AC Battery container, and will participate actively in the development process through design reviews at all critical stages.

5. Supplemental Evaluations and Field Tests

Nickel/Hydrogen Evaluation

Johnson Controls Battery Group, Inc., contract #78-8203, provided technical support for the testing of four 2-kWh Common Pressure Vessel nickel/hydrogen batteries, two each at the Florida Solar Energy Center (FSEC) and the Southwest Technology Development Institute (TDI), and the testing of a 7-kWh boilerplate CPV battery at JCBGI.

Program Background

Development of the CPV nickel/hydrogen battery was performed by JCBGI under a series of previous cost-shared contracts with SNL. The program focused on development of a terrestrial nickel/hydrogen battery with a cost compatible broad range of terrestrial applications. Design and process improvements developed in the program brought the cost of the nickel/hydrogen technology down from the \$25,000/kWh cost of previous state-of-the-art aerospace Individual Pressure Vessel (IPV) designs to under \$700/kWh for a mass produced terrestrial design.

In 1988, a 7-kWh CPV battery composed of four separate 10-cell stacks, each contained in a boilerplate pressure vessel, was delivered to SNL. The battery was connected to a photovoltaic array at SNL and performed admirably for over 2 yr of testing. At the culmination of this test program, the battery was returned to JCBGI where it was stored for about a year in anticipation of extended testing.

The last contract in the development series focused on the development of a field-deployable prototype 12-V, 2-kWh unit for remote energy storage. That contract culminated in the delivery of the four 2-kWh units, two each to the FSEC and the TDI.

Battery Design

The 2-kWh batteries are composed of ten series-connected, nominal 160-Ah cells, providing a nominal 12 V. Cells are composed of nine modules (18 positive plates) contained in sealed polyethylene containers. A 10-cell stack is shown in Figure 5-1, prior to insertion into the pressure vessel. Filament-wound vessels with stainless steel liners were specifically developed to pro-

vide a man-safe, leak-before-burst design. The metal liner contains the hydrogen while the filament winding provides the required strength. A pair of 2-kWh batteries in the filament wound vessels is shown in Figure 5-2.

Florida Solar Energy Center Tests

The two FSEC 2-kWh batteries, #P010 and #P022, were delivered in late May of 1990. Initial testing was limited to simple charge/discharge cycling performed with a power supply to facilitate completion and troubleshooting of the data acquisition and test facilities.

The two parallel batteries were then interfaced to a photovoltaic (PV) array with a 1.6-ohm continuous resistive load providing a nominal 7.5-A discharge current for a daily discharge of 180 Ah. This profile was run from October 1990 through January 1991. Maximum daily state-of-charge and minimum daily state-of-charge, as determined from battery pressure monitoring, averaged 50% and 20%, respectively, for the period. However, high-voltage charge (100% state-of-charge) and low-pressure discharge (0% state-of-charge) control terminations were encountered several times during periods of high and low insolation, respectively. Based on this experience the overcharge/overdischarge control schemes appear to work very well.

From February through September of 1991, a series of three simulated application load profiles including lighting, vaccine refrigeration, and repeater station was initiated. Periodically during these application tests, a characterization cycle was run on each of the two batteries independently to provide a baseline test for battery state-of-health. The characterization cycle consists of a C/6 rate (27-A) charge run off a power supply and terminated when the slope of the battery pressure increase reaches 70% of its initial value, and a resistive load discharge approximating a C/5 rate (32 A) to a 10-V cut-off. The two batteries accepted 209 Ah and 206 Ah, respectively, before reaching the charge pressure slope termination. Maximum battery temperatures approached 40°C at the end of the charge. During discharge the batteries delivered 183 Ah and 182 Ah, respectively, well above the 160-Ah nominal rating. Cell pair voltages, measured via voltage taps on every other cell, indicated excellent cell matching.

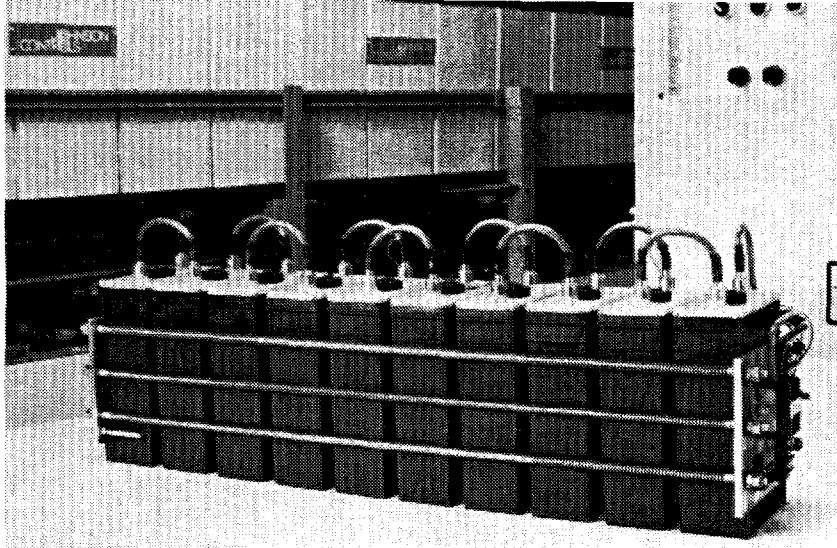


Figure 5-1. 10-Cell Battery Stack

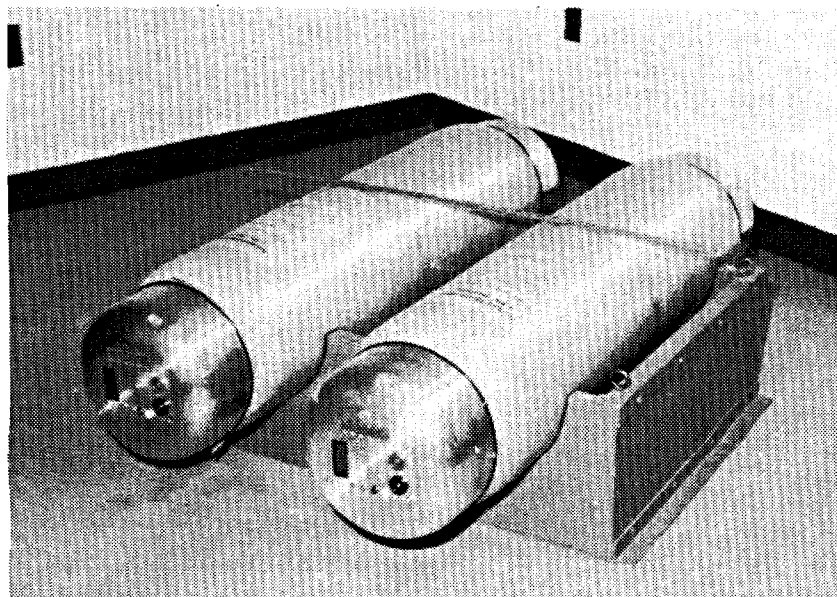


Figure 5-2. 2-kWh Batteries in Filament-Wound Vessels

Following the initial characterization cycles, the batteries were reconnected in parallel to the array. The profile was changed to a simulated lighting profile by doubling the load to 15 A and using a timer to operate the load for a 12-hr period from 6 pm to 6 am.

Figure 5-3 displays typical battery, array, and insolation data for one of the daily cycles. Battery state-of-charge can be followed based on the pressure data in the upper right quadrant of Figure 5-3, based on the predetermined extremes of 300 psi for full charge and 75 psi for full discharge. On this particular day, state-of-charge varied from 90% (250 psi) at the end of the daylight hours to 20% state-of-charge (120 psi) just before sunrise the following day.

A summary of the battery performance during the entire lighting profile test period is provided in Table 5-1. Average daily battery state-of-charge varied between 20% and 65%, with excursions to full discharge, 0%, and full charge, 100%.

After running another set of characterization cycles, the load profile was changed to a simulated vaccine refrigeration cycle for the period from April through June of 1991. The load profile consisted of a 12-A load operated by a repeat cycle timer set to trigger on for 5 min and off for 15 min on a continuous basis. Under this profile the battery experienced a relatively mild depth-of-discharge under normal insolation conditions, allowing several days of autonomy in the event of an extended period of poor insolation.

During the test period, a loss of pressure was observed from the vessel of one of the two batteries. Investigation suggested a vessel leak, possibly related to fatigue from the pressure cycling. Following a brief down period, cycling of the second battery continued. The leaking battery was purged of the remaining hydrogen and returned to JCBGI for failure investigation. At JCBGI, the battery stack was removed from the vessel and placed in a boilerplate vessel for storage.

A destructive analysis was performed on the failed vessel. In general, the condition of the adhesive was excellent and the bond strength between the adhesive and stainless steel components was impressive. However, the source of failure was identified as a fault in the adhesive bonded joint between the dome and cylinder. A large air bubble, apparently trapped in the bond area during initial assembly of the vessel, caused a significant reduction in the width of the bond. As a result, the bond failed prematurely through fatigue stresses induced by the pressure cycling encountered during normal daily operation of the battery. After reviewing these observations, the manufacturer of the adhesive suggested that they develop a modified, less viscous

version of the adhesive to alleviate the problem. The existing adhesive formulation is thixotropic, having a consistency similar to that of whipping cream, and thus has a tendency to trap air bubbles during application and assembly.

While the vessel failure analysis proceeded at JCBGI, the array was reconfigured at FSEC to allow continued testing of the remaining battery on the vaccine refrigeration cycle. Figure 5-4 displays typical battery, array, and insolation data for a daily cycle. As evidenced by the mild fluctuation in pressure, the battery state-of-charge does not drop extensively as long as insolation is good. This provides a significant reserve battery capacity in the event of an extended period of poor insolation, allowing support of the critical refrigeration load. Table 5-2 provides a summary of the entire test period. Due to poor insolation during the period, the average daily maximum state-of-charge averaged only 55%, while average daily minimum state-of-charge averaged 41%. Maximum and minimum state-of-charge during the period was 75% and 25%, respectively.

Following another characterization cycle the load profile was changed to simulate a repeater station, telecommunications application. The resistive load drew approximately 18 A for a period of 1.25 hr, four times a day. Typical daily and weekly data plots are provided in Figure 5-5.

Following the telecommunications profile tests, a final characterization cycle was run on battery P022. The battery accepted 212 Ah to the pressure slope cut-off and delivered 184 Ah on the C/5 discharge to 10 V. This capacity was actually slightly higher than the 182 Ah achieved prior to initiation of the three application profile tests.

Southwest Technology Development Institute Tests

The two 2-kWh TDI batteries, #P004 and #P005, were delivered by JCBGI in mid-July of 1990. These batteries were configured in series to complement the parallel battery testing being done at FSEC. A series of standard system break-in and characterization cycles were run prior to initiating the application profile tests. Table 5-3 and Figure 5-6 provide data from one such cycle. Both batteries delivered 185 Ah, well over the 160-Ah nominal rating. The lower voltage and watt-hour performance of battery #P005 is related to an apparent shorted cell that also affects the battery pressure characteristics (Figure 5-6). Despite the apparent short, battery #P005 continued to operate well and

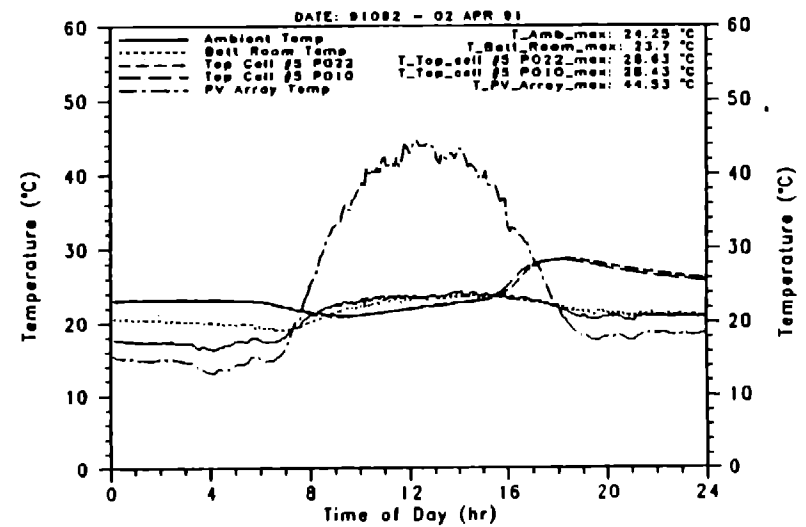
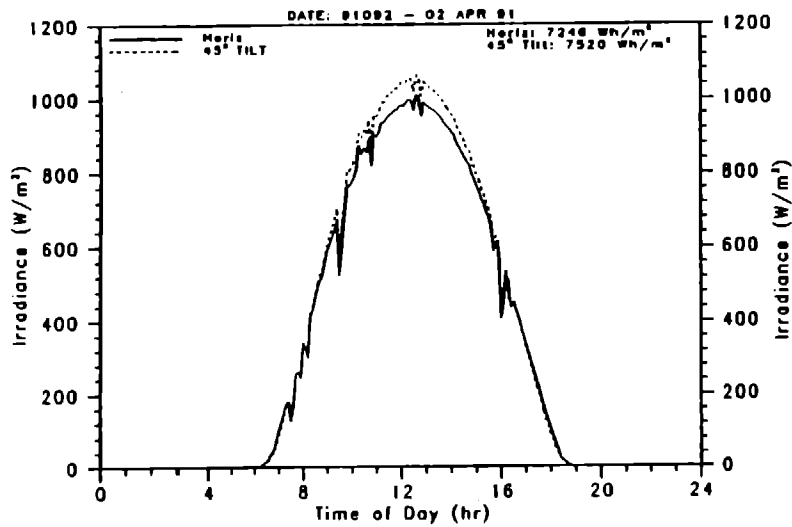
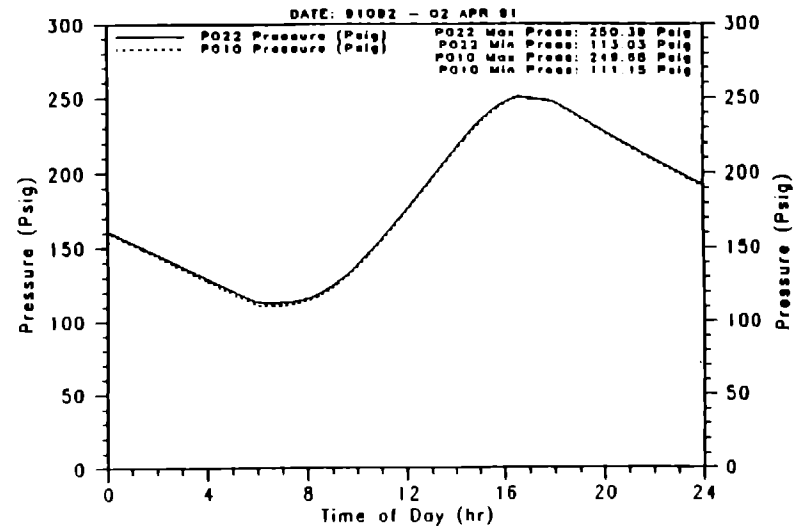
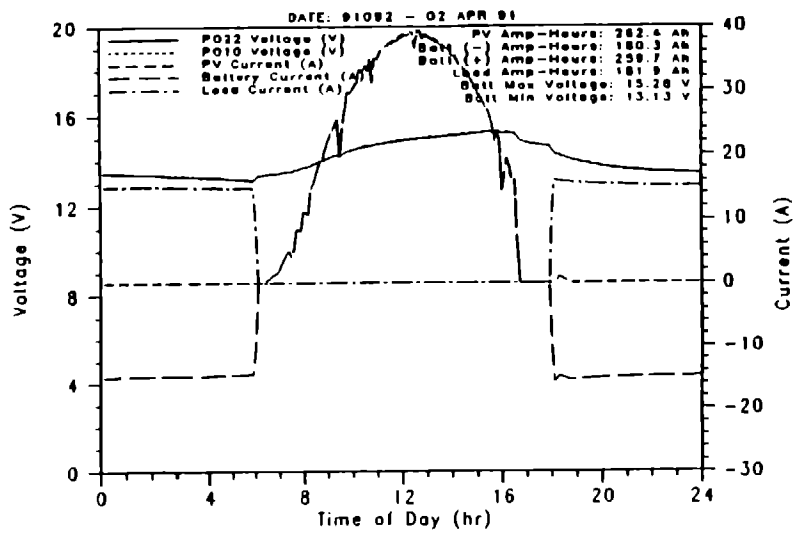


Figure 5-3. Representative Daily Data from Lighting Profile

Table 5-1. Lighting Profile Performance Summary
(2/8/91 – 4/4/91)

| | |
|---|-------------|
| Meteorological Conditions | |
| Avg. Daily Insolation on Array Plane, 45° (kWh/m ²) | 5.16 |
| Avg. Daily Min./Max. Battery Room Temp. (°C) | 18.6/23.8 |
| Min./Max. Battery Room Temp. (°C) | 9.6/26.0 |
| Battery Performance | |
| Average Daily Charge (Ah) | 182.8 |
| Average Daily Discharge (Ah) | 154.5 |
| P022/P010 Average Daily Max. Pressure (psig) | 222/221 |
| P022/P010 Average Daily Min. Pressure (psig) | 125/124 |
| P022/P010 Max. Pressure (psig) | 289/290 |
| P022/P010 Min. Pressure (psig) | 55/54 |
| Average Daily Min./Max. Voltage | 12.72/14.82 |
| Min./Max. Voltage | 10.72/15.65 |
| P022/P010 Average Daily Max. Temperature (°C) | 30.3/29.4 |
| P022/P010 Max. Temperature (°C) | 46.3/42.3 |

Table 5-2. Refrigeration Profile Performance Summary
(5/11/91 – 6/17/91)

| | |
|---|-------------|
| Meteorological Conditions | |
| Avg. Daily Insolation on Array Plane, 45° (kWh/m ²) | 5.02 |
| Avg. Daily Min./Max. Battery Room Temp. (°C) | 24.8/29.1 |
| Min./Max. Battery Room Temp. (°C) | 23.0/32.3 |
| Battery Performance | |
| Average Daily Charge (Ah) | 31.1 |
| Average Daily Discharge (Ah) | 24.0 |
| P022 Average Daily Max. Pressure (psig) | 201 |
| P022 Average Daily Min. Pressure (psig) | 168 |
| P022 Max. Pressure (psig) | 244 |
| P022 Min. Pressure (psig) | 133 |
| Average Daily Min./Max. Voltage | 12.92/14.32 |
| Max. Voltage | 14.62 |
| P022 Average Daily Max. Temperature (°C) | 30.6 |
| P022 Max. Temperature (°C) | 34.3 |

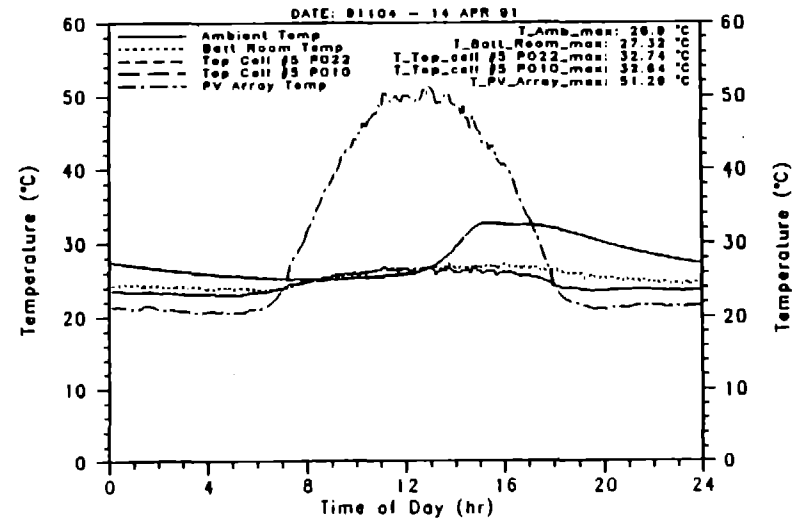
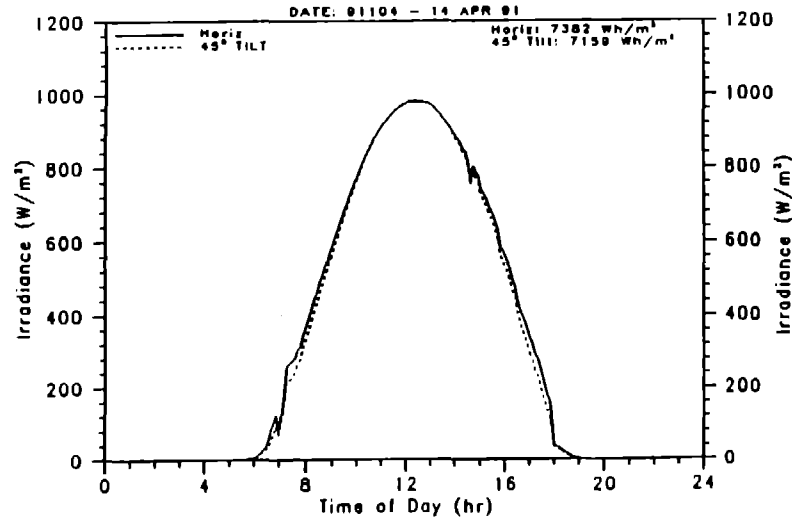
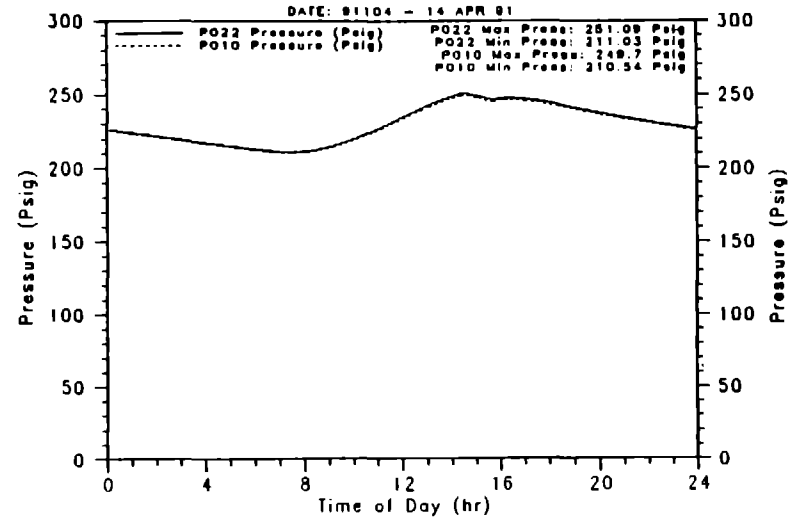
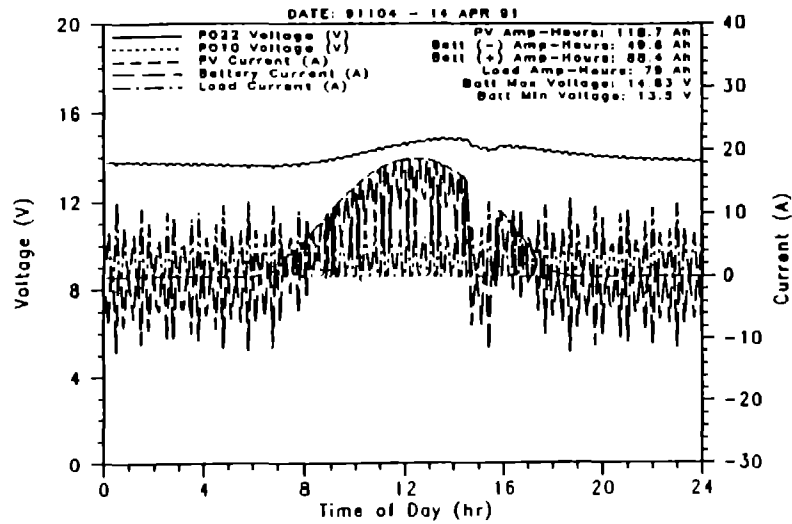


Figure 5-4. Representative Daily Data from Vaccine Refrigeration Profile

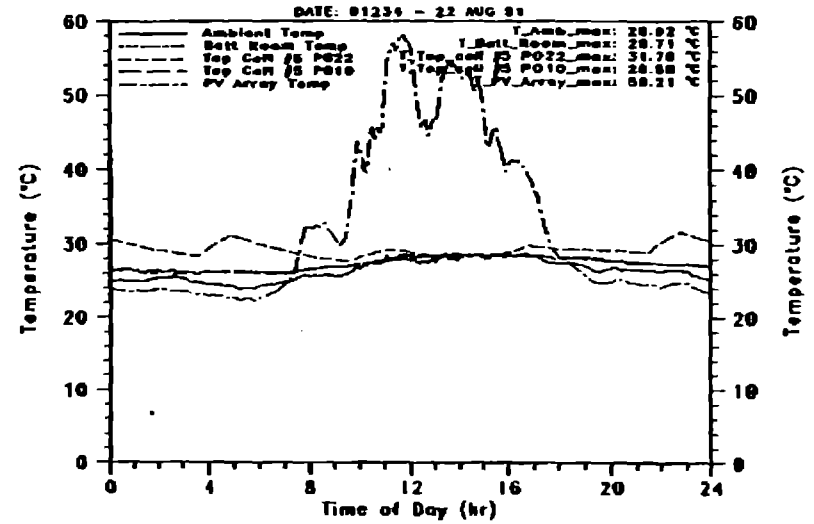
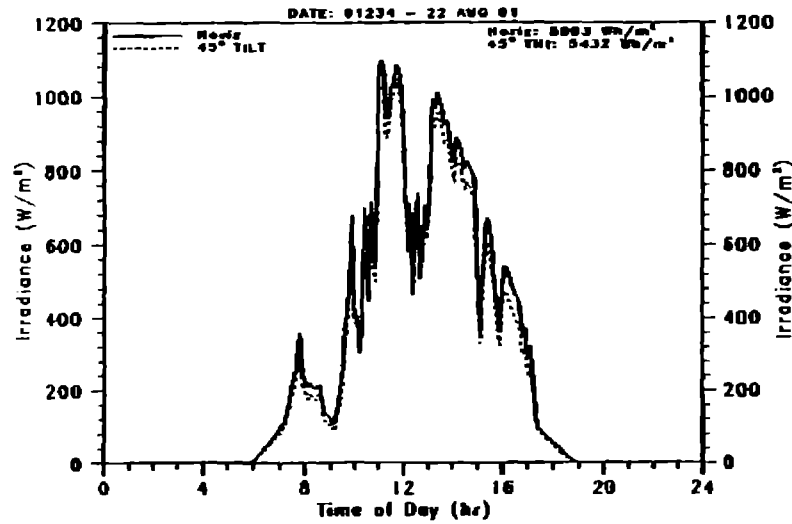
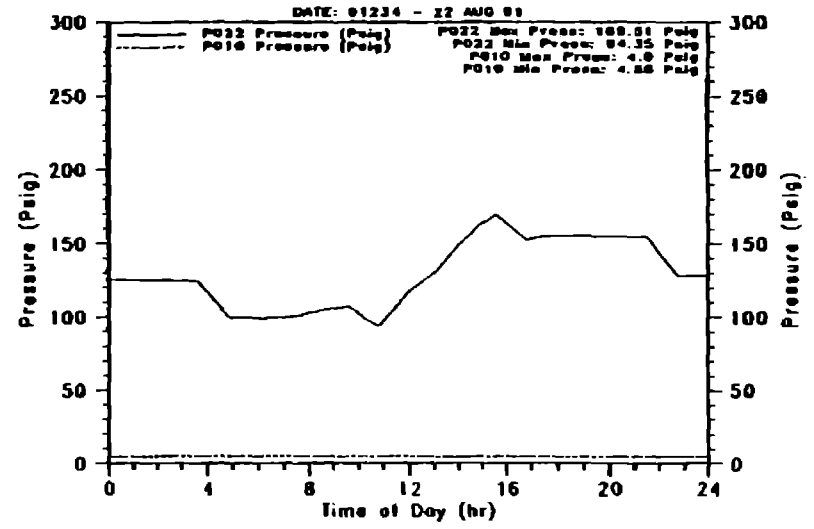
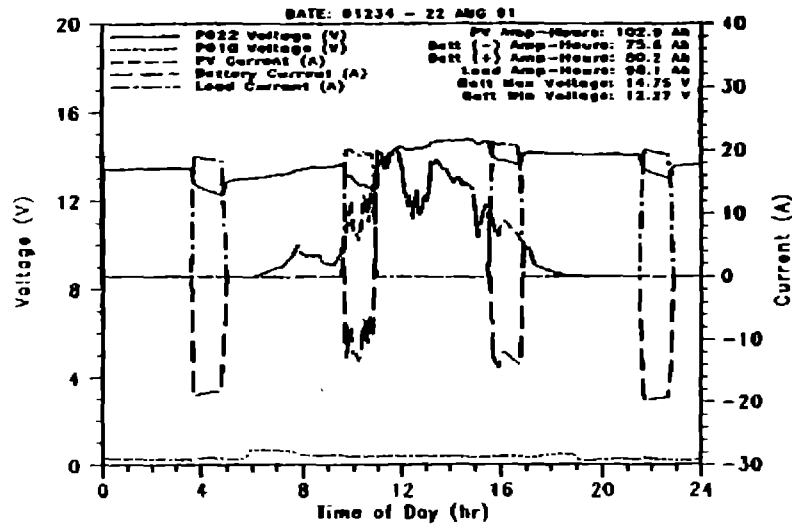


Figure 5-5. Representative Daily Data from Telecommunications Profile

Table 5-3. Characterization Cycles of Batteries P004 and P005

| | P004 | P005 |
|-------------------|---------|---------|
| Pressure (psig) | | |
| Start Cycle | 31.11 | 29.64 |
| End Charge | 258.7 | 235.9 |
| End Cycle | 52.45 | 50.09 |
| System Voltage | | |
| Start Cycle | 0.403 | 1.229 |
| End Charge | 15.03 | 14.88 |
| Start Discharge | 14.09 | 12.47 |
| End Cycle | 8.79 | 8.4 |
| Average Discharge | 12.54 | 11.09 |
| Energy | | |
| Total In (Wh) | 3364.82 | 3195.77 |
| Total Out (Wh) | 2331.48 | 2061.47 |
| Efficiency | 69.29 | 64.51 |
| Ampere Hour In | 229.70 | 229.70 |
| Ampere Hour Out | 185.25 | 185.25 |
| Efficiency | 80.65 | 80.65 |

delivered slightly more than the 2-kWh rated energy capacity. Following the final characterization cycle, the series battery combination was interfaced with a PV array with a load profile simulating a vaccine refrigeration application. Due to the configuration of the series, the load current was set at 5 A, approximately half that used for the parallel battery test run at FSEC.

Following these tests, an apparent leak was identified in the vessel of battery #P004. As in the case of the FSEC battery, the failure was not catastrophic. Plans were made to continue testing the second battery. Unfortunately reconfiguration of the array for that testing has experienced an extensive delay.

7-kWh Battery (JCBGI)

The 7-kWh battery basic cell and stack design is nearly identical to that used subsequently in the 2-kWh batteries. The major difference lies in the pressure vessels. Boilerplate vessels were used for the 7-kWh battery since the fiber-wound vessel concept had not yet been developed.

The 7-kWh design consists of four 12-V battery modules, wired in a series/parallel arrangement to deliver 300 Ah at 24 V, and packaged in a rectangular framework (49" x 34" x 39") covered with decorative panels (Figure 5-7). Passive cooling assists thermal management; no active cooling was provided. Electrical taps are provided on a panel to allow series testing in 12-V multiples up to 48 V with a capacity of 150 to 600 Ah. Each battery module contains 10 prismatic cells. Each cell contains nine cell-modules, a concept developed to reduce manufacturing costs and promote ease of handling. One cell-module, which is the building block of the prismatic cell, consists of two sintered and electrochemically impregnated nickel positives in a back-to-back configuration with an electrolyte absorber between them, two separators, and two negative electrodes. The components of the cell-module are bound together by two outside diffusion screens.

In the summer of 1991, JCBGI and SNL decided to initiate a series of parametric tests on the four batteries comprising the 7-kWh module. Planned tests include a series of cycles of varying discharge rates (C/20 to C/3), varying charge rates (C/20 to C/5), and stand loss tests.

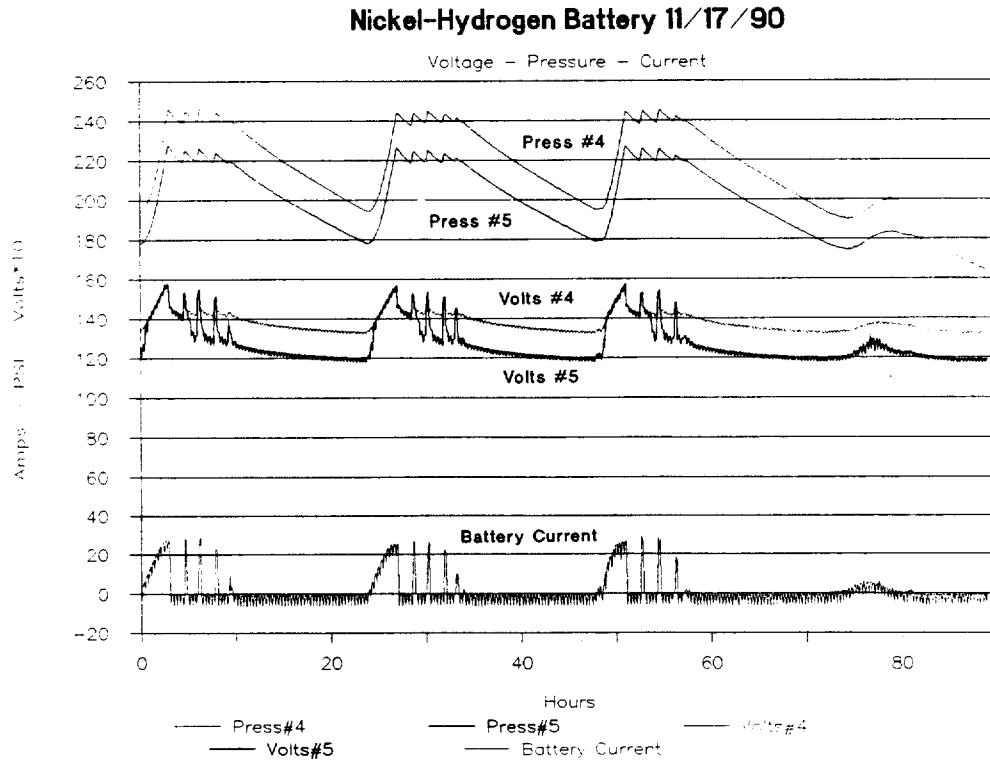


Figure 5-6. Typical Daily Operation of Batteries #P004 and #P005 on the Vaccine Refrigeration Profile

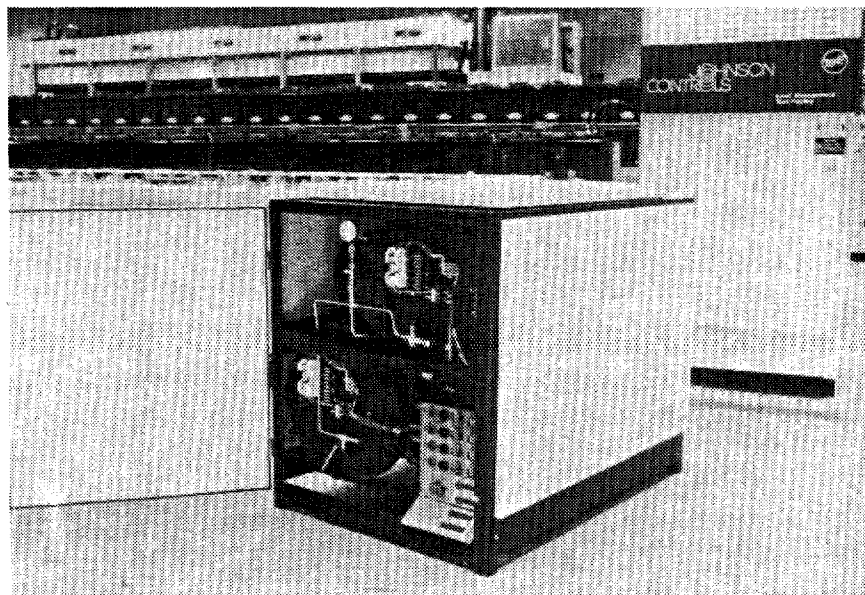


Figure 5-7. 7-kWh Boilerplate CPV Nickel/Hydrogen Battery

In preparation for the renewed testing at JCBGI, a brief series of cycles was run, establishing that the batteries, stored in a fully discharged, open circuit condition at room temperature for almost a full year, were still in excellent condition. The four batteries were then split into two separate sets of series-connected stacks for the parametric tests.

To date, a set of C/5 discharge baseline cycles and C/10 rate discharge cycles have been completed, as summarized in Tables 5-4 and 5-5. The results have been extremely impressive considering the history of these batteries. The batteries have been delivering over 190 Ah and 9.5 kWh in total, well over the 7.85 kWh achieved in initial testing.

Future Plans

Testing of the 7-kWh battery stacks will continue at JCBGI through December, at which time an accelerated

life-test regime will be considered. Battery #P005 at TDI will be inspected by JCBGI personnel to confirm the vessel leak. If confirmed, the battery will be returned to JCBGI for further analysis. Operational battery #P004 at TDI will be shipped to FSEC, where it will be coupled in series with battery #P022 and tested on the three application profiles. Possible rebuild of the two battery stacks from the failed vessels using an improved vessel design is being considered by JCBGI and SNL.

SNL Evaluation

Contracts for the development of nickel/hydrogen batteries at JCBGI provided for periodic delivery of cells and batteries to SNL for evaluation purposes. Typically, these cells consisted of several modules and represented state-of-the-art technology or contained experimental components modified to reduce cost or improve performance.

Table 5-4. Parametric Testing of Series-Configured 10-Cell Modules #1 and #3 from 7-kWh Battery

| Cycle | Charge | | Discharge | | | |
|---|---------|-----|-----------|-------|------|-------------------|
| | Current | Ah | Current | Ah | Wh | Avg. Cell Voltage |
| 1 | 16 | 200 | 32 | 191.3 | 4737 | 1.24 |
| 2 | 16 | 200 | 32 | 191.5 | 4738 | 1.24 |
| 3 | 16 | 200 | 32 | 191.5 | 4732 | 1.24 |
| 4 | 16 | 200 | 32 | 191.6 | 4734 | 1.24 |
| 5 | 16 | 200 | 32 | 191.6 | 4729 | 1.23 |
| 6 | 16 | 200 | 32 | 191.4 | 4721 | 1.23 |
| 7 | 16 | 200 | 32 | 192.4 | 4752 | 1.23 |
| 8 | 16 | 200 | 32 | 191.4 | 4720 | 1.23 |
| Average for C/5 Rate Discharge Cycles: | 16 | 200 | 32 | 191.5 | 4733 | 1.24 |
| 9 | 16 | 200 | 16 | 197.6 | 5093 | 1.29 |
| 10 | 16 | 200 | 16 | 194.4 | 5015 | 1.29 |
| 11 | 16 | 200 | 16 | 194.6 | 5025 | 1.29 |
| 12 | 16 | 200 | 16 | 194.1 | 5010 | 1.29 |
| 13 | 16 | 200 | 16 | 194.6 | 5028 | 1.29 |
| 14 | 16 | 200 | 16 | 194.7 | 5028 | 1.29 |
| 15 | 16 | 200 | 16 | 195.3 | 5044 | 1.29 |
| Average for C/10 Rate Discharge Cycles: | 16 | 200 | 16 | 195.0 | 5032 | 1.29 |

Table 5-5. Parametric Testing of Series-Configured 10-Cell Modules #2 and #4 from 7-kWh Battery

| Cycle | Charge | | Discharge | | | |
|---|---------|-----|-----------|-------|------|-------------------|
| | Current | Ah | Current | Ah | Wh | Avg. Cell Voltage |
| 1 | 16 | 200 | 32 | 193.1 | 4828 | 1.25 |
| 2 | 16 | 200 | 32 | 192.7 | 4815 | 1.25 |
| 3 | 16 | 200 | 32 | 192.9 | 4816 | 1.25 |
| 4 | 16 | 200 | 32 | 192.9 | 4816 | 1.25 |
| 5 | 16 | 200 | 32 | 192.8 | 4810 | 1.25 |
| 6 | 16 | 200 | 32 | 192.9 | 4811 | 1.25 |
| 7 | 16 | 200 | 32 | 194.8 | 4861 | 1.25 |
| 8 | 16 | 200 | 32 | 193.0 | 4812 | 1.25 |
| Average for C/5 Rate Discharge Cycles: | | | | | | |
| | 16 | 200 | 32 | 193.1 | 4821 | 1.25 |
| 9 | 16 | 200 | 16 | 197.6 | 5126 | 1.30 |
| 10 | 16 | 200 | 16 | 194.5 | 5048 | 1.30 |
| 11 | 16 | 200 | 16 | 194.7 | 5056 | 1.30 |
| 12 | 16 | 200 | 16 | 194.5 | 5049 | 1.30 |
| 13 | 16 | 200 | 16 | 194.9 | 5064 | 1.30 |
| 14 | 16 | 200 | 16 | 194.8 | 5059 | 1.30 |
| 15 | 16 | 200 | 16 | 194.8 | 5059 | 1.30 |
| Average for C/10 Rate Discharge Cycles: | | | | | | |
| | 16 | 200 | 16 | 195.1 | 5066 | 1.30 |

Three nickel/hydrogen cells were on test during this period. Table 5-6 lists their configurations and the test conditions.

Cycle Tests

Cell #144. This cell has a Gortex backing on the negative electrodes and represents the baseline design used in the 7-kWh battery evaluated by SNL in 1988. The cell has been subjected to the standard cycle test. During its life-cycling, it was observed that the end-of-charge (EOC) pressure would gradually increase, resulting in a high pressure alarm at 330 psig. Each time this occurred, pressure was reduced to a level of 50 psig at EOD and testing resumed.

After 1500 cycles, it was noted that the capacity was gradually diminishing. EOD pressure was still showing an upward trend, but EOC pressure was not increasing

at the same slope. The cell was subjected to an activation cycle, but the capacity continued to drop. When the cell had accumulated 1896 cycles, the capacity had dropped to 126 Ah, 72% of the initial baseline value. Testing was discontinued at this point and the cell returned to JCBGI for evaluation.

Cell #185. The negative electrodes of this cell have a lower cost fluoroplastic film as a hydrophobic backing. During initial testing using the standard cycle, the EOC pressure increased an average of 0.42 psig per cycle such that the high limit of 330 psi was reached several times. Also, on discharge, the temperature reached the high limit of 40.0°C several times. To overcome these problems, charging was terminated after an input of 160 Ah. This type of cycling still produced a gradual increase in EOC pressure, necessitating an occasional reduction of end-of-discharge (EOD) pressure to 50 psig.

Table 5-6. Configuration and Test Conditions

| Cell S/N | Positive Electrodes | Positive Th. (in) | Positive Additive | Negative Type | KOH (%) | °C Cool | Current (A) Chrg/Disch. | Cycle Type |
|----------|---------------------|-------------------|-------------------|---------------------------|---------|---------|-------------------------|------------|
| #144 | 18 | .070 | Li | Gortex | 24 | None | 25/25 | Std.* |
| #185 | 18 | .070 | Li | Fluoro-plastic (TFE) Film | 24 | None | 25/25 | Consv.* |
| #P003 | 18 | .070 | Cd | Rolled | 24 | 27 | 25/25 | Std.* |

NOTES: *Standard life-cycle: Discharge to 1.0 V/cell followed by charging until the pressure-time slope drops to 75% of the linear value.

*Conservative cycle: Discharge to 1.0 V/cell followed by charging to an input of 160 Ah.

The cell has now accumulated 1180 cycles. Using the conservative test plan produced a steady coulombic efficiency of 98.6% for many months, but after 1100 cycles, the capacity began to fluctuate and the coulombic efficiency dropped to 96.5%.

Cell #P003. This is a nine-module cell of the same construction as the cells used in the 2-kWh batteries delivered to other field test facilities. The design varies from other cells on test at SNL in the use of a rolled-process negative film with a catalyst loading of 0.4 mg Pt/cm². The nominal capacity rating is 160 Ah.

A series of parametric tests was conducted, first at room temperature and then with a cooling jacket installed on the pressure vessel. A comparison of the capacities showed an increase of 6 Ah when the cell temperature was being controlled by the cooling jacket. Testing continued with the cooling jacket in place. EOC and EOD pressures tended to rise slowly in parallel.

Testing of these nickel/hydrogen cells was suspended on June 30, 1991. Table 5-7 lists the results of testing as of that time.

Aluminum/Air Evaluation

In January 1991, Eltech Research Corp. completed a 3-yr \$2.4M aluminum/air battery development program. Evaluation of the final deliverable, a 400-cm² single cell, was completed in the second quarter of FY91. Final tests included SFUDS discharge with both pure aluminum and an advanced aluminum alloy.

Under SFUDS discharge conditions, the 99.995% aluminum anodes did not operate well due to poor discharge characteristics. After only one or two SFUDS cycles, the cell voltage dropped below 0.5 V, a preset cell cutoff condition, during the SFUDS 79 W/kg requirement. Table 5-8 shows data from the two runs with the 99.995% aluminum anodes. For the 99.995% aluminum anodes, data are not presented for the Faradaic efficiency and caution should be taken in interpreting the corrosion rate data owing to the brief discharge time of the tests.

The advanced alloy data in Table 5-8 indicate that the program task to reduce the corrosion rate via high performance aluminum alloys was successful. The programmatic goal was to reduce the corrosion rate to less than 30 mA/cm². As shown in Table 5-8, the

Table 5-7. Summary of Test Results (as of 6/30/91)

| Cell | Cycles | Capacity (Ah) | | Effic. (%) | | Mid-Point Disch. V/c | Pres. (psig) EOD/EOD |
|-------|--------|---------------|--------|------------|------|----------------------|----------------------|
| | | Nominal | Latest | Ah | Wh | | |
| #185 | 1180 | 160 | 156.2 | 96.5 | 82.3 | 1.268 | 43/268 |
| #P003 | 509 | 160 | 191.8 | 93.7 | 80.9 | 1.279 | 89/318 |

Table 5-8. Aluminum/Air Cell SFUDS Discharge Results

| Test # | Anode Type | Elapsed Time (min) | Al Effic. Fara/Total Wt. Loss (%) | Average Corrosion Rate (mA/cm ²) | Anode Utilization (%) | Total SFUDS Cycles |
|--------|------------|--------------------|-----------------------------------|--|-----------------------|--------------------|
| 1 | Alloy | 795 | 54.7 | 22.6 | 16.3 | 93 ¹ |
| 2 | 99.995% | 79 | * | 150.3 | 0.3 | 2 ² |
| 3 | 99.995% | 45 | * | 32.3 | 0.1 | 1 ² |
| 4 | Alloy | 829 | 57.3 | 20.4 | 17.2 | 93 ¹ |
| 5 | Alloy | 720 | 51.5 | 25.7 | 14.8 | 81 ³ |

* - Insufficient data to calculate

¹ - Test terminated after two days

² - Test terminated due to low voltage cut-off of 1/2 V

³ - Test terminated due to cell leak

average corrosion rate for the alloy under SFUDS was 22.9 mA/cm². The reason for the relatively low anode utilization was due to time and cell operation. For Tests 1 and 4 that each ran 93 SFUDS repetitions, the testing was terminated after two 8-hr periods. Test 5 was ter-

minated after 81 cycles due to a cell leak. Due to the uncertainty in the equivalent weight of the battery, that is, the prescribed weight of the single-cell battery correlated to a full-sized EV battery, vehicle range was not predicted.

Appendix: Presentations and Publications

Presentations

- Akhil, A. A., and A. R. Landgrebe, "Advanced Lead-Acid Batteries for Utility Applications," 3rd International Conference, Batteries for Utility Energy Storage, Kobe, Japan, March 1991.
- Jones, K. R., and J. P. Zagrodnik, "Photovoltaic Energy Storage in Nickel/Hydrogen Batteries," 22nd IEEE Photovoltaic Specialists Conference, Las Vegas, Nevada, October 1991.
- Zagrodnik, J. P., and K. R. Jones, "Photovoltaic Testing of 2-kWh Common Pressure Vessel Nickel/Hydrogen Batteries," 24th Intersociety Energy Conversion Conference (IECEC), Boston, August 1991.

Publications

- Magnani, N. J., P. C. Butler, A. A. Akhil, J. W. Braithwaite, J. M. Freese, S. E. Lott, Exploratory Battery Technology Development Report for FY90, Sandia National Laboratories, SAND91-0672, April 1991.
- Rudd, E. J., and S. Lott, The Development of Aluminum-Air Batteries for Application in Electric Vehicles, Sandia National Laboratories, SAND91-7066, December 1990.

Distribution

Argonne National Laboratory (5)
9700 South Cass Avenue
Argonne, IL 60439
Attn: C. Christianson
W. DeLuca
G. Henriksen
K. Myles
J. Smaga

Best Facility
321 Sunnymeade Road
Somerville, NJ 008876
Attn: G. Grefe

Beta Power, Inc. (3)
489 Devon Park Drive, Suite 315
Wayne, PA 19087
Attn: W. Auxer (3)

Beta Power, Inc.
163 West 1700
South Salt Lake City, UT 84115
Attn: J. Rassmussen

Bonneville Power Administration
Routing EO
PO Box 3621
Portland, OR 97208
Attn: J. Ray

C & D Charter Power Systems
3043 Walton Road
Plymouth Meeting, PA 19462
Attn: S. Misra

California State Air Resources Board
Research Division
PO Box 2815
Sacramento, CA 95812
Attn: J. Holmes

Ceramatec, Inc.
2425 South 900 West
Salt Lake City, UT 84119
Attn: D. Richerson
A. Virkar

Chloride Silent Power, Ltd. (4)
Davy Road
Astmoor Runcorn, United Kingdom
WA71PZ
Attn: I. Jones
M. McNamee (3)

Chrysler Motors Corporation
30900 Stevenson Highway
CIMS 463-00-00
Madison Heights, MI 48071
Attn: B. Heinrich

Chrysler Motors Corporation
12000 Chrysler Drive
CIMS 4180418
Highland Park, MI 48288-1118
Attn: D. Smith

Chugach Electric Corporation
PO Box 195300
5601 Minnesota Drive
Anchorage, AK 99519
Attn: T. Lovas

Decision Focus, Inc.
4984 El Camino Real
Los Altos, CA 94022
Attn: S. Jabbour

Delco-Remy
7601 East 88th Place
Indianapolis, IN 46256
Attn: R. Rider

Eagle-Picher Industries
C & Porter Street
Joplin, MO 64802
Attn: J. DeGruson

EG&G Idaho, Inc. (4)
Idaho National Engineering Lab
PO Box 1625
Idaho Falls, ID 83415
Attn: G. Hunt
G. Cole
J. Hardin
A. Burke

Electric Power Research Institute (3)
PO Box 10412
Palo Alto, CA 94303
Attn: R. Schainker
R. Weaver
R. Swaroop

Electrochemical Engineering Consultants, Inc. (3)
1295 Kelly Park Circle
Morgan Hill, CA 95037
Attn: P. Symons (3)

Electrotek Concepts, Inc.
Electric Vehicle Operations
4605 Amnicola Highway
PO Box 16548
Chattanooga, TN 37416
Attn: H. Barnett

Eltech Systems Corporation (2)
Research and Development Center
625 East Street
Fairport Harbor, OH 44077
Attn: E. Rudd (2)

Energetics (3)
9210 Route 108
Columbia, MD 21044
Attn: J. Hurwitch (2)
H. Lowitt

Energy Research Corporation (2)
Three Great Pasture Road
Danbury, CT 06810
Attn: A. Leo
J. Brown

EnerTech
Route 4, Box 415
Rolla, MO 65401-9335
Attn: S. Eckroad

Exxon Research Company
PO Box 536
1900 East Linden Avenue
Linden, NJ 07036
Attn: P. Grimes

Ford Motor Company (2)
Vehicle Systems Department
PO Box 2053
Dearborn, MI 48121-2053
Attn: M. Dzieciuch
R. Moy

General Motors Technical Center
Engineering West, W3-EVP
30200 Mound Road
PO Box 9010
Warren, MI 48090-9010
Attn: M. D. Eskra

Giner, Inc.
14 Spring Street
Waltham, MA 02254-9147
Attn: A. LaConti

GNB Industrial Battery Company (2)
Woodlake Corporate Park
829 Parkview Blvd.
Lombard, IL 60148-3249
Attn: S. Deshpande (2)

Harza Engineering
Sears Tower
233 South Wacker Drive
Chicago, IL 60606
Attn: H. Chen

Hughes Aircraft Company
PO Box 2999
Torrance, CA 90509-2999
Attn: R. Taenaka

ILZRO
PO Box 12036
Research Triangle Park, NC 27709
Attn: R. Nelson

Johnson Controls, Inc. (2)
Globe Battery Division
5757 North Green Bay Avenue
PO Box 591
Milwaukee, WI 53201-0591
Attn: P. Eidler
W. Tiedeman

Johnson Controls, Inc.
Globe Battery Division
12500 West Silver Spring Drive
PO Box 591
Milwaukee, WI 53201-0591
Attn: J. Zagrodnik

Lawrence Berkeley Laboratory (5)
University of California
No. 1 Cyclotron Road
Berkeley, CA 94720
Attn: E. Cairns
K. Kinoshita
F. McLarnon (3)

New York Power Authority
1633 Broadway
New York, NY 10019
Attn: J. Stilman

Oak Ridge National Laboratories
PO Box X
Oak Ridge, TN 37831
Attn: S. Dale

Oglethorpe Power Company
2100 E. Exchange Place
PO Box 1349
Tucker, GA 30085-1349
Attn: K. Scruggs

Omnion Power Corporation
188 Highway ES
Mukwonago, WI 53149
Attn: H. Meyer

Pacific Gas & Electric
3400 Crow Canyon Road
San Ramon, CA 94583
Attn: J. Meglen

Power Technologies Inc.
One Sierragate Plaza
Suite 340B
Roseville, CA 95678
Attn: H. Clark

Puerto Rico Electric Power Authority
G.P.O. Box 4267
San Juan, Puerto Rico 00936-4267
Attn: W. Torres

R. K. Sen & Associates
3808 Veazey Street NW
Washington, DC 20016
Attn: R. Sen

San Diego Gas & Electric Company
PO Box 1831
San Diego, CA 92112
Attn: J. Wight

Southern California Edison
2244 Walnut Grove Avenue
PO Box 800
Rosemeade, CA 91770
Attn: R. Scheffler

Wright Patterson AFB (2)
Air Force Wright Aeronautical Labs
WRDF/POOS
Wright Patterson AFB, OH 45433
Attn: W. Bishop
S. Vukson

U. S. Department of Energy (21)
Office of Energy Management
CE-142
FORSTL
Washington, DC 20585
Attn: R. Eaton (20)
K. Klunder

U. S. Department of Energy (6)
Office of Propulsion Systems
CE-321
FORSTL
Washington, DC 20585
Attn: K. Barber
E. Dowgiallo
A. Landgrebe
K. Heitner
P. Patil
J. Brogan

U. S. Department of Energy (2)
Albuquerque Operation Office
Energy Technologies Division
Albuquerque, NM 87115
Attn: G. Buckingham (2)

U. S. Department of Energy
Sandia Area Office
PO Box 5800
Albuquerque, NM 87115
Attn: A. Sneddon, Jr.

20 O. Jones
140 M. Owen
143 R. Thorp
4200 D. Arvizu
1811 R. Clough
1811 C. Arnold, Jr.
1812 C. Renschler
1812 R. Assink
2000 H. Schmitt
2500 G. Beeler
2520 N. Magnani
2520A L. Lachenmeyer
2522 R. Clark
2523 R. Diegle

2525 P. Butler (20)
3710 L. Welchel
Attn: D. Wilt
6200 B. W. Marshall
6220 D. Schueler
6221 T. Bickell
6223 G. Jones
8523-2 Central Technical Files
3141 S. Landenberger (5)
3145 Document Processing
For DOE/OSTI (8)
3151 G. C. Claycomb